Doctral Dissertation

Nuclear structure of neutron-rich Mg isotopes studied by β-decay spectroscopy of spin-polarized Na isotopes

Kunihiko Tajiri

Department of Physics,
Graduate School of Science,
Osaka University

March, 2012

Doctral Dissertation

Nuclear structure of neutron-rich Mg isotopes studied by β-decay spectroscopy of spin-polarized Na isotopes

Kunihiko Tajiri

Department of Physics,
Graduate School of Science,
Osaka University

March, 2012

Nuclear structure of neutron-rich Mg isotopes studied by β-decay spectroscopy of spin-polarized Na isotopes

(スピン偏極したNa同位体のβ崩壊による
中性子過剰なMg同位体の核構造の研究)

ABSTRACT

The most modern technologies in particle accelerators and experiments enable us to access more exotic nuclei with very asymmetric proton and neutron numbers than ever before. These nuclei are located in the nuclear chart very far from the β-stability line and the knowledge on their structure is essential to answer the basic question to what extent the idea of the nuclear magic number keeps appropriate. One of the most interesting regions is the so-called "island of inversion", the region of nuclei centering at ^{31}Na. In nuclei of this region, two-particle-two-hole (2p-2h) configurations across the $N = 20$ shall gap are lower in energy than normal configurations, and possibility of a variety of nuclear shapes are being discussed both for the ground and excited states. However, most of the experimental data have been rather limited to the ground states and/or low-lying levels and the spins and parities of many levels are left unknown. The present work aims at experimentally clarifying the structure change as a function of the neutron number by firmly establishing the level schemes of the neutron-rich Mg isotopes.

The experiments were performed in combination of our unique method of β-decay spectroscopy for a *spin-polarized* radioactive nucleus and highly polarized Na isotopes at the state-of-the-art radioactive beam facility of TRIUMF. The β-decay asymmetry of the Na decay enables unambiguous spin-parity assignments of the levels in the daughter Mg, and it becomes possible to compare the experimental data and theoretical predictions on a level-by-level basis. The present thesis discusses in detail the successful results on ^{28}Mg, ^{29}Mg and ^{30}Mg, as the first step of series of experiments towards very neutron-rich Mg isotopes across through the island of inversion.

In ^{28}Mg two levels at high excitation energy were newly found and the overall good agreement of the level scheme with the shell-model calculations in the *sd*-shell model space indicates that the structure of ^{28}Mg is understood mostly based on the normal configurations. In ^{29}Mg spins and parities of seven levels were assigned for the first time. All the experimental levels were reasonably reproduced by the conventional shell-model calculations, except for two levels at 1.094 and 1.430 MeV. We propose that the two levels are the negative-parity ones with 1p-1h intruder configurations, since the large scale shell-model calculation, which

takes into account also the fp-shell model space, predicts two negative-parity levels at 0.68 MeV ($7/2^-$) and 1.01 MeV ($3/2^-$). In the systematics of the negative-parity levels in neutron-rich Mg isotopes, it is found that the negative-parity levels rapidly decrease their energies at ^{29}Mg, when the neutron number is increased. This is one of the experimental evidences for the shell evolution in Mg isotopes. In ^{30}Mg four levels were newly found and the spins and parities of eleven levels were assigned for the first time. From the detailed transition probabilities and level-by-level comparison with the conventional shell-model calculations, it was shown that five levels at 1.788 (0_2^+), 2.466 (2_2^+), 3.460 (2^+), 4.967 (1^+), 5.414 (2^+) MeV exhibit different nature from the spherical nucleus. We propose that the 1.788-, 3.460-, 4.967- and 5.414-MeV levels have deformed shapes with intruder configurations and the 2.466-MeV level is the 2^+ band head of γ-band predicted by the mean-field theory.

TABLE OF CONTENTS

CHAPTER I

Introduction

1.1 Structure of neutron-rich nuclei around "island of inversion"

One of the most important problems in the contemporary nuclear physics is structure change as a function of asymmetry in neutron and proton numbers. In particular, questions on nuclear magic number which has been a guiding principle to understand the nuclear structure for over 50 years are one of the most urgent problems. The first clear evidence for light nuclei was the possible changes of the magic number $N = 20$ suggested by the anomalous 2-neutron separation energy S_{2n} in very neutron-rich nuclei ^{31}Na and ^{32}Na [THI75]. Theoretical predictions based on Hartree-Fock (HF) theory suggested deformed ground states for these Na isotopes [CAM75]. Similar anomaly was also found in ^{31}Mg and ^{32}Mg [DET83]. Shell-model calculations performed for a wide range of neutron-rich nuclei of this vicinity indicated that two-particle-two-hole (2p-2h) configurations across the $N = 20$ shall gap are lower in energy than normal configurations for nuclei with $20 \leq N \leq 22$ and $10 \leq Z \leq 12$. Figure 1.1 shows this region of nuclei as a red region centering at ^{31}Na [BRO10]. The inset of the figure shows schematic configurations of 0p-2h in ^{30}Mg (left), 0p-0h in ^{32}Mg (A) in a framework of classical shell model, and 2p-2h in ^{32}Mg (B) in reality. This region of nuclei, referred to as the "island of inversion" [WAR90], represents a dramatic change of structure with growing neutron-proton asymmetry. The nuclei on and around the island of inversion have been attracting much attention from both experiment and theory.

Succeeding investigations have accumulated more detailed information such as $B(E2; 0_1^+ \rightarrow 2_1^+)$, ground-state spin-parity, ground-state magnetic moment, and spectroscopic factors, etc., and confirmed the disappearance of the $N = 20$ magic number. Large deformation was confirmed for the ground states of the $N \sim 20$ nuclei. Recent experiments concentrated on the boundary of the island also showed transitional characters. Figure 1.1 shows the present understanding of the region around the island of inversion. Nuclei are classified in three

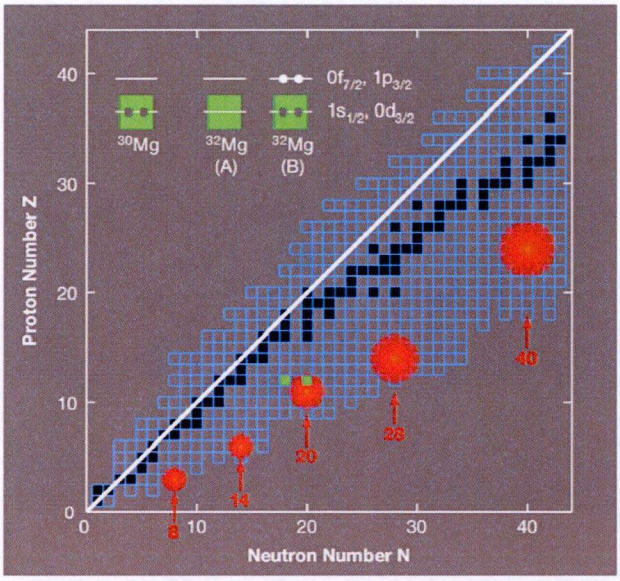

Figure 1.1: Partial nuclear chart [BRO10]. Stable and unstable nuclei are displayed in closed and open squares, respectively. The "island of inversion" is shown by a red square just above the $N = 20$ arrow. It is seen that ^{32}Mg (shown in green) is located on the island, whereas ^{30}Mg is just outside the island. Other regions in red represent the very recently predicted "islands of shell breaking".

categories according to the configurations in the shell-model framework: Nuclei of which ground state is well described with the normal (intruder) configurations are displayed in blue (orange). In the case that the ground state is of the normal configuration and the low-lying excited states are described with the intruder configurations, the nucleus is colored in purple. We define such nucleus as "border" one from its transitional nature to the island of inversion. It is understood that the island has a larger extension from the original island which is displayed by a red square in Fig. 1.2. It should be noted that compared to the ground states, information on the excited states are very limited. In many nuclei in this region, the essential information to discuss the structure or shape such as spins and parities are not known for most of the excited states. This situation prevents us to investigate the shell evolution, i.e., the lowering of the intruder levels as a function of the proton-neutron asymmetry.

A large-scale shell-model calculation has been performed for neutron-rich Na isotopes in a framework of the Monte Carlo shell model (MCSM) [UTS04]. The model space considered was the full *sd*-shell orbits and two lower pf-shell orbits. It was shown that an onset of ground state intruder configurations occurs already at neutron number $N = 19$ and the

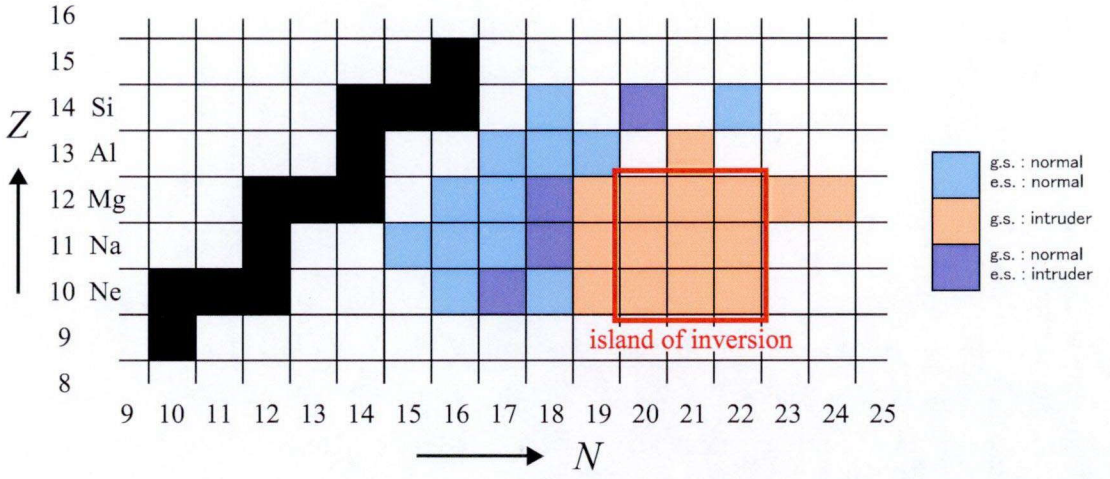

Figure 1.2: Nuclear chart far from the β-stability line. Location of the classical "island of inversion" [WAR90] is surrounded by red square.

narrow $N = 20$ shell gap is caused by the spin-isospin dependence of the nucleon-nucleon interaction [UTS04]. It was also explained that the monopole component of nucleon-nucleon interaction gives rise to the new magic number of $N = 16$ [OTS10].

Another theoretical approaches, which are not based on the shell model, also have made great progresses. The antisymmetrized molecular dynamics (AMD) calculation , which has shown successful reproductions in lighter nuclei such as Li and Be, was applied to predict the structure in the neutron-rich nuclei around island of inversion [KIM07; KIM11]. Furthermore, the constrained-Hartree-Fock-Bogoliubov method with the local quasiparticle random phase approximation (CHFB+LQRPA) predicts the collective behavior such as rotational and γ-vibrational motions in neutron-rich ^{30,32,34}Mg [HIN11]. These theories predict the shape coexistence in Mg around $N = 20$.

Recent discoveries of the second 0^+ levels in ^{30}Mg [SCW09] and ^{32}Mg [WIM10] triggered hot discussions on the properties of these levels [FOR11]. For ^{30}Mg, the excited 0_2^+ level is interpreted as a prolately deformed state which coexists with the spherical ground state. For ^{32}Mg, it is suggested that the 0_2^+ state is a spherical state coexisting with the deformed ground state. These are one of the evidences for the lowering of the intruder levels with increasing neutron number. It is very important to investigate the effects of the intruder configurations in a wide range of excitation energy and with a variation of proton-neutron number asymmetry. However, most of the experimental data have been rather limited to the ground states and/or low-lying levels, and the spins and parities of many levels are left

unknown, although the spin-parity is the key quantity to discuss the nuclear structure. In the case of Mg isotopes, the present status of the spin-parity assignments are not sufficient for isotopes heavier than ^{28}Mg.

1.2 Purpose of the present work

The present work aims at experimentally clarifying the structure change of neutron-rich Mg isotopes as a function of the neutron number by comparing the experimental levels and the theoretical predictions on a level-by-level basis, after firmly establishing the level schemes of the Mg isotopes in a wide excitation energy range. We used our unique method of β-decay spectroscopy which takes advantage of anisotropic β decay of spin-polarized Na isotopes. The asymmetry parameters of the β decay are the effective clues to unambiguously assign the spin-parity of levels in the daughter nucleus Mg, as shown by the successful work which assigned the spins and parities of 7 levels in ^{11}Be for the first time [HIR05]. The experiments were performed at the state-of-the-art radioactive beam facility of TRIUMF in Canada, where the world-highest polarized alkali beams are available. The combination of our powerful method and the highly-polarized and high-intensity Na beams enable systematic studies of Mg isotope structures from lighter region outside of the island of inversion to heavier one across through the island. The present work has been done on ^{28}Mg, ^{29}Mg and ^{30}Mg, as the first step of series of experiments on a number of Mg isotopes.

CHAPTER II

Structures of ^{28}Mg, ^{29}Mg, and ^{30}Mg

2.1 Structure of ^{28}Mg

The level structure of ^{28}Mg has been investigated by the experimental methods of β-decay of ^{28}Na [DET79; GUI84] and nucleon-transfer reactions [HIN61; MID64; FIS73; RAS74] as listed in Table 2.1. The levels observed in these experiments are summarized in Fig. 2.1. The spin-parity assignments have been investigated as outlined below.

Middleton *et al.* [MID64] assigned the spins and parities of 9 levels by the angular distribution of proton. Rastegar *et al.* [RAS74] reported another assignments for 5 levels from the angular correlation between proton and γ ray. They revised the previous 0^+ assignment [MID64] for the 5.272-MeV level to 1^-. Later, the level structure of ^{28}Mg was also investigated in the β decay of ^{28}Na by Détraz *et al.* [DET79] and Guillemaud-Mueller *et al.* [GUI84]. Confirmed were the allowed β transitions leading to the g.s. as well as the known levels including the 5.272-MeV level [GUI84]. By taking into account the positive parity of the ^{28}Na$_{\text{g.s.}}$ (1^+ [NND11]), Endt concluded that the level at 5.272 MeV is of 1^+ [END90].

Thus the spins and parities of ^{28}Mg have been reported for many levels. However, since the highest 6.759-MeV level reported so far [HIN61] is somewhat lower in energy than the neutron-threshold energy of 8.5034(20) MeV [AUD03], the undiscovered levels might be found between these energies.

2.2 Structure of ^{29}Mg

The level structure of ^{29}Mg has been investigated by the experimental studies of β-decay of ^{29}Na [GUI84; BAU87], β-n decay of ^{30}Na [BAU89], multinucleon transfer reactions [SCO74; FIF85; WOO88], and fusion-evaporation reaction [PAN81] as listed in Table 2.2. The levels observed in these experiments are summarized in Fig. 2.2. For ^{29}Mg, firm spin-

Table 2.1: Overview of experimental observations for levels in ^{28}Mg.

Experiment	Observables	Reference
^{26}Mg$(t,p)^{28}$Mg	Observations of 18 excited levels	[HIN61]
^{26}Mg$(t,p)^{28}$Mg	Observations of 11 excited levels; New I^π assignments of 9 excited levels by angular-distribution measurement of proton[a]	[MID64]
^{26}Mg$(t,p)^{28}$Mg	Observations of 8 excited levels including 2 new levels; I^π assignments of 8 excited levels including 2 new assignments by γ-ray angular-distribution measurement	[FIS73]
^{26}Mg$(t,p)^{28}$Mg	Observations of 13 excited levels including 2 new levels at 4.561 and 5.185 MeV; I^π assignments of 12 excited levels including 5 new and 1 revised assignments by angular correlation measurement between proton and γ-ray	[RAS74]
β decay of ^{28}Na	β-decay leading to 4 excited levels[b]	[DET79]
β decay of ^{28}Na	β-decay leading to 10 excited levels[c] including 1 revised $(0, 1, 2)^+$ assignment at 5.272-MeV level	[GUI84]

[a] The level at 5.169 MeV was tentatively assigned to be (3^-).
[b] β decay leading to the 4.878-MeV level was reported by measurement of the 3405-keV γ ray which depopulate this level with $I_\gamma < 0.8$.
[c] β decay leading to the 4.878-, 5.193-, 5.469-, 5.678-, and 5.702-MeV levels were reported with the β branches of $I_\beta < 0.48$, < 0.18, < 0.12, < 0.4, and < 0.6, respectively.

parity assignment has been only performed at the ground state to be $3/2^+$ [KOW08][1]. For other levels, the spin-parity assignments are only discussed based on the comparison with shell-model calculations as described below.

Fifield *et al.* firstly proposed the spin assignments of the ^{29}Mg levels with positive parity by comparing with the shell-model calculation in the *sd*-shell model space [FIF85] as shown in Fig. 2.2(e). It is to be noted that the 2 levels at 1.095 and 1.46 MeV are not reproduced by the calculation. Therefore, they proposed the $3/2^-$ and $7/2^-$ assignments for the 1.095- and 1.46-MeV levels, respectively, with the $\nu(2p_{3/2})$ and $\nu(1f_{7/2})$ configurations for respective levels[2]. Later, Woods *et al.* showed supporting results for these negative-parity assignments by the large cross sections to these levels observed in the ^{30}Si(^{13}C,^{14}O)^{29}Mg reaction, which are approximately equal to those for the population of the first $3/2^-$ and $7/2^-$ states in ^{27}Mg observed in the same mechanism experiment of ^{28}Si(^{13}C,^{14}O)^{27}Mg reaction [WOO88]. They also discussed the assignments of the 0.055 MeV: $1/2^+$, 1.395 MeV: $5/2^+$, and 3.201 MeV:

[1]This assignment is supported by the large β branches to the firmly assigned levels of $1/2^+$, $3/2^+$, and $5/2^+$ in ^{29}Al in the β-decay study of ^{29}Mg [GUI84].

[2]These spin-parity assignments were proposed by following reasons: (i) no prediction by shell-model calculation with *sd*-shell space, (ii) negligibly small β transitions to these levels by ^{29}Na β-decay study [GUI84], (iii) the observation of the strong γ transition of 1040 keV (1.095 $\rightarrow$ 0.055 MeV), and (iv) large populations of these levels obtained largely same as the 3.53-MeV $(3/2^-)$ and 3.13-MeV $(7/2^-)$ levels in ^{31}Si, and the 3.56-MeV $(3/2^-)$ and 3.76-MeV $(7/2^-)$ levels in ^{27}Mg, respectively, by the same mechanism reaction experiments of (^{18}O,^{15}O).

Table 2.2: Overview of experimental observations for levels in ^{29}Mg.

Experiment	Observables	Reference
^{26}Mg(^{11}B,^{8}B)^{29}Mg	Observations of 4 excited levels	[SCO74]
^{13}C(^{18}O,2p)^{29}Mg	Observations of 4 excited levels	[PAN81]
β decay of ^{29}Na	β-decay leading to 6 excited levels	[GUI84]
^{26}Mg(^{18}O,^{15}O)^{29}Mg	Observations of 6 excited levels; I^{π} assignments by comparison with SM calculation with *sd* shell; Suggestions of $3/2^-$, $7/2^-$ at 1.095- and 1.431-MeV levels	[FIF85]
β-n decay of ^{30}Na	Observations of 5 excited levels in ^{29}Mg after neutron emission following the β decay of ^{30}Na	[BAU87]
^{30}Si(^{12}C,^{14}O)^{29}Mg	Observations of 5 excited levels; I^{π} assignments of 4 levels by comparison with SM calculation	[WOO88]
β decay of ^{29}Na	Observations of 10 excited levels	[BAU89]
Laser spectroscopy of ^{29}Na	$3/2^+$ assignment for the ground state of ^{29}Mg	[KOW08]
1n knockout from ^{30}Mg	Unplaced γ rays of 1.79(1), 2.23(1), and 3.41(1) MeV	[TER08]

$5/2^+$ based on the shell-model calculations.

Thus, the spin-parity assignments of excited states in ^{29}Mg have been only discussed by the theoretical calculations, and not firmly determined by the experimental facts.

2.3 Structure of ^{30}Mg

The level structure of ^{30}Mg has been investigated by means of β-decay of ^{30}Na [GUI84; BAU89; MAC05; SCW09], β-n decay of ^{31}Na [KLO93], 2 neutron removal from ^{32}Mg in proton inelastic scattering [TAK09], and fusion-evaporation reaction [DEA10], as listed in Table 2.2. The ^{30}Mg levels observed in these experiments are summarized in Fig. 2.2. The anomalous structures of ^{30}Mg levels have been becoming clear as described below.

The 2 experiments of ^{30}Na β decay [GUI84; BAU89] had shown the precise level scheme of ^{30}Mg for the first time. By the small $B(E2; 0^+_{\text{g.s.}} \rightarrow 2^+_1)$ value [295(26)e^{2}fm^4] measured in the Coulomb excitation experiment [PRI99], the ground state of ^{30}Mg has been concluded to be the "normal" configuration, and ^{30}Mg was regarded as the nucleus out of the island of inversion. The small spectroscopic strengths to the $3/2^-$ and $7/2^-$ states in ^{29}Mg in the neutron knockout experiment of ^{30}Mg support this result [TER08]. However, recent β-decay experiments have discovered the 2nd 0^+ state at quite anomalously low-lying 1.789 MeV in ^{30}Mg [MAC05; SCW09][3]. The large prolate deformation was proposed for this level, resulting

[3]The assignment of 0^+_2 at the 1.789-MeV level has been firstly proposed by the revised γ transitions of 1789 and 1820 keV; The two γ transitions of 1789 keV (1.789 MeV $\rightarrow$ g.s.) and 1820 keV (1.820 MeV $\rightarrow$ g.s.) [GUI84] were revised by the γ-γ coincidence study as, 1789 keV (5.091 $\rightarrow$ 3.303 MeV (new level)) and 1820 keV (3.303 $\rightarrow$ 1.482 MeV) [MAC05].

Table 2.3: Overview of experimental observations for levels in ^{30}Mg.

Experiment	Observables	Reference
β decay of ^{30}Na	Observations of 10 excited levels; unplaced γ ray of 4685 keV	[GUI84]
β decay of ^{30}Na	Observations of 11 excited levels	[BAU89]
β-n decay of ^{31}Na	Observations of 5 excited levels	[KLO93]
Coulomb excitation of ^{30}Mg	Small $B(E2; 0^+_{\text{g.s.}} \rightarrow 2^+_1)$ value of 295(26) e^{2}fm^4	[PRI99]
β decay of ^{30}Na	Suggestion of the excited 0^+ level at 1.789 MeV	[MAC05]
$1n$ knockout from ^{30}Mg	Normal and intruder configurations in g.s. and excited 0^+ level in ^{30}Mg by the small C^2S value to the ^{29}Mg negative-parity states	[TER08]
β decay of ^{30}Na	0^+ assignment at 1.789 MeV by $E0$ decay measurement	[SCW09]
$2n$ removal in ^{32}Mg(p,p')	4^+ assignment at 3.302-MeV level	[TAK09]
^{14}C(^{18}O,$2p$)^{30}Mg	Observations of 9 excited levels; I^π assignments of 6 excited levels including 4 new assignments	[DEA10]

in the coexistence of different shapes [SCW09]. Thus, ^{30}Mg has been revised as a "border" nucleus toward the island of inversion.

Not only that revision, very recently, many new levels were observed by the fusion-evaporation experiment of ^{14}C(^{18}O,$2p$)^{30}Mg including the new spin-parity assignments of 3.379 MeV: 4^+, 3.455 MeV: 4^+, 4.181 MeV: 5, and 2.541 MeV: 2^- or 3^- [DEA10]. These levels have not been understood by any theoretical predictions.

Furthermore, quite attracting predictions have been performed by the theoretical calculation of CHFB+LQRPA method; Large-amplitude collective dynamics of shape phase transition in the low-lying states of ^{30}Mg [HIN].

Thus, the structure of ^{30}Mg have been under hot discussion because many anomalous structures were observed and predicted.

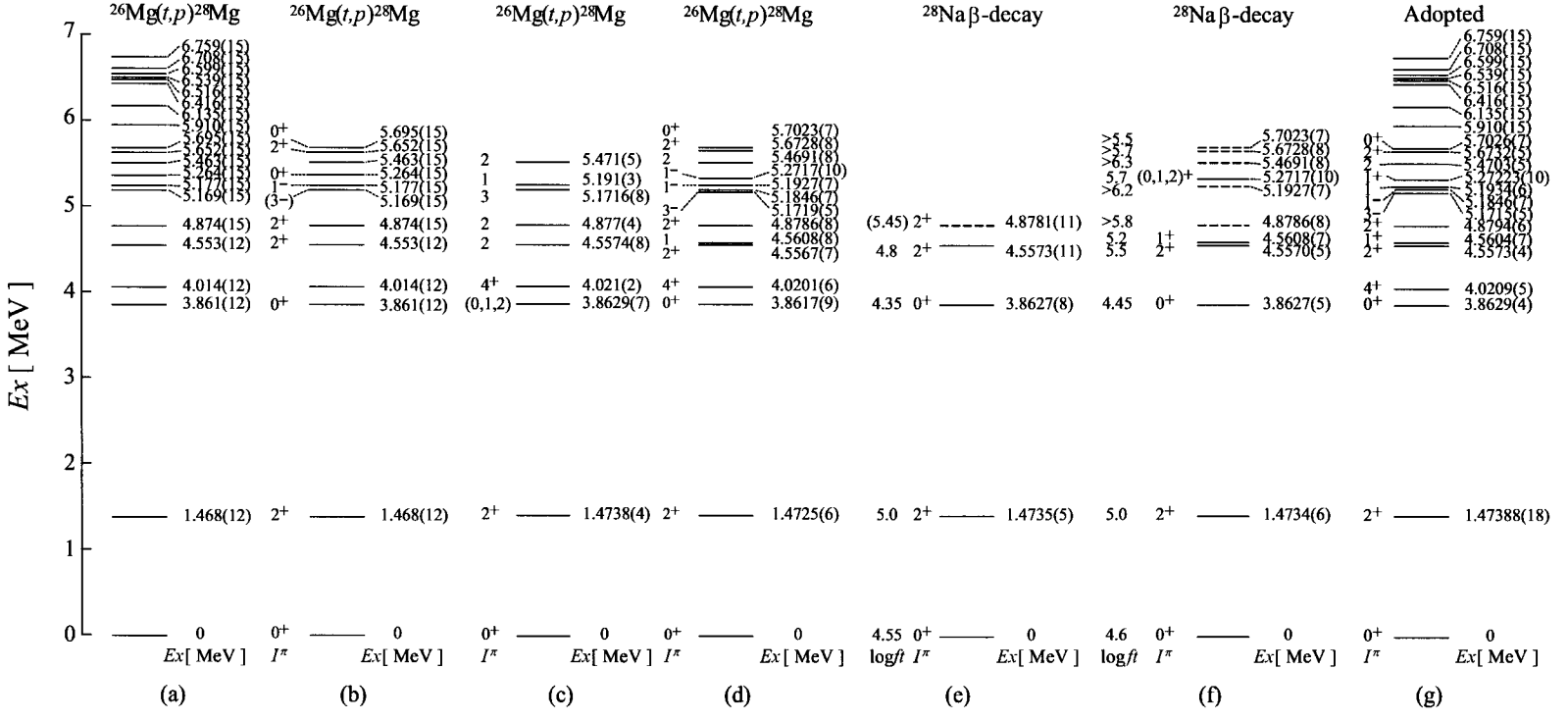

Figure 2.1: Compilation of the experimental levels in ^{28}Mg. The levels were observed in the experiments of (a): ^{26}Mg$(t,p)^{28}$Mg [HIN61], (b): ^{26}Mg$(t,p)^{28}$Mg [MID64], (c): ^{26}Mg$(t,p)^{28}$Mg [FIS73], (d): ^{26}Mg$(t,p)^{28}$Mg [RAS74], (e): β decay of ^{28}Na [DET79], (f): β decay of ^{28}Na [GUI84]. The levels in (g) is the compilation of all the experiments shown in Ref. [NND11]. The level energies in (b) and (f) are taken from Refs. [HIN61] and [RAS74], respectively. It is to be noted that the spin-parity assignments for the 5.272-MeV levels are inconsistent between the (b), (c), (d), and (f) (see text in detail). The levels denoted by dashed lines in (f) and (g) represent the ones which were reported in the corresponding references, but γ transitions populating and/or depopulating these levels were not observed. The 4.878-MeV level in (e) is also denoted by dashed line because the depopulating γ ray of 3405-keV was reported with $I_\gamma < 0.8$.

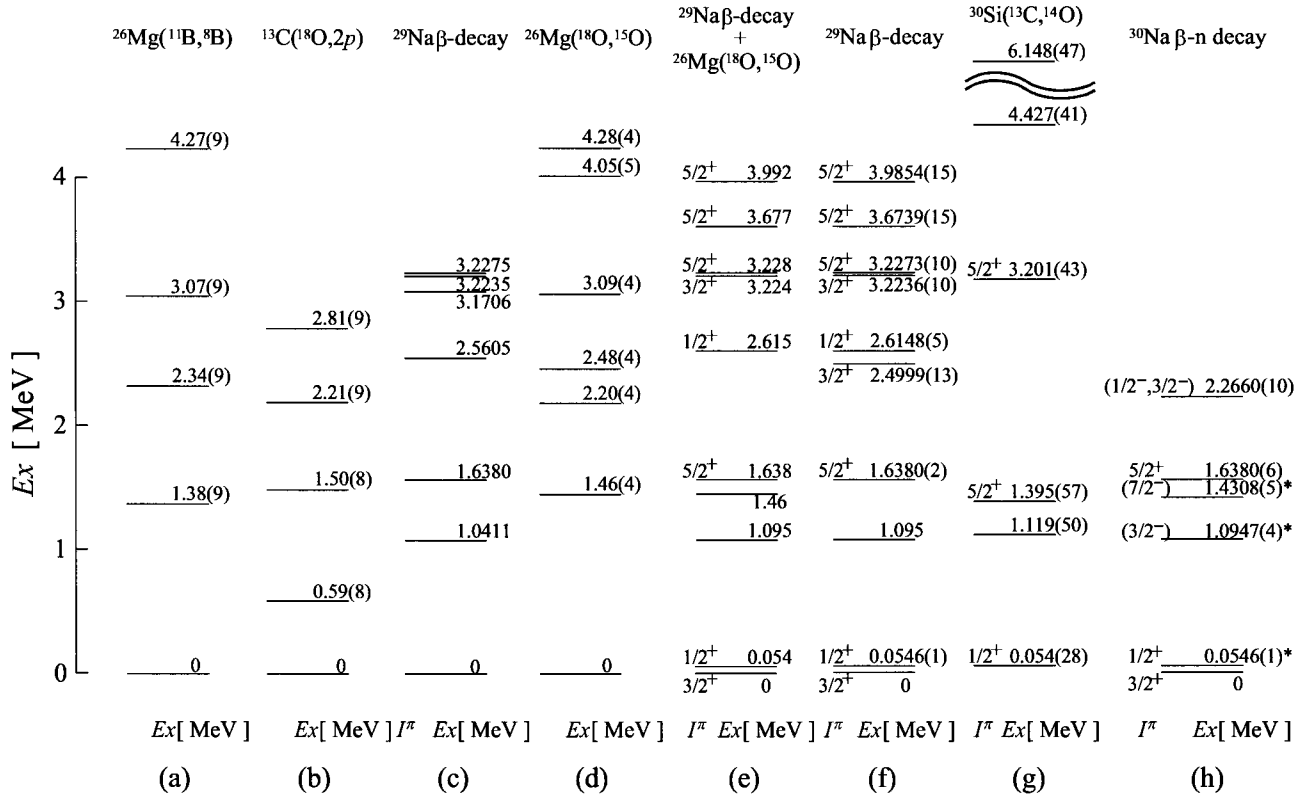

Figure 2.2: Compilation of the experimental levels in ^{29}Mg. The levels were observed in the experiments of (a): ^{26}Mg(^{11}B,^{8}B)^{29}Mg [SCO74], (b): ^{13}C(^{18}O,2p)^{29}Mg [PAN81], (c): β decay of ^{29}Na [GUI84], (d): ^{26}Mg(^{18}O,^{15}O)^{29}Mg [FIF85], (e): compilation of ^{26}Mg(^{18}O,^{15}O)^{29}Mg [FIF85] and β decay of ^{29}Na [GUI84], (f): β decay of ^{29}Na [BAU87], (g): ^{30}Si(^{13}C,^{14}O)^{29}Mg [WOO88], (h): β-n decay of ^{30}Na[BAU89].The spin-parity assignments in (e), (f), (g), and (h) were deduced by the comparison with shell-model calculations in the *sd*-shell model space.

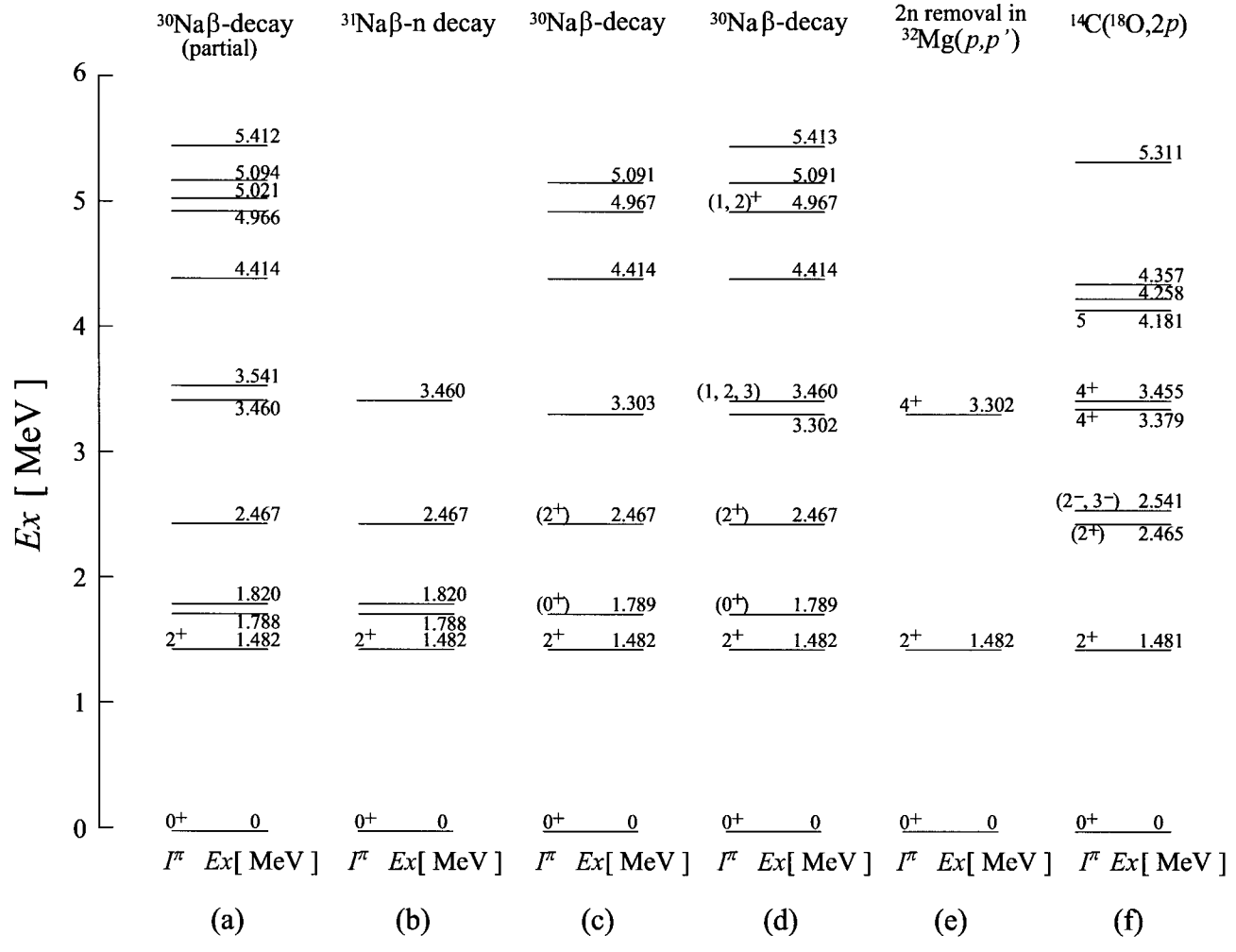

Figure 2.3: Compilation of the experimental levels in ^{30}Mg. The levels were observed in the experiments of (a): β decay of ^{30}Na [BAU89], (b): β-n decay of ^{31}Na [KLO93], (c): β decay of ^{30}Na [MAC05], (d): β decay of ^{30}N [SCW09], (e): 2 neutron removal in ^{32}Mg(p,p') [TAK09], (f): ^{14}C(^{18}O,2p)^{30}Mg [DEA10].

CHAPTER III

Principle of measurement

3.1 Spin-Parity assignment

The levels of Mg isotopes were populated by the β-decay of Na isotopes and the decay scheme was constructed by the β-γ and γ-γ coincidence measurement. We are using unique technique of using spin-polarized Na. The spins and parities of the Mg states were unambiguously assigned from the β-decay asymmetry as follows. The β-ray angular distribution from a polarized nucleus is given by

$$W(\theta) \simeq 1 + (v/c)AP\cos\theta, \tag{3.1}$$

for an allowed transition, where v, c, A, P, and θ are the velocity of the emitted electron, the light velocity, the asymmetry parameter of the β transition, polarization of the parent nucleus, and the β-ray emission angle with respect to polarization direction, respectively. In the case of a large Q_β value, the β-ray velocity v can be approximately regarded as $v/c \simeq 1$. The asymmetry parameter A takes three different values depending on possible final state spin I_f with a given initial state spin I_i, as

$$A = \begin{cases} -1 & (I_\mathrm{f} = I_\mathrm{i} - 1) \\ \dfrac{-1/(I_\mathrm{i}+1) - 2\tau\sqrt{I_\mathrm{i}/(I_\mathrm{i}+1)}}{1+\tau^2} & (I_\mathrm{f} = I_\mathrm{i}) \\ \dfrac{I_\mathrm{i}}{I_\mathrm{i}+1} & (I_\mathrm{f} = I_\mathrm{i}+1) \end{cases} \tag{3.2}$$

Table 3.1: Asymmetry parameters A of GT-transition for ^{28}Na, ^{29}Na, and ^{30}Na to possible spins in ^{28}Mg, ^{29}Mg, and ^{30}Mg, respectively.

Transition	I_i^π	I_f^π	A
$^{28}\mathrm{Na} \rightarrow {}^{28}\mathrm{Mg}$	1^+	0^+	-1.0
		1^+	-0.5
		2^+	$+0.5$
$^{29}\mathrm{Na} \rightarrow {}^{29}\mathrm{Mg}$	$3/2^+$	$1/2^+$	-1.0
		$3/2^+$	-0.4
		$5/2^+$	$+0.6$
$^{30}\mathrm{Na} \rightarrow {}^{30}\mathrm{Mg}$	2^+	1^+	-1.0
		2^+	-0.33
		3^+	$+0.67$

where τ is the ratio of Fermi (M_F) to Gamow-Teller (M_{GT}) matrix elements.

$$\tau = (C_V \mid M_F \mid)/(C_A \mid M_{GT} \mid). \tag{3.3}$$

In the case of neutron-rich nuclei ^{28}Na, ^{29}Na, and ^{30}Na, the β-decays to the levels below the neutron threshold are mostly due to the Gamow-Teller transition. Therefore, it is plausible to approximate $\tau \sim 0$ in Eq. (3.2) and the asymmetry parameters for the β-decay of ^{28}Na, ^{29}Na, and ^{30}Na are evaluated as listed in Table 3.1. The very discrete values enable us to firmly assign the spins and parities of the states in ^{28}Mg, ^{29}Mg, and ^{30}Mg.

3.2 Measurement of β asymmetry

The asymmetry parameters are evaluated from the β counts N_R^+ and N_L^+ in the same ($\theta = 0$) and opposite ($\theta = \pi$) directions with respect to polarization, respectively, as follows. The β counts are expressed as

$$N_R^+ = \epsilon_R N(1 + AP), \tag{3.4}$$

$$N_L^+ = \epsilon_L N(1 - AP), \tag{3.5}$$

where N is the number of disintegration, and ϵ_R and ϵ_L are the efficiency of the respective detectors (see Fig. 3.1). In order to cancel out spurious asymmetry due to difference in the

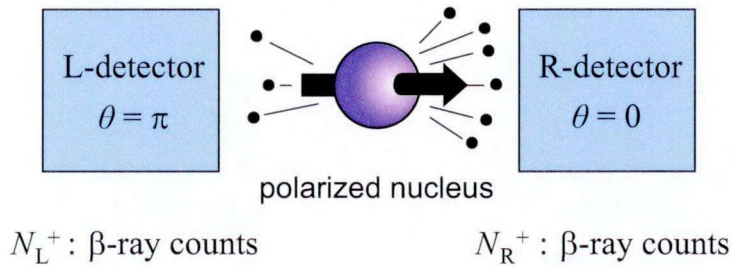

Figure 3.1: Schematic illustration of β-decay asymmetry measurement.

efficiency, the spin orientation is rotated by 180 degrees. Then the counts are expressed as

$$N_R^- = \epsilon_R N(1 - AP), \tag{3.6}$$

$$N_L^- = \epsilon_L N(1 + AP). \tag{3.7}$$

By taking a double ratio of the counts, the product of AP is deduced, freely from the efficiency, as

$$AP = \frac{\sqrt{R} - 1}{\sqrt{R} + 1} \left(R = \frac{N_R^+ / N_L^+}{N_R^- / N_L^-} \right). \tag{3.8}$$

The asymmetry parameter A can be obtained if the polarization P is known.

3.3 Beta- and β-delayed γ-ray spectroscopy

The β rays and β-delayed γ rays associated with the β decay of Na isotopes were measured by the β-γ, γ-γ, and β-γ-γ coincidence methods using multiple radioactive detectors. The decay scheme of Na isotopes can be established by finding new γ transitions and associated energy levels. By using β-γ coincidence method, the β ray which populates the specific level in Mg isotope are selected. As shown in Fig. 3.2, for example, β decays of β_1 and β_2 which populate the level "1" and "2", respectively, are selected by measuring γ_1, and γ_2 and γ_3, respectively. Then, the spin of each level in Mg can be assigned by measuring β-decay asymmetry (see Sec. 3.2). The spin and parity of level in Mg with small β branch can also be speculated by γ-transition intensities associated with the transition(s) from and/or to the spin-known level(s). Finally, the revised nuclear level structure of Mg isotopes can be obtained.

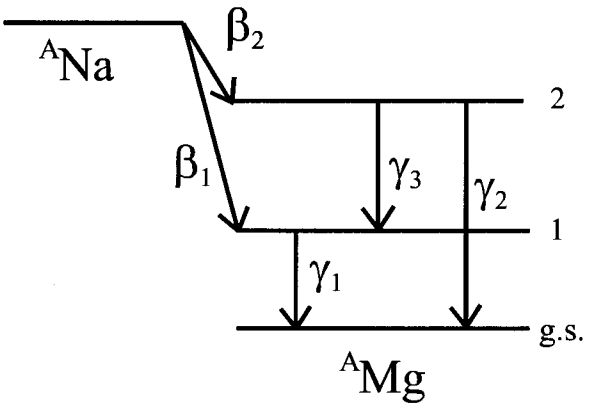

Figure 3.2: Schematic decay scheme of a neutron-rich Na isotope.

3.3.1 Gamma-ray intensities and β-decay branching ratios

Since the Q_β values of neutron-rich Na isotopes are very high compared with the neutron separation energy of daughter nucleus Mg isotopes, neutron emission takes place after the β decay of Na. To evaluate the population of Mg isotopes after the β decay of Na, the β decay of neutron-rich (Z, A) isotope, where Z and A represent the proton and mass number, respectively, are discussed below.

When direct β and β-n decays to the ground states of $(Z+1, A)$ and $(Z+1, A-1)$ are negligibly small as described in Fig. 3.3(a), the populations of $(Z+1, A)$ and $(Z+1, A-1)$ are deduced by intensities of γ transitions (I_γ) in both nuclei. Figure 3.4 shows the schematic decay scheme of a neutron-rich isotope when the direct β decay to the ground state in $(Z+1, A)$ is negligible. The sum of the β-decay intensities (I_β) to all the levels in $(Z+1, A)$ is calculated by using the γ-transition intensities as,

$$\begin{aligned} \Sigma I_\beta &= I_{\beta 1} + I_{\beta 2} + I_{\beta 3} \\ &= I_{\gamma 1} + I_{\gamma 2} + I_{\gamma 3} + I_{\gamma 4} + I_{\gamma 5} - I_{\gamma 3} + I_{\gamma 6} - I_{\gamma 2} - I_{\gamma 5} \\ &= I_{\gamma 1} + I_{\gamma 4} + I_{\gamma 6}. \end{aligned} \tag{3.9}$$

Note that this number can be obtained only by the sum of the γ-transition intensities which directly populate the ground state of $(Z+1, A)$. The population of $(Z+1, A-1)$ in the β-n decay of (Z, A) can also be calculated in the same way.

When the direct β-decay to the ground state of $(Z+1, A)$ nucleus are observed, the population of $(Z+1, A)$ nucleus cannot be calculated by its γ-ray intensities. In this case,

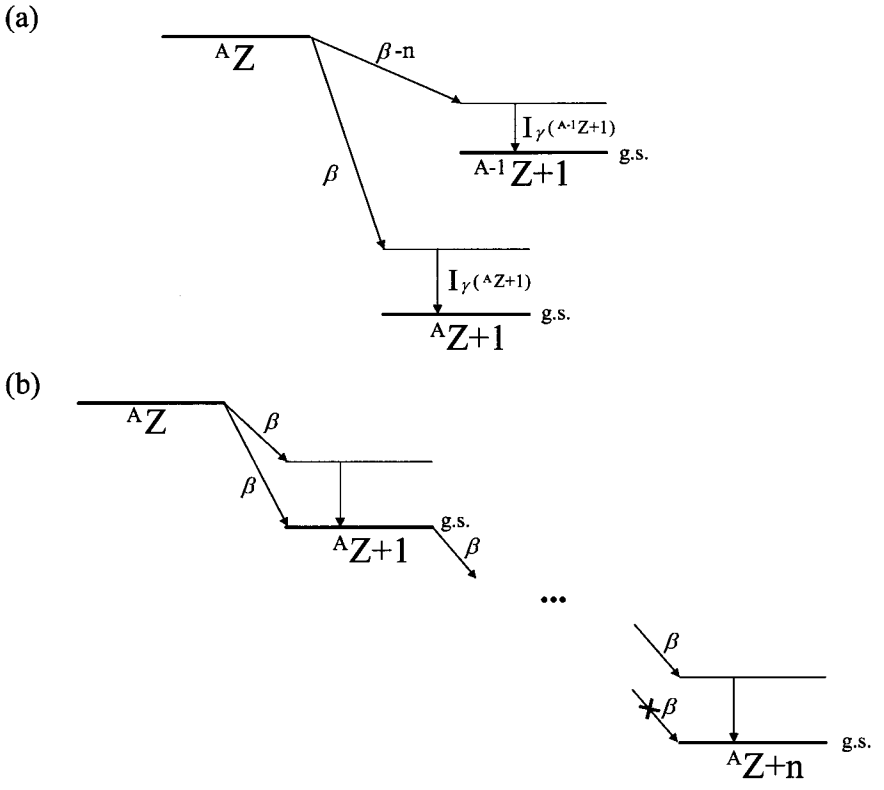

Figure 3.3: (a) Schematic β and β-n decay scheme of a neutron-rich (Z, A) isotope with the proton and mass number of Z and A, respectively. (b) Schematic β-decay chain of neutron-rich (Z, A) isotope.

the population of $(Z+1, A)$ nucleus can be obtained from the γ-transition intensities of $(Z+n-1, A)$ nucleus with the negligible direct β-decay population of the ground state as shown in Fig. 3.3(b). The same way can be applied to deduce the population of $(Z+1, A-1)$ nucleus when the direct β-n decay to the ground state of $(Z+1, A-1)$ are observed. Thus, the γ-ray and β-decay intensities of Mg isotopes are obtained.

3.3.2 Effect from the residual polarization of Na isotopes

Since the polarization of Na is very high, the γ-ray emissions in Mg have angular dependence on the emission angle to the polarization axis because of the residual polarization. Therefore, the angular distribution of γ transition depending on spin change of levels are estimated as follows. According to Morinaga and Yamazaki [MOR76], the angular distribution

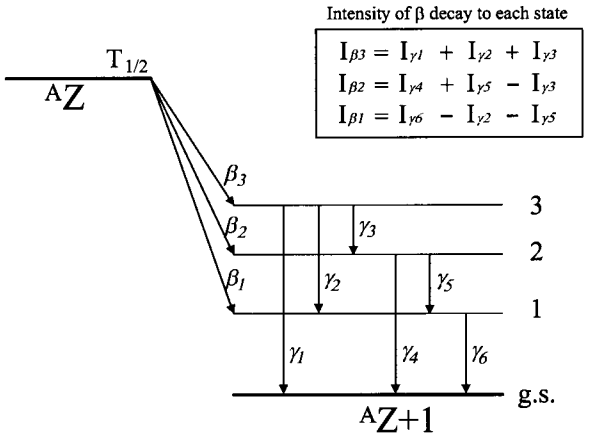

Figure 3.4: Schematic decay scheme of a neutron-rich (Z, A) isotope. The β-decay branching ratio to each level in $(Z+1, A)$ is calculated from the intensity valance of populating and depopulating γ rays as listed in the upper right.

of γ-ray emission is expressed as

$$\begin{aligned} W(\theta) &= \Sigma_k A_k \times P_k(\cos\theta) \\ &= \Sigma_k \rho_k(j_\mathrm{i}) F_k(j_\mathrm{i}\lambda j_\mathrm{f}) P_k(\cos\theta), \end{aligned} \tag{3.10}$$

where j_i, j_f, λ, θ, and P_k represent the spin of initial and final states, multiplicity of γ transition, angle of γ-ray emission from polarization axis, and Legendre polynomial, respectively. The $\rho_k(j_\mathrm{i})$ is called statistical tensor, expressed as

$$\rho_k(j_\mathrm{i}) = \sqrt{2j_\mathrm{i}+1} < j_\mathrm{i} m j_\mathrm{i} - m | k0 > P(m), \tag{3.11}$$

where $P(m)$ represents the probability of pure state. The value $F_k(j_\mathrm{i}\lambda j_\mathrm{f})$ are expressed by using Racah coefficient as

$$\begin{aligned} F_k(j_\mathrm{i}\lambda j_\mathrm{f}) &= (-1)^{1+j_\mathrm{i}-j_\mathrm{f}} \sqrt{2j+1} < \lambda 1 \lambda - 1 | k0 > \\ &\quad \times W(j_\mathrm{i} j_k \lambda\lambda; k j_\mathrm{f}). \end{aligned} \tag{3.12}$$

Assuming the pure transition, λ takes one value for each transition.

When the nucleus is 100% spin-polarized, Eq. (3.11) is expressed as

$$\rho_k(j_\mathrm{i}) = \sqrt{2j_\mathrm{i}+1} < j_\mathrm{i} j_\mathrm{i} j_\mathrm{i} - j_\mathrm{i} | k0 > \tag{3.13}$$

using $m = j_i$. Figure 3.5(a) and (b) show the angular distributions of γ transition as a function of γ-ray emission angle from the polarization axis in the case of integer spin and half-integer spin, respectively. In a practical case, the angular distribution is reduced because of small residual polarization and finite volume of the detectors. The anisotropy due to the angular distribution caused by residual polarization was estimated by using the most effected γ transition of 1482 keV [1.482 MeV(2^+) $\rightarrow$ g.s.(0^+)] in ^{28}Mg. It is found that the γ-ray counts measured by the detector placed at 0° to the polarization axis are 13% smaller than that measured by the detector placed at 90° in the present work (see details in Sec. 6.4).

3.3.3 Spin assignment of the practical case

The levels in Mg are identified by taking β-γ coincidence. The asymmetry parameter of a specific transition is determined simply from the β-γ counts, if no γ transition populates such final state as schematically shown by the level "2" in Fig. 3.2. However, in many cases the levels, such as level "1" in Fig. 3.2, are populated by γ transitions from higher levels. In this case, the asymmetry parameter determined from β-γ coincidence is affected by the asymmetry of β transitions to the higher levels, as

$$A_1^{\gamma} = A_2 \times \frac{I_{\gamma 3}}{I_{\gamma 1}} + A_1 \times \frac{I_{\beta_1}}{I_{\gamma 1}}, \tag{3.14}$$

where I_γ and I_β are intensities of γ- and β-rays, respectively. The asymmetry parameter A_1 can be deduced as

$$A_1 = A_1^{\gamma} \times \frac{I_{\gamma 1}}{I_{\beta_1}} - A_2 \times \frac{I_{\gamma 3}}{I_{\beta_1}}. \tag{3.15}$$

Accordingly, the spin-parity of the state "1" is assigned.

3.4 Effectiveness of using large polarization

The error of Eq. (3.8) is calculated as

$$\begin{aligned} \Delta(AP) &= \frac{\partial(AP)}{\partial R}\Delta R \\ &= \frac{\partial}{\partial R}\left(\frac{\sqrt{R}-1}{\sqrt{R}+1}\right)\Delta R \\ &= \frac{1}{\sqrt{R}(\sqrt{R}+1)^2}\Delta R. \end{aligned} \tag{3.16}$$

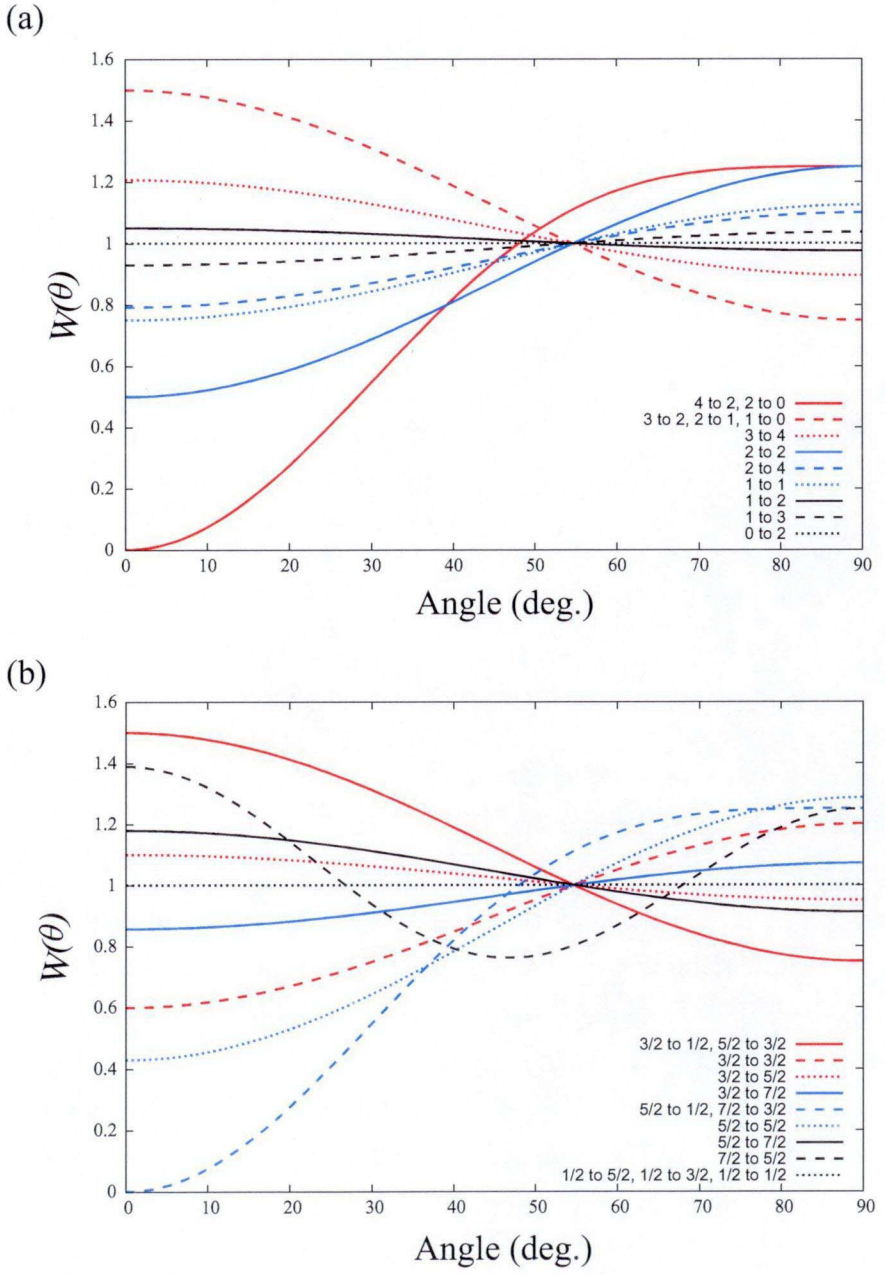

Figure 3.5: Angular distributions of γ transitions between (a) integer spin states and (b) half integer spin states emitted from spin-polarized nucleus as a function of γ-ray emission angle from polarization axis.

ΔR is calculated by error propagation as

$$\begin{aligned}\Delta R &= \left\{\left(\frac{\partial R}{\partial N_{R+}}\right)^2 \Delta N_{R+}^2 + \left(\frac{\partial R}{\partial N_{L+}}\right)^2 \Delta N_{L+}^2 + \left(\frac{\partial R}{\partial N_{R-}}\right)^2 \Delta N_{R-}^2 + \left(\frac{\partial R}{\partial N_{L-}}\right)^2 \Delta N_{L-}^2\right\}^{1/2} \\ &= R\left\{\frac{1}{N_{R+}} + \frac{1}{N_{R+}} + \frac{1}{N_{R+}} + \frac{1}{N_{R+}}\right\}^{1/2}. \end{aligned} \tag{3.17}$$

By assuming $N_{R+} = N_{L+} = N_{R-} = N_{L-} = N_{total}/4$ (N_{total} denotes total β-ray counts by two detectors for β-ray asymmetry measurement), Eq. (3.16) is calculated by using Eq. (3.17), as

$$\begin{aligned}\Delta(AP) &= \frac{1}{\sqrt{R}(\sqrt{R}+1)^2}\frac{4R}{\sqrt{N_{total}}} \\ &= \frac{4\sqrt{R}}{(\sqrt{R}+1)^2}\frac{1}{\sqrt{N_{total}}}. \end{aligned} \tag{3.18}$$

The relative error of AP can therefore be deduced by using $R = ((1-AP)/(1+AP))^2$, as

$$\left|\frac{\Delta(AP)}{AP}\right| = \left|\frac{1-(AP)^2}{AP}\right|\frac{1}{\sqrt{N_{total}}}. \tag{3.19}$$

It is understood that higher polarization is more important than statistics. This deduction is discussed quantitatively by showing the case of distinguishing $A = -1.0$ from $A = -0.33$ for ^{30}Mg as an example, as follows. Figure 3.6 shows Monte Carlo simulations for the distribution of asymmetry parameter A deduced from the β-ray counts measured by two detectors with finite volume placed along the polarization axis as shown in Fig. 3.1 assuming polarization $P = 0.05$ and 0.4 . In the case $P = 0.05$, A cannot be distinguished with the β-ray counts of 100 [Fig. 3.6(a)]. By counting 4×10^4 counts as shown in Fig. 3.6(b), $A = -1.0$ can be distinguished from $A = -0.33$ in good accuracy. Meanwhile, in the case of $P = 0.4$, $A = -1.0$ can be distinguished from $A = -0.33$ with good accuracy by measuring only 100 events as shown in Fig. 3.6(c). Thus, the effectiveness of large polarization can be understood.

In order to use highly spin-polarized Na isotopes, we are carrying out the experimental study at TRIUMF, Canada. This facility provides the world's largest polarized Alkali beam as described precisely in the next chapter. Table 3.2 shows the estimation of typical beam intensities of Na isotopes with 50% polarization using 40 μA proton beam and Ta target fragmentation reaction at TRIUMF.

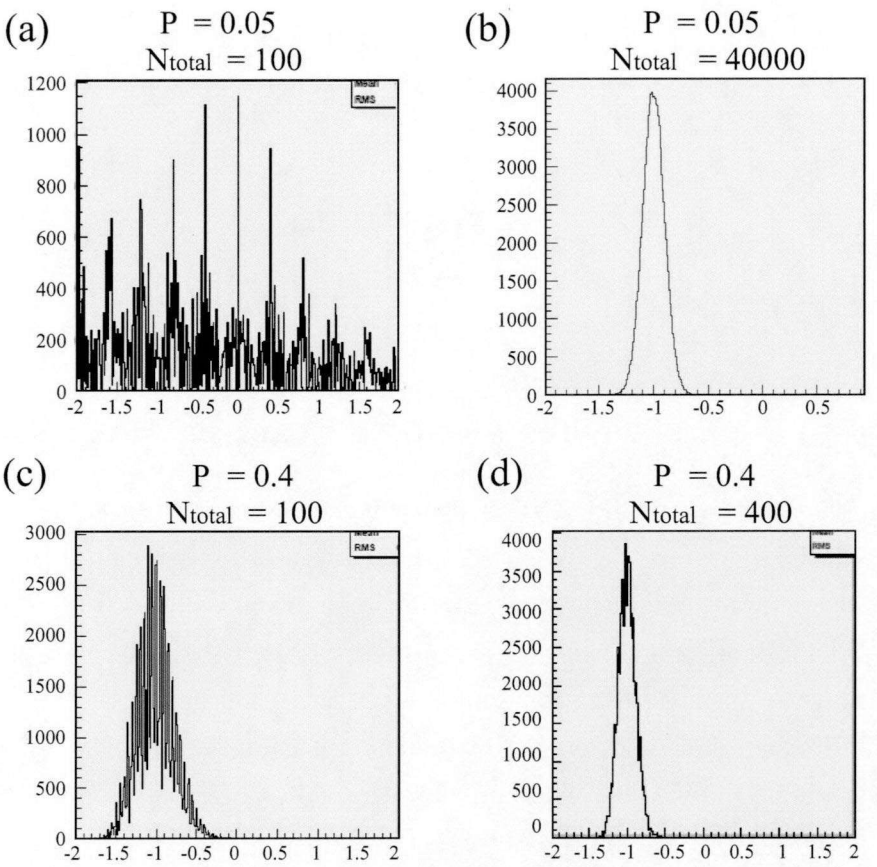

Figure 3.6: Simulation of yield with polarization P of 5 and 40 %.

Table 3.2: Estimation of the beam intensities of Na isotopes with 50% polarization obtained by 40 μA proton induced fragmentation reaction with Ta target at TRIUMF.

Beam	Intensity (pps)
^{28}Na	2×10^3
^{29}Na	5×10^2
^{30}Na	1×10^2
^{31}Na	15
^{32}Na	2

CHAPTER IV

Experiment

4.1 Production of neutron-rich Na beam at ISAC facility

Figure 4.1(a) shows the ISAC-1 facility which consists of target ion modules, a high resolution mass separator, and beam lines for variety of experiments. Unstable nuclei are produced by a target fragmentation reaction of a primary beam of proton at 500 MeV provided by TRIUMF cyclotron and a production target. A wide variety of isotopes are released from the surface ionization source heated to 2000 degree, and alkali are preferentially ionized because of their low ionization energy. Diffused isotopes are accelerated up to the energy of 12-60 keV. Then the ions pass through a high resolution mass spectrometer ($\Delta M/M = 10000$) so that only the isotope of interest are delivered to the experimental area. Particle identification is performed by measuring the lifetime at the YIELD station. The intensity of the radioactive beam is also measured at the YIELD station.

For the present study, unstable isotopes of ^{28}Na, ^{29}Na, and ^{30}Na are produced by target fragmentation reaction using 70 μA proton beam and stack of tantalum (Ta) target (21.8 g/cm^2 in total thickness). These isotopes are transported upstairs after the mass separator, and reach to the polarization beam line with kinetic energy of $\sim$30 keV. Afterward, these beams are spin-polarized as going through the polarizer shown in Fig. 4.2, as described precisely in the following section.

4.2 Production of spin-polarized Na beam

4.2.1 Procedure of producing spin-polarized Na beam

Spin-polarization of ^{28}Na, ^{29}Na, and ^{30}Na isotopes are produced by means of the collinear optical pumping technique [LEV04]. Figure 4.2(a) shows the schematic layout of the beam line of collinear optical pumping (polarizer). A detailed layout of the polarizer is shown in

(a)

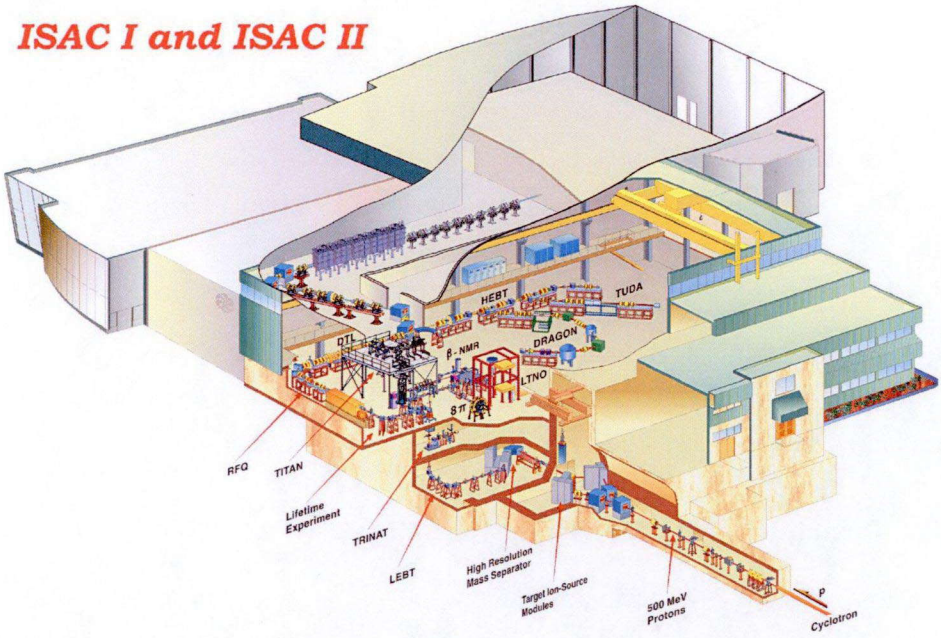

(b)

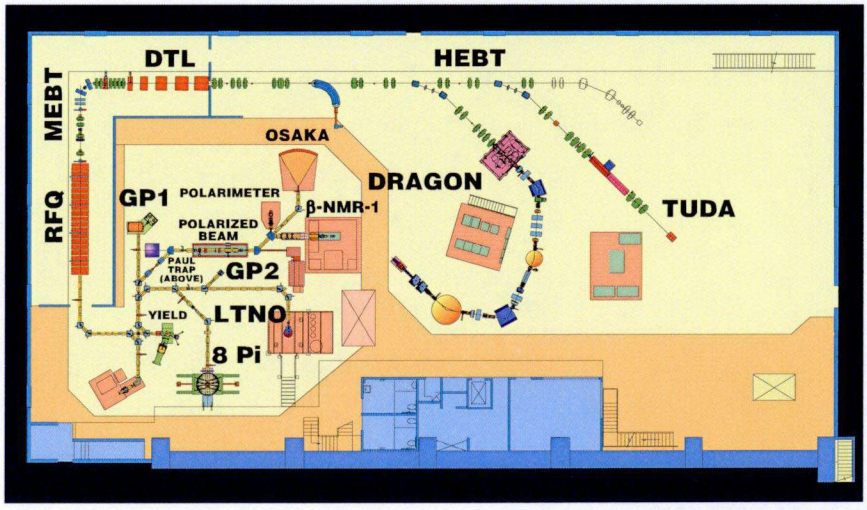

Figure 4.1: (a) Overview of the facility of ISAC experimental hall at TRIUMF. (b) Schematic layout of ISAC-1 experimental hall.

Fig. 4.2(b). The Na^+ ion beam with 30 keV was neutralized by receiving an electron in the cell filled with Na gas. The temperature of the Na cell was 480 °C. The neutralized atoms of ^{28}Na, ^{29}Na, and ^{30}Na were optically pumped by a collinear circularly polarized laser beam tuned to the respective D_1 transition. A 10 Gauss magnetic field parallel to the beam line was applied to the optical pumping region by six Helmholtz coils to define the polarization axis. The precise mechanism of spin-polarization is described in the next subsection. Spin-polarized Na beam is re-ionized by transferring an electron in a helium gas cell which was cooled to 12 K by a cryogenerator, and delivered to the OSAKA beam line where the polarization direction was perpendicular to the beam direction as shown in Fig. 4.2(c). In order to avoid spin relaxation of Na atom during beam transportation, electric field was applied for changing the direction of Na beam. We can avoid the influence from laser system because the detector setups are away from the polarizer and laser system.

4.2.2 Principle of Optical Pumping

Figure 4.3 shows the principle of optical pumping. The total angular momentum of nucleus and atom $\vec{F}$ is described as the sum of the angular momenta of electron ($\vec{J}$) and nucleus ($\vec{I}$). As the electronic angular momentum J is 1/2 for the $^2S_{1/2}$ ground state and for the $^2P_{1/2}$ first excited state, the angular momentum F for every ^{28}Na, ^{29}Na, and ^{30}Na takes 2 different values as shown in Fig. 4.3(a), (b) and (c), as a possible results of the summation of $\vec{F} = \vec{J} + \vec{I}$ depending on the angular momenta of the ground states of these isotopes. For every state of F, there are $2F + 1$ possibilities as characterized by the magnetic quantum number m_F, by Zeeman splitting in the weak magnetic field of $\vec{B}_0 = 10$ Gauss as shown in Fig. 4.3(a), (b) and (c).

The hyperfine energy levels of ^{28}Na, ^{29}Na, and ^{30}Na, generated by electromagnetic multipole interactions of the nucleus with surrounding electrons were calculated by using the hyperfine structure Hamiltonian for the $^2S_{1/2}$ and $^2P_{1/2}$ states as

$$W_F = \frac{(A\vec{I}\cdot\vec{J})}{\hbar^2} + hB\frac{\frac{3}{2}K(K+1) - 2I(I+1)J(J+1)}{2I(2I-1)2J(2J-1)}, \tag{4.1}$$

where $K = F(F+1) - I(I+1) - J(J+1)$. A is magnetic dipole hyperfine coupling constant expressed as

$$A = \frac{g_I\mu_N B_J}{\sqrt{J(J+1)}} = \frac{\mu_I}{I}\frac{B_J}{\sqrt{J(J+1)}}, \tag{4.2}$$

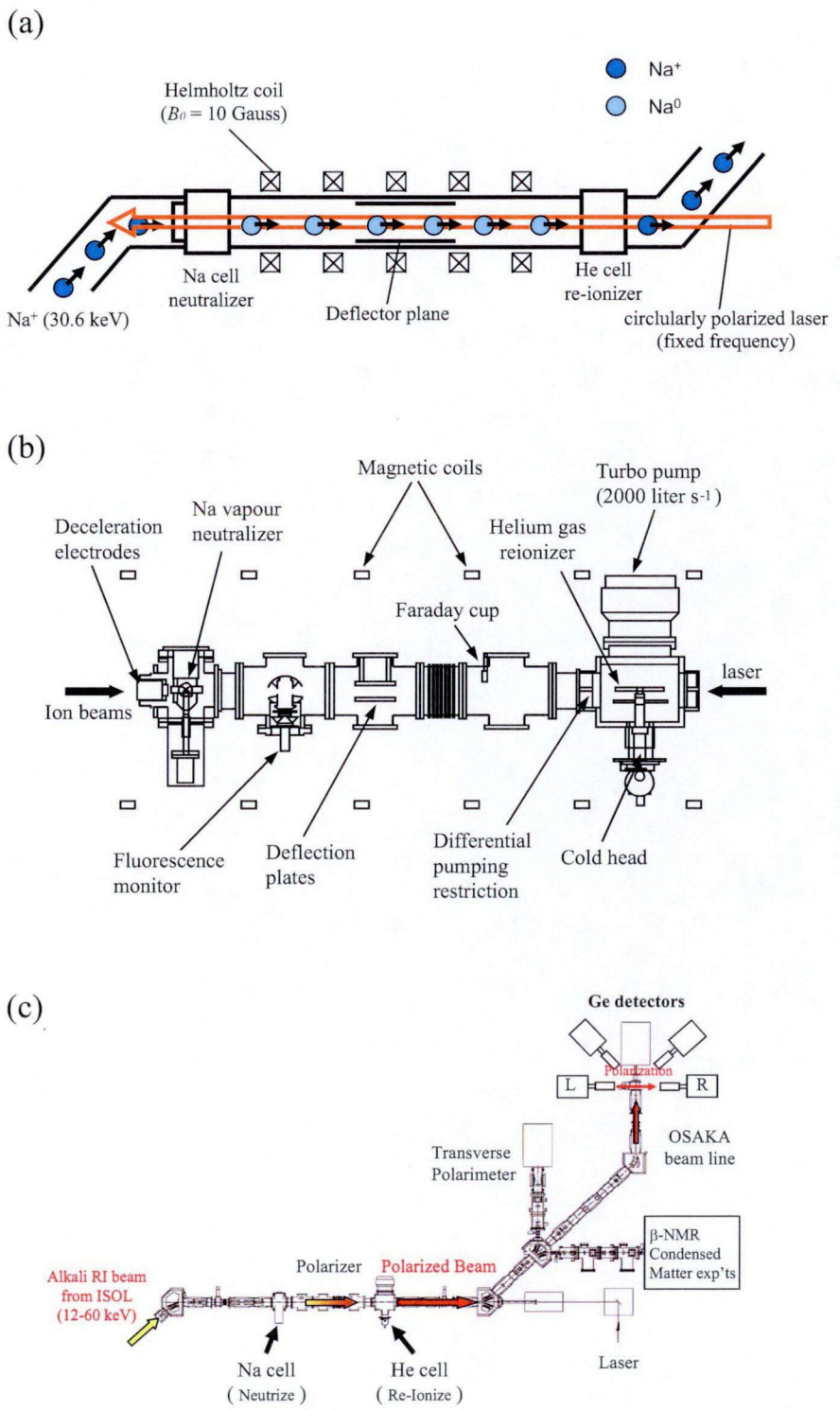

Figure 4.2: (a) Schematic layout of the polarizer at ISAC-1 and transportation of Na beam. (b) Detailed layout of the polarizer. (c) Transportation of spin-polarized Na beams.

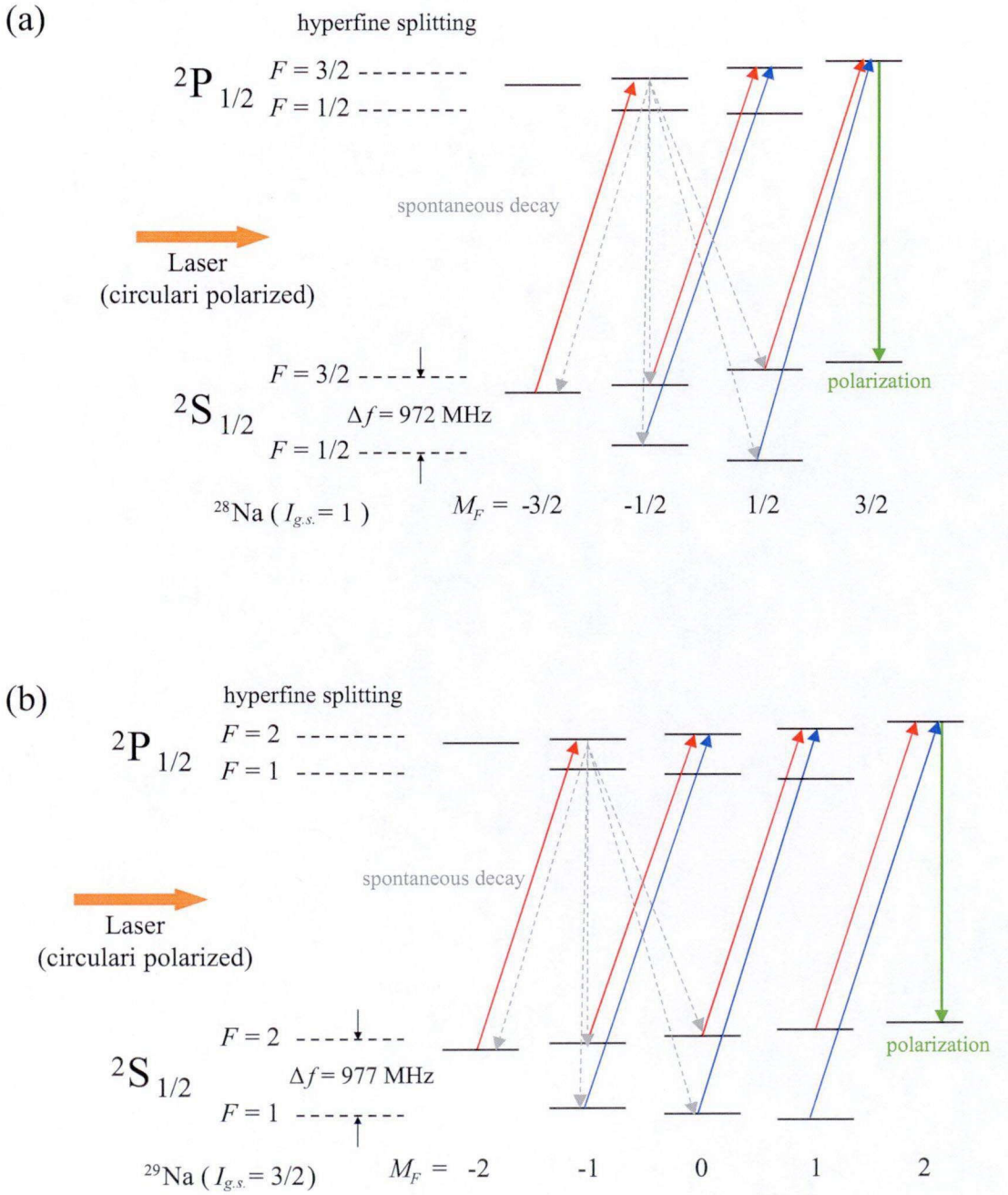

Figure 4.3: (a)(b)(c) Principle of optical pumping using circularly polarized laser. The hyperfine levels of ^{28,29,30}Na and optical transitions induced by σ^+ laser absorption (solid lines) and in spontaneous decay (dotted lines). (d) Spectrum of the laser light split into three different frequencies by electro optical modulator (EOM).

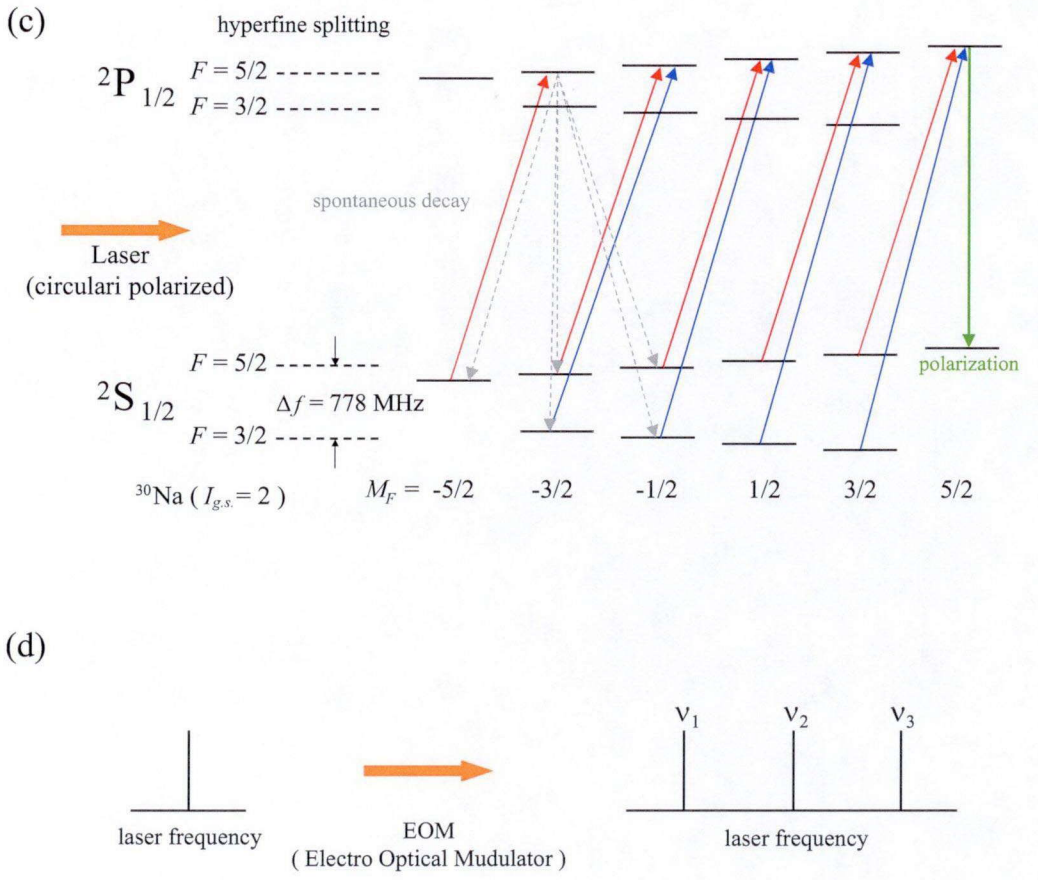

Figure 4.3: *Continued.*

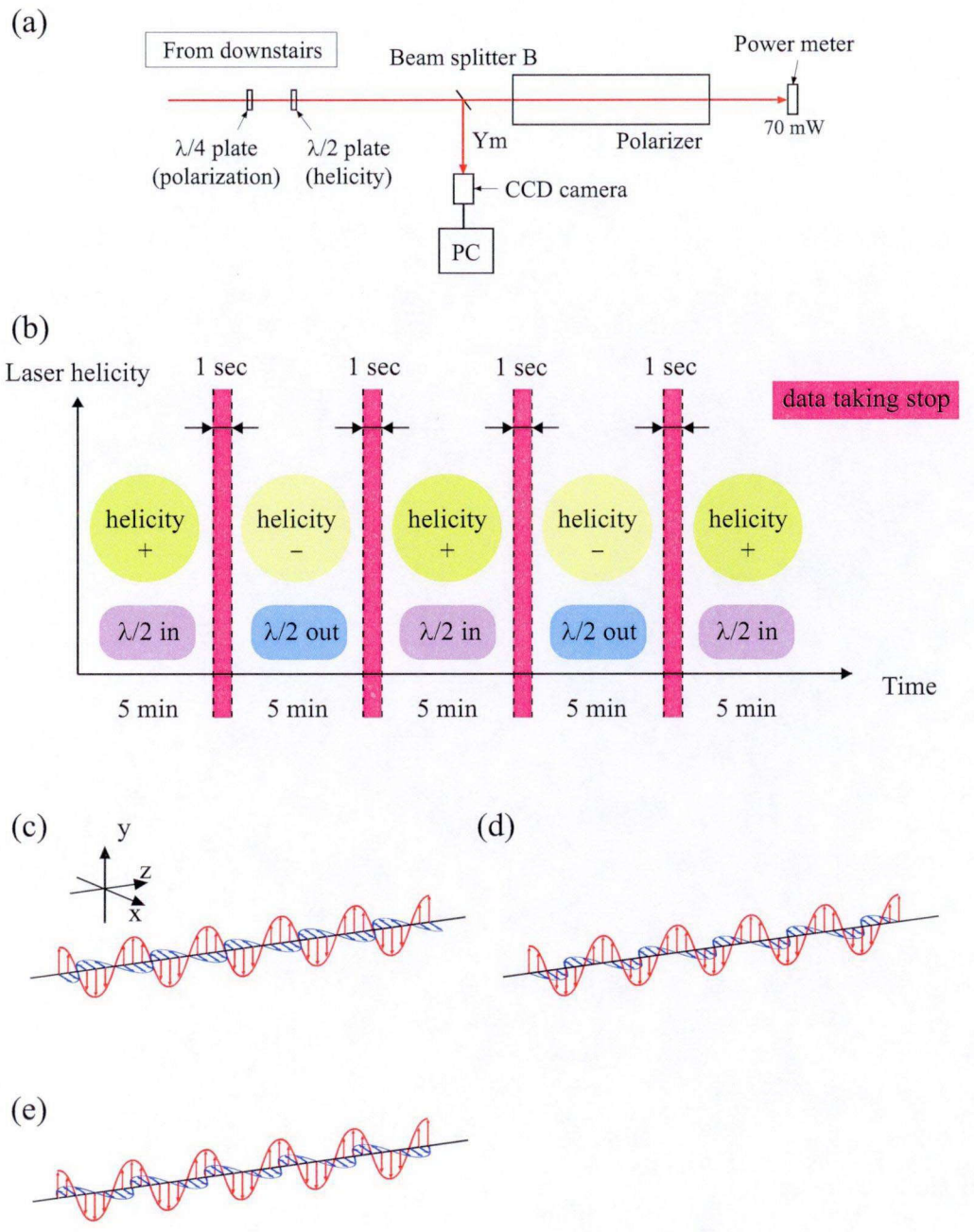

Figure 4.4: (a) Schematic view of laser system in the floor of ISAC-1 experimental hall. The laser transported from downstairs is circularly polarized by inserting $\lambda/4$ plate. Helicity flip is achieved by inserting $\lambda/2$ plate in the laser. (b) Time chart of helicity flip and data taking in the case of ^{28}Na beam. The periods for helicity flip are 30 and 100 s for ^{29}Na and ^{30}Na beams, respectively. (c) Linearly polarized laser. (d) and (e) shows circularly polarized lasers of right-handed (σ^+) and left-handed (σ^-), respectively.

with g_I, μ_N, and B_J being nuclear g-factor, nuclear magneton, and the magnetic field strength produced by the electrons at the nucleus, respectively. B is electric quadrupole hyperfine coupling constant expressed as

$$B = eQ_s\varphi_{jj}(0), \tag{4.3}$$

where Q_s and $\varphi_{jj}(0)$ are electric quadrupole moment of nucleus and the electric field gradient generated by the surrounding electrons at the position of nucleus. To deduce the energy distance ΔW_F between hyperfine levels in the ground $^2S_{1/2}$ state of $^{28-30}$Na, A and B values were speculated as follows. The B_J value, which cannot be measured directly in general, was speculated from $A_{2S_{1/2}}$ and g_I deduced from μ_N of well established ^{23}Na [HUB78] under the assumption of same magnetic field of B_J in all Na isotopes. Then, the magnetic dipole hyperfine coupling constant A of $^{28-30}$Na were obtained by using known spin and magnetic moment μ_I values. By using well established values of Q and $\varphi_{jj}(0)$ for ^{28,29}Na [KEI00], the electric quadrupole hyperfine coupling constant B can be obtained. In the case of ^{30}Na, although the Q and $\varphi_{jj}(0)$ values have not been measured, the B value can be speculated by assuming the same electric field gradient at nucleus position. Consequently, the distances between the hyperfine levels of the $^2S_{1/2}$ ground states in ^{28}Na, ^{29}Na, and ^{30}Na were calculated to be $\Delta E_{2S1/2}$ = 972, 977, and 778 MHz, respectively [see Fig. 4.3(a), (b) and (c)].

In a weak magnetic field of B_0, additional splitting by Zeeman effect is caused as

$$\Delta W = -\vec{\mu}_F \cdot \vec{B}_0. \tag{4.4}$$

The magnetic moment $\vec{\mu}_F$ is expressed as

$$\vec{\mu}_F = \frac{g_F \mu_B \vec{F}}{\hbar}, \tag{4.5}$$

with

$$g_F = g_J \frac{F(F+1) + J(J+1) - I(I+1)}{2F(F+1)} \tag{4.6}$$

$$+ g_I \frac{\mu_N}{\mu_B} \frac{F(F+1) + I(I+1) - J(J+1)}{2F(F+1)}, \tag{4.7}$$

where g_J, μ_B, and μ_N are electron g-factor, Bohr magneton, and nuclear magneton, respec-

tively. The electron g-factor g_J is expressed by Lande's equation, as

$$g_J = g_L \frac{J(J+1) + L(L+1) - S(S+1)}{2J(J+1)} \tag{4.8}$$

$$+ g_S \frac{J(J+1) + S(S+1) - L(L+1)}{2J(J+1)}, \tag{4.9}$$

where L is electron orbital angular momentum and S is electron spin. The electron g-factor g_L and g_S are -1 and -2.0023193134, respectively.

The polarizations of $^{28-30}$Na are achieved as follows. The exciting laser light is a σ^+ circularly polarized one and is split into three lines with equally spaced frequencies by electro optic modulator (EOM) as shown in Fig. 4.3(d). The difference of frequency between ν_1 and ν_2 (and also ν_2 and ν_3) corresponds to the energy splitting between the $^2S_{1/2}$ ($F = 1/2$ for ^{28}Na; $F = 1$ for ^{29}Na; $F = 3/2$ for ^{30}Na) and $^2S_{1/2}$ ($F = 3/2$ for ^{28}Na; $F = 2$ for ^{29}Na; $F = 5/2$ for ^{30}Na) levels. To excite both of the hyperfine levels of ground state $^2S_{1/2}$, the beams of the frequency ν_1 and ν_2 are tuned, for example in the case of ^{29}Na, to the $^2S_{1/2}$ ($F = 2$)-$^2P_{1/2}$ ($F = 2$) [the red line in Fig. 4.3(b)] and the $^2S_{1/2}$ ($F = 1$)-$^2P_{1/2}$ ($F = 2$) (the blue line) transitions, respectively. When the ^{29}Na atom in the $^2S_{1/2}$ ($|F, m_F\rangle = |2, -2\rangle$) state absorbs the light (red line), it is excited to the $^2P_{1/2}$ ($|F, m_F\rangle = |2, -1\rangle$) state, which then decays to the $^2P_{1/2}$ state either of $|F, m_F\rangle = |2, -2\rangle$, $|2, -1\rangle$, $|2, 0\rangle$, $|1, -1\rangle$, and $|1, 0\rangle$ (gray dotted line) according to the selection rule $\Delta F = 0, \pm 1$ and $\Delta m_F = 0, \pm 1$. Since the absorption always imparts $\Delta m_F = +1$ to the ^{29}Na atom, all the $^2S_{1/2}$ atoms will be moved to the $|F, m_F\rangle = |2, 2\rangle$ state. On the contrary, when the exciting laser is σ^- circularly polarized, the absorption of the σ^- light always imparts $\Delta m_F = -1$ to the ^{29}Na atom to move all the $^2S_{1/2}$ ($|F, m_F\rangle = |2, -2\rangle$) state. Thus, the spin orientation is rotated by 180 degrees by flipping the laser helicity. This is made by inserting $\lambda/2$ plate in the laser system as shown in Fig. 4.4(a). The polarization direction of Na beam is converted at the same interval of time for every Na beam, as shown in Fig. 4.4(b). Consequently, the polarized atoms of Na isotopes are produced, and nuclear polarization for Na isotopes is achieved.

The laser wave numbers were set to be fixed values of 16930.37, 16930.84, and 16932.45 for the ^{28}Na, ^{29}Na, and ^{30}Na beams, respectively, which correspond to the D_1 line energies.

4.2.3 Production of circularly polarized laser

The circularly polarized laser for the optical pumping was produced as follows. The COHERENT ring dye laser was split to three frequencies by EOM [see Fig. 4.3(d)] and linearly polarized as shown in Fig. 4.4(c). The right-handed σ^+ laser was produced by phase

shift of 90 degree [Fig. 4.4(c) to (d)] with a $\lambda/4$ (quarterwave) plate. Using additional $\lambda/2$ (halfwave) plate, left-handed σ^- laser was produced by phase shift of 180 degree from σ^+ laser (Fig. 4.4(d) to (e)).

4.3 Beam stopper and surrounding devices

Figure 4.5 and 4.6 show the experimental setups and surrounding devices around Pt stopper in the experiment performed in 2007 and 2010, respectively. The brief overview of the setup is outlined as follows. A Pt foil was placed at OSAKA beam line for stopping Na beam transported from polarizer. The foil is sustained by supporting instrument attached to the flange upstream. The foil is surrounded by FPR (fiber-reinforced plastic) vacuum chamber. A permanent magnet is placed around the stopper to apply magnetic field along the polarization direction to prevent the relaxation of Na polarization. The SmCo and Nd magnets were used for the experiments of 2007 and 2010, respectively. Germanium (Ge) detectors and plastic scintillators are placed around the stopper to detect the β and β-delayed γ rays emitted from β decay of neutron-rich Na isotopes in Pt stopper. These detectors are sustained by detector frame. Each devices are explained in detail in the following subsections.

4.3.1 FRP vacuum chamber and beam current monitor

A FRP (fiber-reinforced plastic) vacuum chamber in the shape of cylindrical cap was connected to the end of the OSAKA beam line. Figure 4.7(a) and (b) show the design and picture of the FRP chamber. The wall thickness of the chamber is 2 mm at the left side, and 1 mm at the right side (around Pt stopper) in Fig. 4.7(a). The 1 mm thickness was designed to minimize the attenuations and scatterings of the radiations and to withstand the atmospheric pressure.

Figure 4.7(c) shows the schematic illustration of beam current monitors around stopper position. The detailed parts and attachment of the beam current monitors are shown in Fig. 4.7(d) and (e), respectively. The beam is tuned to minimize the current at Cu baffle and maximize the current at Faraday cup.

4.3.2 Pt stopper

In the present experiment, one of the most important requirement for the stopper is preserving the nuclear polarization of Na inside the material for a period enough longer than the life times of ^{28}Na (τ = 30.5 ms), ^{29}Na (τ = 44.9 ms), and ^{30}Na (τ = 48.4 ms).

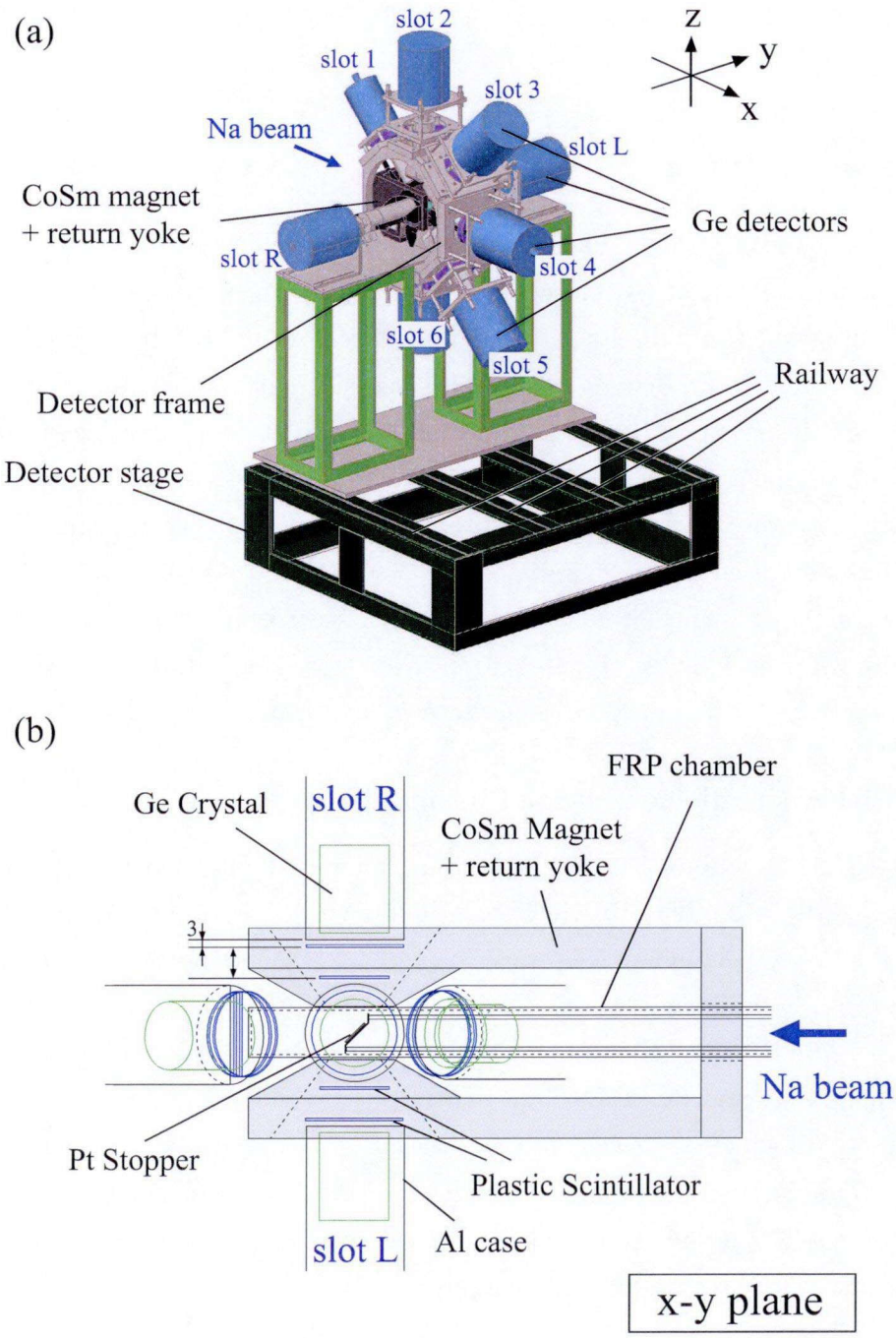

Figure 4.5: (a) Detector setups for the experiment of 2007. (b)(c)(d) The arrangement of the experimental devices around Pt stopper for the experiment of 2007 (not to scale).

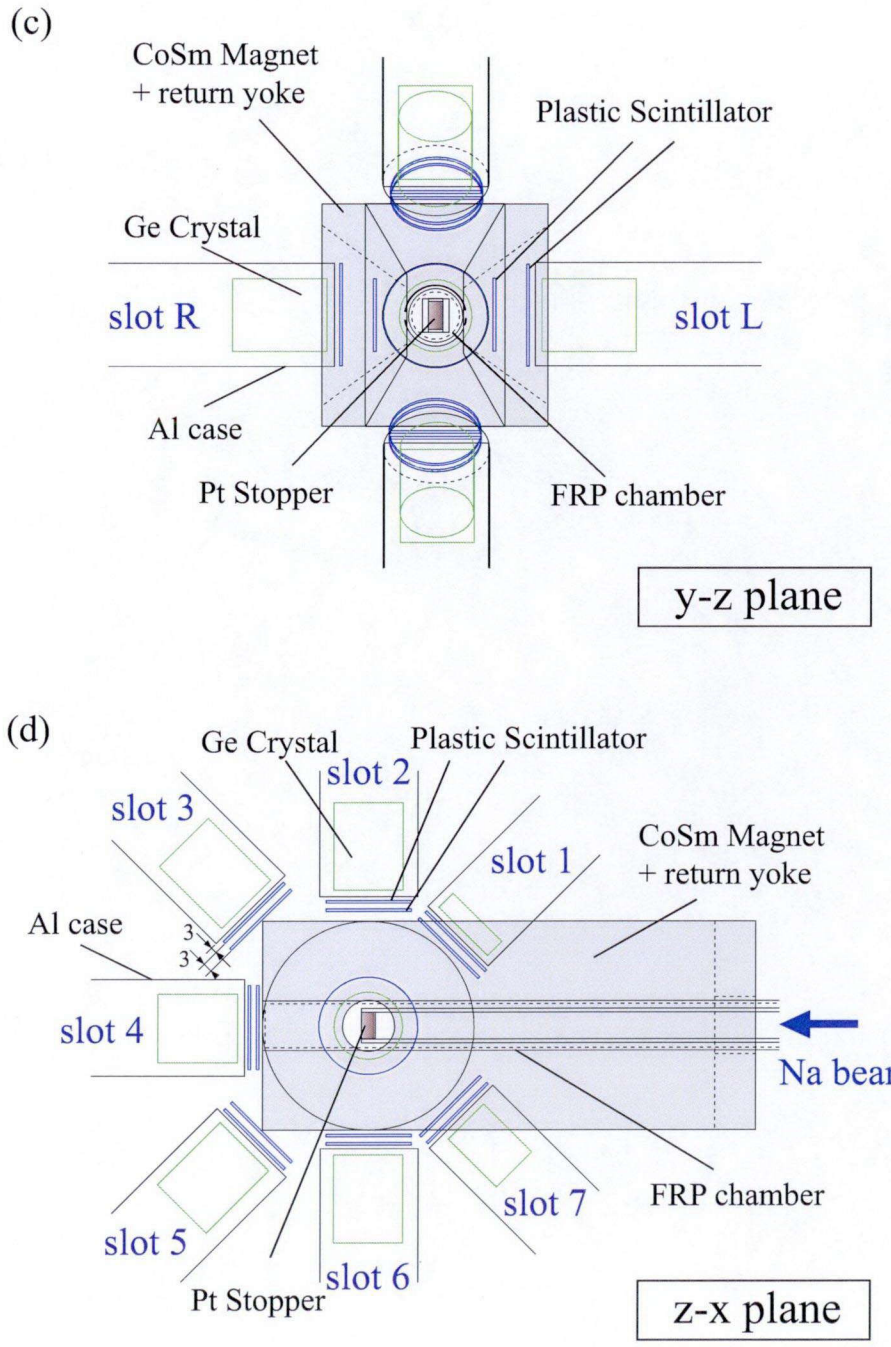

Figure 4.5: *Continued.*

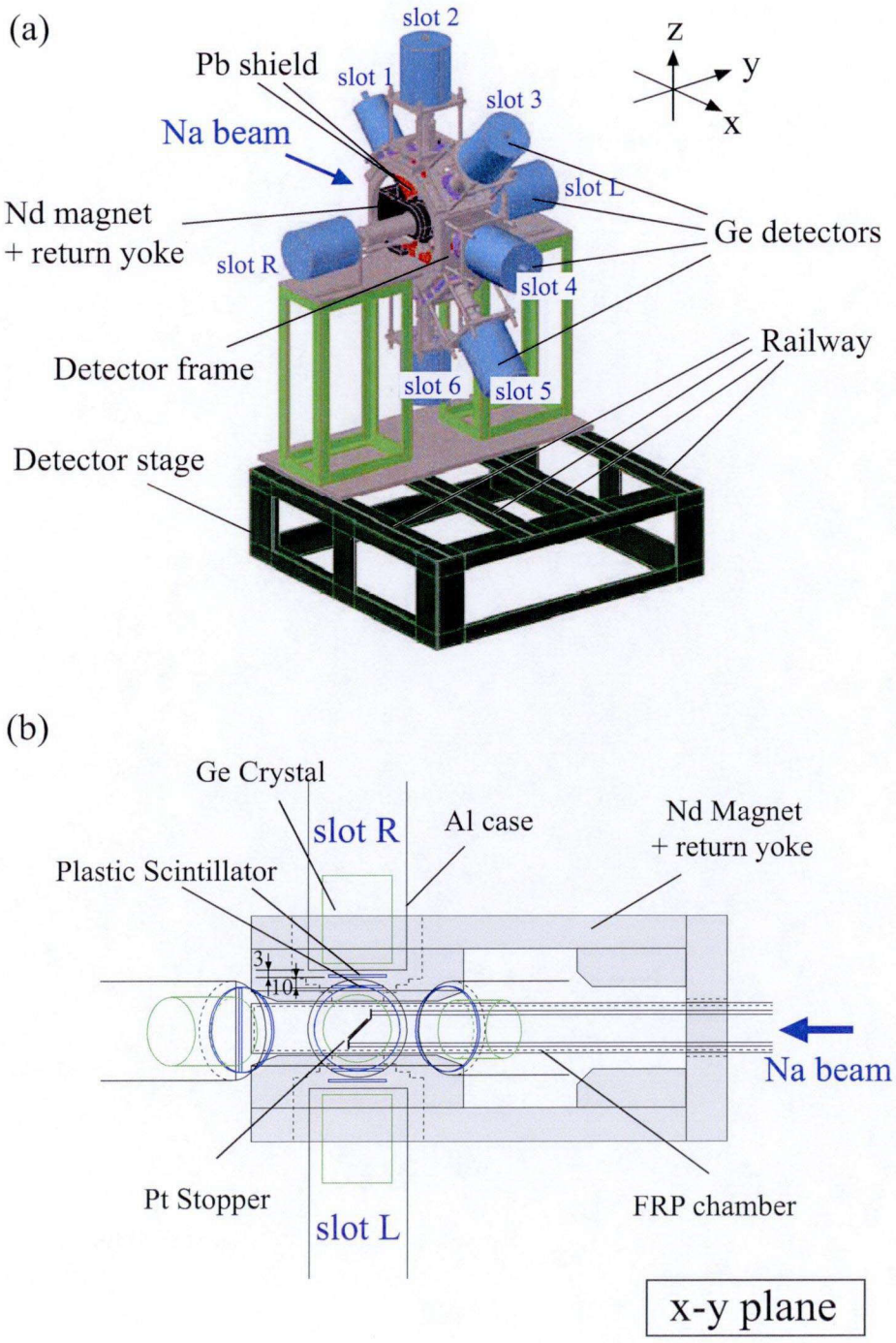

Figure 4.6: (a) Detector setups for the experiment of 2010. (b)(c)(d) The arrangement of the experimental devices around Pt stopper for the experiment of 2010 (not to scale).

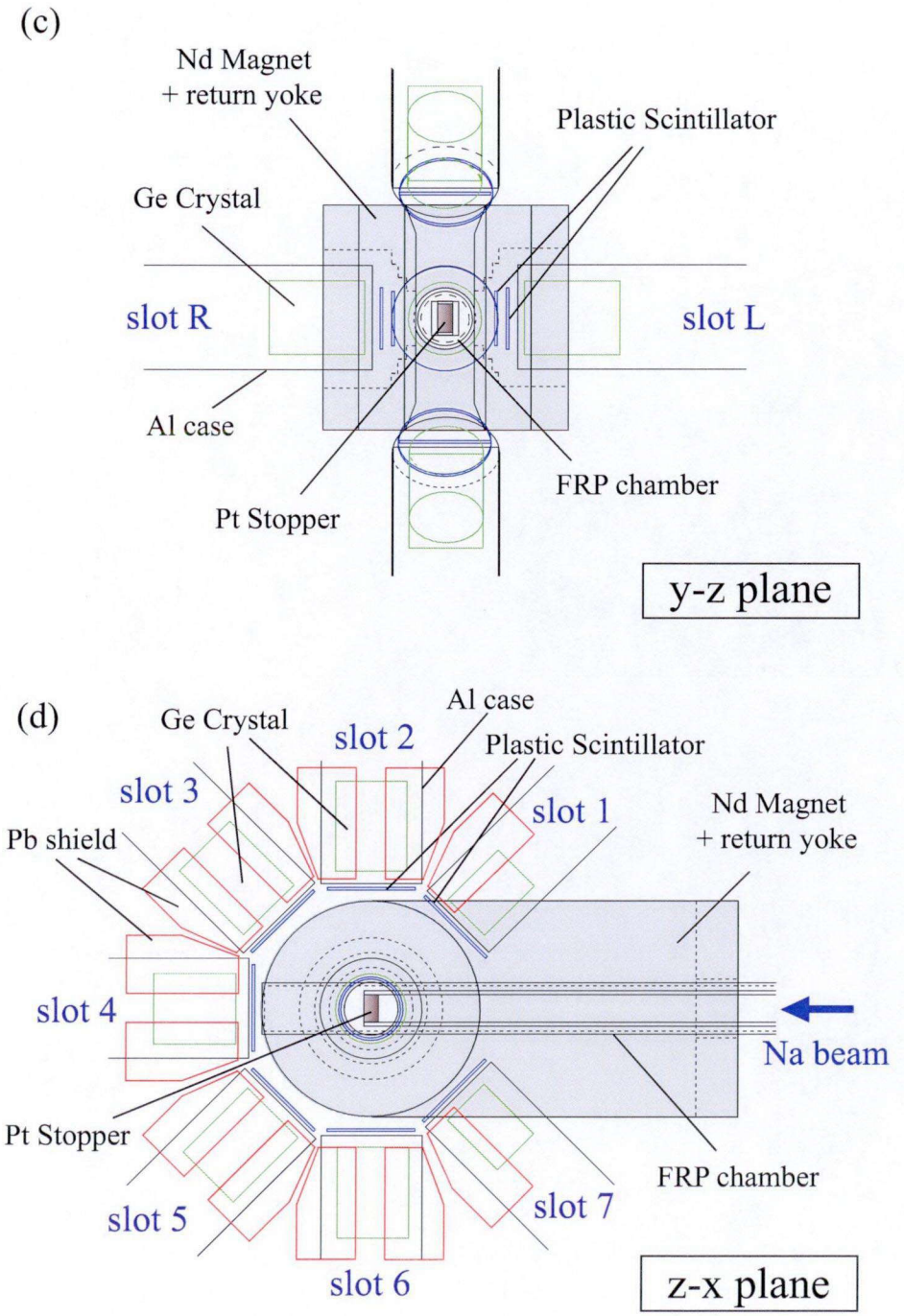

Figure 4.6: *Continued.*

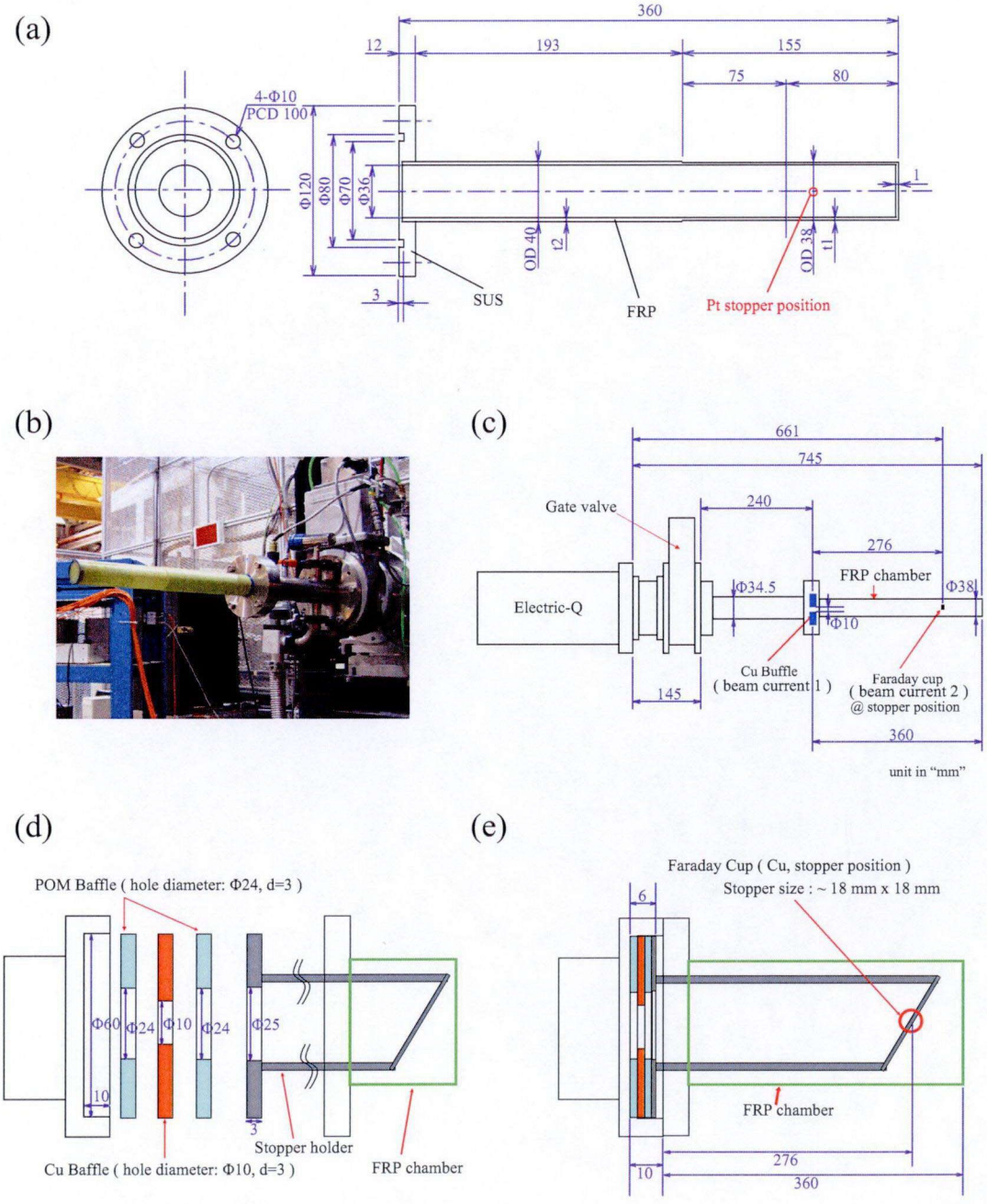

Figure 4.7: (a) Design of FRP (fiber-reinforced plastic) chamber used in the experiment of 2007 and 2010. The thickness of 1 mm at downstream side is thicker than upstream side (2 mm) to reduce energy loss of β ray. (b) Picture of FRP chamber. (c) Positions of beam current monitors (not to scale). (d)(e) Attachment of devices for beam current monitor to the beam line (not to scale). All the dimensions are given in mm.

Table 4.1: Estimation of the spin relaxation time T_1 of Na nuclei in Pt at room temperature ($T = 300$ K) by using Korringa's relation. The experimental values were obtained at the condition of room temperature and a magnetic field of $B = 5.25$ kGauss.

Nucleus	Relaxation time T_1 [s]	Half-life $T_{1/2}$[ms]
^{20}Na	22.0(19)[a]	447.9
^{27}Na	0.3, 0.78(8)[a]	301
^{28}Na	0.1	30.5
^{29}Na	0.3	44.9
^{30}Na	0.6	48.4
^{31}Na	0.3	17.0
^{32}Na	-	13.2

[a]Ref. [MIN04]

Pt foil meets this requirement, since the spin relaxation time (T_1) of Na isotopes at room temperature in Pt metal has been estimated to be long enough than these half-lives [MIN05]. The spin relaxation times at room temperature $T = 300$ K were estimated to be $T_1 = 0.1, 0.3$, and 0.6 s for ^{28}Na, ^{29}Na, and ^{30}Na, respectively, by using Korringa's relation [$T_1 \times T \propto (1/\gamma)^2$, $\gamma = \mu/Ih$], as listed in Table 4.1. Furthermore, Pt is non-magnetic material and the lattice is face-centered structure which guarantees the absence of electric field gradient at the normal sites of the atoms.

A Pt foil of 10 μm in thickness and 24 mm $\times$ 24 mm in area was placed to stop the spin-polarized Na beams. The foil was placed 45 degree to the beam axis to reduce energy loss of β ray in the foil emitted to the detectors for the measurement of β-ray asymmetry [see the cross section of x-y plane in Fig. 4.5(b) or 4.6(b)]. To satisfy this requirement, a holder for Pt stopper was made as shown in Fig. 4.8. Cupper plates to monitor beam current and a standard γ-ray source can also be attached at the stopper position as shown in Fig. 4.8(c) and (d).

The foil was annealed, in advance, for the purpose of removing the local stress in the foil and avoiding relaxation of Na polarization inside the foil caused by inhomogeneous magnetic field as derived from distortion or lack of lattice. The annealing procedure of Pt foil is outlined as follows. The foil was placed in vacuum at the center of an electric furnace and first pre-heated to 1400 °C for 2 hours. Then the temperature was lowered gradually to 1200 °C in 2 hours, kept constant for 7 hours, lowered gradually to 800 °C in 2 hours, again kept constant in 10 hours, and finally lowered to room temperature in 2 hours.

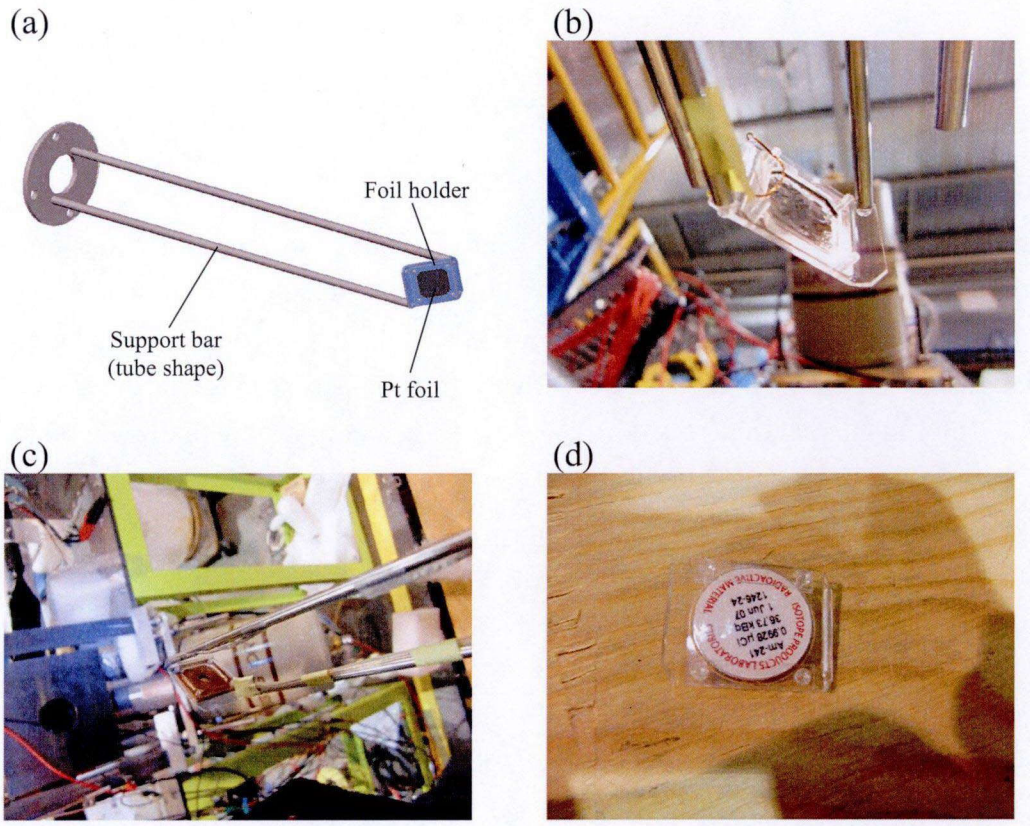

Figure 4.8: (a) Design of Pt stopper and stopper holder. Tube shape is used for he support bar to put conducting wire in. (b) Picture of Pt stopper. The charge of Na ions are carried and earthed through the conducting wire. (c) Picture of the beam current monitor attached to the stopper support. (d) Picture of standard source attached to the foil holder of stopper support.

4.3.3 Permanent magnet

In order to avoid the relaxation of Na spin polarization inside Pt foil, magnetic field along the Na polarization direction was applied by using permanent magnet. Figure 4.9(a) and 4.10(a) show the designs of SmCo and Nd permanent magnets used for the experiments of 2007 and 2010, respectively. To prevent the scattering of β rays to two detectors for β-decay asymmetry measurement, the shape of these magnets were designed with large holes of an opening angle of 90 degree along z-axis. To enforce the magnetic field at stopper position along z-axis, return yoke of stainless steel was attached to each magnet. The shape of magnet and return yoke was designed to minimize the distances between Pt stopper and radiation detectors. The hole of $\phi 50$ was created in the return yoke to pierce FRP chamber and set to the stopper position. To fulfill all the requirements, the shape of return yoke was simulated by using the code TOSCA in OPERA3D [TOS11]. The magnetic field along z-axis by the simulation and the actual SmCo magnet as a function of distance from $(x, y) = (0, 0)$ are shown in Fig. 4.11(a) and (b), respectively. Magnetic field of about 820 Gauss at stopper position was achieved in both cases. Fig. 4.11(c) shows the magnetic field along z-axis of Nd magnet as a function of distance from $(x, y) = (0, 0)$. About 6.5 times larger magnetic field at stopper position along z-axis (5300 Gauss) compared with SmCo was attained. The effect of this increased magnetic field will be discussed in Chapter 4. As shown in Fig. 4.9(c) and 4.9(c), these magnet can be installed to the Pt stopper position coupled with the detector setups by sliding on the rail of detector stage [see also Fig.4.5(a) or 4.6(a)].

4.3.4 Compton cross talk shield

Since γ rays are measured by nine Ge detectors placed in very close to Pt stopper, coincidence event derived from one γ ray are detected with high probability. This is Compton cross talk event; a γ ray is Compton-scattered in one Ge detector and all the residual energy of the γ ray is absorbed in another Ge detector. Therefore, the fake energy peak appears in the analysis of γ-γ coincidence. In the experiment of ^{28}Mg and ^{29}Mg carried out in 2007, many cross talk peaks are observed in γ-γ coincident analysis (see Sec. 7.1). In order to reduce the probability of Compton cross talk event, two lead shields were placed between adjacent Ge detectors in slot 1 to 7 as shown in Fig. 4.12 for the experiment of ^{30}Mg in 2010. As a result, Compton cross talk events were remarkably reduced.

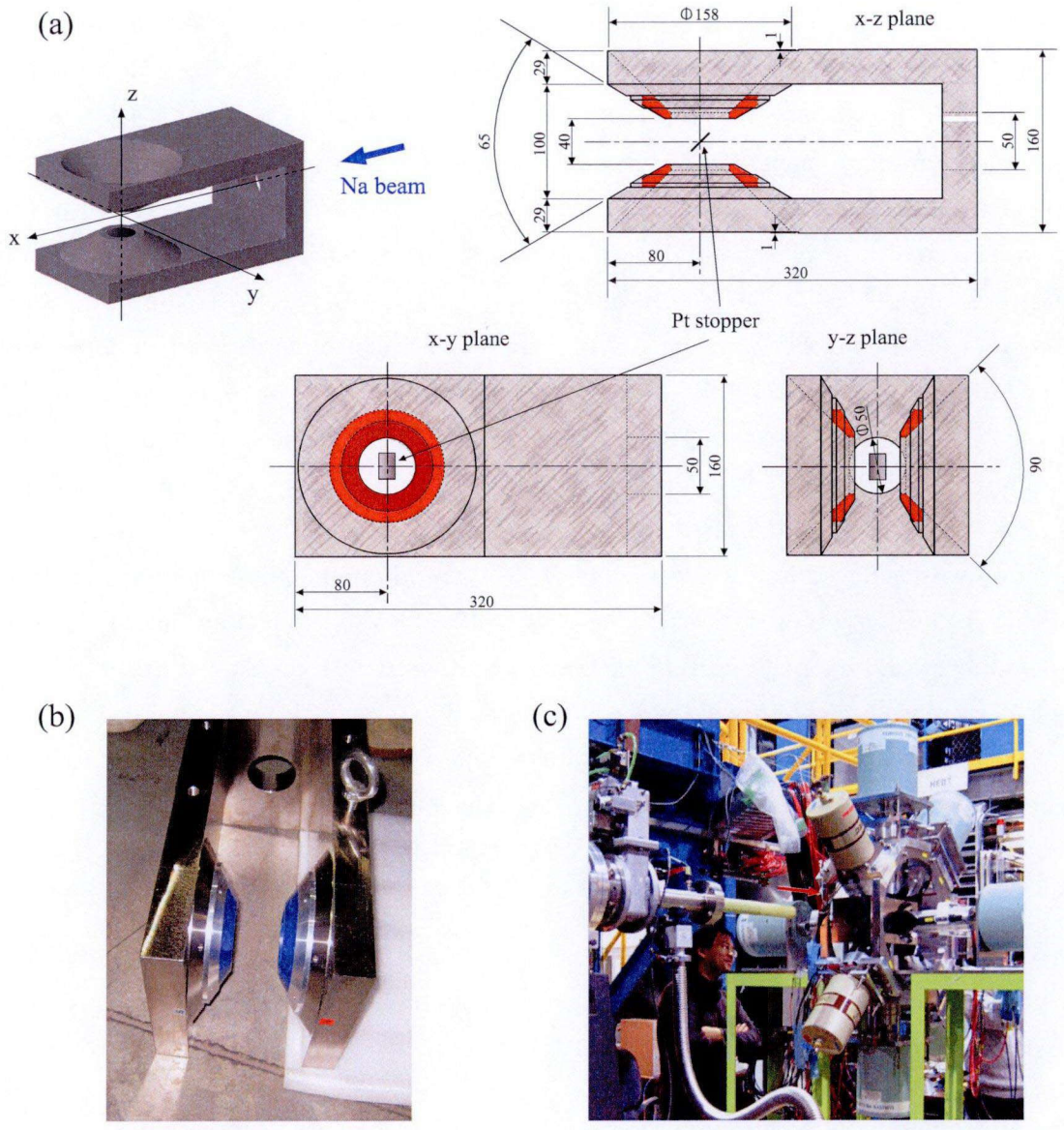

Figure 4.9: (a) Design of the permanent magnet of SmCo enforced by return yoke. The hole in the yoke is for the installment of FRP chamber into the magnet. All the dimensions are given in mm. (b) Picture of the SmCo magnet and return yoke. (c) Picture of the magnet installed to the detector setup. The detector setups with magnet is installed to the Pt stopper position by moving the upper frame of detector on a rail (see Fig.4.5 or 4.6).

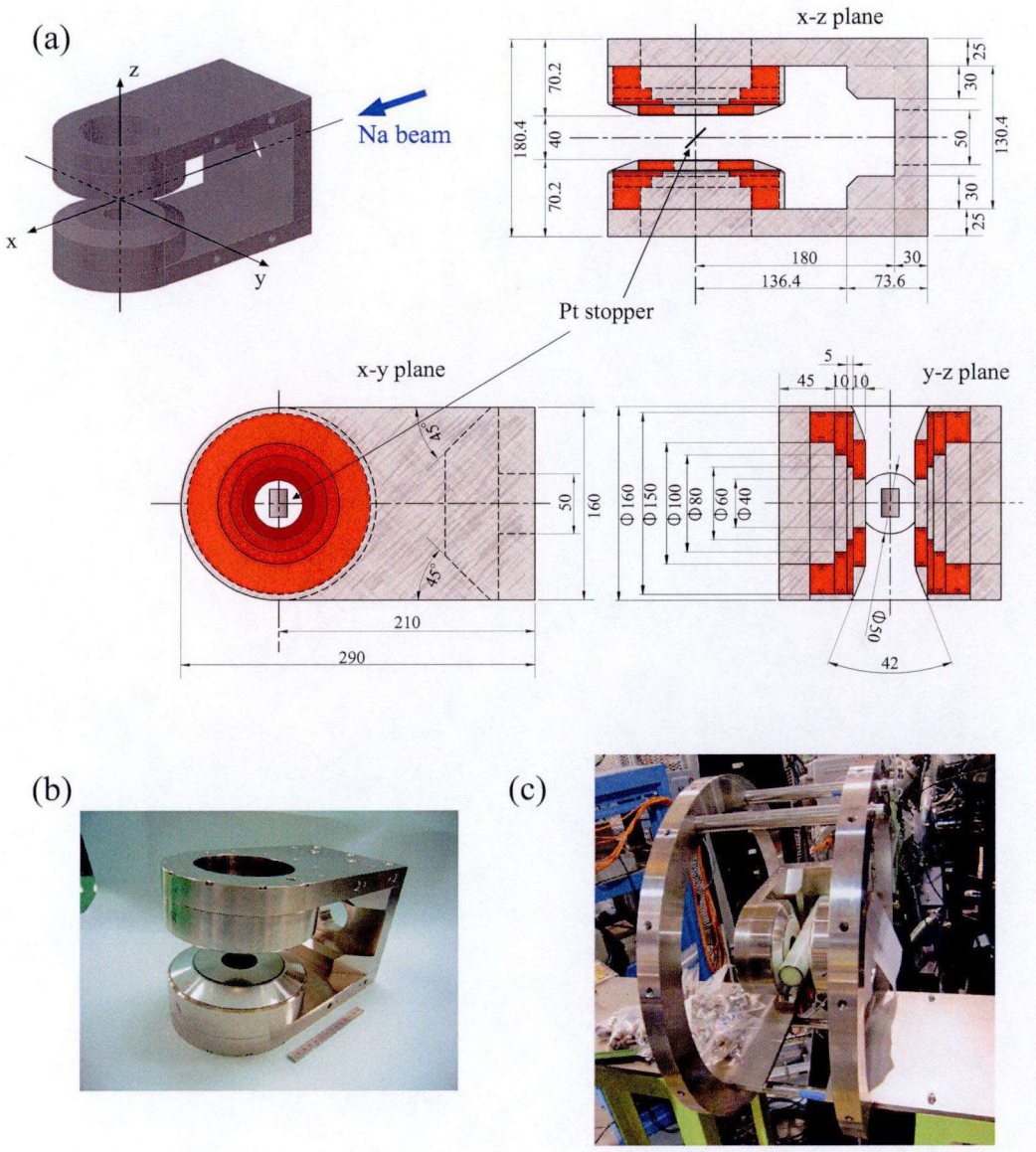

Figure 4.10: (a) Design of the permanent magnet of Nd enforced by return yoke. All the dimensions are given in mm. (b) Picture of the Nd magnet and return yoke. (c) Picture of the magnet set in the Pt stopper position (all the detectors are not attached).

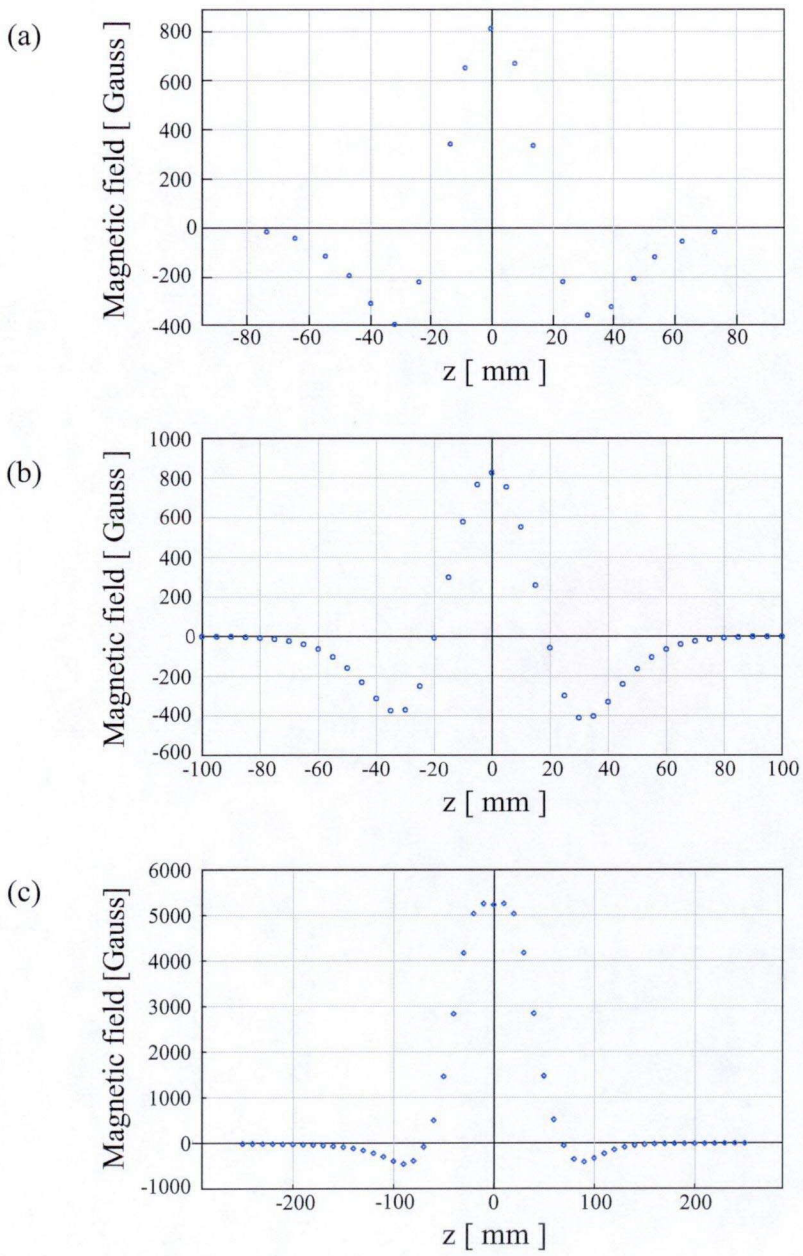

Figure 4.11: (a) Simulation of magnetic field distribution of SmCo permanent magnet enforced by return yoke along z-axis as a function of distance from the beam axis (x-axis). The calculation was carried out by using TOSCA in OPERA-3D [TOS11]. (b) Magnetic field distribution of actual SmCo permanent magnet enforced by return yoke along z-axis as a function of distance from the beam axis (x-axis).. (c) Magnetic field distribution of Nd permanent magnet enforced by return yoke along z-axis as a function of distance from the beam axis (x-axis).

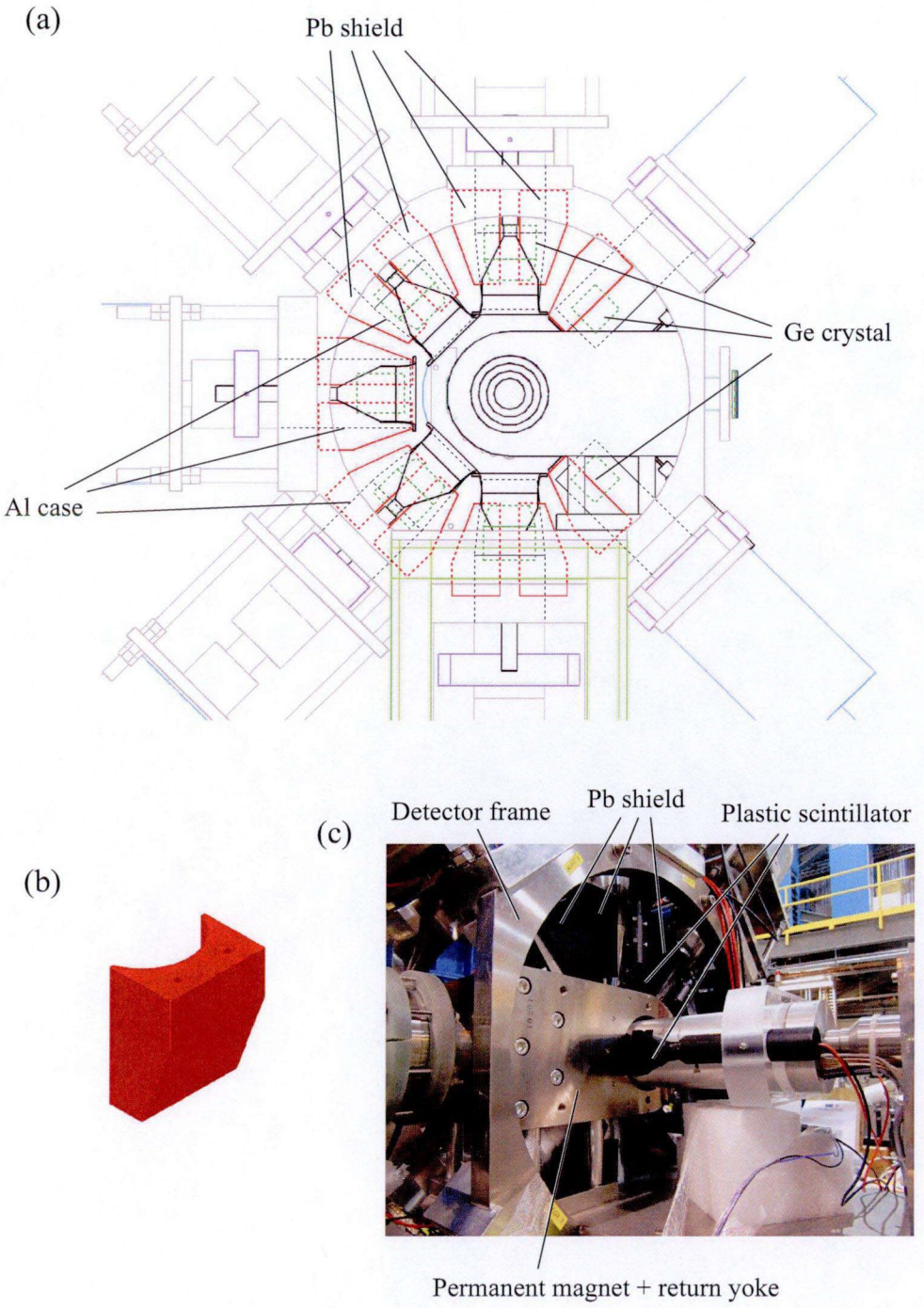

Figure 4.12: (a) Layout drawing of the Pb Compton cross talk shield used for experiment in 2010. Two lead shields are placed between each adjacent Ge detectors for slot 1 to 7. (b) Design of the Pb shield. The shape of the shield was designed to fit to the curved surface of Al cap of Ge detector. (c) Picture of Pb shields and detectors.

4.4 Detector setups

For the measurement of β rays and β-delayed γ rays associated with the β decay of ^{28}Na, ^{29}Na, and ^{30}Na, nine telescopes which consists of germanium (Ge) detector and a thin plastic scintillator (1.5 mm thickness) were used. Fig. 4.13(a) shows the schematic view of detector telescopes. The detector frame was designed and built to put these nine detector telescopes (see Fig. 4.5 and 4.6). Nine slots were allocated for each telescope; Two telescopes for the measurement of β-ray asymmetry are placed in slot R and L, and other seven Ge detectors are placed perpendicular to the polarization axis at every 45° as shown in Fig 4.13.

4.4.1 Germanium (Ge) detectors and plastic scintillators

In the experiment of 2007 (2010), nine Ge detectors and eighteen (eleven) plastic scintillators were used to measure β and γ rays. To distinguish β and γ rays, a pair of plastic scintillators was placed in front of each Ge detector as shown in Fig. 4.13(b) and 4.15(a). In the experiment of 2010, one plastic scintillator was placed in front of each Ge detector for the slot of 1 to 7, for the purpose of increasing efficiency of Ge detectors. Specifications of the detectors for the experiment of 2007 and 2010 are listed in Table 4.2 and Table 4.3, respectively.

Figure 4.14 shows the figure of plastic scintillator. The probability of excitation of scintillator crystal by γ ray is almost negligible because the thicknesses of all the scintillator crystals are thin (1.5 or 2 mm). The shape of the light guide is designed not to decrease the efficiency of guiding light from crystal to PMT. All the PMT tubes are covered with cylindrical magnetic shield of steel. The plastic scintillators and PMTs were attached to Al case of Ge detectors by using Acryl support as shown in Fig. 4.15(b).

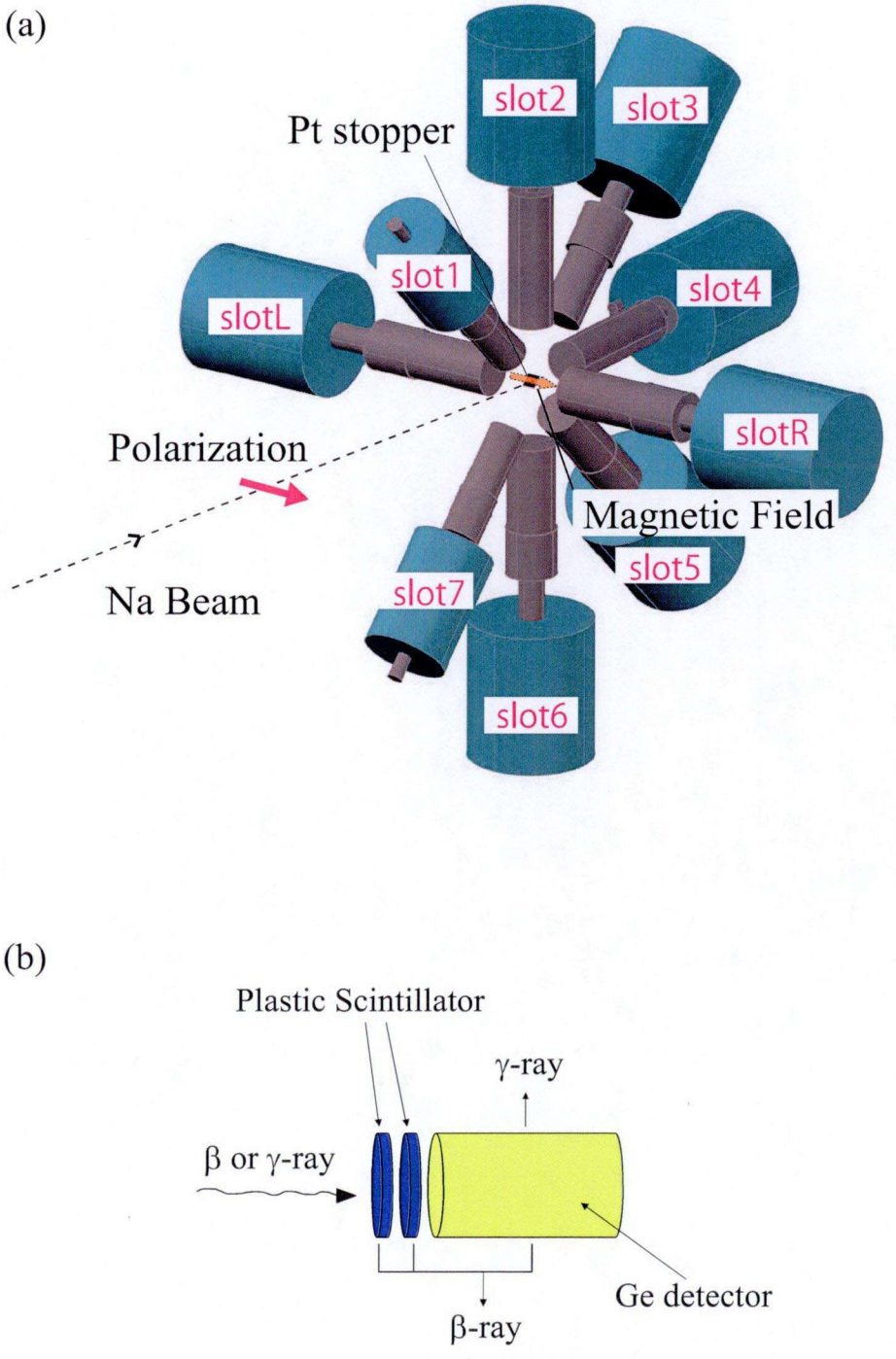

Figure 4.13: (a) Schematic view of detector setups. (b) Schematic figure of telescope consists of Ge detector and two plastic scintillators for measurement of β and γ rays.

Table 4.2: Specification of Ge detectors for the experiment in 2007. Two kind of gains were applied for 2-split signals for slot 5, R, and L.

Slot	1	2	3	4	5	6	7	R	L
Type	planner	co-axial	co-axial	co-axial	co-axial	co-axial	co-axial	co-axial	co-axial
Manufacturer	ORTEC	EURYSIS	EURYSIS	ORTEC	EURYSIS	EURYSIS	ORTEC	EURYSIS	EURYSIS
Operation high voltage (V)	−1700	−4500	−4000	+3000	−5000	−4500	−2300	−5000	−4000
Relative efficiency (%)	10	50	60	40	60	45	30	60	60
Pair scintillator size	ϕ70 & ϕ70	ϕ70 & ϕ70	ϕ70 & ϕ70	ϕ83 & ϕ83	ϕ70 & ϕ70	ϕ70 & ϕ85	ϕ70 & ϕ70	ϕ45 & ϕ90	ϕ45 & ϕ80

Table 4.3: Specification of Ge detectors for the experiment in 2010. Two kind of gains were applied for 2-split signals for slot R and L.

Slot	1	2	3	4	5	6	7	R	L
Name	CINDY	GUOC7	GFIC37	KEK	GFIC38	GFIC39	ALICE	H50%	H45%
Type	co-axial	co-axial	co-axial	co-axial	co-axial	co-axial	co-axial	co-axial	co-axial
Manufacturer	ORTEC	EURYSIS	EURYSIS	ORTEC	EURYSIS	EURYSIS	ORTEC	EURYSIS	EURYSIS
Operation high voltage (V)	−2300	−3500	−4000	−5000	−4000	−4000	−3000	−4500	−5000
Relative efficiency (%)	30	70	70	44	70	70	30	50	45
Pair scintillator size	ϕ70	ϕ70	ϕ70	ϕ70	ϕ70	ϕ85	ϕ70	ϕ42 & ϕ50	ϕ42 & ϕ50

4.5 Data acquisition

For measuring β rays and β-delayed γ rays, pulse height data from Ge detectors and timing data from all the detectors were collected for the experiments of 2007 and 2010. In the experiment of 2007, charge amount data from the plastic scintillators were also collected. For acquiring each of the singles and coincidence events detected, a cluster of the data from all the detectors and relevant devices are formed and transferred to a computer. A CAMAC system was used for processing the detector signals.

4.5.1 MIDAS and electronic circuit

As a software interface to process the event-based data acquisition, MIDAS [TRI11] was used for the experiment of 2007. The conceptual diagram of the system is shown in Fig. 4.16. The analog signals from all the Ge detectors and plastic scintillators were fed to the individual analog-to-digital converters (ADC) and charge ADC (QDC), respectively, and all the fast-timing signals to the STOP inputs of the individual time-to-digital converters (TDC). The signal from β-singles of slot R and L, reduced γ-singles, γ-γ signal, and β-γ signal generate a PRIMARY TRIGGER which initiates all the ADC's, QDC's, TDC's and coincidence registers into operation. In the case of ^{29}Na experiment, latter two signals were not used for a PRIMARY TRIGGER. The signals for the helicity flip were sent to EPICS [ARG07] which control the laser system every 5 min (30 s) for ^{28}Na (^{29}Na). The detailed circuit diagram to obtain the signals from all the detectors are shown in Fig. 4.17(a). The condition of every coincidence signal in Fig. 4.17(a) is shown in Fig. 4.17(b) to (f). The START signal for TDC is generated by every signal for the PRIMARY TRIGGER. The gains of shaping amplifiers for all the Ge detectors were set to the maximum ADC range of 6 MeV. For the Ge detectors of slot R and L, energy signals were split for measuring energy data up to 14 MeV in order to measure the β rays with the end point energy of 14.029(13) MeV (^{28}Na) [AUD03] and 13.284(19) MeV (^{29}Na) [AUD03]. The Ge detector signal of slot 6 was also split for measuring low energy signal by setting high gain which correspond to the ADC range of 3 MeV. The corresponding maximum ADC range and energy resolutions of all the signals from Ge detectors are listed in Table. 4.4.

In the case of ^{28}Na, every β signal was created from coincidence of "coincidence of a pair plastic scintillators of the same telescope" and "Ge detector signal with threshold level $E > 1.5$ MeV". The β ray from ^{28}Mg and ^{28}Al were eliminated by selecting high energy signals corresponding to $E > 4$ MeV because the $Q_\beta = 14.03$ MeV of ^{28}Na is high enough

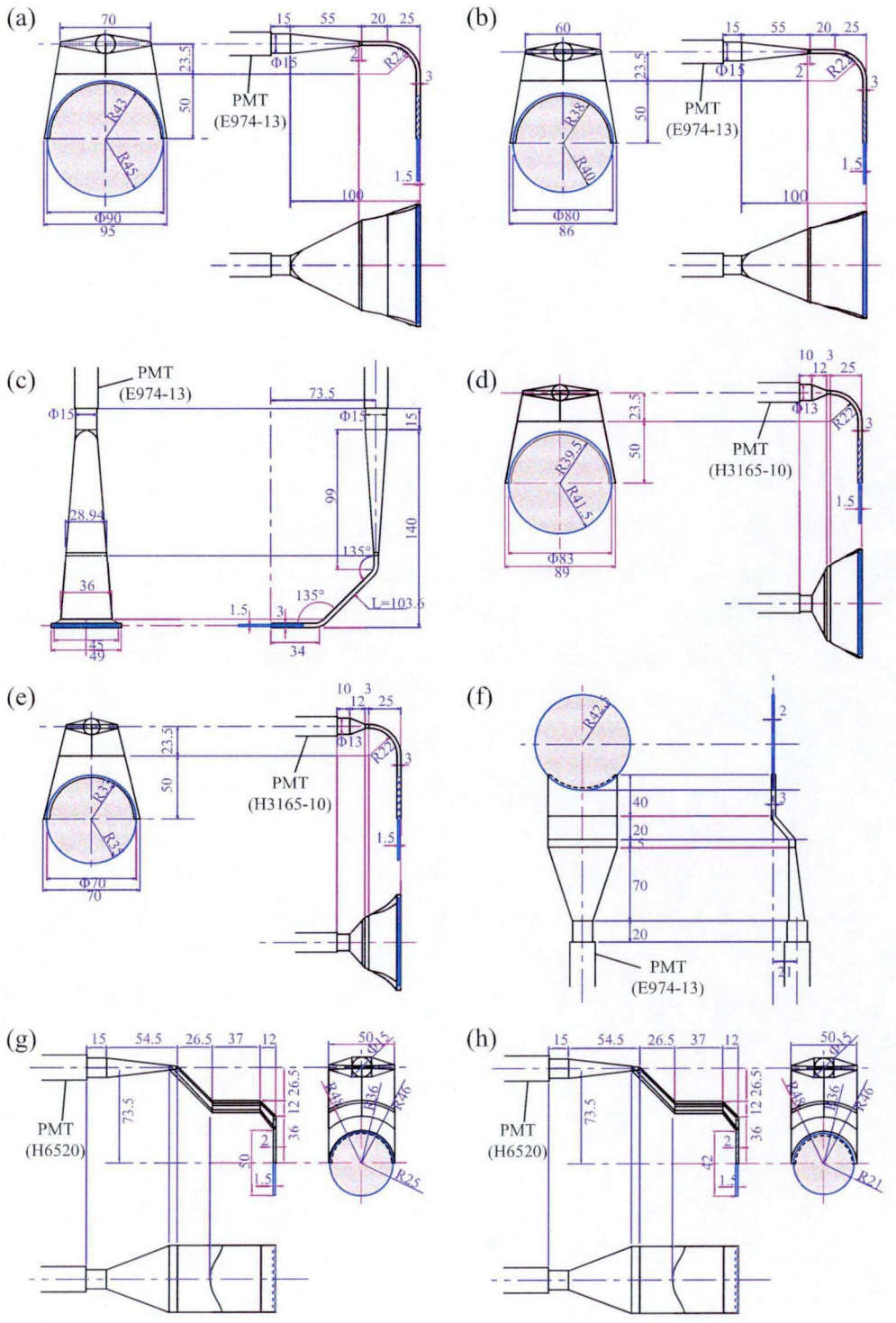

Figure 4.14: Plastic scintillators used in the experiment of 2007 [(a)−(f)] and 2010[(d)−(h)]. Material of plastic scintillator is BC408. All the numbers are the dimensions in mm (not to scale).

(a)

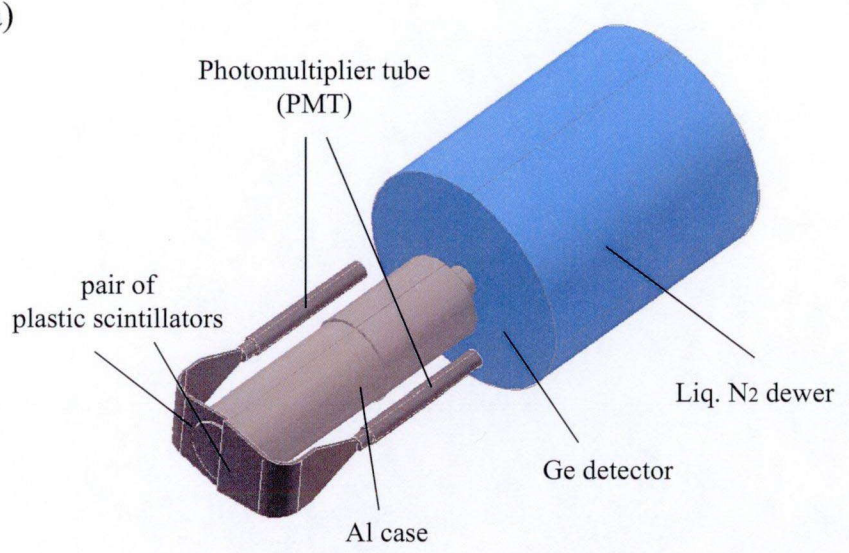

(b)

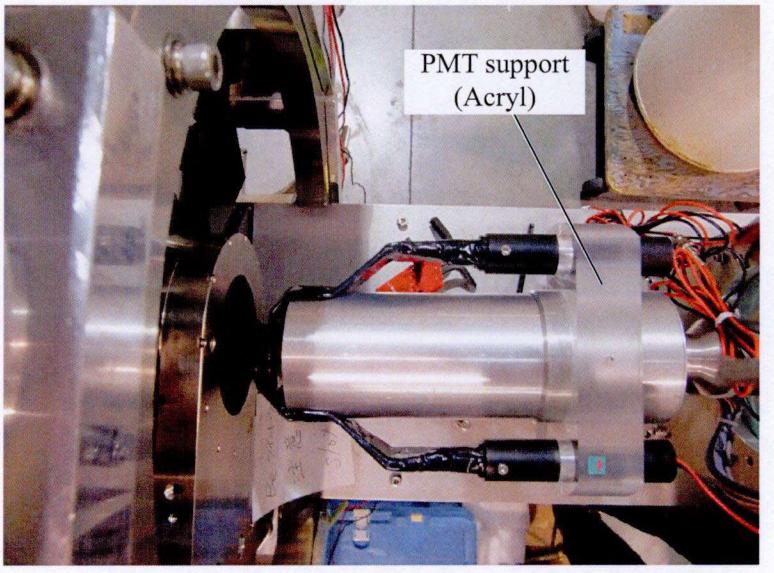

Figure 4.15: (a) Schematic view of a pair plastic scintillators and Ge detector in the same telescope. All the PMT tube is covered with cylindrical magnetic shield. (b) Picture of the telescope for slot R in the experiment of 2010. The plastic scintillator and PMT are attached to the Al cap of Ge detector by using Acryl support.

Table 4.4: Specification of the signals from Ge detectors for the experiment of 2007.

Signal	ADC range [MeV]	Original signal	Energy resolution @1408 keV
1	3	1	2.0
2	6	2	2.8
3	6	3	3.1
4	6	4	2.4
5	6	6	3.5
6	6	5	3.0
6 high	3	5	4.1
7	6	7	2.6
R low	14	R	3.7
R	6	R	3.9
L low	14	L	4.9
L	6	L	2.9

to distinguish from the beta ray of those progeny nuclei. The threshold level of the discriminator was set to the level corresponding to 1.5 MeV to consider the energy loss of β ray in the materials between Pt stopper and Ge crystals. To avoid too much dead time of data acquisition by too frequent event rate, the rates of the γ-singles events were reduced by the factor of 1/3.

In the case of ^{29}Na, every β signal was created from coincidence of a pair plastic scintillators of the same telescope. The β ray from the contaminant of ^{29}Al were measured in this case because the beam rate was not too high. The PRIMARY TRIGGER was generated by γ-singles, and β-singles of slot R and L.

Figure. 4.18 shows the data cluster obtained by using MIDAS system. The data is composed of file header, and following four kinds of event data; normal, scaler, epics, and final event. Each event is identified by event ID.

4.5.2 NBBQ and electronic circuit

For the experiment in 2010, data acquisition system using NBBQ interface was applied to process the event-based data. The conceptual diagram of data acquisition using NBBQ system is shown in Fig. 4.19. The analog signals from all the Ge detectors were fed to the individual analog-to-digital converters (ADC) and all the fast-timing signals to the STOP inputs of the individual time-to-digital converters (TDC).

The signal from β-singles of slot R and L, ORed signals from Ge detectors generate a PRIMARY TRIGGER which initiates all the ADC's, TDC's and coincidence registers. The signals from output register were generated every 100 s for the helicity flip by changing laser condition. The detailed circuit diagram to obtain the signals from all the detectors are

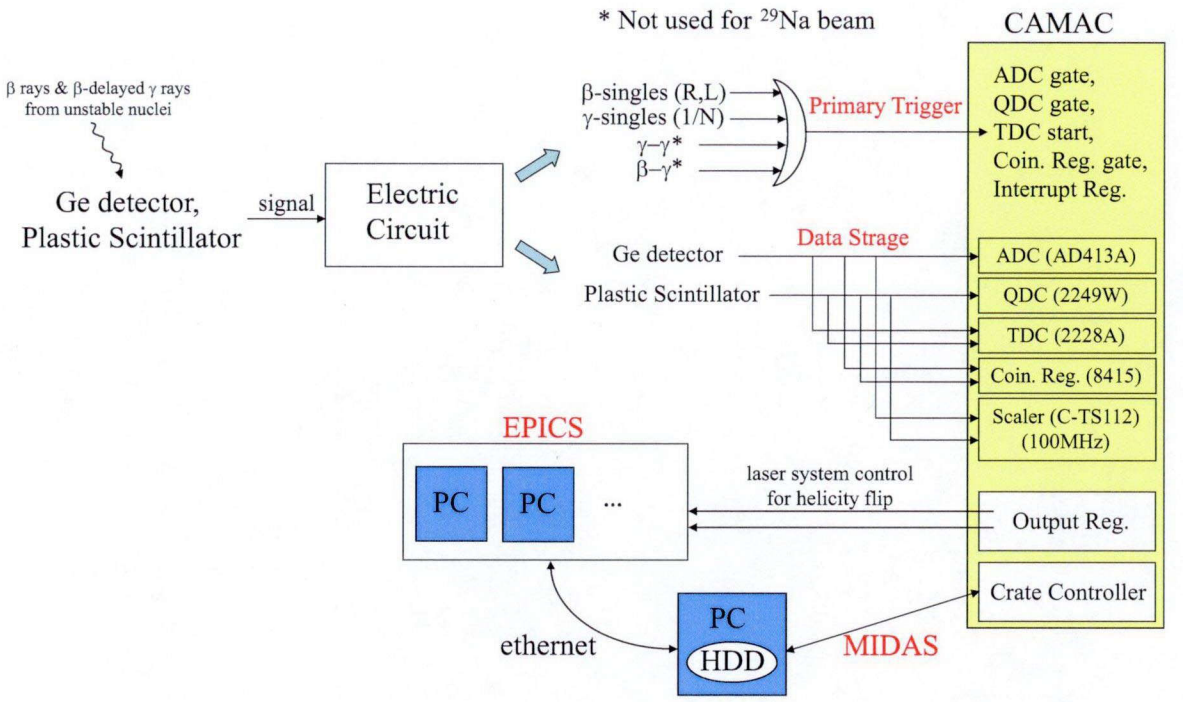

Figure 4.16: Conceptual diagram of data acquisition system using MIDAS.

shown in Fig. 4.20(a). The condition of every coincidence signal in Fig. 4.20(a) is shown in Fig. 4.20(b) and (c). The data structure of the system using NBBQ is shown in Fig. 4.21. The data is composed of the blocks of header, event, and ender, which are identified by first 4 word of 0001, 0000, and ffff, respectively.

4.6 Experimental Procedure

4.6.1 Beam tuning of ^{28}Na

The electric quadrupole strengths and deflector voltages of Na beam line were determined by using a stable ^{23}Na beam (unpolarized). The beam currents were measured on the collimator placed at the position of FRP chamber's flange and the Faraday cup placed at the Pt stopper position. The schematic illustration of beam monitor system is shown in Fig. 4.7(c). The ^{23}Na beam was optimized so that the current at the collimator was minimized (2×10^{-11} A), and that at Faraday cut was maximized (6.5×10^{-10} A). The Faraday cut was replaced with the Pt stopper position. The ^{28}Na beam was optimized by setting both of the asymmetries of the β-ray counts (N_U/N_D, N_L/N_R) to be 1.

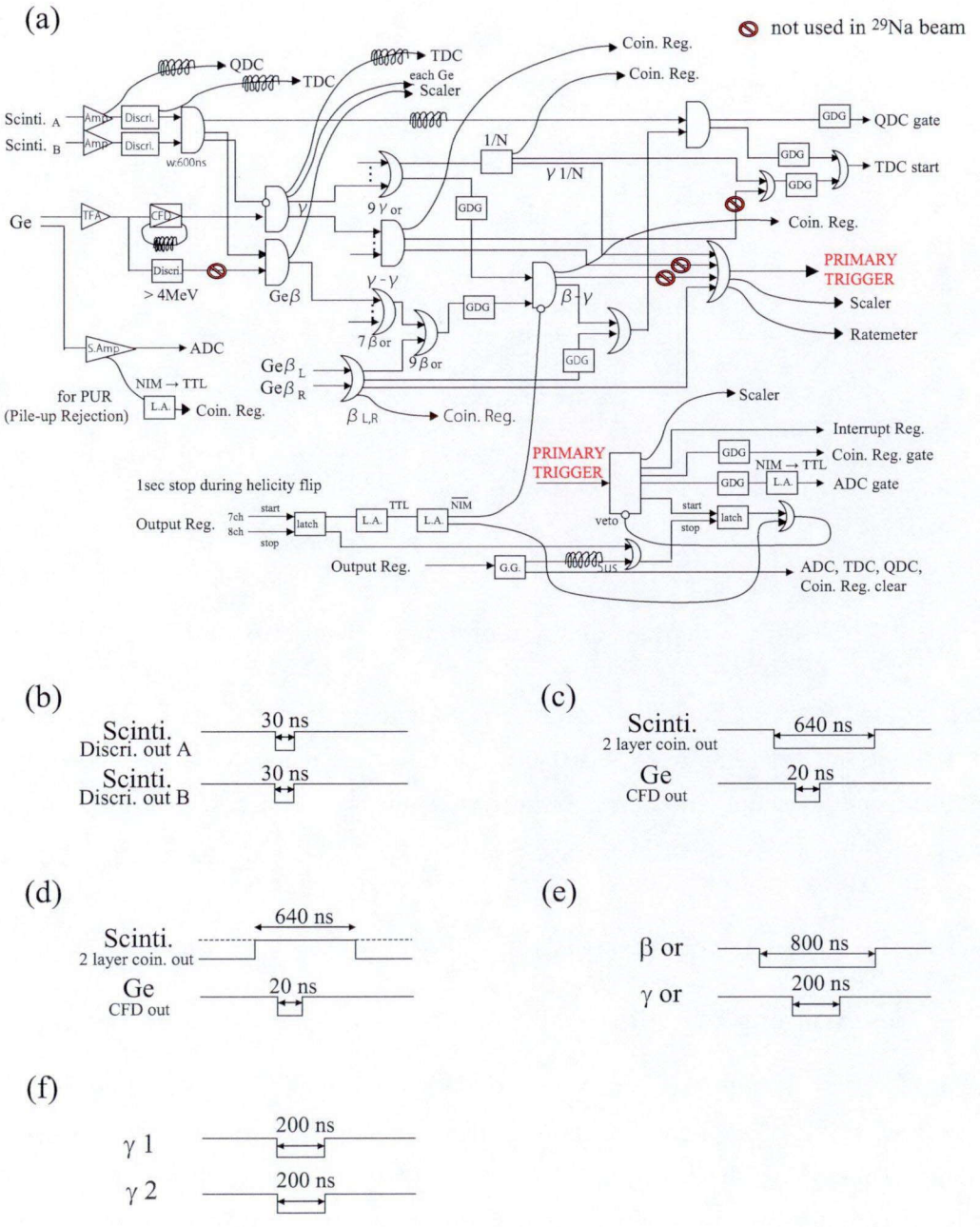

Figure 4.17: (a) Circuit diagram for the experiment of 2007. The condition of two signals in each coincidence module is listed in (b) to (f).

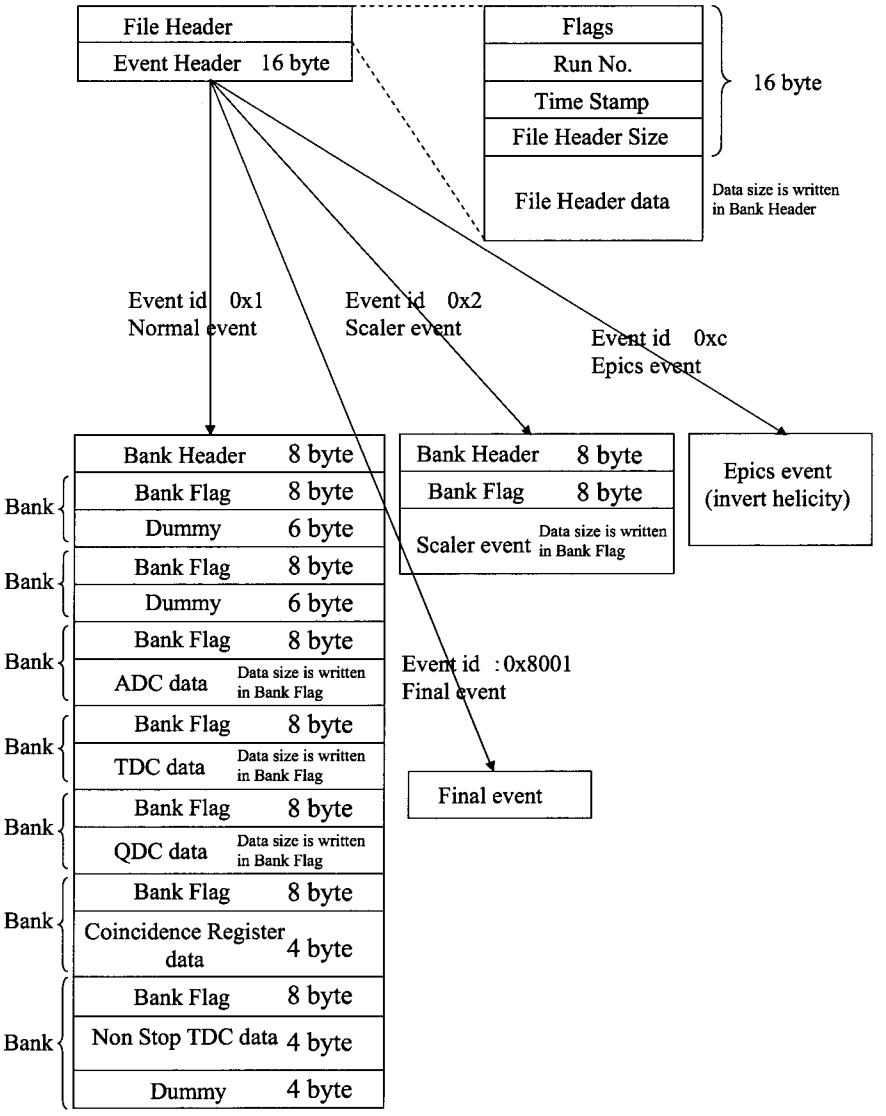

Figure 4.18: Structure of data obtained by the data acquisition system using MIDAS. The data was fixed length.

Table 4.5: Specification of the signals from Ge detectors for the experiment of 2010.

Signal	ADC range [MeV]	Original signal	Energy resolution @1332 keV
1	6	1	2.7
2	6	2	5.2
3	6	3	3.1
4	6	4	2.3
5	6	5	3.4
6	6	6	2.6
7	6	7	2.5
R low	16	R	7.5
R	6	R	2.7
L low	16	L	5.1
L	6	L	3.1

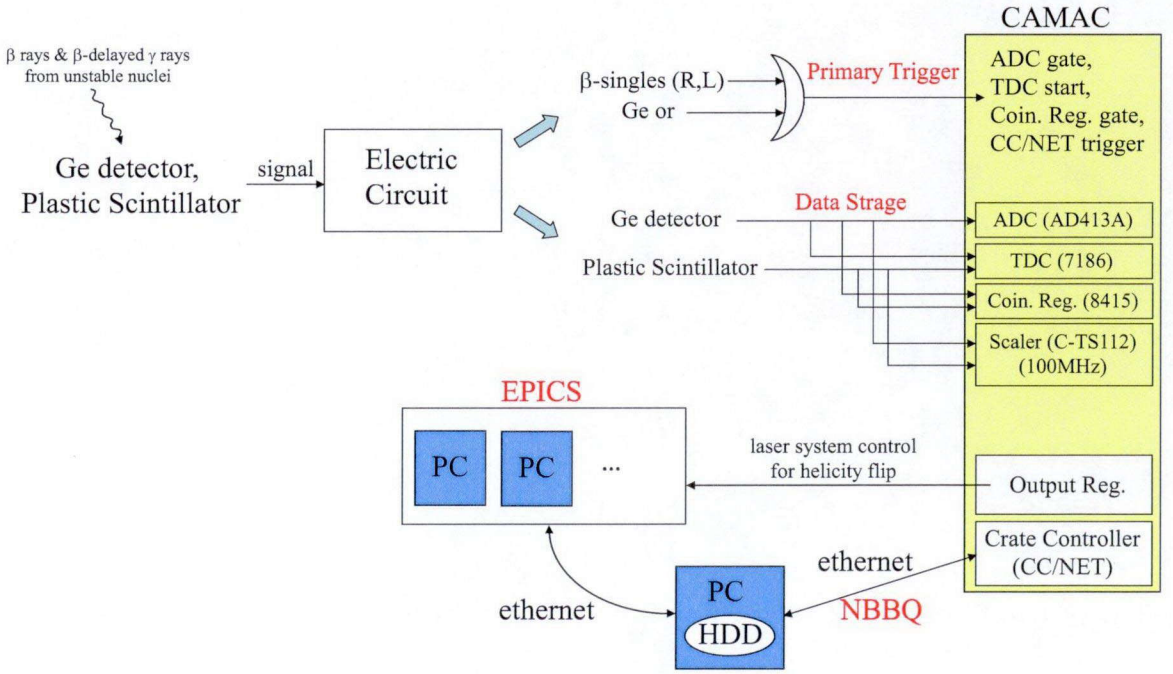

Figure 4.19: Conceptual diagram of data acquisition system using NBBQ.

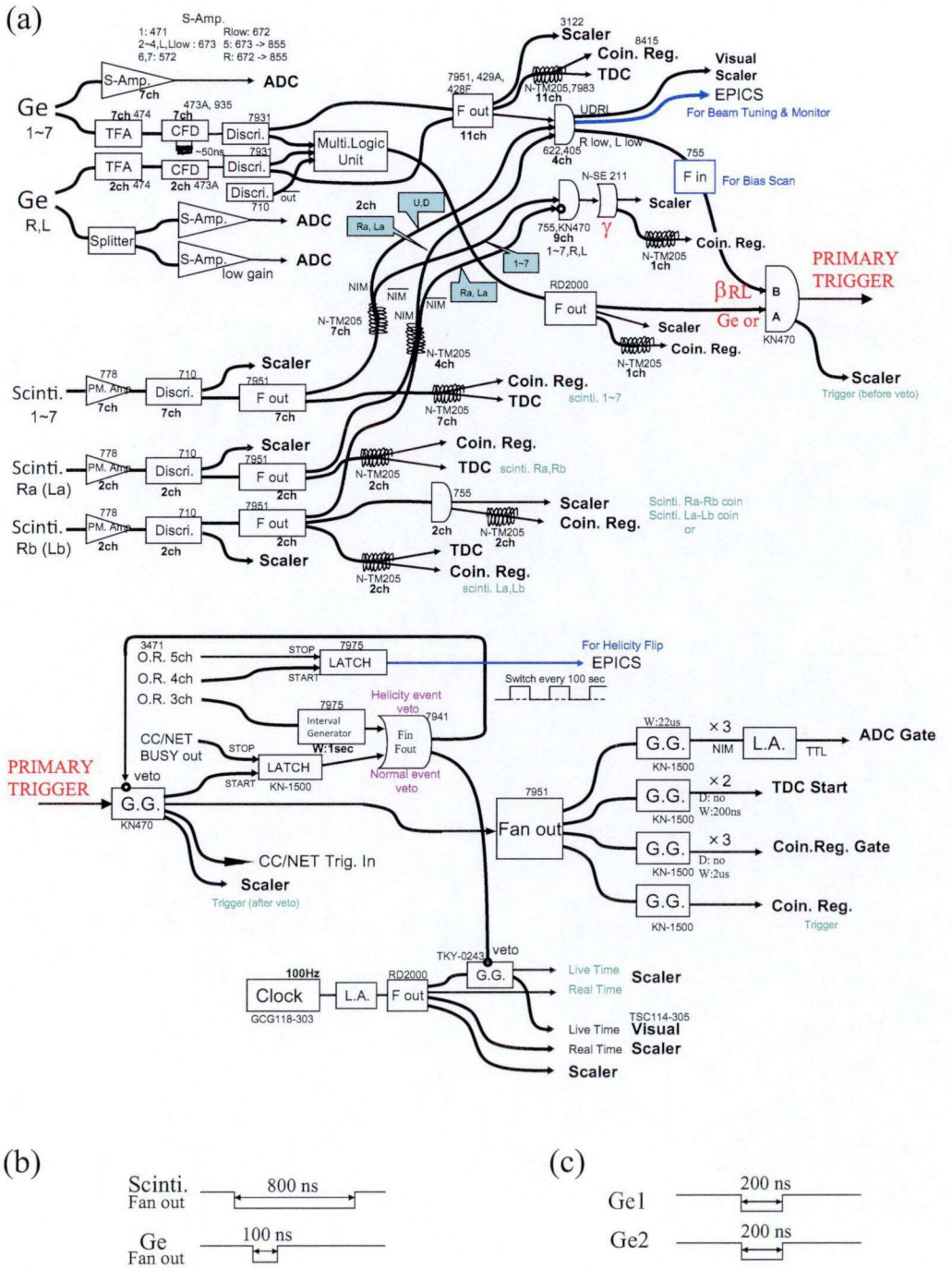

Figure 4.20: (a) Circuit diagram for the experiment of 2010. The condition of two signals in each coincidence module is listed in (b) and (c).

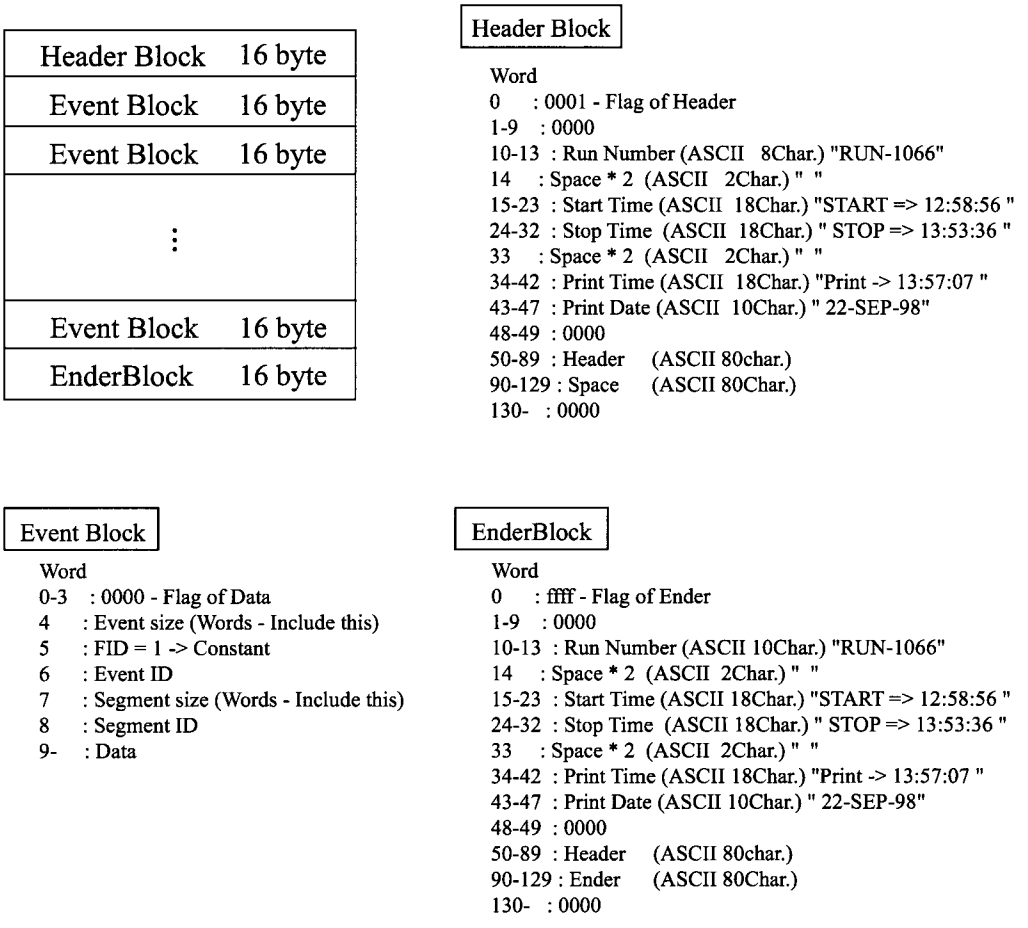

Figure 4.21: Structure of data obtained by the data acquisition system using NBBQ. The data of fixed length was defined.

Subsequently, the polarization of ^{28}Na was carried out as follows. The dye laser was tuned to a wave number of 16930.37 cm^{-1} and split into three as shown in Fig. 4.3. To correctly realize a resonance condition, the beam energy of ^{28}Na was tuned by changing the deceleration voltage of the Na cell to change the Doppler correction. Figure 4.22(a), (b), and (c) show the asymmetries of the β-ray counts from ^{28}Na, ^{29}Na, and ^{30}Na, respectively, in the left and right telescopes as a function of bias voltage. Since the laser frequencies of ν_1, ν_2, and ν_3 was generated by EOM (see Fig. 4.3), four possible resonances can be seen. The biggest resonance with D_1 energy distance was achieved by $\nu_1 + \nu_2$ laser at the voltage of 109 V shown in Fig. 4.22(a). Therefore, the Na cell voltage of 109 V was settled for the polarization of ^{28}Na. The average polarization of ^{28}Na over the whole experiment was measured to be 28.3(5)%, as will be described in the following section.

The total events of 3.0×10^7 were accumulated in 42.8 h with the average ^{28}Na beam intensity of ~450 pps.

4.6.2 Beam tuning of ^{29}Na

The experiment using ^{29}Na beam was performed shortly after the ^{28}Na experiment. To avoid the contaminant from the γ rays associated with the β decay of ^{28}Mg with relatively long half-life (20.915 h), Pt stopper was exchanged. By the same process as ^{28}Na, the polarized ^{29}Na beam was optimized. The beam was optimized by setting the β-ray asymmetry of up-down, and left-right (N_U/N_D, N_L/N_R) to be 1. Then the polarization of ^{28}Na was carried out by the optical pumping method. The wave number of the dye laser was set to be 16934.8408 cm^{-1} with EOM splitting by 977 MHz (see Fig. 4.3). The resonance voltage of 114 V in the Na cell was obtained by searching the resonance point to measure the β-ray counts asymmetry of left and right telescopes as shown in Fig. 4.22(b).

The total events of 1.7×10^7 were accumulated in 56 h with the average ^{28}Na beam intensity of ~82 pps.

4.6.3 Beam tuning of ^{30}Na

The ^{30}Na beam was tuned as follows. The ^{27}Al beam with kinetic energy of 28 keV was optimized to minimize and maximize the current at the collimator and Faraday cut, respectively. The electric quadrupole strengths and deflector voltages of Na beam line were determined by using a stable ^{23}Na beam (unpolarized). Then, the Faraday cut was replaced with the Pt stopper position. The ^{30}Na beam was optimized by setting both of the asymmetries of the β-ray counts (N_U/N_D, N_L/N_R) to be 1. Subsequently, the polarization of ^{30}Na

was carried out by the optical pumping method. The dye laser was tuned to a wave number of 16932.45 cm^{-1} and split into three as shown in Fig. 4.3. By changing the deceleration voltage of the Na cell to change the Doppler correction, the resonance point voltage of 322 V was obtained for maximum polarization of ^{30}Na. The average polarization of ^{30}Na over the whole experiment was measured to be 32(3)%, as will be described in the following section.

The total events of 7.1×10^6 were accumulated in 142 h with the average ^{30}Na beam intensity of ~14 pps.

4.6.4 Contaminant in Na beams

The ^{28}Al and ^{29}Al contaminants are observed as mixtures in the ^{28}Na and ^{29}Na beams, respectively, as shown in Fig. 4.23(a) and (b). The average intensities of ^{28}Al and ^{29}Al contaminants at the stopper position were ~70 and ~32 pps, respectively. By using the Q_β values of ^{28}Na [14.029(13) MeV [AUD03]] and ^{28}Mg [1.8318(20) MeV [AUD03]], the mass difference between ^{28}Na and ^{28}Al is estimated to be

$$\frac{Q_{^{28}\mathrm{Na}} - Q_{^{28}\mathrm{Mg}}}{A \times M_N} = \frac{14.029 + 1.832}{28 \times 935} \simeq \frac{1}{1650}, \tag{4.10}$$

where M_N represent the mass of nucleon. The mass difference of ^{29}Na and ^{29}Al is also estimated to be $\simeq$1/1300 by using the Q_β values of ^{29}Na [13.284(19) MeV] and ^{29}Mg [7.596(14) MeV [AUD03]]. Since the mass resolution of ISAC mass separator is $\Delta M/M \simeq$ 1/10000, it is understood that it is difficult to separate ^{28}Na (^{29}Na) from ^{28}Al (^{29}Al) when these nuclei have momentum broadening.

On the contrary, the ^{30}Al contaminant was not observed in ^{30}Na beam experiment in spite of the similar extent of mass difference between ^{30}Na and ^{30}Al ($\simeq$1/1160) compared to the cases of ^{28}Na and ^{29}Na beams. This result might be due to finer tuning was obtained in the case of ^{30}Na beam.

In the case of analysis in β-ray energy spectrum as described in the following sections, the β rays emitted from the ^{28}Al and ^{29}Al can be cut out by choosing high energy β-rays estimated from the mass differences of ^{28}Na [14.029(13) MeV [AUD03]] and ^{28}Al [4.64224(14) MeV [AUD95]], and ^{29}Na [13.284(19) MeV [AUD03]] and ^{29}Al [3.6797(12) MeV [AUD03]].

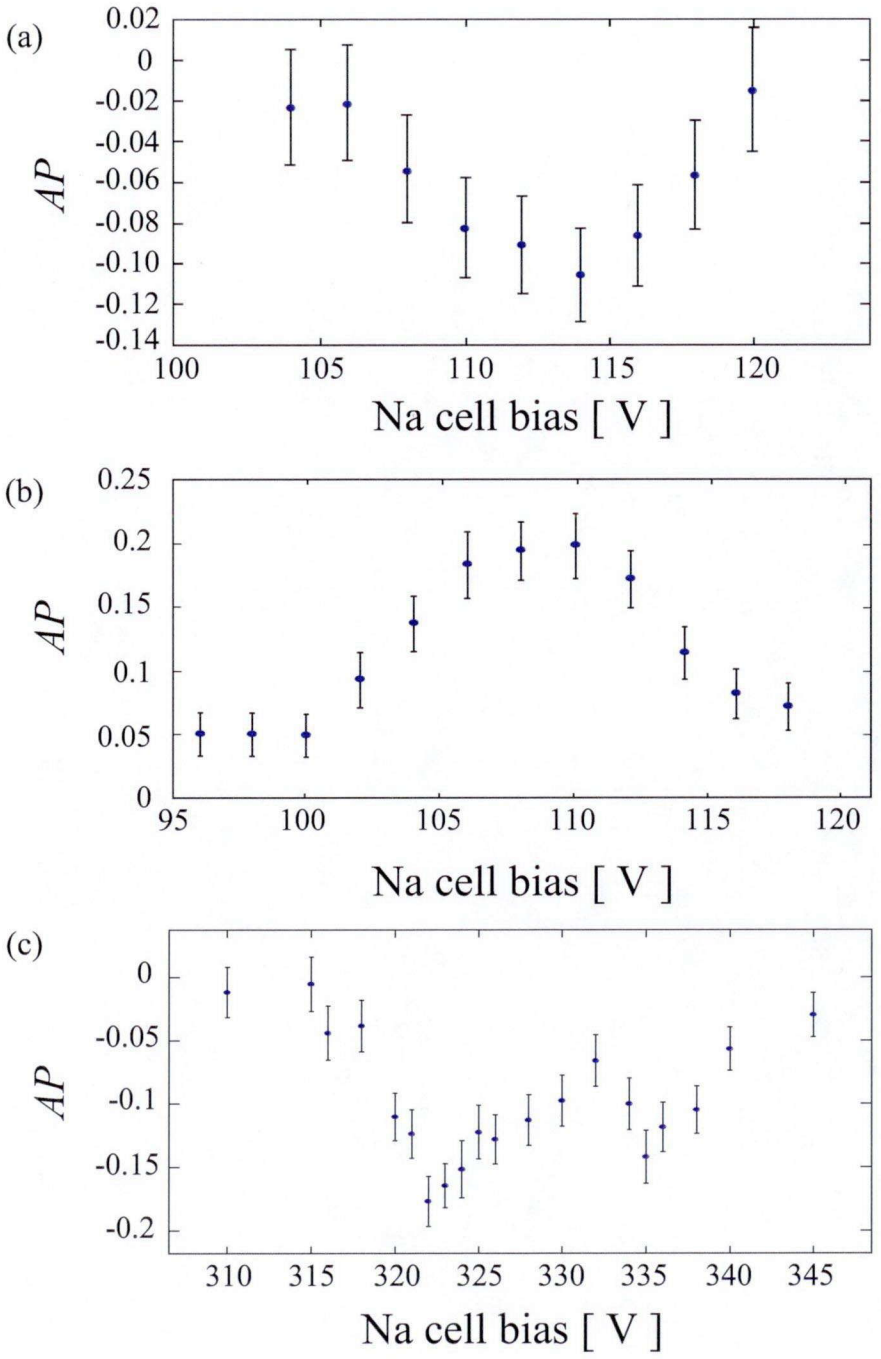

Figure 4.22: Asymmetries of the β-ray emission from spin-polarized (a) ^{28}Na, (b) ^{29}Na, and (c) ^{30}Na as a function of deceleration bias of the Na cell. The lasers were tuned to wave numbers of 16930.37, 16930.8408, and 16932.4540 cm^{-1} for ^{28}Na, ^{29}Na, and ^{30}Na, respectively.

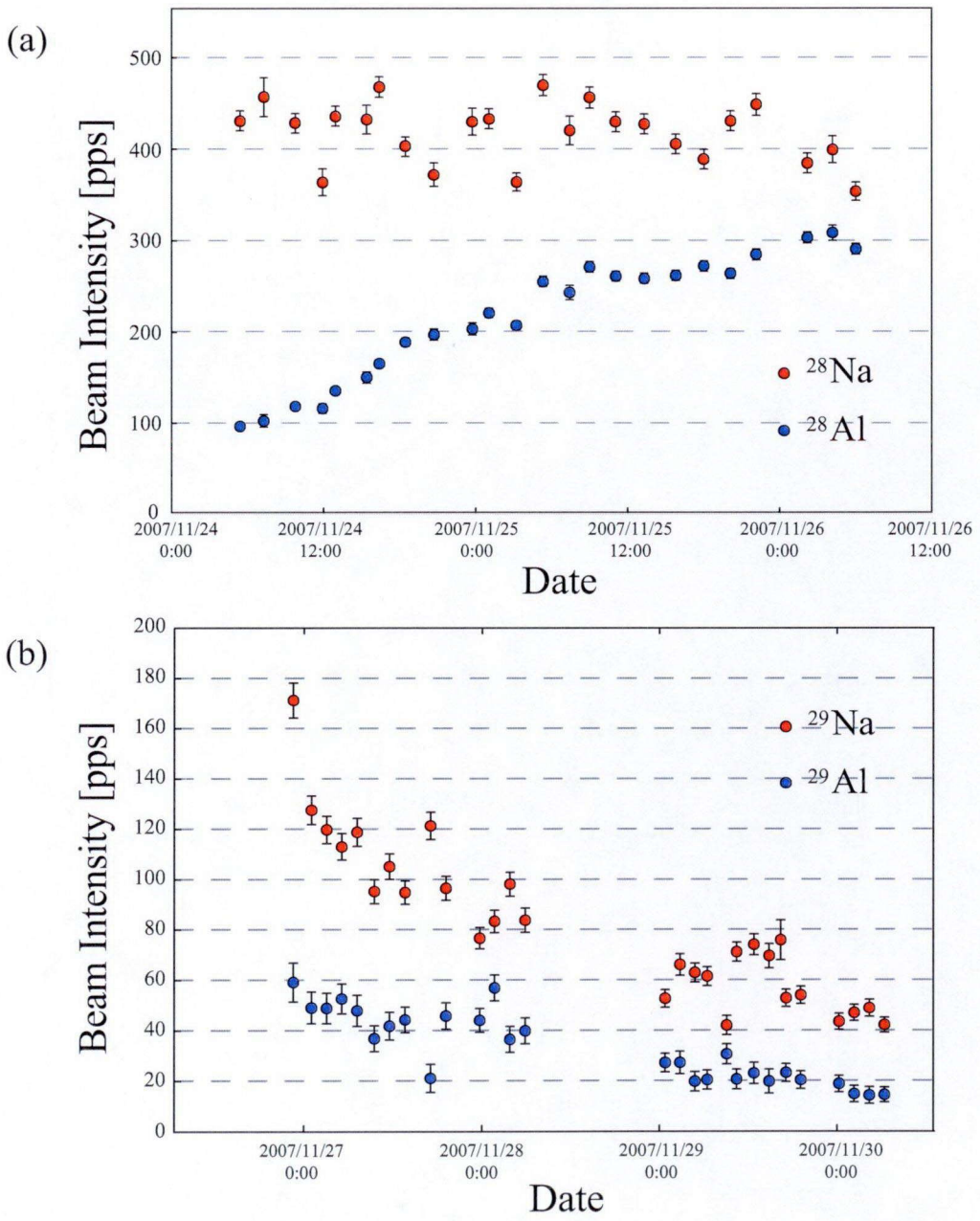

Figure 4.23: Beam intensities of (a) ^{28}Na, (b) ^{29}Na, and (c) ^{30}Na during experimental times. The contaminants of ^{28}Al and ^{29}Al were observed in ^{28}Na and ^{29}Na beam times, respectively. The increasing of ^{28}Al contaminant is due to the accumulation as derived from the beta decay of ^{28}Mg with long half-life ($T_{1/2} = 20.915$ h).

(c)

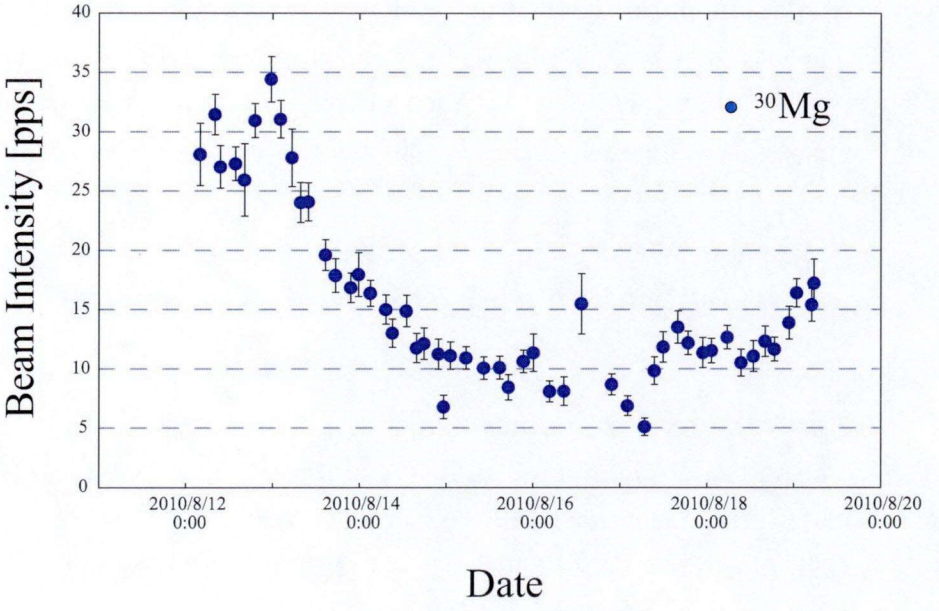

Figure 4.23: *Continued.*

CHAPTER V

Data Analysis

The event data of all the modules in CAMAC is collected as the data structure shown in Fig. 4.18. The events of β rays, γ rays, etc. were extracted by the condition of ADC, TDC, etc., by using off-line sorting program. The processed data was constructed as a data array. The data array was analyzed by using the analysis software of gf3 in RADWARE package [RAD11].

5.1 Energy Calibration and Gain Shift Correction

All the energy signals in ADC were calibrated by using the data of γ-ray peaks from ^{56}Co (847 to 3253 keV), ^{60}Co (1173 to 1332 keV), ^{241}Am (60 keV), and ^{152}Eu (122 to 1408 keV) sources. The source data was obtained before and after the experimental time of each Na beams. The calibration parameters were obtained for each of the ^{28}Na, ^{29}Na, and ^{30}Na experiment. The γ rays of 3272, 3451 and 3548 keV in ^{56}Co were not used because of low statistics. The channels of respective ADC was calibrated by using the linear expression of

$$E = a \times channel + b. \tag{5.1}$$

All the parameters were obtained by fitting the energy source data as a function of ADC channel with least-square method. The fitting region was divided into low and high energy region for all the ADC channels because the fitting results were better than one linear fitting. The differences of calibrated and source energy for analyses of ^{28}Mg, ^{29}Mg, and ^{30}Mg for all the Ge detectors are shown in Fig. 5.1(a), (b), and (c), respectively. Since the efficiency of planner type detector (slot 1) is low, only one set of parameters were used for energy region of $E < 1000$ keV.

The gains of shaping amplifier fluctuate due to the aging deterioration of internal circuit

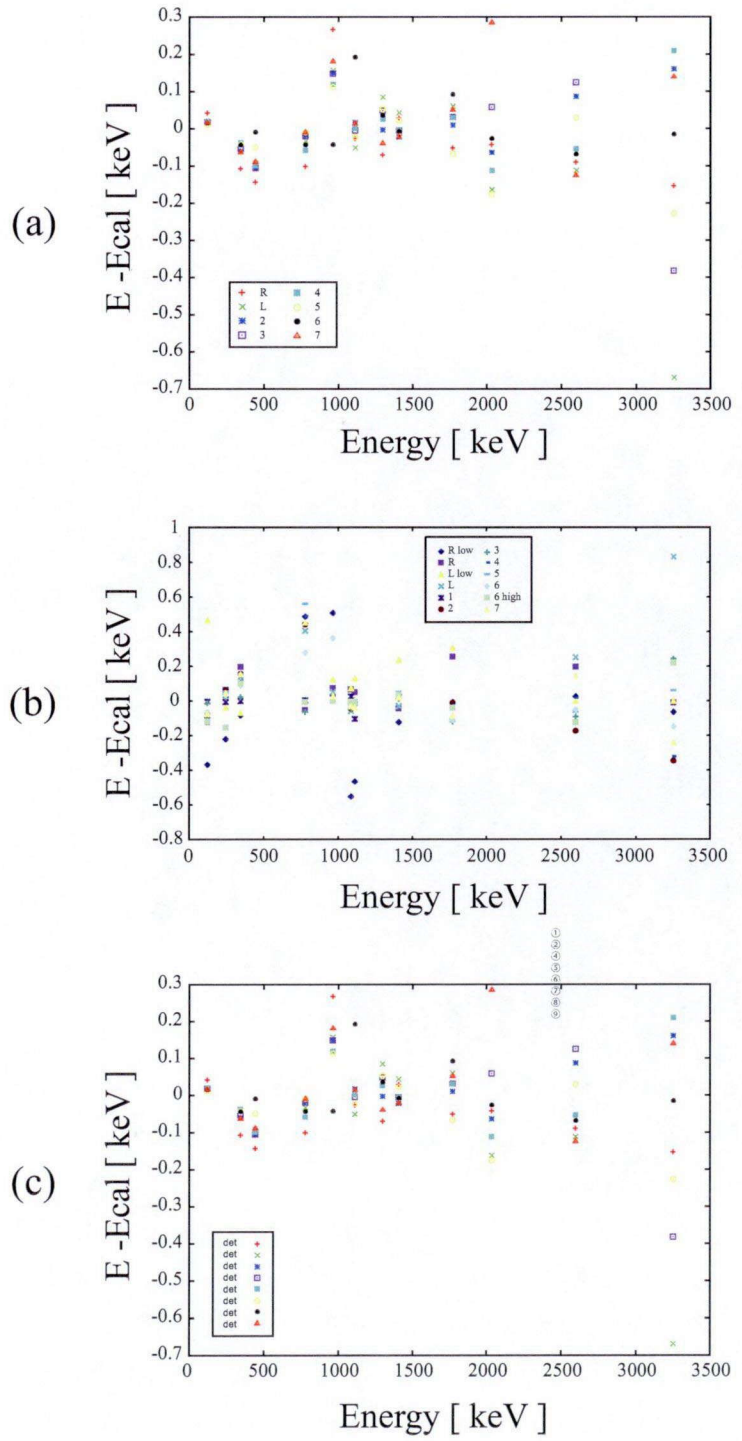

Figure 5.1: Differences of source energies and calibrated results for the experiment of (a) ^{28}Na, (b) ^{29}Na, and (c) ^{30}Na, respectively.

of the module or temperature of the experimental hall, etc., during the experimental time. Therefore, the calibration parameters of ADC channel was corrected by according γ-ray peak positions to the same for every block data (RUN) if gain shift was detected. Figure 5.2(a) and (b) show the raw and gain-shift corrected γ-ray energy spectra, respectively, around the 2560- and 2614-keV photo peaks detected by the Ge detector of slot 5 for first 20 RUNs during the experiment of ^{29}Mg. It is to be found that the obvious gain shift from RUN 1 to 2 are corrected.

5.2 Gamma-ray efficiencies of Ge detectors

The relative γ-ray efficiencies of Ge detectors were deduced as follows. In the case of Ge detectors used for the data analysis of the experiment of 2007, the efficiency was deduced by using the γ rays in ^{56}Co and ^{152}Eu sources. Because of inaccurate source intensities, the efficiencies deduced from ^{56}Co and ^{152}Eu show big discrepancy. Therefore, we introduced the factor to correct the source intensity of ^{56}Co. The factor was calculated to minimize the qai-square value of fitting results.

Figure 5.3(a) shows the efficiency used in the analysis of ^{28}Na beam data. One linear fitting was applied for all the fitting, except that the 8th degree equation was used for the low energy region ($E < 300$ keV) in (a) because of the better fitting result. The fitting equation used for all the fittings is

$$\log\epsilon = \sum_{n=1}^{N} p_{\mathrm{n}} \times \log(\frac{E}{1332})^{n}. \tag{5.2}$$

where N represents the number of degrees of fitting equation. In order to reduce the fluctuation of parameters in the fitting procedure, energy E is divided by 1332 keV. The parameters for all the fittings are shown in Fig. 5.3.

The γ-ray efficiencies of Ge detectors used for the data analysis of the experiment of 2010 (^{30}Mg) shown in Fig. 5.3(b) was deduced by using the γ rays of 244 and 444 keV in ^{30}Al and 2236 and 3598 keV in ^{30}Si following the β decay of ^{30}Mg because the efficiency of each Ge detector deduced from the standard sources of ^{56}Co and ^{152}Eu shows big discrepancy, especially between the Ge R and Ge L. This may be because the position of ^{30}Na beam spot was not in the center of Pt stopper. The intensities of these four γ rays were referred from [HIN08].

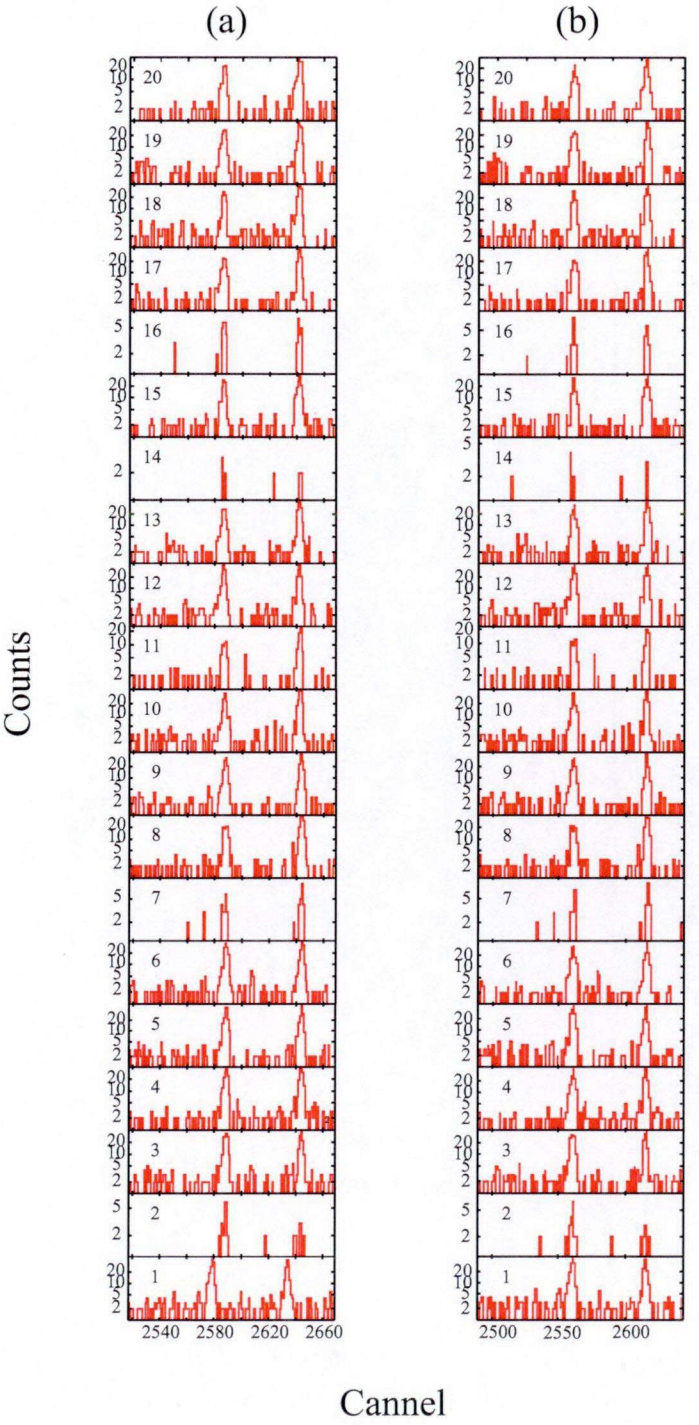

Figure 5.2: Gamma-ray energy spectra of Ge detector in slot 5 for each RUN of ^{29}Mg (a) before and (b) after gain shift correction.

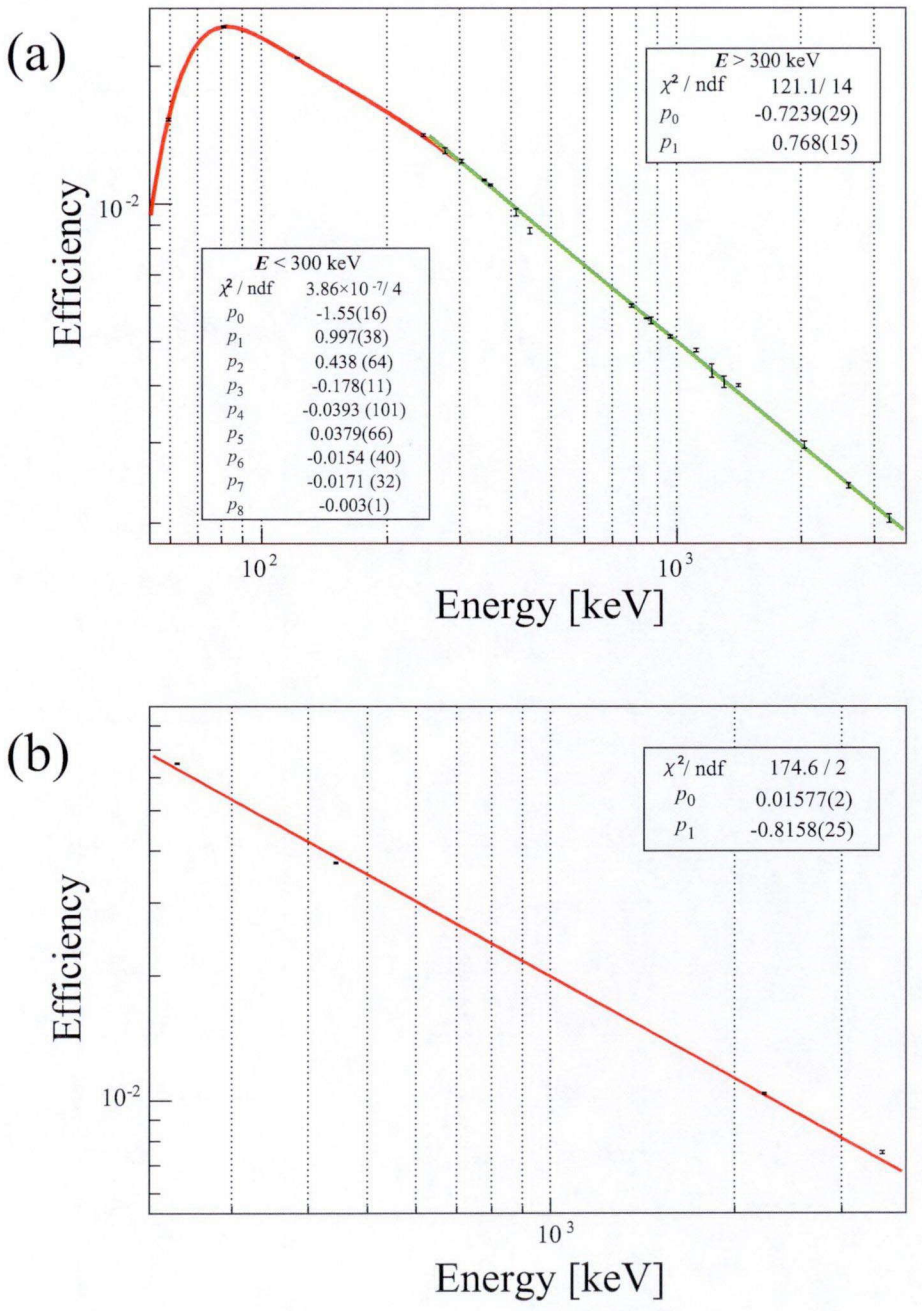

Figure 5.3: Gamma-ray efficiencies of Ge detectors used for the data analysis for the present experiments; (a) Ge R for ^{28}Mg, (b) all Ge detectors for ^{30}Mg. The γ rays emitted from the calibration sources of ^{56}Co and ^{152}Eu, and γ rays in ^{30}Al and ^{30}Si following the β decay of ^{30}Mg were used to calculate the efficiencies of (a) and (b), respectively. The 8th degree equation was used in the energy lower than 300 keV, whereas linear fitting was applied for the energy higher than 300 keV for (a) ^{28}Mg. The one linear fitting was applied for (b) ^{30}Mg. The fitting parameters are also shown.

Table 5.1: Conditions of choosing β ray for the experiment of ^{28}Na, ^{29}Na, and ^{30}Na. TAC gate represents choosing prompt region on time different spectrum of Ge detector and scintillator in the same telescope (see Fig. 5.5).

Beam(slot)	Ge E	Ge T	Scinti. a E	Scinti. a T	Scinti. b E	Scinti. b T	TAC gate
^{28}Na (all)	○	○	○	○	○	○	○
^{29}Na (all)	○	○	○	○	○	○	-
^{30}Na (R,L)	○	○	–	○	–	○	○
^{30}Na (1–7)	○	○	–	○	–	–	○

5.3 Energy Spectra of β and γ ray

Beta and γ rays were extracted by the condition of ADC and TDC of Ge detector and plastic scintillators as follows. Figure 5.4(a), (b), and (c) show ADC spectra of slot 6 Ge detector of energy-calibrated, β, and γ rays, respectively, in the experiment of ^{30}Na. The β ray was sorted out by the coincidence data of Ge detector and plastic scintillators in the same telescope. Table. 5.1 shows the conditions of β ray for the experiment of ^{28}Na, ^{29}Na, and ^{30}Na. To eliminate accidental event, only the prompt element of time different spectrum of Ge detector and plastic scintillator in the same telescope was selected. Figure 5.5 shows the time different spectrum of Ge detector and plastic scintillator of the slot R for ^{28}Na experiment. The background signals were eliminated by choosing the data in the range between two blue lines.

The γ ray was sorted out by choosing ADC and TDC of Ge detector in the anti-coincidence with TDC of plastic scintillator in the same telescope.

5.4 Matrix data and γ-γ coincidence analysis

To analyze γ-γ coincidence event, two dimensional data array of 4096 $\times$ 4096 channel was constructed. The ADC data of Ge detector was filled to the array when γ-ray event of more than 2 coincidence was detected. Figure 5.6(a) shows schematic figure of matrix data array. When coincidence data of x ch and y ch was detected, the data of [x][y] is filled. The matrix data can be analyzed by gf3, for example, when we gate on x channel, we can extract y-projected spectrum of the matrix as shown in Fig. 5.6(b). Thus, the γ-γ coincidence data can be analyzed.

In actual data analysis of γ-γ coincidence data, tha background components of Compton scattering and chance coincidence must be subtracted from the γ-ray gated spectrum. Fig-

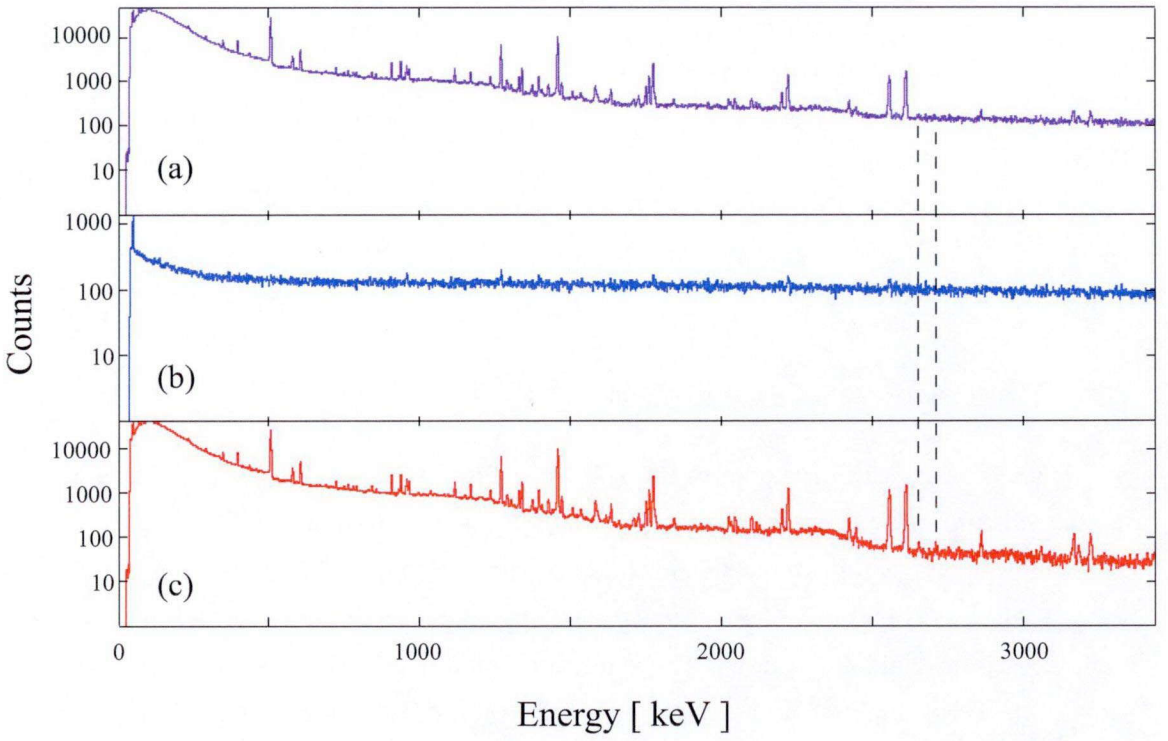

Figure 5.4: ADC spectra of (a) raw data (energy is calibrated), (b) β ray, and (c) γ ray in the experiment of ^{29}Na. In (c), γ-ray peaks can be confirmed which are not seen in ADC raw data (a) as indicated by dotted lines.

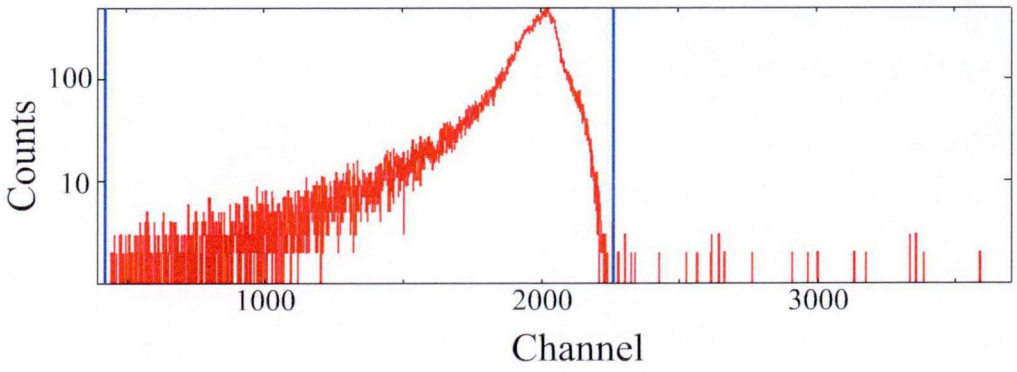

Figure 5.5: Time different spectrum of Ge detector and plastic scintillator in the same telescope in the experiment of ^{28}Na.

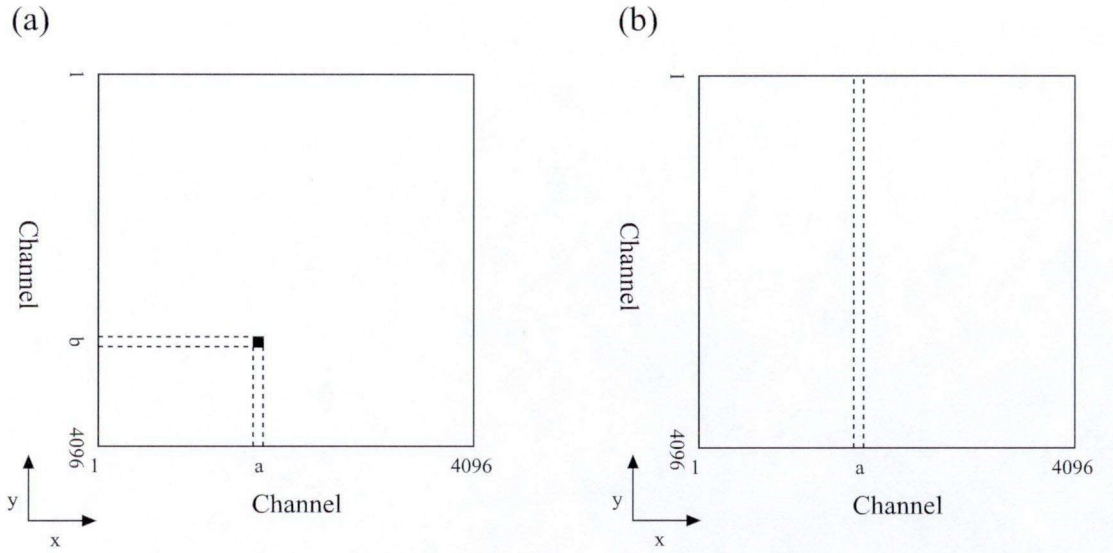

Figure 5.6: (a) Schematic figure of matrix data array. When coincidence data of x ch and y ch was detected, the data of [x][y] is filled. (b) Schematic figure of matrix analysis. When a ch of x-axis is chosen, y-projected spectrum is obtained.

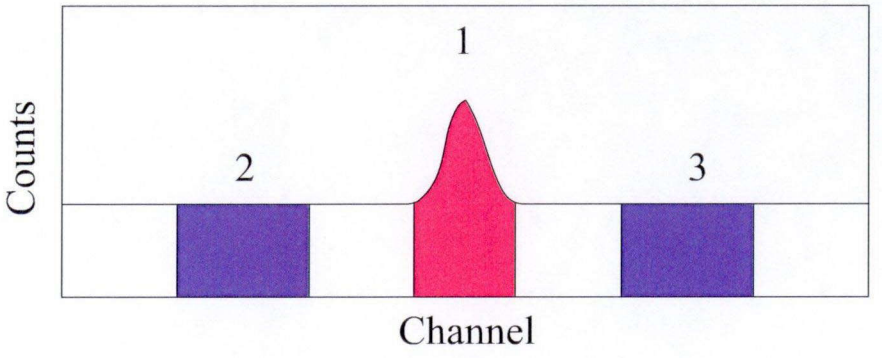

Figure 5.7: Schematic illustration of background subtraction in γ-γ analysis.

ure 5.7 shows a schematic illustration of background subtraction in γ-γ coincidence analysis. The coincidence events by the background region ("2" and "3" in Fig. 5.7) are subtracted from the coincidence events of the peak ("1" in Fig. 5.7) after normalizing by channel number. Then, we obtain the coincidence energy spectrum gated purely on the γ-ray.

CHAPTER VI

Analysis of experimental data and results: ^{28}Mg

6.1 Levels observed for the first time in β decay of ^{28}Na

Figure 6.1 shows the projection spectrum of γ-γ coincidence data. Peaks with asterisks, closed squares, triangles and circles denote the γ-ray peaks of ^{28}Mg, ^{28}Al, ^{28}Si and background, respectively. By the β-γ and γ-γ coincidence relations, twenty-four peaks with asterisks were found as the transitions in ^{28}Mg. Their energies and intensities are listed in Table 6.2. It is to be noted that seven γ rays (1373, 1991, 2008, 2192, 2291, 2907, and 4443 keV) have been newly observed in the present work. Six γ rays of 1152, 2548, 3405, 3694, 3995, and 5193 keV, which were observed in the ^{26}Mg$(t,p)^{28}$Mg reaction [FIS73; RAS74], were also newly found as the transitions after the β decay of ^{28}Na. The rest five γ rays (1474, 2388, 3081, 3088, and 5269 keV) depopulating the levels at 1.474, 3.862, 4.555, 4.562, and 5.269 MeV were confirmed.

The cascade relations between these transitions were examined by the analysis of γ-γ coincidence with a time window of $\pm$400 ns, as shown in Table 6.1. The symbol $\bigcirc$ ($\times$) denotes that the γ-ray peak was (not) observed in the gated spectrum. As will be discussed in the following, a new decay scheme of ^{28}Na has been established as shown in Fig. 6.2. Asterisks in the figure indicate new findings.

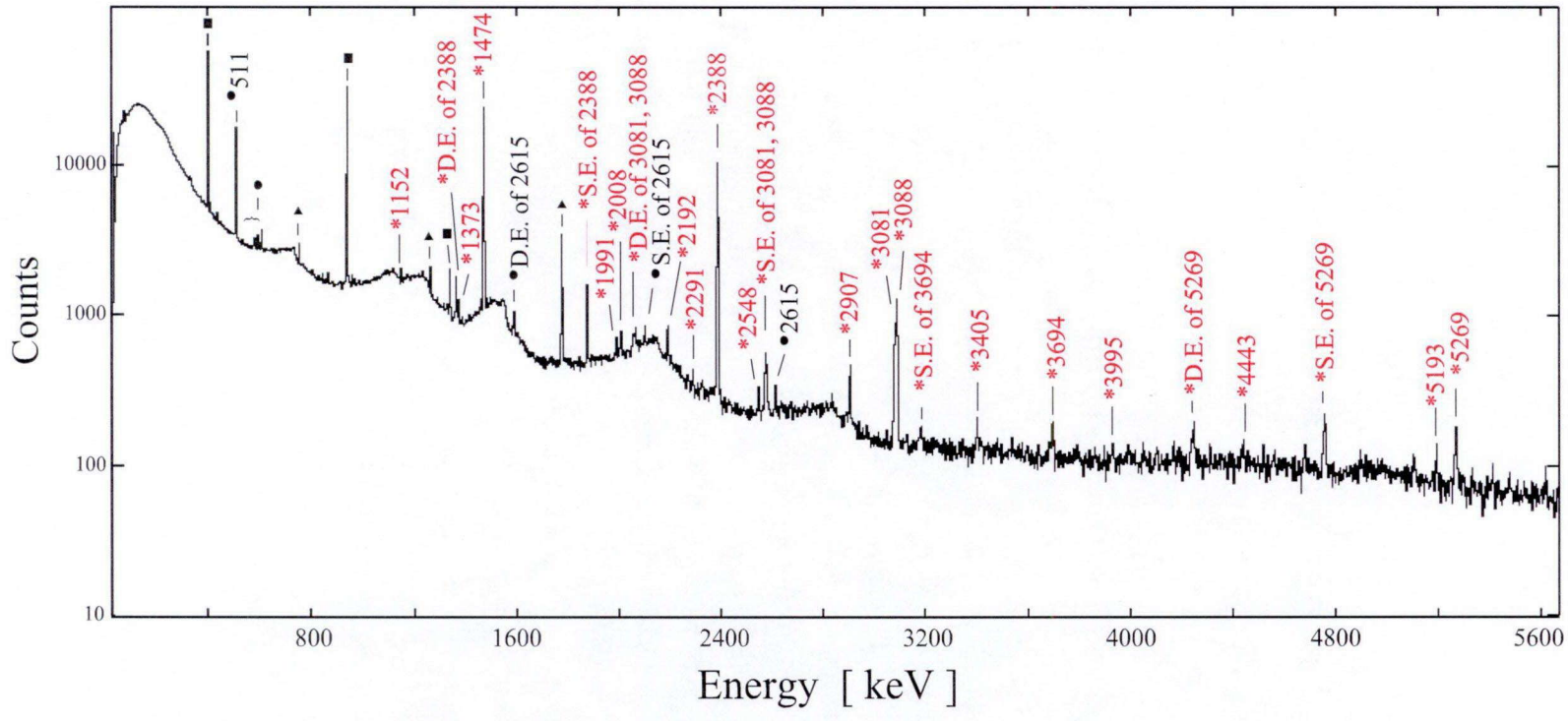

Figure 6.1: Total projection spectrum of γ-γ coincidence data for ^{28}Mg. The γ rays of ^{28}Mg attributed to the β decay of ^{28}Na are labeled with asterisks and the corresponding γ-ray energies in keV. The peaks of ^{28}Al, ^{28}Si, and background are labeled with open circle, triangle, and square, respectively.

Table 6.1: Coincidence relations of γ rays in ^{28}Mg observed in the present work: Whether or not the γ ray peak was observed in the gated spectrum is displayed by a ◯ or a ×, respectively.

gated by \ coincident	1152	1373	1474	1991	2008	2192	2291	2388	2548	2907	3081	3088	3405	3694	3995	4443	5193	5269
1152	–	◯	◯	×	×	×	×	×	◯	×	×	×	×	×	×	×	×	×
1373	◯	–	◯	×	×	×	×	×	×	×	×	×	×	×	×	×	×	×
1474	◯	◯	–	◯	×	×	×	◯	◯	◯	◯	◯	◯	◯	◯	◯	×	×
1991	×	×	◯	–	×	×	×	×	×	×	◯	×	×	×	×	×	×	×
2008	×	×	×	×	–	×	×	×	×	×	×	×	×	×	×	×	◯	×
2192	×	×	×	×	×	–	×	×	×	×	×	×	×	×	×	×	×	◯
2291	×	×	×	×	×	×	–	×	×	×	×	×	×	◯	×	×	×	×
2388	×	×	◯	×	×	×	×	–	×	×	×	×	×	×	×	×	×	×
2548	◯	◯	◯	×	×	×	◯	×	–	×	×	×	×	×	×	×	×	×
2907	×	×	◯	×	×	×	×	×	×	–	◯	×	×	×	×	×	×	×
3081	×	×	◯	◯	×	×	×	×	×	◯	–	×	×	×	×	×	×	×
3088	×	×	◯	×	×	×	×	×	×	×	×	–	×	×	×	×	×	×
3405	×	×	◯	×	×	×	×	×	×	×	×	×	–	×	×	×	×	×
3694	×	×	◯	×	×	×	◯	×	×	×	×	×	×	–	×	×	×	×
3995	×	×	◯	×	×	×	×	×	×	×	×	×	×	×	–	×	×	×
4443	×	×	◯	×	×	×	×	×	×	×	×	×	×	×	×	–	×	×
5193	×	×	×	×	◯	×	×	×	×	×	×	×	×	×	×	×	–	×
5269	×	×	×	×	×	◯	×	×	×	×	×	×	×	×	×	×	×	–

6.2 Energy levels and γ transitions observed for the first time in the β decay of ^{28}Na

The high efficiency of γ-γ coincidence measurements in the present work enabled us to find three γ rays from the known levels; the 4443-keV transition depopulating the 5.917-MeV level and 1373- and 1991-keV γ rays emitted from the 6.545-MeV level (see Table 6.2 and Fig. 6.2). These levels have been found in the ^{26}Mg$(t,p)^{28}$Mg reaction experiment [HIN61], but not observed in the β decay of ^{28}Na. The present work established the first observation of the β decays to these levels, as shown by the β-decay paths with asterisks in Fig. 6.2. Since it was confirmed that there were no γ rays populating these levels, the β decay intensities to the respective levels were determined directly from the intensities of the newly found γ rays, as listed in Table 6.2 and Table 6.3.

Small peaks at 1152, 2548, 3694, and 5193 keV in Fig. 6.1 are found as the transitions depopulating the known levels found in the ^{26}Mg$(t,p)^{28}$Mg reaction [FIS73; RAS74]. These levels have not been observed in the β decay of ^{28}Na[5]. It was found that the 5.193-MeV level ($I = 1$) is populated by the 2008-keV γ ray which depopulates a new level at 7.200 MeV (The new levels found in the present work will be discussed in Sec. 6.3). From the γ-ray intensity balance, the branching ratio of β decay to the 5.193-MeV level was estimated to be negligibly small. This forbidden nature suggests negative parity of this level which agrees with the first assignment of 1^- [MID64], whereas the later assignments removed the parity assignment [GUI84; NND11]. The 1152- and 3694-keV γ rays have their origins in the 5.171 MeV level ($I^\pi = 3^-$). Also the 2548-keV γ ray is assigned as the transition from the 4.021-MeV level (4^+) to the first 2^+ level at 1.474 MeV. The resultant negligibly small β-decay branching ratios to these levels support the previous spin-parity assignments.

The known γ rays of 3405 and 3995 keV, which depopulate the levels at 4.878 ($I^\pi = 2^+$) and 5.468 ($I = 2$) MeV, respectively, were also observed in the present work. Although these levels were reported in the β decay of ^{28}Na [GUI84; DET79], the detail is not clear. Accordingly, the β decays to these levels were not adopted in Ref. [NND11]. In the present work, the β decays were established for the first time and the β-decay branching ratios were determined to be 0.2(1) and <0.1% for the 4.878- and 5.468-MeV levels, respectively.

[5]The β-decay branch to the 5.193-MeV level was reported in Ref. [GUI84], but not adopted in their decay scheme of ^{28}Na.

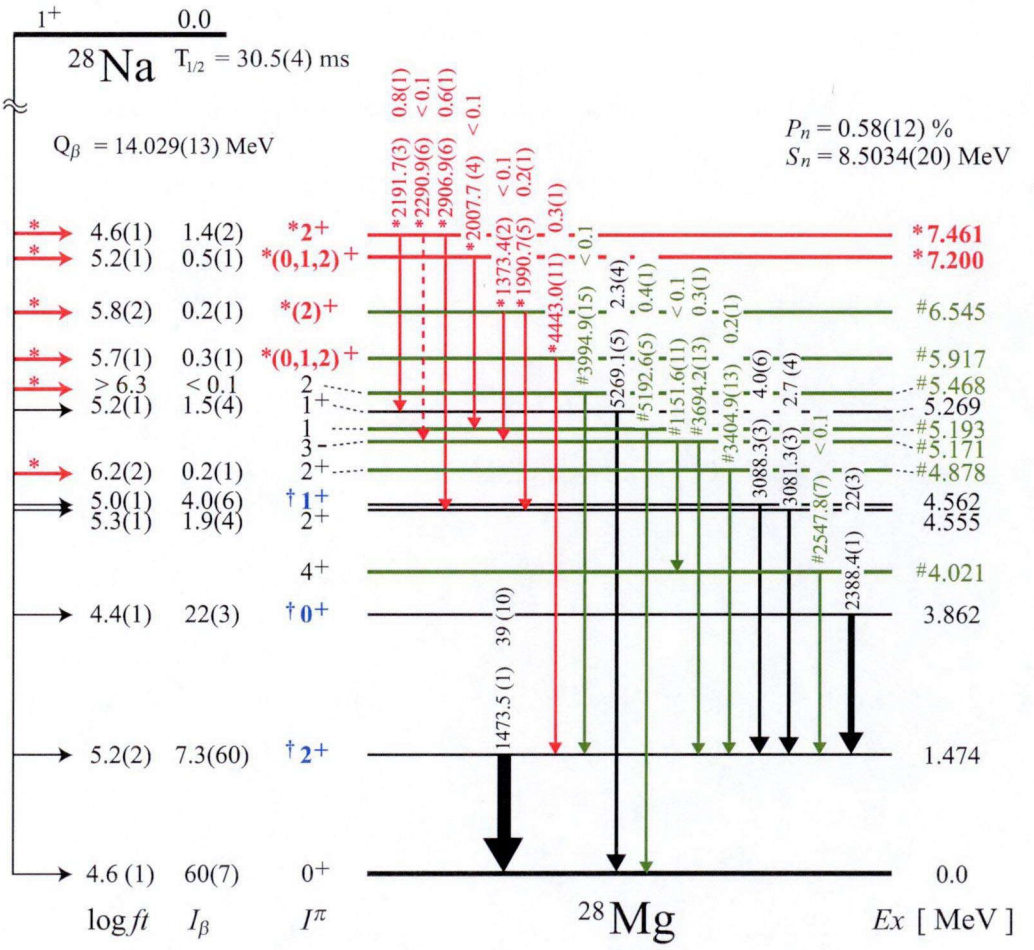

Figure 6.2: Revised decay scheme of ^{28}Na. The newly observed γ rays, β transitions, and energy levels, and newly assigned spins and parities in the present work are indicated by asterisks in red color. The spins and parities which were reconfirmed in the present work are indicated by daggers in blue color. The energy levels and γ rays which has been reported in the ^{26}Mg$(t,p)^{28}$Mg reaction experiments [HIN61; FIS73; RAS74] and firstly observed in the β decay of ^{28}Na in the present work are denoted by sharps in green color. Reported values of $T_{1/2}$ [ROE74], Q_β [AUD03], P_n [ROE74], and S_n [AUD03] are also shown.

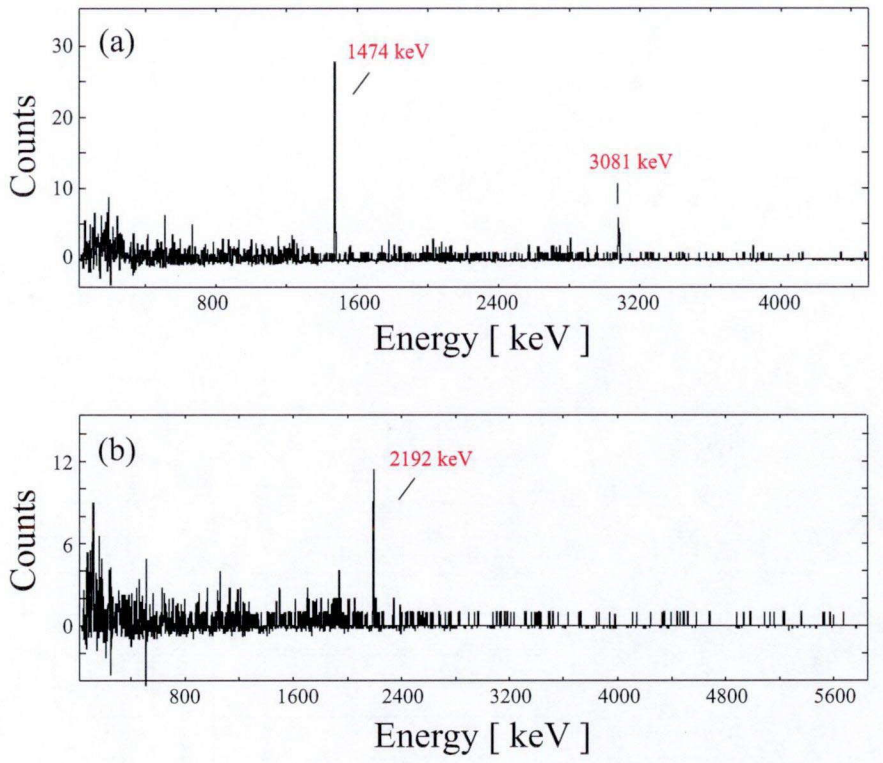

Figure 6.3: Gamma-ray energy spectrum gated on the γ rays of (a) 2907 keV and (b) 5269 keV.

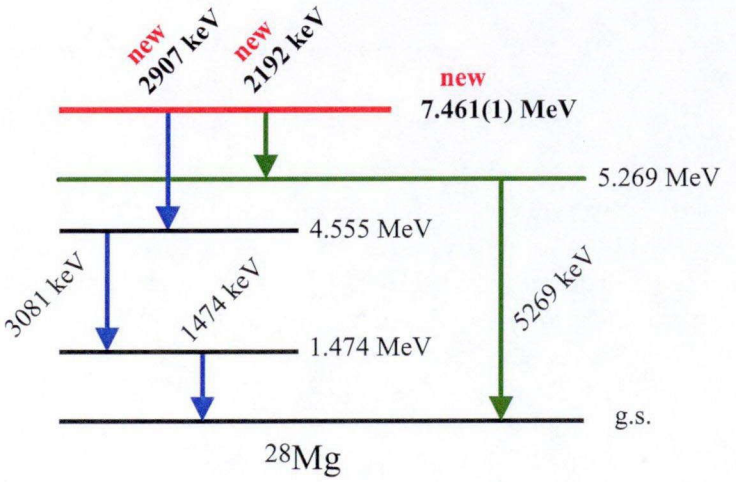

Figure 6.4: Partial level scheme of ^{28}Mg. New energy level at 7.461(1) MeV was proposed by the cascade lines of 1474-3081-2192 keV and 5269-2907 keV.

6.3 New levels at 7.200 and 7.461 MeV

In the present work, four more γ-ray peaks were newly found at 2008, 2192, 2291, and 2907 keV. Their origins could not be assigned to the known levels in ^{28}Mg. From the γ-ray coincidence relations, two levels with small logft values were newly established in the excitation-energy region between the reported highest 6.759-MeV level [HIN61] and the neutron-threshold energy (around 8.5 MeV): the higher one at 7.461 MeV [logft = 4.6(1)] and lower one at 7.200 MeV [5.2(1)] (see Fig. 6.2). The new level assignment will be discussed below.

Fig. 6.3(a) and (b) show the γ-ray energy spectra gated on the 2907 and 5269 keV, respectively. The newly observed 2907-keV γ ray was coincident with the 1474- and 3081-keV γ rays. Similarly the new 2192-keV γ ray was found in coincidence with the 5269-keV γ ray. The sum energies of these cascade γ rays, 1473.5(1) + 2906.9(6) + 3081.3(3) = 7461.7(7) and 2191.7(3) + 5269.1(5) = 7460.8(6) keV were consistent with each other. Therefore, the energy of the new level was determined to be 7.4611(4) MeV.

The 2291-keV γ ray was newly found in the projection spectrum of γ-γ coincidence data in Fig. 6.1. Figure 6.5(a)−(c) show the γ-ray energy spectra gated on the 1152-keV (5.171 $\rightarrow$ 4.021 MeV), 3694-keV (5.171 $\rightarrow$ 1.474 MeV), and 2548-keV (4.021 $\rightarrow$ 1.474 MeV) γ rays, respectively. The 1373-keV γ transition (6.545 $\rightarrow$ 5.171 MeV) can be confirmed in all the energy spectra, whereas the 2291-keV γ ray was not confirmed in the γ-ray energy spectrum gated on the 1152-keV γ ray [Fig.6.5(a)]. In the γ-ray energy spectrum gated on the 2291-keV γ ray as shown in Fig. 6.5(d), the 3694 keV (5.171 $\rightarrow$ 1.474 MeV) γ transition can only be observed. Although the coincidence relation of the 2291-keV γ ray was confirmed to be incomplete, we propose the placement of this γ transition indicated by the dashed line in Fig. 6.2, because the energy difference between the levels, 2289(1) keV [= 7461(1) − 5172(1)], is consistent with this γ-ray energy 2290.9(6) keV within 2σ accuracy.

Another newly found 2008-keV γ ray was coincident only with the 5193-keV γ ray (5.193 MeV $\rightarrow$ g.s.). This observation required another new level and the excitation energy was reasonably determined to be 7.2003(6) MeV [= 5.1926(5) + 2.0077(4)].

All the γ-ray energy spectra gated on the γ rays in ^{28}Mg except for the ones gated on the 1152-, 2291-, 2548-, 2907-, 3694-, and 5269-keV γ rays which are represented in this chapter (Fig. 6.3 and 6.5) are shown in Fig. A.1 to A.12 in Appendix A.

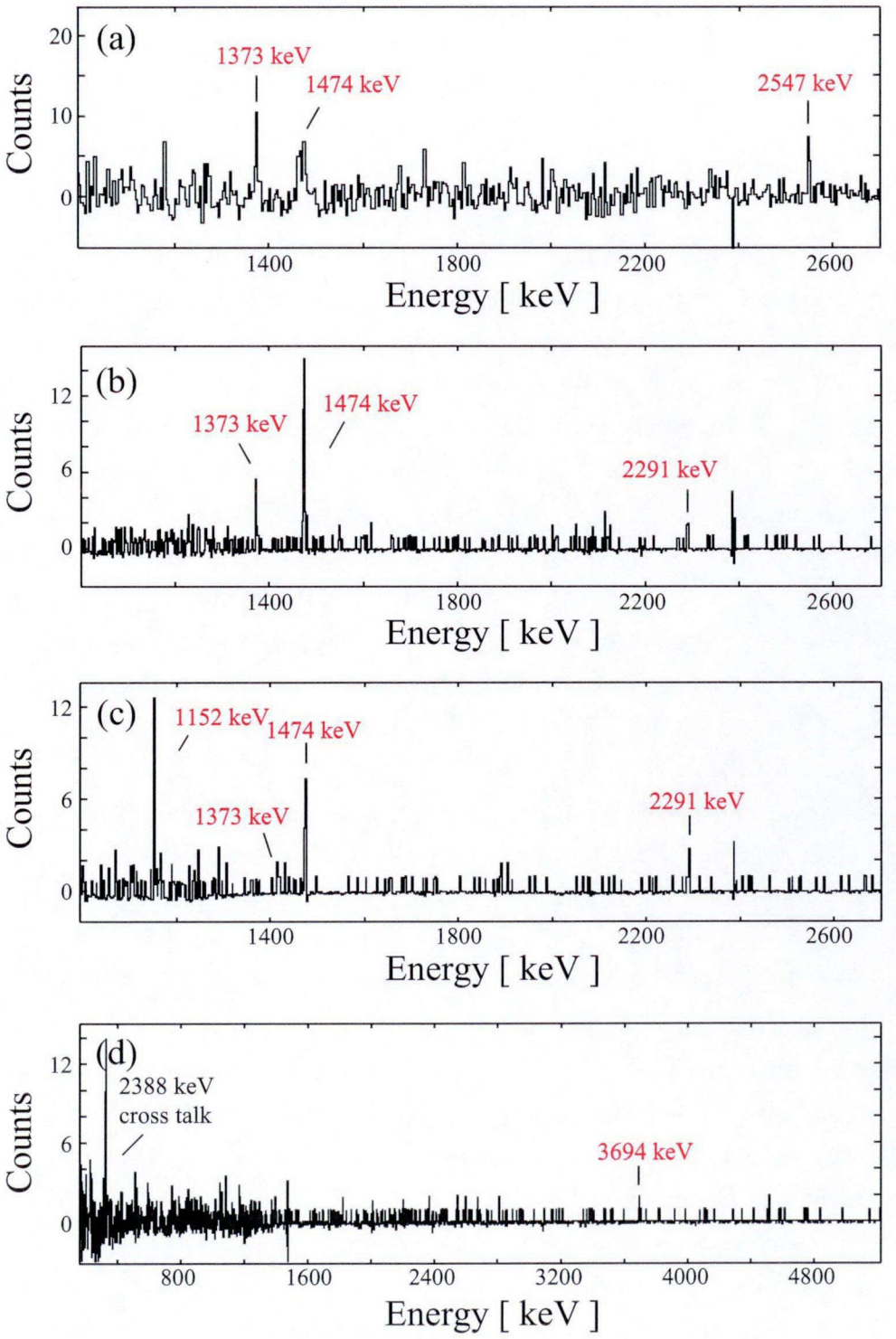

Figure 6.5: Gamma-ray energy spectra in coincidence with the γ rays of (a) 1152 keV, (b) 3694 keV, (c) 2548 keV, and (d) 2291 keV.

Table 6.2: Gamma transitions in ^{28}Mg observed in present work. E_i and E_f are the energies of initial and final levels, respectively. The intensities are shown in percent of ^{28}Na β decay.

E_γ [keV][a]	$E_i \rightarrow E_f$	I_γ [%][a]	E_γ [keV][b]	I_γ [%][c]
1151.6(11)	5.913 → 4.021	<0.1	1151.5(8)	–
1373.4(2)	6.545 → 5.913	<0.1	–	–
1473.5(1)	1.474 → g.s.	37(5)[d]	1473.4(7)	37(5)
1990.7(5)	6.545 → 4.555	0.2(1)	–	–
2007.7(4)	7.000 → 5.193	0.5(1)	–	–
2191.7(3)	7.461 → 5.269	0.8(1)	–	–
2290.9(6)	7.461 → 5.171	<0.1	–	–
2388.4(1)	3.862 → 1.474	22(3)	2389.1(8)	18.7(25)
2547.8(7)	4.021 → 1.474	<0.1	2546.6(9)	–
2906.9(6)	7.461 → 4.555	0.6(1)	–	–
3081.3(3)	4.555 → 1.474	2.7(4)	3083.4(8)	1.3(3)
3088.3(3)	4.562 → 1.474	4.0(6)	3087.4(7)	2.6(5)
3404.9(13)	4.878 → 1.474	0.2(1)	3404.9(11)	–
3694.2(13)	5.171 → 1.474	0.3(1)	3698.1(8)	–
3994.9(15)	5.468 → 1.474	<0.1	3995.3(11)	–
4443.0(11)	5.917 → 1.474	0.3(1)	–	–
5192.6(5)	5.193 → g.s.	0.4(1)	5190(3)	–
5269.1(5)	5.267 → g.s.	2.3(4)	5271.7(8)	0.50(15)

[a]Present work.
[b]Taken from Ref. [RAS74].
[c]Taken from Ref. [END90].
[d]Taken from Ref. [NND11].

Table 6.3: The ^{28}Mg levels observed in the β decay of ^{28}Na. Asterisks indicate that the β-decay branching ratios (I_β) to these levels were less than the sensitivity of the present measurement.

E_x [MeV]	I_β [%][a]	I_β [%][b]	log ft[a]	log ft[b]
g.s.	60(7)	63(6)	4.6(1)	4.57(5)
1.4735(1)	7.3(60)	14(6)	5.2(2)	4.99(19)
3.8619(1)	22(3)	19(3)	4.4(1)	4.42(8)
4.0213(7)	*	–	*	–
4.5548(3)	1.9(4)	1.3(3)	5.3(2)	5.43(11)
4.5618(3)	4.0(6)	2.6(5)	5.0(1)	5.13(9)
4.878(1)	0.2(1)	–	6.2(2)	–
5.1713(7)	*	–	*	–
5.1926(5)	*	–	*	–
5.2691(5)	1.5(4)	0.50(15)	5.2(1)	5.68(14)
5.468(1)	<0.1	–	>6.3	–
5.917(1)	0.3(1)	–	5.7(1)	–
6.5452(5)	0.2(1)	–	5.8(2)	–
7.2003(6)	0.5(1)	–	5.2(1)	–
7.4611(4)	1.4(2)	–	4.6(1)	–

[a]Present work.
[b]Taken from Ref. [END90]

6.4 Gamma-ray intensities and β-decay branching ratios

The absolute intensities would have been deduced by normalizing the intensity of 1342-keV γ transition in the granddaughter nucleus ^{28}Al, if the ^{28}Na beam intensity had been stable enough during a time span of the order of ^{28}Mg half-life (20.9 hours). In the present work, the intensities were estimated by normalizing the ^{28}Mg 1474-keV γ-ray intensity to the previously reported value of 37(5)% [NND11].

The γ-ray intensities were evaluated based on the counts in the Ge detector (Right) placed along the polarization direction, assuming isotropic γ-ray emission. However, possible residual polarization in the ^{28}Mg levels may cause anisotropic γ-ray emission [MOR76]. From the observed 90°/0° anisotropy for the most polarization-affected $2^+ \rightarrow 0^+$ transition of the 1474-keV γ ray, it was found that the isotropic assumption underestimates the γ-ray intensities by 7%. The effect in other transitions should be less than this amount. The intensities listed in Table 6.2 do not include this ambiguity.

6.5 Polarization of ^{28}Na

To deduce the β-decay asymmetry parameter A for each β transition from Eq. (3.8), the polarization P has to be known. The polarization P can be evaluated by using the β transition which populates the level with known spin. Therefore, we selected the $^{28}\mathrm{Na}_{\mathrm{g.s.}}(1^+) \rightarrow {}^{28}\mathrm{Mg}_{\mathrm{g.s.}}(0^+)$ transition by setting a β-ray energy gate on a range 9.7−11.4 MeV to cut off the transitions to the excited levels in ^{28}Mg. These gate energies were determined by taking into account the β-ray energy losses in the materials between the Pt stopper and the Ge detector. The AP value was obtained to be $-0.283(5)$. Since the asymmetry parameter of this transition is $A = -1$, the polarization P was deduced to be 28.3(5)%. This value is smaller than the reported one [MIN05]. This reduction may be caused by the spin-relaxation in the Pt foil, because the external magnetic field was lower than in the reported experiment.

6.6 Spin-Parity assignments of ^{28}Mg levels

In the present work, the β decay to the 2^+ level at 4.878 MeV [MID64] was observed for the first time. Since its logft value was determined to be 6.2(2), all the decays with log$ft \leq 6.2$ can be regarded as GT transitions. As a result, the levels associated with log$ft \leq 6.2$ are assigned to be of positive parity. Spins of these levels were assigned in the present work as discussed in this subsection. The assigned spins and parities for the levels

at 1.474, 3.862, and 4.562 MeV were consistent with the reported ones [END90]. This fact demonstrates the effectiveness of the present method. It is to be emphasized that the newly found 7.461-MeV level was assigned to be 2^+.

6.6.0.1 Spin-parity of the 1.474-, 3.862- and 4.562-MeV levels

The details of spin assignment are discussed here in the order of simplicity. Since the levels at 3.862 and 4.562 MeV are not populated by the γ transitions from the higher levels, the asymmetry parameters of the β decay to these levels were obtained by simply counting the γ rays of 2388 and 3088 keV in coincidence with the β rays (see Fig. 6.2). Figure 6.6 shows the γ-ray energy spectra around the 2388-keV peak in four patterns according to the polarization direction (+ or −) and the β-ray detector (L or R) expressed as the Eq. (3.4) to (3.7). Larger peak counts of N_R^+ and N_L^- than those of N_R^- and N_L^+ indicate a positive and sizable asymmetry (see Eq. (3.8)). From the peak counts in Fig. 6.6, the value of $A_{3.862}$ was obtained to be $-0.85(6)$ (Hereafter the asymmetry parameter of the β decay to the daughter level with excitation energy E is expressed as A_E). Among the expected values of A in Table 3.1, $A = -1$ ($I^\pi = 0^+$) is mostly consistent with the experimental result. Thus the 3.862-MeV level was assigned to be 0^+. This assignment agrees with the previous one [MID64].

In the same way, $A_{4.562} = -0.54(19)$ was obtained from the 3088-keV γ-ray counts in coincidence with β ray. This result enabled 1^+ assignment for the 4.562-MeV level. Note that the spin-parity assignment is again consistent with the reported one [END90].

The first excited level of ^{28}Mg at 1.474 MeV is populated not only by the direct β transition, but also by eight γ transitions from higher levels (see Fig. 6.2). In order to select the direct β transition, we set the β-ray energy gate with $E_\beta = 7.7 - 9.7$ MeV so that the β transitions to the levels higher than the 3.862-MeV level were rejected. Figure 6.7 shows the γ-ray energy spectra around the 1474-keV peak in 4 patterns according to the direction of polarization (+ or −) and the β-ray detector (L or R) in coincidence with above mentioned β-ray energy range. From these γ-ray counts, $A_{1.474} = 0.48(3)$ was obtained, indicating very reasonable assignment of 2^+ for the first excited state [END90].

Figure 6.8 compares the experimental asymmetry parameters of $A_{1.474}$, $A_{3.862}$, and $A_{4,562}$ with the expected 3 values. It is seen that the value of $A_{3.862}$ is somewhat away beyond the 1σ error range from the expected value of $A = -1.0$. It must be due to the assumption on the β-ray emission angle θ, as mentioned in Sec. 3.2.

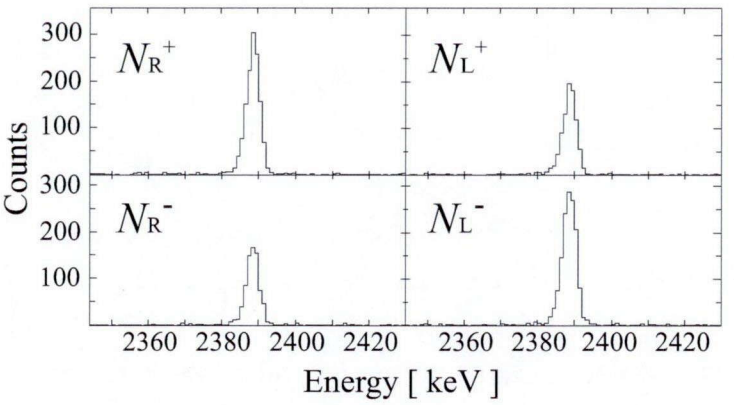

Figure 6.6: Gamma-ray energy spectra around the 2388-keV peak in coincidence with the β rays detected in the Left (L) or Right (R) detector when polarization is in the direction to the R-detector (+) or L-detector (−).

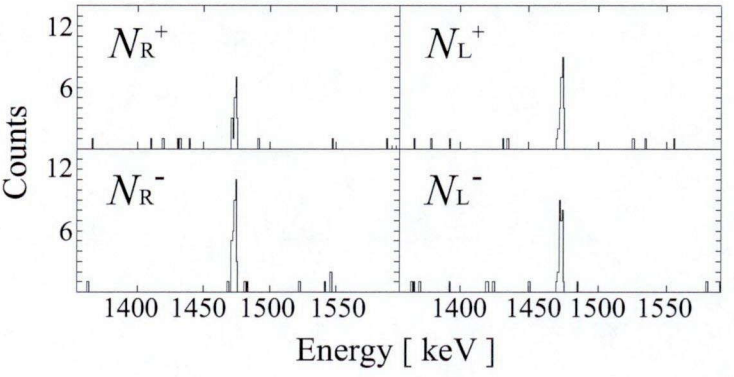

Figure 6.7: Peaks of the 1474-keV γ ray coincident with β rays of $E = 7.7 - 9.7$ MeV.

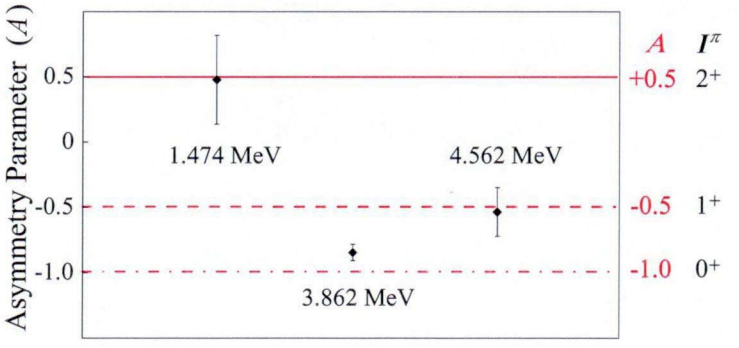

Figure 6.8: Asymmetry parameters of the β transitions to the 1474-, 3.862-, and 4.562-MeV levels.

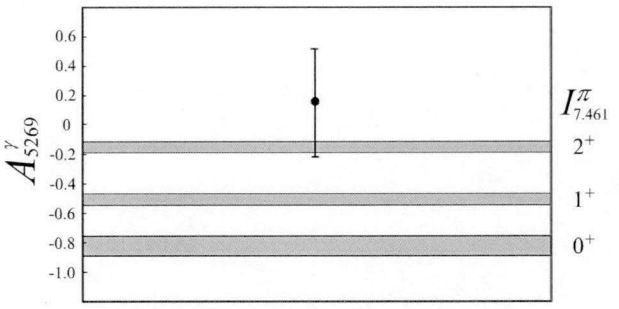

Figure 6.9: Asymmetry parameter of β decay in coincidence with the 5269-keV γ ray.

6.6.0.2 Spin-parity of the new level at 7.461 MeV

The intensities of γ rays deexciting the new level at 7.461 MeV were too weak to determine the asymmetry parameter of $A_{7.461}$. Therefore, the following indirect method of spin assignment was used, based on discussion in Sec. 3.3.3. The key is the known 1^+ assignment for the 5.269-MeV level. Because of the cascade relation of the 2192-keV (7.461 MeV $\rightarrow$ 5.269 MeV) and 5269-keV (5.269 MeV $\rightarrow$ g.s.) transitions, the relation in Eq. (3.14) is applied as

$$A^{\gamma}_{5269} = A_{5.269} \times \frac{I^{5.269}_{\beta}}{I^{5269}_{\gamma}} + A_{7.461} \times \frac{I^{2192}_{\gamma}}{I^{5269}_{\gamma}}, \tag{6.1}$$

where the asymmetry parameter A^{γ}_{5269} is deduced by the β-decay asymmetry in coincidence with the 5269-keV γ ray. Taking into account $A_{5.269}(1^+) = -0.5$ and transition intensities (I_{γ}, I_{β}) in Tables 6.2 and 6.3, the values of A^{γ}_{5269} were calculated for the three possible values of $A_{7.461}$. The results are compared with the experimental A^{γ}_{5269} as shown in Fig. 6.9. It is found that only 2^+ case is consistent with the experimental result. Thus the spin-parity of the 7.461-MeV level was assigned to be 2^+.

6.6.0.3 Spin-parity of the 6.545 MeV level

The level at 6.545 MeV was identified in the ^{26}Mg$(t,p)^{28}$Mg reaction [HIN61]. The present work observed the β decay to this level for the first time. The logft value of 5.8(2) indicates that the transition is allowed one.

The asymmetry parameter of the β decay leading to the 6.545-MeV level could not be determined because of weak intensities of the 1373- and 1991-keV γ rays which deexcite the 6.545-MeV level. Therefore, the spin-parity of this level was determined based on the

γ-transition probabilities as follows. The 1373- and 1991-keV γ rays populate the 5.171-(3^- [RAS74]) and the 4.555-MeV levels (2^+ [RAS74]), respectively, as shown in Fig. 6.2. The experimental intensities ($I_\gamma^{\rm exp}$) and transition probabilities by Weisskopf estimate [$T_W(\sigma\lambda)$] for the transitions from the 6.545-MeV level are compared for the possible spin-parity of 0^+, 1^+, or 2^+ of this level in Table 6.4. It is found that the ratio of intensities can be explained by neither 0^+ nor 1^+ case even with hindrance or enhancement factor for the transition probabilities. In order to consider if the 2^+ assignment is reasonable, the hindrance factors of $E1$ and $M1$ transitions were examined as follows. The known half-life of the 5.171-MeV

Table 6.4: Experimental intensities ($I_\gamma^{\rm exp}$) and transition probabilities by Weisskopf estimates [$T_W(\sigma\lambda)$] for the γ transitions depopulating the 6.545-MeV level.

γ transition (keV)	$I_\gamma^{\rm exp}$ (%)	I^π(6.545 MeV)	$\sigma\lambda$	$T_W(\sigma\lambda)$ (Weisskopf estimate)
		0^+	$E3$	2.5×10^5
1373	< 0.1	1^+	$M2$	1.0×10^9
		2^+	$E1$	2.4×10^{15}
		0^+	$E2$	2.0×10^{11}
1991	0.2	1^+	$M1$	2.4×10^{14}
		2^+	$M1$	2.4×10^{14}

level ($T_{1/2} = 120$ fs [END90]) enables us to deduce the hindrance factors of $E1$ transitions for the transitions of 5.171 MeV(3^-) $\rightarrow$ 4.021 MeV(4^+) and 5.171 MeV(3^-) $\rightarrow$ 1.474 MeV(2^+) to be 10^{-3}–10^{-4}. Since the 1991-keV transition is most likely an ℓ-forbidden $M1$ transition, a hindrance factor of 10^{-2} is reasonably estimated [MOR76]. By taking these hindrance factors, the experimental data are consistent with the 2^+ assignment. Thus the spin-parity of the 6.545-MeV level is proposed to be $(2)^+$.

6.6.0.4 Other levels

Other three levels at 4.878, 5.468, and 5.917 MeV were also found as the final states of the ^{28}Na β decay for the first time. These levels have been identified in the ^{26}Mg(t,p)^{28}Mg reaction [HIN61]. The spins and parities of the 4.878- and 5.468-MeV levels were reported to be 2^+ and 2, respectively. The former assignment is consistent with the presently measured logft values of 6.2(2), as mentioned before. The spins and parities of the 5.917- and 7.200-MeV levels are newly proposed to be both $(0, 1, 2)^+$ based on logft = 5.7(1) and 5.2(1), respectively.

The spins and parities assigned in the present work are summarized in Table 6.5.

Table 6.5: Spins and parities of levels in ^{28}Mg.

E_x [MeV]	$I^{\pi a}$	$I^{\pi b}$	$I^{\pi c}$	$I^{\pi d}$	$I^{\pi e}$	$I^{\pi f}$
g.s.	0^+	0^+	0^+	0^+	0^+	0^+
1.474	2^+	2^+	2^+	2^+	2^+	2^+
3.862	0^+	0^+	(0, 1, 2)	0^+	0^+	0^+
4.021	4^+	–	4^+	4^+	4^+	4^+
4.555	2^+	2^+	2	2^+	2^+	2^+
4.562	1^+	–	–	1	1^+	1^+
4.878	2^+	2^+	2	2^+	2^+	2^+
5.171	3^-	(3^-)	3	3^-	–	3^-
5.193	1	–	1	1^-	1	1
5.269	1^+	0^+	–	1^-	$(1, 2, 3)^+$	1^+
5.468	2	–	2	2	2	2
5.673	–	2^+	–	–	–	2^+
5.702	–	0^+	–	0^+	0^+	0^+
5.917	$(0, 1, 2)^+$	–	–	–	–	–
6.545	$(2)^+$	–	–	–	–	–
7.200	$(0, 1, 2)^+$	–	–	–	–	–
7.461	2^+	–	–	–	–	–

[a]Present work.
[b]Taken from Ref. [MID64]
[c]Taken from Ref. [FIS73]
[d]Taken from Ref. [RAS74]
[e]Taken from Ref. [GUI84]
[f]Taken from Ref. [END90]

CHAPTER VII

Analysis of experimental data and results: ^{29}Mg

7.1 New γ transitions in ^{29}Mg

Figure 7.1 shows the total γ-ray energy spectrum of β-γ coincidence data in the β decay of ^{29}Na. The γ rays of ^{29}Mg in the β decay of ^{29}Na are clearly observed (labeled by asterisks and corresponding energies in keV in red color). The γ rays of ^{29}Al and ^{29}Si associated with the β decay of ^{29}Mg, and those of ^{28}Mg, ^{28}Al, and ^{28}Si in the β-n decay of ^{29}Na were also observed (labeled by closed circle). As will be discussed in the following, a new decay scheme of ^{29}Na has been established as shown in Fig. 7.2. New findings are labeled by asterisks in Fig. 7.2. We have confirmed all the β-delayed γ rays in ^{29}Mg reported in Ref. [BAU87], except for the two γ rays of 2445 and 2500 keV deexciting the level at 2.500 MeV. These two γ rays with very low intensities, 0.4(1) and 0.2(1), respectively, are out of sensitivity in the present experiment by the estimation from background noise in the energy spectrum. However, γ-γ coincidence analysis using nine Ge detectors enabled us to find new γ transitions of 1583 and 1794 keV shown as follows. The energy of the levels and γ rays in ^{29}Mg were re-evaluated in the present work.

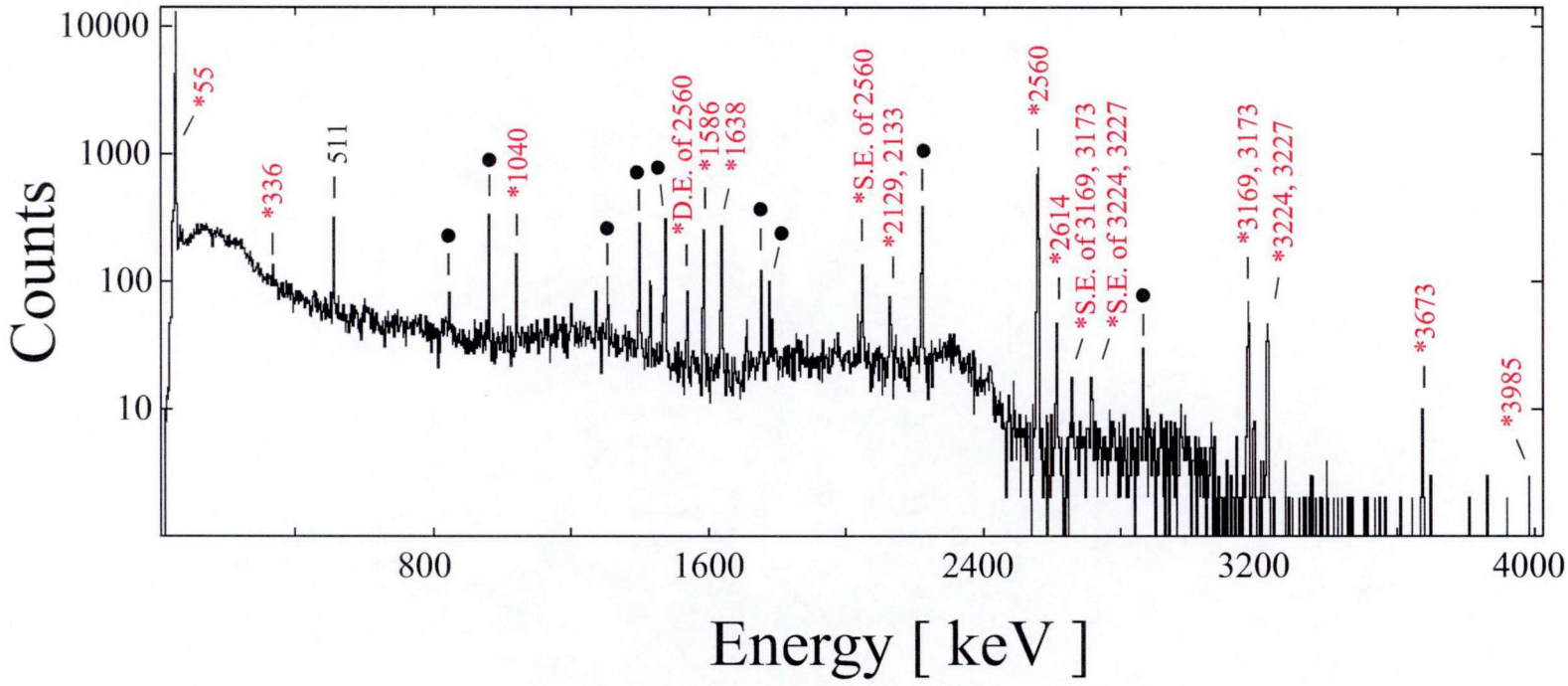

Figure 7.1: Gamma-ray energy spectrum of β-γ coincidence data in the β decay of ^{29}Na. The γ-ray peaks of ^{29}Mg are labeled by asterisk and the corresponding γ-ray energies in keV. The peaks of the descendants (^{29}Al, ^{29}Si, ^{28}Mg, ^{28}Al, and ^{28}Si) are labeled by closed circles.

The γ-ray peak of 336 keV found in Fig. 7.1 which was reported as the transition between levels at 1.431 and 1.095 MeV in ^{29}Mg in the β-n decay experiment of ^{30}Na [BAU89], was firstly observed in the β decay experiment of ^{29}Na in the present work. Figures 7.3(a) and (b) show the γ-ray spectra in coincidence with the γ rays of 336 and 1040 keV, respectively. The peaks indicated by black dots are the spurious peaks due to Compton cross talk between two Ge detectors. It is confirmed that the 336-keV γ ray is in coincidence with the 1040-keV γ ray. This assures the γ transition of 336 keV (1.430 $\rightarrow$ 1.095 MeV) reported in [BAU89].

In Fig. 7.3(a), γ-ray peak of 1794 keV is also observed. By the γ-γ coincidence analysis gated on the 1794 keV shown in Fig. 7.3(c), the 1794-keV γ ray was confirmed to be in coincidence with the 55-, 336-, and 1040-keV γ rays. We propose the new γ transition of 1794 keV (3.223 $\rightarrow$ 1.430 MeV) from the consistent energy of $55+1040+336+1794 = 3223$. It is strongly suggested that this transition is the same as the one observed and left unplaced in the single-neutron knockout experiment of ^{30}Mg [TER08].

The γ-ray energy spectrum gated on range of 1582$-$1587 keV is shown in Fig. 7.3(d). The γ-ray peak of 55 keV, which cannot be in coincidence with 1586-keV γ ray can be seen clearly. In the latest decay scheme of ^{29}Mg [NND11], the γ transitions of 1586 keV (3.223 $\rightarrow$ 1.638 MeV) and 55 keV cannot be in cascade relation unless the γ transition(s) which finally lead(s) to the 0.055-MeV level as shown in Fig. 7.4. No γ rays of 208 keV [$= 1638 - 1430$] and 543 keV [$= 1638 - 1095$] in Fig. 7.3(d) indicate that the small γ-ray peak next to the 1638 keV γ ray in Fig. 7.3(d) is doublet of 1583-keV and 1586-keV (3.223 $\rightarrow$ 1.638 MeV) γ rays with the consistent energy difference of $1638 - 55 = 1583$ keV. Thus, the new γ transition of 1583 keV (1.638 $\rightarrow$ 0.055 MeV) was proposed.

The coincidence relations investigated by the analysis of γ-γ coincidence with a time window of $\pm$400 ns are summarized in Table 7.1. The symbol $\bigcirc$ ($\times$) denotes that the γ-ray peak was (not) observed in the gated spectrum. All the γ-ray energy spectra gated on γ transitions in cascade relation in ^{29}Mg are listed in Fig. A.13 to A.17 in Appendix A, except for the ones gated on the 336, 1040, 1794, and 1582-1587 keV which are represented in this chapter (Fig. 7.3).

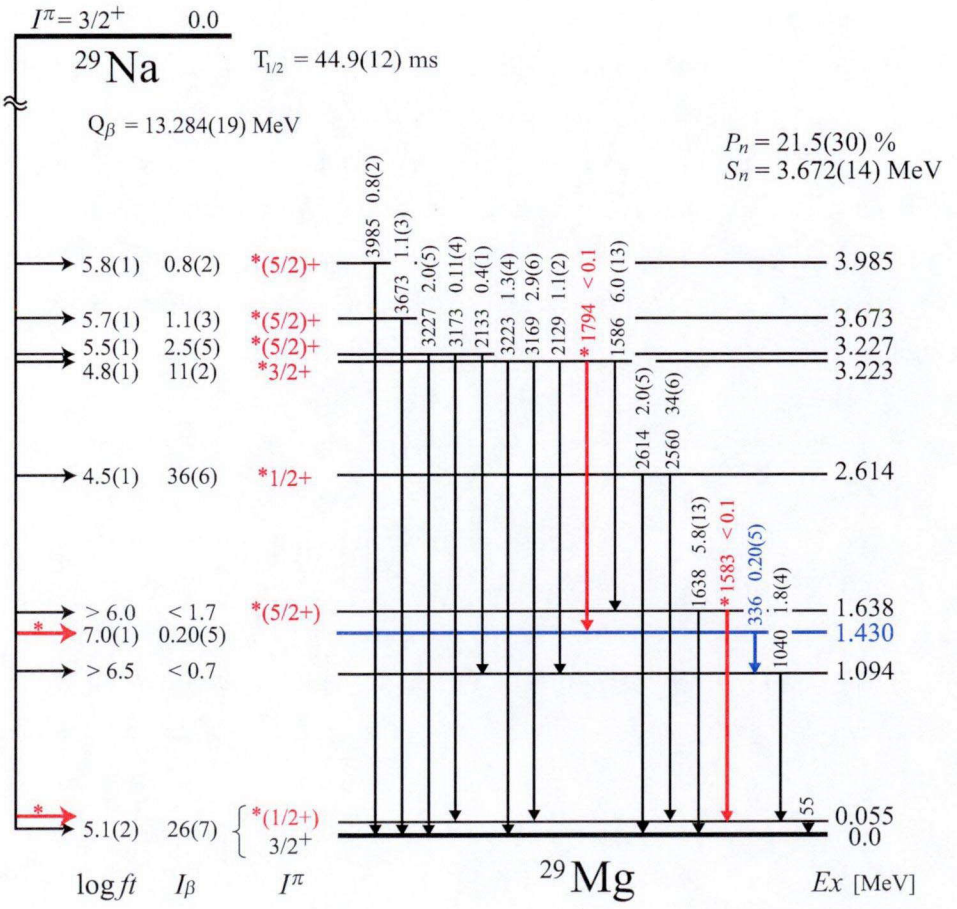

Figure 7.2: Revised decay scheme of ^{29}Na. The physical quantities and decay paths labeled by asterisks are newly found ones in the present work. The blue lines show the level and the γ transition observed in β-n decay of ^{30}Na [BAU89], and firstly observed in the β decay of ^{29}Na in the present work. Reported values of $T_{1/2}$ [GUI84], Q_β [AUD03], P_n [DET79], and S_n [AUD03] are also shown.

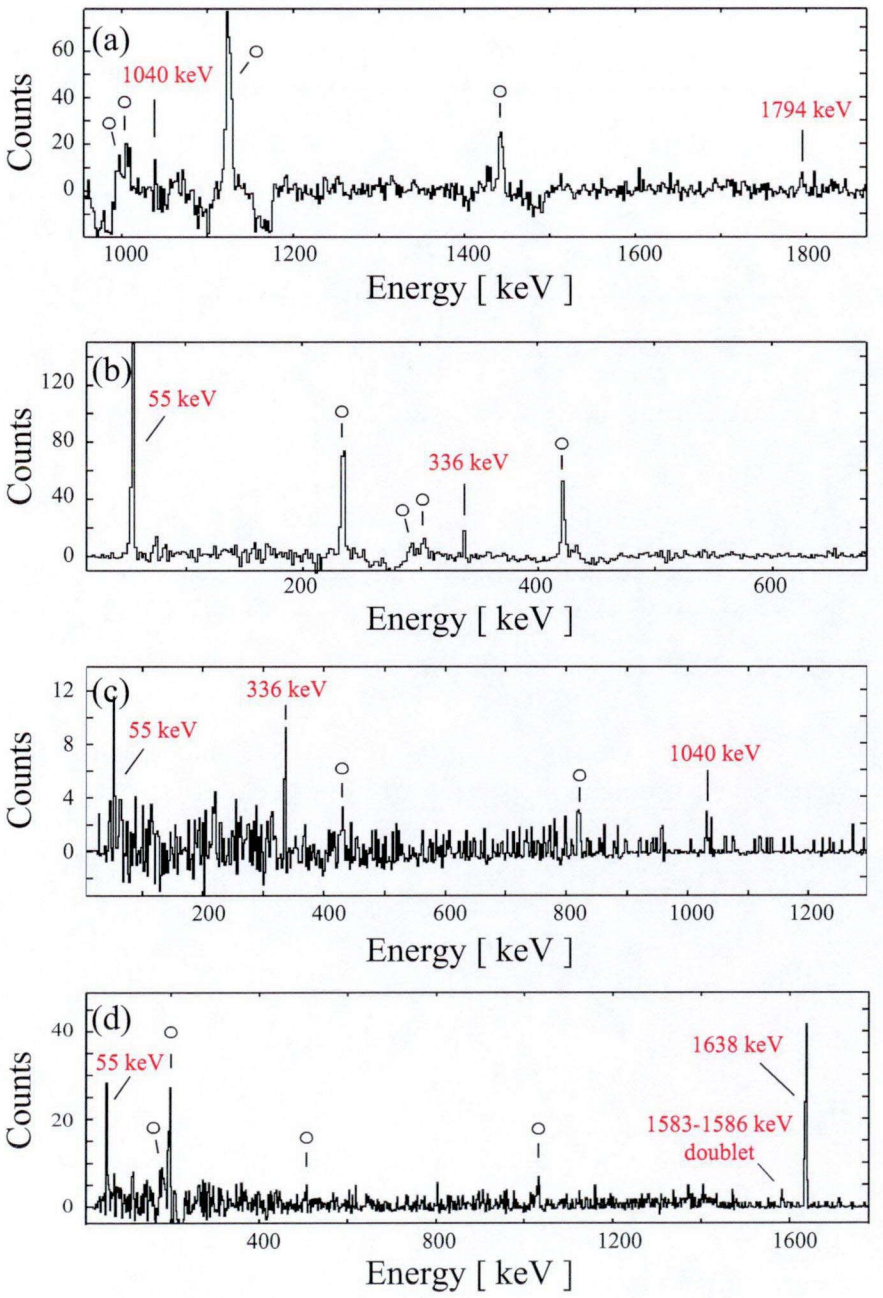

Figure 7.3: Gamma-ray energy spectrum in coincidence with the γ rays of (a) 336 keV, (b) 1040 keV, (c) 1794 keV, and (d) the energy range of 1582-1587 keV. The spurious peaks caused by Compton cross talk are labeled by open circles.

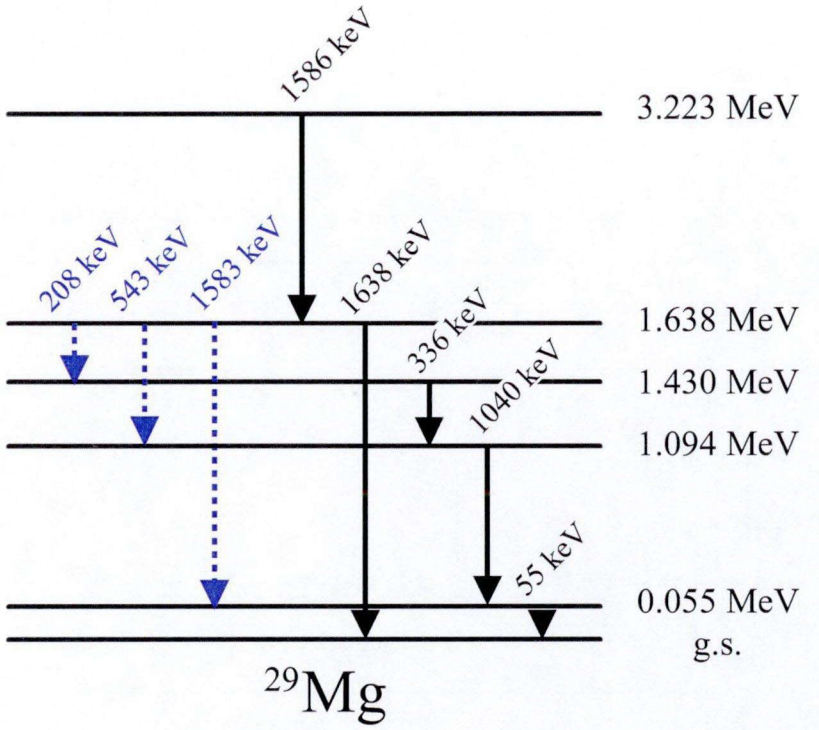

Figure 7.4: Partial level scheme of ^{29}Mg. Three γ transitions indicated by dashed lines in purple color are possible considered from Fig. 7.3(d).

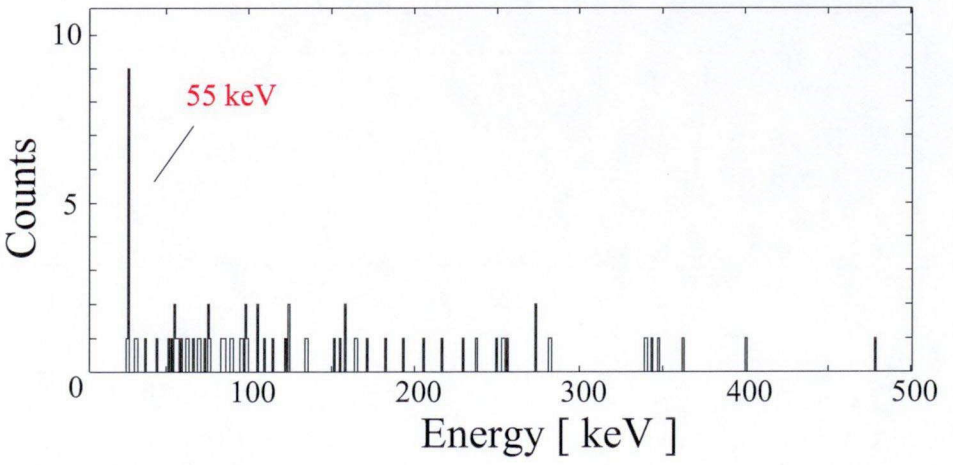

Figure 7.5: Gamma-ray energy spectrum in coincidence with the β ray with the energy over 12 MeV.

Table 7.1: Coincidence relations of γ rays in ^{29}Mg observed in the present work: Whether or not the γ ray peak was observed in the gated spectrum is displayed by a ◯ or a ×, respectively.

gated by \ coincident	55	336	1040	1583	1586	1638	1794	2129	2133	2560	2614	3169	3173	3223	3227	3673	3985
55	–	◯	◯	◯	◯	×	×	×	×	◯	×	×	×	×	×	×	×
336	◯	–	◯	×	×	×	◯	×	×	×	×	×	×	×	×	×	×
1040	◯	◯	–	×	×	×	×	×	×	×	×	×	×	×	×	×	×
1583	◯	×	×	–	◯	×	×	×	×	×	×	×	×	×	×	×	×
1586	◯	×	×	×	–	◯	×	×	×	×	×	×	×	×	×	×	×
1638	×	×	×	×	◯	–	×	×	×	×	×	×	×	×	×	×	×
1794	◯	◯	◯	×	×	×	–	×	×	×	×	×	×	×	×	×	×
2129	◯	◯	×	×	×	×	×	–	×	×	×	×	×	×	×	×	×
2133	◯	◯	×	×	×	×	×	×	–	×	×	×	×	×	×	×	×
2560	◯	×	×	×	×	×	×	×	×	–	×	×	×	×	×	×	×
2614	×	×	×	×	×	×	×	×	×	×	–	×	×	×	×	×	×
3169	◯	×	×	×	×	×	×	×	×	×	×	–	×	×	×	×	×
3173	◯	×	×	×	×	×	×	×	×	×	×	×	–	×	×	×	×
3223	×	×	×	×	×	×	×	×	×	×	×	×	×	–	×	×	×
3227	×	×	×	×	×	×	×	×	×	×	×	×	×	×	–	×	×
3673	×	×	×	×	×	×	×	×	×	×	×	×	×	×	×	–	×
3985	×	×	×	×	×	×	×	×	×	×	×	×	×	×	×	×	–

7.2 Beta decay to the 1st excited state in ^{29}Mg

In the result of Ref. [BAU87], the β decay of ^{29}Na to the 1st excited state in ^{29}Mg (0.055 MeV) was not confirmed and the sum of the β-decay intensity to the ground and the 1st excited states was reported. In the present experiment, the β decay to the 0.055-MeV level was observed for the first time. Fig. 7.5 shows the γ-ray energy spectrum in coincidence with the β ray with the energy over 12 MeV, which corresponds to the end point energy of the ^{29}Na$_{\mathrm{g.s.}}$ $\rightarrow$^{29}Mg (1.094 MeV) β ray. The attenuation of β-ray energy in the materials between Ge crystal and Pt stopper (Pt stopper, FRP chamber, plastic scintillators, and Al cap of Ge detector) was estimated to be $\sim$2 MeV by using GEANT4 code [AGO03; ALI06]. By choosing energy above 12 MeV, the β ray from the ^{29}Na$_{\mathrm{g.s.}}$ to the ground or 1st excited state in ^{29}Mg can be selected. The 55-keV γ ray peak clearly seen in Fig. 7.5 indicates the evidence for the β decay to the 0.055-MeV level from ^{29}Na.

7.3 Gamma-ray intensities and β-decay branching ratios

Because of the residual polarization of levels in ^{29}Mg associated with the β decay of largely spin-polarized ^{29}Na, the anisotropic emission of the γ ray causes the angular distribution. In the case of ^{28}Mg, 1474-keV γ ray ($2^+ \rightarrow 0^+$) which shows the maximum angular distribution detected by 0 degree detectors along the polarization axis was measured 13% lower than 90 degree (see Sec. 6.4). The γ-ray intensities in ^{29}Mg was deduced by using seven Ge detectors placed 90 degree along the polarization axis because an effect of γ-ray angular distribution can be ignored (see Fig. 3.5).

The γ-ray intensities in ^{29}Mg in the present work are listed in Table 7.2, with the values reported in Ref. [BAU87]. The relative intensities of the γ rays are normalized to the strongest γ ray of 2560 keV as 100%. The intensity of the 55-keV γ ray cannot be obtained because the low energy γ-ray efficiency of Ge detectors could not be clearly determined. The absolute γ-ray intensity in ^{29}Mg and β-decay branching ratio leading to the levels in ^{29}Mg were deduced as follows. The yield of ^{29}Mg was calculated by using the well-established intensity value of 36% for the 2224-keV γ ray in granddaughter ^{29}Al in the β decay of ^{29}Mg with the half-life of 1.3 sec [GUI84]. Then, the absolute γ intensity of ^{29}Mg were obtained by using the ^{29}Na β-decay probability of 78.5(30)% referred from the value of β-n decay probability P_n = 21.5(30)% [LAN84].

The β-decay branching ratio and logft values deduced from the absolute γ-ray intensity are listed in Table 7.3. Since the intensity of the 55-keV γ ray was not obtained, sum of the

Table 7.2: Gamma transitions in ^{29}Mg observed in the β decay of ^{29}Na in the present work. E_i and E_f are the energies of initial and final levels, respectively. The absolute intensities are shown in percent of ^{29}Na β decay. Asterisks indicate that the intensities were less than the sensitivity of the present measurement. The intensity of 55-keV γ ray was not obtained because the γ-ray efficiency at low energy could not be clearly determined.

E_γ [keV][a]	$E_i \rightarrow E_f$ [MeV][a]	I_γ(rel.)[a] [%]	I_γ(abs.)[a]	I_γ(rel.)[b] [%]
54.56(1)	0.055 $\rightarrow$ g.s.	–	–	$\geq$115
335.5(2)	1.430 $\rightarrow$ 1.094	0.57(7)	0.20(5)	–
1039.7(2)	1.094 $\rightarrow$ 0.055	5.4(5)	1.8(4)	4.6(3)
1583.2(1)	1.638 $\rightarrow$ 0.055	<0.1	<0.1	–
1585.7(2)	3.224 $\rightarrow$ 1.638	17(1)	6.0(13)	15.6(9)
1637.7(1)	1.638 $\rightarrow$ g.s.	17(1)	5.8(13)	16.3(9)
1793.6(3)	3.223 $\rightarrow$ 1.430	<0.1	<0.1	–
2129.1(3)	3.223 $\rightarrow$ 1.094	3.2(3)	1.1(2)	3.7(3)
2132.8(8)	3.227 $\rightarrow$ 1.094	1.3(2)	0.4(1)	1.5(2)
2445.1[b]	2.500 $\rightarrow$ 0.055	*	*	0.4(1)
2499.9[b]	2.500 $\rightarrow$ g.s.	*	*	0.2(1)
2559.51(8)	2.614 $\rightarrow$ 0.055	100	34(6)	100
2614.3(4)	2.614 $\rightarrow$ g.s.	5.8(6)	2.0(5)	4.7(3)
3168.8(2)	3.223 $\rightarrow$ 0.055	8.4(5)	2.9(6)	10.3(6)
3172.5(8)	3.227 $\rightarrow$ 0.055	0.33(9)	0.11(4)	0.4(1)
3223.4(2)	3.223 $\rightarrow$ g.s.	3.8(10)	1.3(4)	4.4(4)
3227.1(8)	3.227 $\rightarrow$ g.s.	5.7(10)	2.0(5)	6.6(5)
3673.1(4)	3.673 $\rightarrow$ g.s.	3.3(3)	1.1(3)	2.3(2)
3984.6(7)	3.985 $\rightarrow$ g.s.	2.2(2)	0.8(2)	0.8(1)

[a]Present work.
[b]Taken from Ref. [BAU87]

β decay to the ground and 1st excited states is listed.

7.4 Spin-Parity assignments of ^{29}Mg levels and polarization of ^{29}Na

7.4.1 Spin-Parity assignments of 2.614- and 3.223-MeV levels and polarization of ^{29}Na

For the investigation of the spins and parities of the excited levels in ^{29}Mg, AP values of the β rays from ^{29}Na in coincidence with the γ ray which deexcite the state in ^{29}Mg were

Table 7.3: The ^{29}Mg levels observed in the β decay of ^{29}Na. The β-decay branching ratio to the ground state and 0.055-MeV level were deduced as the sum of them.

E_x [MeV]	I_β [%][a]	I_β [%][b]	log ft[a]	logft[b]
g.s.	26(7)	24(10)	5.1(2)	5.3(2)
0.05456(1)				
1.0943(2)	<0.7	<0.2	>6.5	>7.0
1.4298(2)	0.20(5)	–	7.0(1)	–
1.6377(1)	<1.7	<0.4	>6.0	>6.6
2.6143(4)	36(6)	37.8(72)	4.46(9)	4.4(1)
3.2234(2)	11(2)	12.3(24)	4.84(8)	4.8(1)
3.2271(8)	2.5(5)	3.1(6)	5.5(1)	5.4(1)
3.6731(4)	1.1(3)	0.8(2)	5.7(1)	5.9(1)
3.9846(7)	0.8(2)	0.29(6)	5.8(1)	6.2(1)

[a]Present work.
[b]Taken from Ref. [BAU87]

calculated using Eq. (3.8). For calculating asymmetry parameter A, polarization P of parent nucleus ^{29}Na is necessary. P value of ^{29}Na can be calculated from AP value from β decay leading to spin-know level in ^{29}Mg. However, the P value cannot be calculated because the β decay to the ground state in ^{29}Mg, which the spin-parity is only reported to be $3/2^+$, cannot be separated from the decay to the 0.055-MeV level. Therefore, the spins and parities in ^{29}Mg were investigated as follows.

The AP values of the two energy levels at 2.614 and 3.223 MeV were calculated by using the β-γ coincidence event gated on the γ rays of 2559 keV (2.614 $\rightarrow$ 0.055 MeV) and 1586 keV (3.223 $\rightarrow$ 1.638 MeV), respectively, as

$$A_{2.614}P = 0.352(20) \tag{7.1}$$

$$A_{3.223}P = 0.161(42). \tag{7.2}$$

The ratio of these AP values was calculated as

$$\frac{A_{2.614}P}{A_{3.223}P} = \frac{A_{2.614}}{A_{3.223}} = 2.19(59). \tag{7.3}$$

This value is only consistent with the case that the asymmetry parameter of the 2.614- and 3.223-MeV levels are -1.0 ($I^\pi = 1/2^+$) and -0.4 ($I^\pi = 3/2^+$), respectively. Therefore, the spins and parities of the 2.614- and 3.223-MeV levels in ^{29}Mg were assigned to be $1/2^+$ and

$3/2^+$, respectively, for the first time.

The polarization of ^{29}Na was deduced from the AP values of the 2.614- and 3.223-MeV levels in Eq. (7.2) divided by the A values these levels ($A_{2.614} = -1.0$, $A_{3.223} = -0.4$). The value of 35 $\pm$ 2% was obtained from the average of polarization values of these two levels.

7.4.2 3.227-MeV level

The spin-parity of the 3.227-MeV level was investigated as follows. For deducing the asymmetry parameter $A_{3.227}$ associated with the 3.227-MeV level, the counts of γ rays deexciting this state in coincidence with β rays are needed. However, the closely located γ-ray peaks deexciting the 3.223-MeV level made it difficult to precisely obtain the counts because of poor statistics. Therefore, we regarded the doublet peaks as one peak and estimated the asymmetry parameter as a whole, $A_{doublet}$. $A_{doublet}$ can be described as $(A_{3.223} \times I_\gamma^{3.223} + A_{3.227} \times I_\gamma^{3.227})/(I_\gamma^{3.223} + I_\gamma^{3.227})$, where $I_\gamma^{3.223}$ and $I_\gamma^{3.227}$ represent intensities of the doublet γ-rays from the 3.223- and 3.227-MeV levels, respectively. The established assignment of $3/2^+$ for the 3.223-MeV level requires $A_{3.223}$ to be -0.4. Then, $A_{3.227}$ can be calculated from the experimental value of $A_{doublet}$. This method was applied for the doublet γ-ray peaks of 3223 - 3227 keV and 2129 - 2133 keV to determine the same $A_{3.227}$. The 3169 - 3173 keV doublet was eliminated because of low statistics. $A_{3.227}$ values from each doublet peaks were deduced to be 0.27 ± 0.68 and 1.03 ± 1.89, respectively, as plotted in Fig. 7.6, together with expected asymmetry parameters in horizontal lines. The experimental data are consistent with $+0.6$ or -0.4, which correspond to $3/2^+$ or $5/2^+$. By comparing the γ transitions from the 3.223- and 3.227-MeV levels to the ground and 1st excited state, the significant contrast of γ-decay intensity can be seen. Therefore, we propose the spin-parity assignment of $(5/2)^+$ for the 3.227-MeV level.

7.4.3 0.055- and 1.638-MeV levels

The spins and parities of levels at 0.055 and 1.638 MeV are investigated as follows. From parallel γ transition with the relative intensity of $I_{2614} : I_{2560} = 1 : 17$ for 2614 keV [2.614 MeV $(1/2^+) \rightarrow$ g.s. $(3/2^+)$; $M1$] and 2560 keV [2.614 MeV $(1/2^+) \rightarrow$ 0.055 MeV], $M1$ transition is more likely for 2560-keV γ ray than $E2$. Then, the spin-parity of the 0.055-MeV level was assigned tentatively to be $(1/2^+, 3/2^+)$. The relative γ-transition intensity of $I_{1638} : I_{1583} = 20 : 1$ for the 1638 keV [1.638 MeV $\rightarrow$ g.s. $(3/2\ ^+)$] and 1583 keV (1.638 $\rightarrow$ 0.055 MeV) suggest that $M1$ and $E2$ transitions for 1638 and 1583 keV, respectively, are favored. Therefore, the most probable spins and parities of the levels at 0.055 and 1.638 MeV

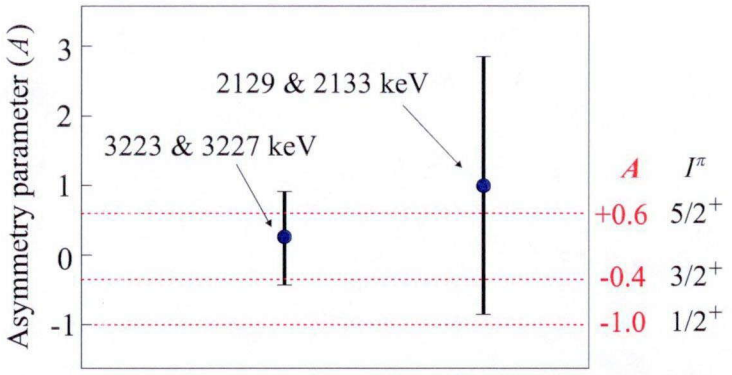

Figure 7.6: Asymmetry parameter associated with the 3.227-MeV level deduced from two doublet γ-ray peaks of 3223-3227 keV and 2129-2133 keV.

are $1/2^+$ and $5/2^+$, respectively.

7.4.4 3.673- and 3.985-MeV levels

The logft values of 5.8(1) for the both transitions leading to the 3.673- and 3.985-MeV levels support the assumption of their allowed nature. The possible spins and parities of these states are both $(1/2, 3/2, 5/2)^+$. The only observed γ transition from the these levels to the ground state $(3/2^+)$ [not to the first excited level at 0.055 MeV $(1/2^+)$] suggest the different spin-change between these γ transitions; $E2$ and $M1$ decays. Therefore, $5/2^+$ assignment is favored for the 3.673- and 3.985-MeV levels. Thus, the spin and parity of level at 3.985 MeV with logft value of 5.8(1) were proposed to be $(5/2)^+$.

To summarize, the spins and parities of all the levels except for 1.094 and 1.430 MeV were successfully assigned in ^{29}Mg in present work as listed in Table 7.4. The assignments of spins will be discussed later in Discussion. Figure 7.2 shows the decay scheme of ^{29}Na. The newly observed γ rays of 1583 and 1794 keV and β transition to the level at 1.430 MeV are described in red lines. The 336-keV γ ray and level at 1.430 MeV which were firstly observed in the β decay of ^{29}Na are described in blue lines. The spins and parities labeled in red color are newly assigned ones.

Table 7.4: Spins and parities of levels in ^{29}Mg.

E_x [MeV]	$I^{\pi a}$	$I^{\pi b}$	$I^{\pi c}$
g.s.	$3/2^+$	$3/2^+$	$3/2^+$
0.055	$(1/2)^+$	–	$1/2^+$
1.094	–	–	$(3/2^-)$
1.430	–	–	$(7/2^-)$
1.638	$(5/2)^+$	–	$5/2^+$
2.266	–	–	$(1/2^-, 3/2^-)$
2.614	$1/2^+$	–	–
3.223	$3/2^+$	–	–
3.227	$(5/2)^+$	–	–
3.673	$(5/2)^+$	–	–
3.985	$(5/2)^+$	–	–

[a]Present work.
[b]Taken from Ref. [BAU87]
[c]Taken from Ref. [BAU89]

CHAPTER VIII

Analysis of experimental data and results: ^{30}Mg

8.1 New γ transitions and levels in ^{30}Mg

Figure 8.1 shows the total γ-ray energy spectrum of β-γ coincidence data in the β decay of ^{30}Na. The γ rays of ^{30}Mg in the β decay of ^{30}Na are clearly confirmed (indicated by the asterisk and corresponding energy in keV in red color). The γ rays of ^{30}Al and ^{30}Si in the β decay of ^{30}Mg, and those of ^{29}Mg, ^{29}Al, and ^{29}Si in the β-n decay of ^{29}Na were also observed (labeled with open circle). The γ rays of 305, 984, 1482, 1505, 1559, 1791, 1820, 1871, 1952, 1978, 2059, 2499, 2627, 3179, 3484, 3542, 3930, 4967, 5022, 5095, 5413 keV, and single and double escape (s.e. and d.e.) peaks of the γ rays of 3179, 3930, 4967, 5022, 5095, and 5413 keV in ^{30}Mg were observed. The new γ rays of 2604, 2684, 3211, and 3431 keV in ^{30}Mg are also found in Fig. 8.1. The 1898 keV γ ray which was observed as the transition of 3.379 $\rightarrow$ 1.481 MeV in ^{30}Mg in the fusion reaction experiment of ^{14}C(^{18}O,2p) [DEA10], was firstly observed in the β decay of ^{30}Na in the present work. By γ-γ analysis with the coincidence time width of $\pm$400 ns, fourteen γ transitions and four energy levels were newly observed in ^{30}Mg as summarized in Table 8.3 and described in the revised decay scheme of ^{30}Na as shown in Fig. 8.2. Asterisks in the figure indicate new findings. The energy of the levels and γ transitions in ^{30}Mg were re-evaluated in the present work.

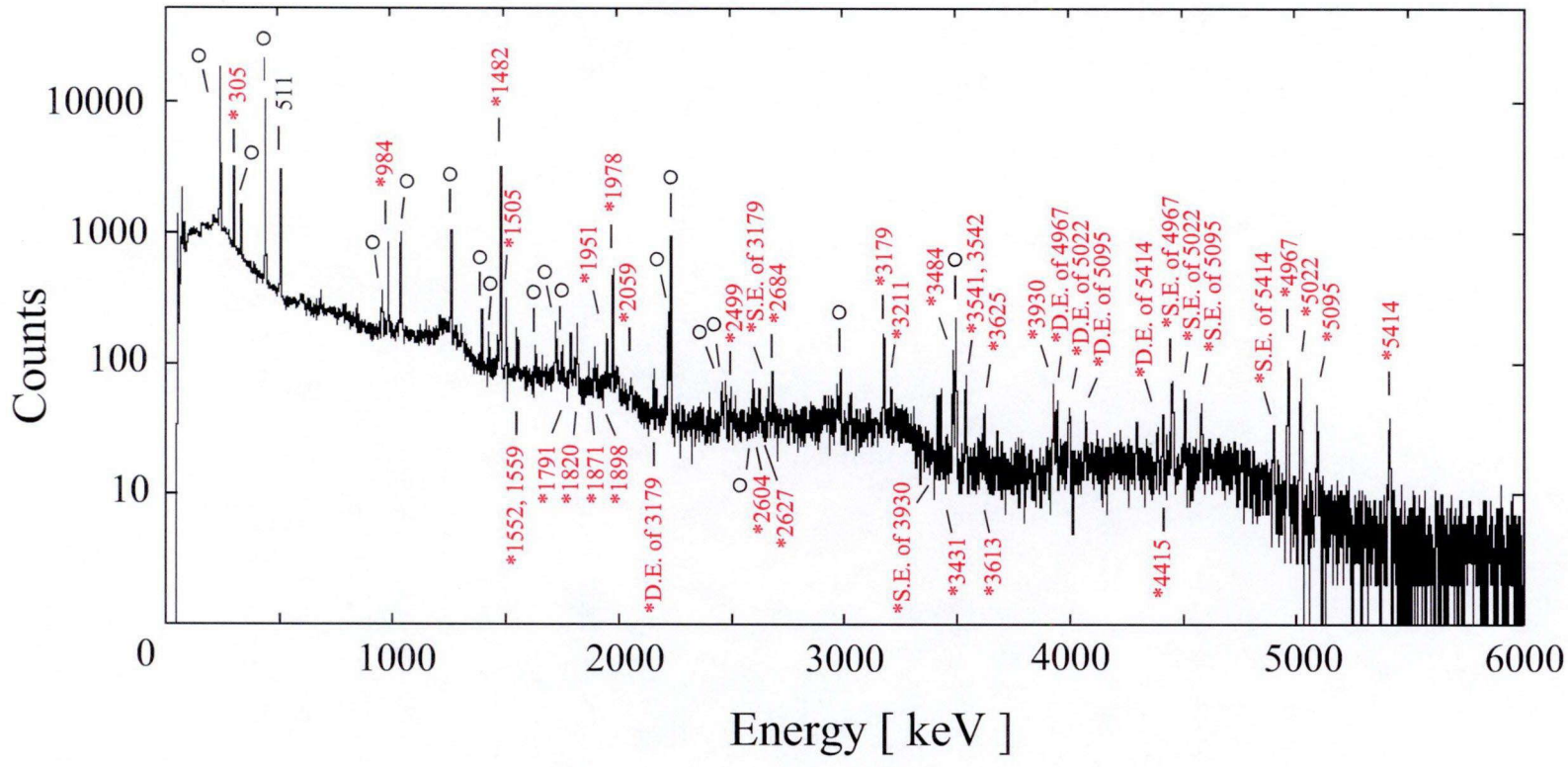

Figure 8.1: Gamma-ray energy spectrum of β-γ coincidence data for the β decay of ^{30}Na. The γ-rays of ^{29}Mg associated with β decay of ^{30}Na are labeled by asterisks and the corresponding γ-ray energies in keV. The peaks of the descendants (^{30}Al, ^{30}Si, ^{29}Mg, ^{29}Al, and ^{29}Si) are labeled with open circles.

The energy level at 6.064 MeV and γ rays of 2684 keV and 2604 keV were newly found in ^{30}Mg as follows. Figure 8.3(a) and (b) show the γ-ray energy spectra gated on the 1898- and 1978-keV γ rays, respectively. The clearly observed 2684- and 2604-keV γ ray peak in Fig. 8.3(a) and (b) indicate the coincidence relations of 1482-1898-2684 keV and 1482-1978-2604 keV, respectively. Figure 8.3(c) and (d) shows the γ-ray energy spectra gated on the 2684- and 2604-keV γ rays, respectively. The clearly observed γ-ray peaks of (1482, 1898 keV) and (1482, 1978 keV) supports the coincidence relations of 1482-1898-2684 keV and 1482-1978-2604 keV, respectively. The consistent sum energies of these cascade γ rays, $1482 + 1898 + 2684 = 6064$ keV and $1482 + 1978 + 2604 = 6064$ keV, indicate the cascade relations shown in Fig. 8.4. Thus, the new energy level at 6.064 MeV, and γ transitions of 2684 keV (6.064 $\rightarrow$ 3.380 MeV) and 2604 keV (6.064 $\rightarrow$ 3.460 MeV) were proposed in ^{30}Mg for the first time.

Similarly, the γ rays of 1635, 2216, 2227, 2437, 2554, 2946, 3201, 3211, 3431, 3598, and 4582 keV, and energy levels at 4.683, 4.694, and 5.897 MeV were newly confirmed by γ-γ coincidence analysis in the present work. The γ transitions in ^{30}Mg observed in the β decay of ^{30}Na in the present work are listed in Table 8.3. The energies of the γ rays were deduced by fitting of the observed photo peaks. Table 8.1 and 8.2 show the coincidence relations of γ rays in ^{30}Mg investigated by γ-γ analysis. The symbol $\bigcirc$ ($\times$) denotes that the γ-ray peak was (not) observed in the gated spectrum. Note that the γ rays of 1948 keV (4.415 $\rightarrow$ 2.466 MeV) was not observed in the present work. Besides, the 4415-keV γ ray was confirmed to be in coincidence with the 1482-keV γ ray as shown in Fig. 8.5. The energy difference of $5.897 - 1.482 = 4.415$ MeV suggests that the 4415-keV γ ray is the transition between 5.897- and 1.482-MeV levels. Therefore, we propose that the 4415-keV γ ray is the transition of 5.897 $\rightarrow$ 1.482 MeV as substitute for the transition of 4.415 MeV $\rightarrow$ g.s reported previously. All the γ-ray energy spectra gated on the γ rays in ^{30}Mg except for the 1898-, 1978-, 2604-, 2684-, and 4415-keV γ rays (Fig. 8.3 and 8.5) are shown in Fig. A.18 to A.40 in Appendix A. The 1635-keV γ ray, which is indicated by dashed line in Fig. 8.2, was deduced as the transition of 5.095 $\rightarrow$ 3.460 MeV from the incomplete coincidence relation between the 1978 keV [see Table 8.1, Fig. A.24 and 8.3(b)].

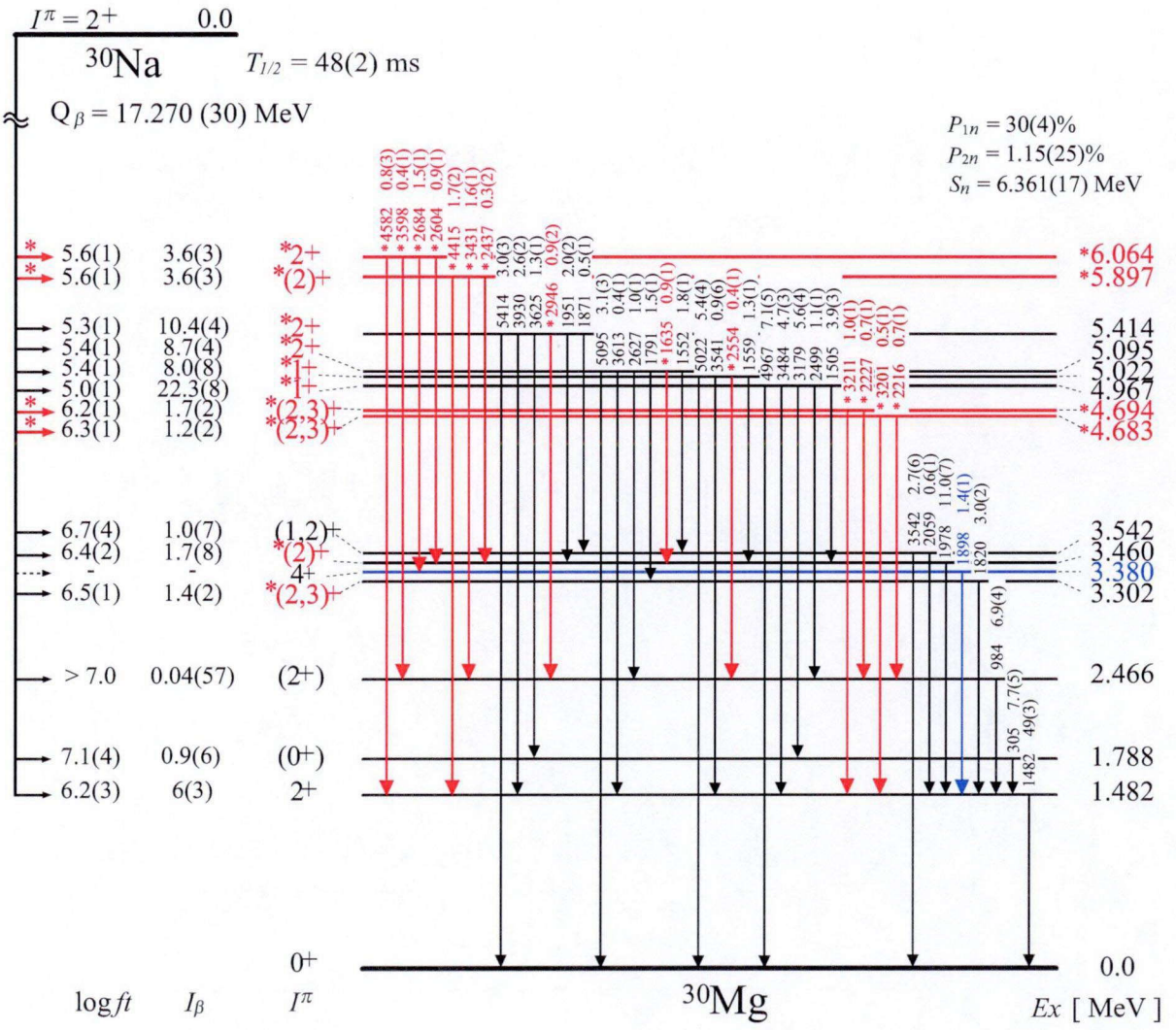

Figure 8.2: Revised decay scheme of ^{30}Na. The physical quantities and decay paths newly found in the present work are labeled by asterisks. The 1635-keV γ transition (5.095 $\rightarrow$ 3.460 MeV) is labeled by dashed line because 1635-keV γ-ray peak could not be found in the γ ray energy spectrum gated on the 1978-keV γ ray. The 1898-keV γ ray and 3.380-MeV level labeled in blue are observed in the fusion reaction experiment of ^{14}C(^{18}O,2p) [DEA10], and firstly observed in the β decay of ^{30}Na in the present work. Reported values of $T_{1/2}$ [LAN84], Q_β [AUD03], P_{1n} [GUI84], P_{2n} [GUI84], and S_n [AUD03] are also shown.

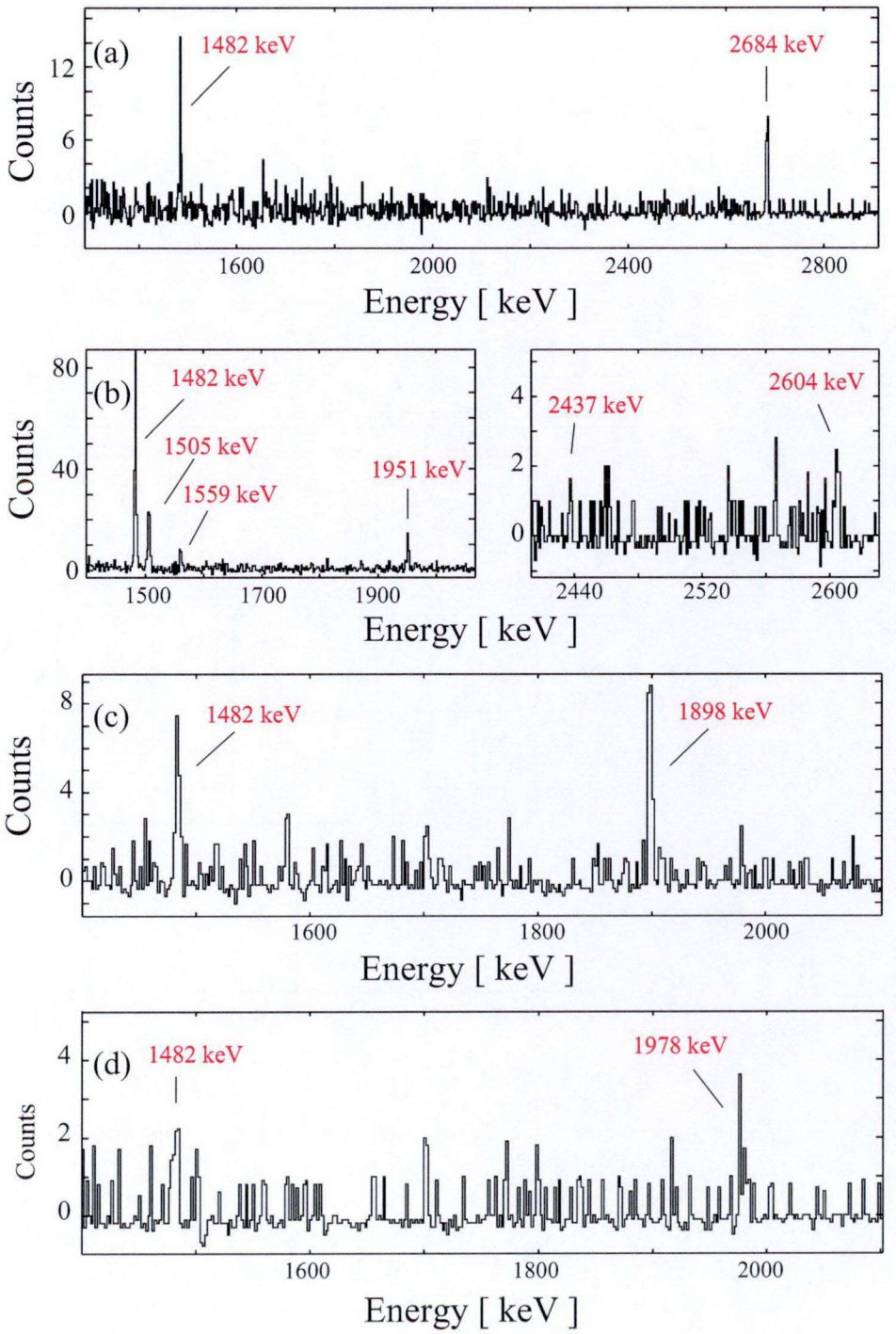

Figure 8.3: Gamma-ray energy spectra in coincidence with the (a) 1898-keV, (b) 1978-keV, (c) 2684-keV, and (d) 2604-keV γ rays, respectively.

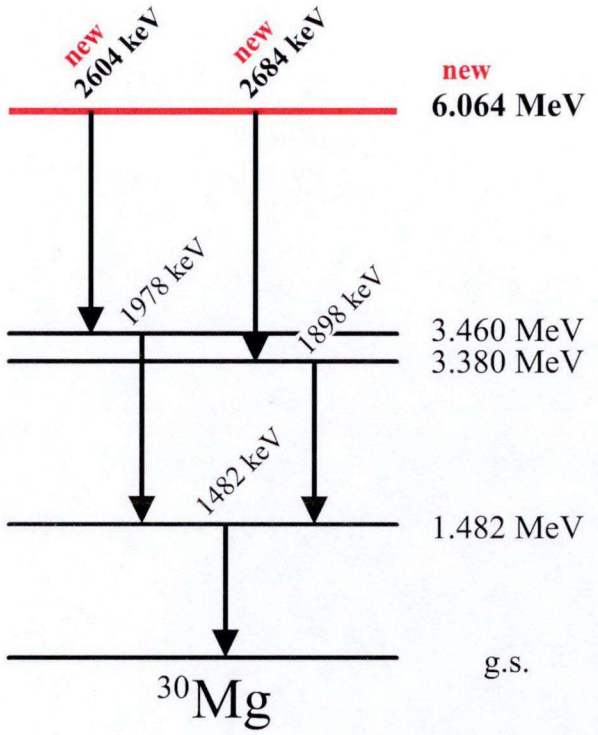

Figure 8.4: Partial level scheme of ^{30}Mg. New energy level at 6.064 MeV was proposed by the cascade lines of 1482-1898-2684 keV and 1482-1978-2604 keV.

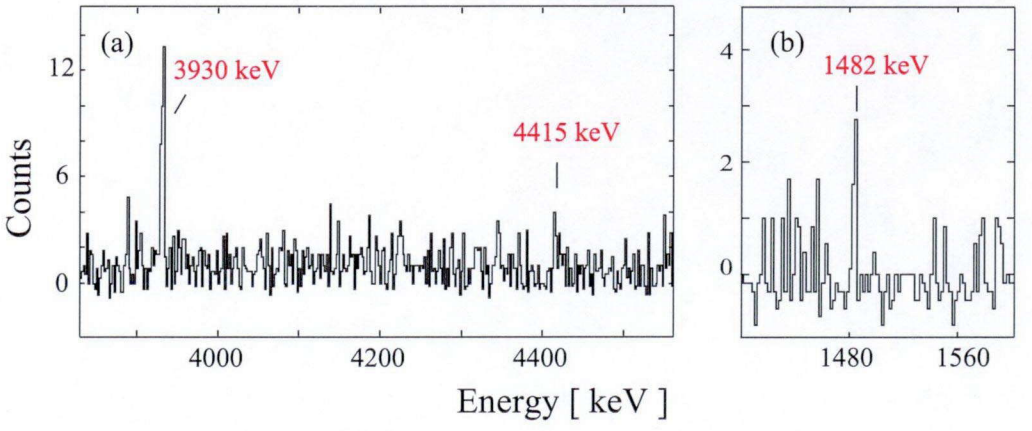

Figure 8.5: Gamma-ray energy spectra in coincidence with the (a) 1482-keV and (b) 4415-keV γ rays, respectively.

Table 8.1: Coincidence relations of γ rays in ^{30}Mg observed in the present work I: Whether or not the γ ray peak was observed in the gated spectrum is displayed by a ◯ or a ×, respectively. The 3541- and 3542-keV γ rays could not be separated within the energy resolution of Ge detectors.

gated by \ conicident	305	984	1482	1505	1552	1559	1635	1791	1820	1871	1898	1951	1978	2059	2216	2227	2437	2499	2554	2604	2627	2684
305	–	×	◯	×	×	×	×	×	×	×	×	×	×	×	×	×	×	×	×	×	×	×
984	×	–	◯	×	×	×	×	×	×	×	×	×	×	×	◯	◯	×	◯	◯	×	◯	×
1482	◯	◯	–	◯	◯	◯	◯	◯	◯	×	◯	◯	◯	×	◯	◯	×	◯	×	◯	◯	◯
1505	×	×	◯	–	×	×	×	×	×	×	×	×	◯	×	×	×	×	×	×	×	×	×
1552	×	×	◯	×	–	×	×	×	×	×	×	×	×	×	×	×	×	×	×	×	×	×
1559	×	×	◯	×	×	–	×	×	×	×	×	×	◯	×	×	×	×	×	×	×	×	×
1635	×	×	◯	×	×	×	–	×	×	×	×	×	◯	×	×	×	×	×	×	×	×	×
1791	×	×	◯	×	×	×	×	–	◯	×	×	×	×	×	×	×	×	×	×	×	×	×
1820	×	×	◯	×	×	×	×	◯	–	×	×	×	×	×	×	×	×	×	×	×	×	×
1871	×	×	◯	×	×	×	×	×	×	–	×	×	×	◯	×	×	×	×	×	×	×	×
1898	×	×	◯	×	×	×	×	×	×	×	–	×	×	×	×	×	×	×	×	×	×	◯
1951	×	×	◯	×	×	×	×	×	×	×	×	–	◯	×	×	×	×	×	×	×	×	×
1978	×	×	◯	◯	×	◯	×	×	×	×	×	◯	–	×	×	×	◯	×	×	◯	×	×
2059	×	×	×	×	◯	×	×	×	×	◯	×	×	×	–	×	×	×	×	×	×	×	×
2216	×	◯	◯	×	×	×	×	×	×	×	×	×	×	×	–	×	×	×	×	×	×	×
2227	×	◯	◯	×	×	×	×	×	×	×	×	×	×	×	×	–	×	×	×	×	×	×
2437	×	×	◯	×	×	×	×	×	×	×	×	×	◯	×	×	×	–	×	×	×	×	×
2499	×	◯	◯	×	×	×	×	×	×	×	×	×	×	×	×	×	×	–	×	×	×	×
2554	×	◯	◯	×	×	×	×	×	×	×	×	×	×	×	×	×	×	×	–	×	×	×
2604	×	×	◯	×	×	×	×	×	×	×	×	×	◯	×	×	×	×	×	×	–	×	×
2627	×	◯	◯	×	×	×	×	×	×	×	×	×	×	×	×	×	×	×	×	×	–	×
2684	×	×	◯	×	×	×	×	×	×	×	◯	×	×	×	×	×	×	×	×	×	×	–
2946	×	◯	◯	×	×	×	×	×	×	×	×	×	×	×	×	×	×	×	×	×	×	×
3179	◯	×	◯	×	×	×	×	×	×	×	×	×	×	×	×	×	×	×	×	×	×	×
3201	×	×	◯	×	×	×	×	×	×	×	×	×	×	×	×	×	×	×	×	×	×	×
3211	×	×	◯	×	×	×	×	×	×	×	×	×	×	×	×	×	×	×	×	×	×	×
3431	×	◯	◯	×	×	×	×	×	×	×	×	×	×	×	×	×	×	×	×	×	×	×
3484	×	×	◯	×	×	×	×	×	×	×	×	×	×	×	×	×	×	×	×	×	×	×
3541, 3542	×	×	◯	×	◯	×	×	×	×	◯	×	×	×	×	×	×	×	×	×	×	×	×
3598	×	◯	◯	×	×	×	×	×	×	×	×	×	×	×	×	×	×	×	×	×	×	×
3613	×	×	◯	×	×	×	×	×	×	×	×	×	×	×	×	×	×	×	×	×	×	×
3625	◯	×	◯	×	×	×	×	×	×	×	×	×	×	×	×	×	×	×	×	×	×	×
3930	×	×	◯	×	×	×	×	×	×	×	×	×	×	×	×	×	×	×	×	×	×	×
4415	×	×	◯	×	×	×	×	×	×	×	×	×	×	×	×	×	×	×	×	×	×	×
4582	×	×	◯	×	×	×	×	×	×	×	×	×	×	×	×	×	×	×	×	×	×	×
4967	×	×	×	×	×	×	×	×	×	×	×	×	×	×	×	×	×	×	×	×	×	×
5022	×	×	×	×	×	×	×	×	×	×	×	×	×	×	×	×	×	×	×	×	×	×
5095	×	×	×	×	×	×	×	×	×	×	×	×	×	×	×	×	×	×	×	×	×	×
5414	×	×	×	×	×	×	×	×	×	×	×	×	×	×	×	×	×	×	×	×	×	×

Table 8.2: Coincidence relations of γ rays in ^{30}Mg observed in the present work II: Whether or not the γ ray peak was observed in the gated spectrum is displayed by a ◯ or a ×, respectively. The 3541- and 3542-keV γ rays could not be separated within the energy resolution of Ge detectors.

gated by \ conicident	2946	3179	3201	3211	3431	3484	3541	3542	3598	3613	3625	3930	4415	4582	4967	5022	5095	5414
305	×	◯	×	×	×	×	×	×	×	×	◯	×	×	×	×	×	×	×
984	◯	×	×	×	◯	×	×	×	◯	×	×	×	×	×	×	×	×	×
1482	×	◯	◯	◯	◯	◯	◯	×	×	◯	◯	◯	◯	◯	×	×	×	×
1505	×	×	×	×	×	×	×	×	×	×	×	×	×	×	×	×	×	×
1552	×	×	×	×	×	×	×	◯	×	×	×	×	×	×	×	×	×	×
1559	×	×	×	×	×	×	×	×	×	×	×	×	×	×	×	×	×	×
1635	×	×	×	×	×	×	×	×	×	×	×	×	×	×	×	×	×	×
1791	×	×	×	×	×	×	×	×	×	×	×	×	×	×	×	×	×	×
1820	×	×	×	×	×	×	×	×	×	×	×	×	×	×	×	×	×	×
1871	×	×	×	×	×	×	×	◯	×	×	×	×	×	×	×	×	×	×
1898	×	×	×	×	×	×	×	×	×	×	×	×	×	×	×	×	×	×
1951	×	×	×	×	×	×	×	×	×	×	×	×	×	×	×	×	×	×
1978	×	×	×	×	×	×	×	×	×	×	×	×	×	×	×	×	×	×
2059	×	×	×	×	×	×	×	×	×	×	×	×	×	×	×	×	×	×
2216	×	×	×	×	×	×	×	×	×	×	×	×	×	×	×	×	×	×
2227	×	×	×	×	×	×	×	×	×	×	×	×	×	×	×	×	×	×
2437	×	×	×	×	×	×	×	×	×	×	×	×	×	×	×	×	×	×
2499	×	×	×	×	×	×	×	×	×	×	×	×	×	×	×	×	×	×
2554	×	×	×	×	×	×	×	×	×	×	×	×	×	×	×	×	×	×
2604	×	×	×	×	×	×	×	×	×	×	×	×	×	×	×	×	×	×
2627	×	×	×	×	×	×	×	×	×	×	×	×	×	×	×	×	×	×
2684	×	×	×	×	×	×	×	×	×	×	×	×	×	×	×	×	×	×
2946	–	×	×	×	×	×	×	×	×	×	×	×	×	×	×	×	×	×
3179	×	–	×	×	×	×	×	×	×	×	×	×	×	×	×	×	×	×
3201	×	×	–	×	×	×	×	×	×	×	×	×	×	×	×	×	×	×
3211	×	×	×	–	×	×	×	×	×	×	×	×	×	×	×	×	×	×
3431	×	×	×	×	–	×	×	×	×	×	×	×	×	×	×	×	×	×
3484	×	×	×	×	×	–	×	×	×	×	×	×	×	×	×	×	×	×
3541, 3542	×	×	×	×	×	×	–	×	×	×	×	×	×	×	×	×	×	×
3598	×	×	×	×	×	×	×	×	–	×	×	×	×	×	×	×	×	×
3613	×	×	×	×	×	×	×	×	×	–	×	×	×	×	×	×	×	×
3625	×	×	×	×	×	×	×	×	×	×	–	×	×	×	×	×	×	×
3930	×	×	×	×	×	×	×	×	×	×	×	–	×	×	×	×	×	×
4415	×	×	×	×	×	×	×	×	×	×	×	×	–	×	×	×	×	×
4582	×	×	×	×	×	×	×	×	×	×	×	×	×	–	×	×	×	×
4967	×	×	×	×	×	×	×	×	×	×	×	×	×	×	–	×	×	×
5022	×	×	×	×	×	×	×	×	×	×	×	×	×	×	×	–	×	×
5095	×	×	×	×	×	×	×	×	×	×	×	×	×	×	×	×	–	×
5414	×	×	×	×	×	×	×	×	×	×	×	×	×	×	×	×	×	–

8.2 Gamma-ray intensities and β-decay branching ratios

The γ-ray intensities were deduced by using γ-ray counts measured by all Ge detectors. As discussed in Sec. 3.3.2 and 6.4, the intensities are affected by angular distribution caused by the residual polarization. Therefore, the obtained γ-ray intensities in ^{30}Mg have an ambiguity as discussed in Sec. 6.4. The γ-ray intensities in ^{30}Mg in the present work are listed in Table 8.3, with the values reported in Ref. [GUI84] and [BAU89]. The relative intensities are normalized to the strongest γ ray of 1482 keV as 100%. The absolute values were obtained by using the intensities of γ rays populating the ^{30}Mg ground state (see Sec. 3.3.1) and the neutron emission probabilities of P_{1n} = 30(4)% and P_{2n} = 1.15(25)% taken from Ref. [GUI84].

The β-transition intensities and logft values in the present work and Ref. [NND11] are summarized in Table 8.4. It is to be noted that significant changes of intensities of the β decays leading to the 1.788- and 2.466-MeV levels were deduced in the present work compared to the reported values [NND11].

8.3 Spin-Parity assignments of ^{30}Mg levels and polarization of ^{30}Na

8.3.1 Spins and parities of 4.967- and 5.022-MeV levels and polarization of ^{30}Na

The asymmetry parameter of the β decay leading to the levels in ^{30}Mg can be evaluated from measured AP values of the β transition to the respective levels, and polarization P of parent nucleus ^{30}Na. Since it is difficult to deduce AP values to the spin-known levels in ^{30}Mg because there are many populating γ transitions from higher levels (i.e., 1.482 MeV), the asymmetry parameters of ^{30}Mg were evaluated as follows.

The AP values of the levels at 4.967 and 5.022 MeV with strong β-decay branching ratios were calculated by using β-ray counts gated on the γ rays of (4967, 3484, 3179, 2499, and 1505 keV) and (5022, 3541, 2554, and 1559 keV), respectively, as $(AP)_{4.967}$ = 0.29(4) and $(AP)_{5.022}$ = 0.38(6). By taking the ratio of these AP values, the ratio only by the asymmetry parameters was calculated to be $A_{4.967}/A_{5.022}$ = 0.78(17). Depending on the 3 possible final spin values of 1, 2, or 3 in the case of allowed β transition, the possible ratio of A takes 9 patterns, resulting in the values of +3.0, +1.0, +0.33, -0.5, -0.67, -1.5, and -2.0. Of these values, the experimental value of 0.78(17) is only consistent with +1.0, which correspond to the assignments of $(I^{\pi}_{4.967}, I^{\pi}_{5.022})$ = $(1^+, 1^+)$, $(2^+, 2^+)$, or $(3^+, 3^+)$. Since the γ transitions

Table 8.3: Energies and intensities of γ transitions in ^{30}Mg populated with β decay of ^{30}Na. E_i and E_f are the energies of initial and final levels, respectively. The absolute intensities are shown in percent of ^{30}Na β decay.

E_γ [keV][a]	$E_i \rightarrow E_f$	I_γ(rel.) [%][a]	I_γ(abs.) [%][a]	I_γ(rel.) [%][b]	I_γ(rel.) [%][c]
305.36(2)	1.788 → 1.482	15.8(2)	7.7(5)	12.5(13)	11.4(7)
984.13(4)	2.466 → 1.482	14.0(3)	6.9(4)	14.2(8)	14.5(9)
1482.19(2)	1.482 → g.s.	100	49(3)	100	100
1505.23(9)	4.967 → 3.460	7.9(3)	3.9(3)	8.2(7)	8.4(6)
1552.0(2)	5.095 → 3.541	3.6(2)	1.8(1)	4.2(6)	4.7(4)
1559.1(2)	5.022 → 3.460	2.7(2)	1.3(1)	3.2(6)	3.6(3)
1634.7(3)	5.095 → 3.460	1.9(1)	0.9(1)	–	–
1790.8(2)	5.095 → 3.302	3.1(2)	1.5(1)	–	4.0(6)
1819.9(1)	3.302 → 1.482	6.0(2)	3.0(2)	6.2(8)	5.4(4)
1870.8(3)	5.414 → 3.541	1.1(1)	0.5(1)	1.7(7)	1.3(2)
1897.9(2)	3.380 → 1.482	2.8(2)	1.4(1)	–	–
1948	4.415 → 2.466	–	–	–	1.6(3)
1950.6(3)	5.414 → 3.460	4.2(2)	2.0(1)	–	4.5(3)
1978.04(5)	3.460 → 1.482	22.6(5)	11.0(7)[d]	24(2)	25(2)
2058.6(5)	3.541 → 1.482	1.2(1)	0.6(1)	–	2.0(3)
2216.4(8)	4.683 → 2.466	1.4(3)	0.7(1)	–	–
2227.3(4)	4.694 → 2.466	1.5(3)	0.7(1)	–	–
2436.8(3)	5.897 → 3.460	0.6(4)	0.3(2)	–	0.3(1)
2498.6(5)	4.967 → 2.466	2.3(2)	1.1(1)	1.9(6)	1.8(2)
2554.2(1)	5.022 → 2.466	0.8(2)	0.4(1)	–	–
2604.1(3)	6.604 → 3.460	1.8(2)	0.9(1)	–	–
2626.5(3)	5.095 → 2.466	2.0(2)	1.0(1)	–	2.3(3)
2684.1(3)	6.064 → 3.380	3.2(2)	1.5(1)	1.1(8)	–
2945.9(1)	5.414 → 2.466	1.7(4)	0.9(2)	–	–
3179.2(1)	4.967 → 1.788	11.4(4)	5.6(2)	11(2)	12.6(9)
3200.5(8)	4.683 → 1.482	1.0(1)	0.5(1)	–	–
3211.4(4)	4.694 → 1.482	2.1(2)	1.0(1)	–	–
3430.7(2)	5.897 → 2.466	3.3(2)	1.6(1)	2.5(8)	–
3484.4(1)	4.967 → 1.482	9.6(4)	4.7(3)	9.8(16)	12.1(8)
3541.2(1)	5.022 → 1.482	1.9(13)	0.9(6)	6.8	1.6(7)
3542.2(3)	3.541 → g.s.	5.5(12)	2.7(6)		6.7(7)
3597.8(6)	6.064 → 2.466	0.8(1)	0.4(1)	–	–
3612.7(3)	5.095 → 1.482	0.8(1)	0.4(1)	–	0.8(1)
3625.4(3)	5.414 → 1.788	2.7(2)	1.3(1)	1.9(7)	3.1(3)
3930.4(2)	5.414 → 1.482	5.3(3)	2.6(2)	6.3(12)	6.6(5)
4414.7(5)	5.897 → 1.482	3.4(3)	1.7(2)	–	2.5(2)
4582.0(4)	6.604 → 1.482	1.7(6)	0.8(3)	–	–
4685	– → –	–	–	2.2(1)	<0.3
4967.0(2)	4.967 → g.s.	14.5(6)	7.1(5)	11(3)	16(1)
5022.4(2)	5.022 → g.s.	11.2(5)	5.4(4)	11(2)	12.7(8)
5094.9(3)	5.095 → g.s.	6.4(4)	3.1(3)	5.8(14)	7.4(5)
5413.6(2)	5.414 → g.s.	6.2(4)	3.0(3)	4.9(12)	6.4(4)

[a]Present work.
[b]Taken from Ref. [GUI84].
[c]Taken from Ref. [BAU89].
[d]Small value of 7.9(5)% was deduced by the γ-γ coincidence data analysis. This discrepancy could not be confirmed in the γ-γ coincidence data.

Table 8.4: The levels of ^{30}Mg observed in the β decay of ^{30}Na. The level at 4.415 MeV was not observed in the present (see text for further detail). Asterisks indicate that the β-decay intensities to these levels were less than the sensitivity of the present measurement.

E_x [MeV]	I_β [%][a]	I_β [%][b]	log ft[a]	log ft[b]
g.s.	*	–	–	–
1.4822(2)	6(3)	9.5(11)	6.2(3)	5.86
1.7875(3)	0.9(6)	–	7.1(4)	–
2.4663(4)	0.04(57)	3.8(5)	>7.0	6.12
3.3021(1)	1.4(2)	0.4(4)	6.5(1)	7.0
3.3801(2)	*	–	–	–
3.46023(5)	1.7(8)	3.5(6)	6.4(2)	6.01
3.5422(3)	1.0(7)	1.3(4)	6.7(4)	6.43
4.415	*	1.80(20)	–	6.15
4.6827(8)	1.2(2)	–	6.4(1)	–
4.6936(4)	1.7(2)	–	6.2(1)	–
4.9670(2)	22.3(8)	21.7(18)	5.0(1)	4.98
5.0224(2)	8.0(8)	7.7(6)	5.4(1)	5.42
5.0949(3)	8.7(4)	8.5(8)	5.4(1)	5.37
5.4136(2)	10.4(4)	9.5(8)	5.3(1)	5.26
5.8970(2)	3.6(3)	–	5.6(1)	–
6.0642(4)	3.6(3)	–	5.6(1)	–

[a]Present work.
[b]Taken from Ref. [NND11].

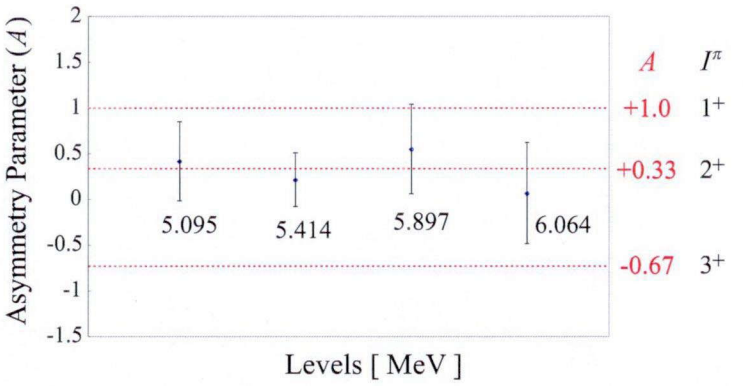

Figure 8.6: Asymmetry parameters of levels at 5.095, 5.414, 5,897, and 6.064 MeV deduced from the AP values divided by polarization $P = 0.32(3)$.

which populate the g.s. (0^+) were observed from both 4.967- and 5.022-MeV levels, the 3^+ assignments are not reasonable for these levels by the γ-ray selection rules. Therefore, the assignments were deduced to be $(I^\pi_{4.967}, I^\pi_{5.022}) = (1^+, 1^+)$ or $(2^+, 2^+)$. Of these 2 patterns, the polarization values P were calculated to be 0.32(3) and 0.94(9) from the AP values divided by A values for the both 1^+ and 2^+ assignments, respectively. As the former value of $P = 0.32(3)$ is reasonable, the spins and parities of these levels are assigned to be 1^+ and 1^+ for the first time.

8.3.2 5.095-, 5.414-, 5,897-, and 6.064-MeV levels

The spins and parities of the levels at 5.095, 5.414, 5,897, and 6.064 MeV were deduced from AP values of these levels and the polarization $P = 0.32(3)$. The AP values of the respective levels were calculated to be 0.134(102), 0.0696(7), 0.228(17), and 0.023(150), respectively, by using β-ray counts gated on the γ rays which deexcite the respective levels. The asymmetry parameter A of these levels were calculated by using $P = 0.32(3)$, as shown in Fig. 8.6. As a result, the spins and parities of these levels are deduced to be 2^+, 2^+, $(1, 2)^+$, and 2^+, respectively.

To discuss the $(1, 2)^+$ assignment of the 5.897-MeV level, experimental γ-ray intensities deexciting this level are compared with Weisskopt estimations in the both spin-parity case as shown in Table 8.5. Assuming the spin-parity of 1^+, γ transition to the ground state should be observed as strongly as other levels due to $M1$ decay nature. However, the γ transition of 5897 keV (5.897 MeV $\rightarrow$ g.s.) was not confirmed in the present work. The detection of this γ ray is out of sensitivity in the present experiment by estimation from background noise at

Table 8.5: Experimental transition intensities and transition probabilities by Weisskopf estimates [$T_W(\sigma\lambda)$] for the γ transitions deexciting the 5.897-MeV level. $T_W(\sigma\lambda)$ values are normalized to the 5.897 $\rightarrow$ 1.482 MeV transition. $T_W(\sigma\lambda)$ values are calculated in the cases of $I^{\pi}_{5.897} = 1^+$ and 2^+.

E_f [MeV] (I^{π})	$T_W(\sigma\lambda)$(normalized)		I^{exp}_{γ}
	$I^{\pi}_{5.897} = 1^+$	$I^{\pi}_{5.897} = 2^+$	
1.482 (2^+)	1.0	1.0	1.6(2)
0 (0^+)	2.4	1.9×10^{-2}	–

this energy ($I^{5897}_{\gamma} < 0.4$). Therefore, we proposed 2^+ assignment for the 5.897-MeV level.

8.3.3 3.302-, 3.380-, 3.460-, and 3.542-MeV levels

The spins and parities of the 3.302-, 3.380-, 3.460-, and 3.542-MeV levels were reported by several experiments as, 3.302 MeV: 4^+ [TAK09], 3.380 MeV: (4^+) [DEA10], 3.460 MeV: (1, 2, 3)$^+$ [SCW09] or (4^+) [DEA10], 3.542 MeV: (1, 2)$^+$ [NND11]. The spin-parity assignments were again investigated in the present work. The β-decay asymmetry measurements for these levels were not possible due to the very small or no β-decay branching ratio in the present work. Therefore, the spins and parities of these four energy levels were speculated by the experimental relative γ-transition intensities as follows.

The β-transition intensities with I_{β} = 1.4(2), 1.6(4), and 1.6(2) for the 3.302-, 3.460-, and 3.542-MeV levels, respectively, indicate the allowed nature, resulting in the possible spins and parities of 1^+, 2^+, or 3^+ for these levels. Table 8.6, 8.7, and 8.8 show the comparisons of experimental γ transition intensities and Weisskopf estimations deexciting the 3.302-, 3.460-, and 3.542-MeV levels, respectively. The 3^+ assignment was excluded for the 3.542-MeV level because the strong γ transition to the ground state are observed. No observations of γ transitions to the ground state suggest that the spin-parity of 1^+ can be excluded for the 3.302- and 3.460-MeV levels. Moreover, strong γ transitions of 1505 keV [4.967 MeV(1^+) $\rightarrow$ 3.460 MeV] and 1559 keV [5.022 MeV(1^+) $\rightarrow$ 3.460 MeV] indicate the preferable assignment of 2^+ for the 3.460-MeV level. By taking into account the hindrance factor of 10^{-2} for l-forbidden $M1$ decay in this nuclear region [MOR76], the assignments of 1^+ and 2^+ for the 3.542-MeV are both plausible. Thus, the spins and parities of the 3.302-, 3.460-, and 3.542-MeV levels were deduced to be (2, 3)$^+$, 2^+, and (1, 2)$^+$,respectively, in the present work. It is to be noted that the obtained result of I^{π} = (2, 3)$^+$ at the 3.302-MeV level shows the contradiction with 4^+ assignment by the proton inelastic scattering experiment

Table 8.6: Experimental transition intensities and transition probabilities by Weisskopf estimates [$T_W(\sigma\lambda)$] for the γ transitions deexciting the 3.302-MeV level. $T_W(\sigma\lambda)$ values are normalized to the 3.302 $\rightarrow$ 1.482 MeV transition. $T_W(\sigma\lambda)$ values are calculated in the cases of $I^\pi_{3.302} = 1^+$, 2^+, and 3^+.

E_f [MeV] (I^π)	$T_W(\sigma\lambda)$(normalized)			I_γ^{exp}
	$I^\pi_{3.302} = 1^+$	$I^\pi_{3.302} = 2^+$	$I^\pi_{3.302} = 3^+$	
1.482 (2^+)	1.0	1.0	1.0	1.3(1)
0 (0^+)	6.0	1.4×10^{-2}	2.4×10^{-8}	–

Table 8.7: Experimental transition intensities and transition probabilities by Weisskopf estimates [$T_W(\sigma\lambda)$] for the γ transitions deexciting the 3.460-MeV level. $T_W(\sigma\lambda)$ values are normalized to the 3.460 $\rightarrow$ 1.482 MeV transition. $T_W(\sigma\lambda)$ values are calculated in the cases of $I^\pi_{3.460} = 1^+$, 2^+, and 3^+.

E_f [MeV] (I^π)	$T_W(\sigma\lambda)$(normalized)			I_γ^{exp}
	$I^\pi_{3.460} = 1^+$	$I^\pi_{3.460} = 2^+$	$I^\pi_{3.460} = 3^+$	
1.482 (2^+)	1.0	1.0	1.0	10.7(7)
0 (0^+)	5.4	1.4×10^{-2}	2.5×10^{-8}	–

[TAK09]. The assignment of $(1, 2)^+$ for the 3.542-MeV level is consistent with the reported one [NND11].

The spin-parity of the 3.380-MeV level has been assigned to be 4^+ by the γ-ray angular distribution measurement in the fusion reaction experiment of ^{14}C(^{18}O,2p) [DEA10]. In the present work, strong γ transitions which populate [2684 keV: 6.064 MeV(2^+) $\rightarrow$ 3.380 MeV] and depopulate [1898 keV: 3.380 $\rightarrow$ 1.482 MeV(2^+)] the 3.380-MeV level were observed, which supports the 4^+ assignment.

Table 8.8: Experimental transition intensities and transition probabilities by Weisskopf estimates [$T_W(\sigma\lambda)$] for the γ transitions deexciting the 3.542-MeV level. $T_W(\sigma\lambda)$ values are normalized to the 3.542 MeV $\rightarrow$ g.s. transition. $T_W(\sigma\lambda)$ values are calculated in the cases of $I^\pi_{3.542} = 1^+$ and 2^+.

E_f [MeV] (I^π)	$T_W(\sigma\lambda)$(normalized)		I_γ^{exp}
	1^+	2^+	
1.482 (2^+)	0.20	70	0.5(1)
0 (0^+)	1.0	1.0	1.0(4)

Table 8.9: Experimental transition intensities and transition probabilities by Weisskopf estimates [$T_W(\sigma\lambda)$] for the γ transitions populating the 3.542-MeV level. $T_W(\sigma\lambda)$ values are normalized to the transitions leading to the g.s.

γ transition [keV]	E_i [MeV] (I^π)	E_f [MeV] (I^π)	$\sigma\lambda$	$T_W(\sigma\lambda)$(normalized)	I_γ^{exp}
5414	5.414 (2^+)	g.s. (0^+)	$E2$	1.0	2.9(3)
1871	5.414 (2^+)	3.542 (1^-)	$E1$	2.0×10^2	0.5(1)
5095	5.095 (2^+)	g.s. (0^+)	$E2$	1.0	3.0(2)
1552	5.095 (2^+)	3.542 (1^-)	$E1$	1.5×10^2	1.8(1)

Table 8.10: Experimental transition intensities and transition probabilities by Weisskopf estimates [$T_W(\sigma\lambda)$] for the γ transitions deexciting the 4.683-MeV level. $T_W(\sigma\lambda)$ values are normalized to the 4.683 $\rightarrow$ 1.482 MeV transition. $T_W(\sigma\lambda)$ values are calculated in the cases of $I^\pi_{4.683} = 1^+$, 2^+, and 3^+.

E_f [MeV] (I^π)	$T_W(\sigma\lambda)$(normalized)			I_γ^{exp}
	$I^\pi_{4.683} = 1^+$	$I^\pi_{4.683} = 2^+$	$I^\pi_{4.683} = 3^+$	
1.482 (2^+)	1.0	1.0	1.0	0.5(1)
0 (0^+)	3.1	1.5×10^{-2}	5.0×10^{-8}	–

8.3.4 4.683- and 4.694-MeV levels

The β transitions to the levels at 4.683 and 4.694 MeV were observed for the first time in the present work. The allowed nature of β transition suggests that the spins and parities of these levels are 1^+, 2^+, or 3^+. The γ-transition intensities deexciting the 4.683-MeV level were compared with Weisskopf estimations as shown in Table 8.10. No observations of γ transitions to the ground state suggest that the spin-parity of 1^+ can be excluded for this level. Therefore, the spin and parity of 4.683-MeV level were deduced to be $(2, 3)^+$. Similarly, the spin and parity of 4.694-MeV level can be deduced to be $(2, 3)^+$.

8.4 1.788- and 2.466-MeV levels

8.4.1 Intensities of β decays to the 1.788- and 2.466-MeV levels

The β branch and spin-parity assignment for the 1.788-MeV level have been investigated by the β-decay experiments [GUI84; BAU89; MAC05; SCW09], and 0^+ assignment has been suggested by the recent measurements of life-time of 1.789-MeV level [MAC05] and conversion electron of the 1789 keV $E0$ transition (1.789 MeV $\rightarrow$ g.s.) [SCW09]. The β branch of this level ($I_\beta^{1.788}$) deduced in these experiments is summarized in Table 8.11. The

Table 8.11: Beta-decay intensity of the 1.788-MeV level reported by the ^{30}Na β-decay experiments.

Author	Reference	$I_\beta^{1.788}$	logft	$I_\beta^{1.788}$ (Corrected)
D. Guillemaud-Mueller *et al.*	[GUI84]	2.6(16)	6.4	0.1(15)[a]
P. Baumann *et al.*	[BAU89]	<0.6	>7.0	−1.9(9)[a]
H. Mach *et al.*	[MAC05]	4.3(12) units	–	1.8(6)[b]
W. Schwerdtfeger *et al.*	[SCW09]	–	–	–
H. Mach *et al.*	–	No[c]	–	–

[a] After relocating the 1789-keV γ transition from 1.789 MeV $\rightarrow$ g.s. to 5.022 $\rightarrow$ 3.302 MeV.
[b] Estimated by normalizing to the 4.8(5)% for the 305-keV γ ray.
[c] Schwerdtfeger *et al.* [SCW09] stressed "according to new high-statistics experimental data no imbalance between feeding and deexcitation of the 1789 keV level exists any more [MAC09]".

$I_\beta^{1.788}$ value has been calculated from the intensity balance of γ rays which excite (3179 and 3625 keV) and deexcites (305 keV) the 1.788-MeV level for all the experiments as shown in Fig. 8.7(a). It is found that the negligibly small intensity [GUI84; BAU89; MAC09] and finite value [MAC05] have been reported. It is to be emphasized that sensitive measurement of β branch is quite important to evaluate 0^+ assignment since the $2^+ \rightarrow 0^+$ β decay corresponds to the second forbidden transition. The distribution of logft value of second forbidden decay is 10−18.[6] At these situation, the β-decay intensity of 0.9 with small error of 0.6 has been deduced in the present measurement, resulting in anomalously small logft value of 7.1(4). This value indicate the contradiction to the 0^+ assignment for the 1.788-MeV level.

Figure 8.8 shows the electron energy spectrum in Ref. [SCW09]. It is found that the peak they insists as $E0$ decay is doubtful to be identified as the 1789-keV energy peak because the possibility of just a fluctuation cannot be denied. Furthermore, the energy of the peak in Fig. 8.8(b) seems to be observed at ∼1784 keV, showing disaccord with the 1789 keV. Therefore, we cannot help but mention that the 0^+ assignment for the 1.788-MeV level is less convincing.

If the 0^+ assignment for the 1.788-MeV level is correct, the possible reasons for the anomalously large β branch of this level are, (i) the 305-keV γ ray intensity is overestimated by counting γ rays which overlaps with the 305-keV γ ray of 1.788 MeV $\rightarrow$ 1.482 MeV in the γ-ray singles energy spectrum, (ii) the intensities of the 3179- and 3625-keV γ rays are

[6] The smallest logft value for the second forbidden decay is 9.58 for the transition of ^{91}Zr$_{g.s.}$ $(9/2^+) \rightarrow$ ^{91}Nb$_{g.s.}$ $(5/2^+)$ [NND11].

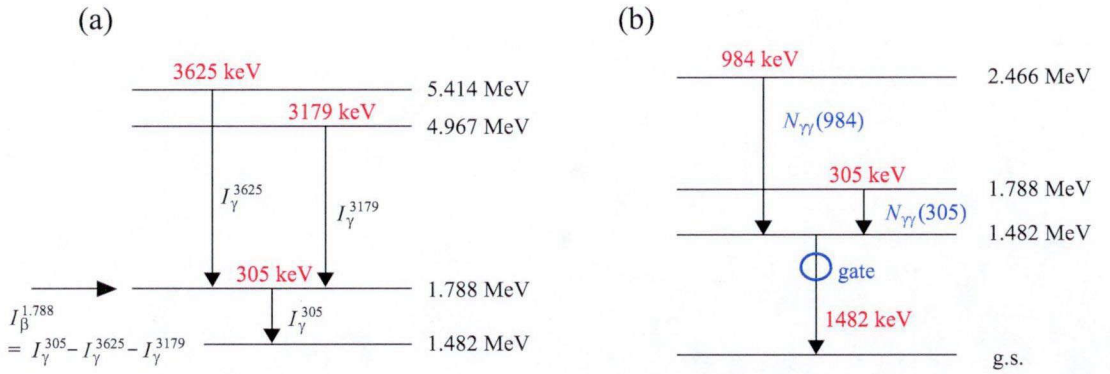

Figure 8.7: (a) Partial level scheme of ^{30}Mg. The β branch of the 1.788-MeV level is calculated by the intensity balance of the 305-, 3179, and 3625-keV; $I_\beta^{1.788} = I_\gamma^{305} - I_\gamma^{3179} - I_\gamma^{3625}$. (b) Partial level scheme of ^{30}Mg for deducing the 305-keV γ ray intensity by the γ-γ coincidence analysis. $N_{\gamma\gamma}(984)$ and $N_{\gamma\gamma}(305)$ represent the γ-ray counts of the 984 and 305 keV, respectively, in coincidence with the 1482-keV γ ray.

underestimated due to the γ-ray angular distribution derived from the residual polarization, or (iii) there are some γ transitions which populate the 1.788-MeV level from higher levels except for the 4.967- and 5.414-MeV levels with the intensities less than the sensitivity of the present measurement. For (i), the 305-keV γ ray intensity was deduced by the analysis of γ-γ coincidence data as follows. The schematic illustration of the γ-γ analysis is shown in Fig. 8.7(b). The counts of the 305- and 984-keV γ-rays which are in coincidence with the 1482-keV γ ray were obtained to be $N_{\gamma\gamma}(305)$ and $N_{\gamma\gamma}(984)$, respectively. By referring to $I_\gamma^{984} = 6.9(4)$ which was deduced from the γ-ray singles counts, the intensity of the 305-

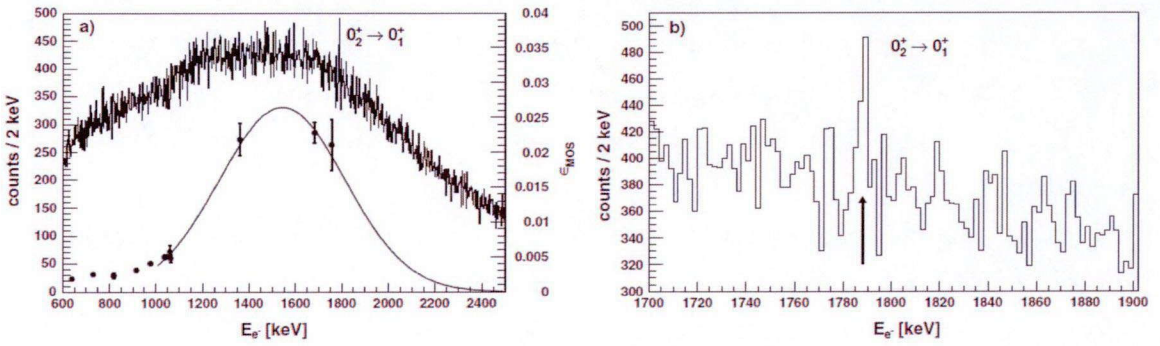

Figure 8.8: Background-subtracted electron spectrum referred from Ref. [SCW09]. (b) is expanded spectrum of (a) around the peak at 1.78 MeV.

keV γ ray is calculated as $I_\gamma^{305} = N_{\gamma\gamma}(305)/N_{\gamma\gamma}(984) \times 6.9(4) = 7.7(5)\%$, showing equal result to the value deduced from the γ-ray singles counts. For (ii), we estimated the 90°/0° anisotropy of the 3179- and 3625-keV γ rays caused by possible residual polarization (see Sec. 3.3.2 and Sec. 6.4). The result is that the isotropic assumption of the emission of these γ rays overestimates the γ-ray intensity of the 3179-keV by 5%, resulting in the 0.3% overestimation. For (iii), the upper limit of intensities of the possible γ rays which populate the 1.788-MeV level was estimated to be ~0.3% from the fluctuation of the background energy spectrum. As a result of discussions for (i)−(iii), the finite β branch of the 1.788-MeV level is concluded to be plausible.

By taking into account the less reliable 0^+ assignment for the 1.788-MeV, another spin-parity assignment can be conceivable. The possible spin-parity assignments for this level were speculated from the comparison of γ-transition intensities with Weisskopf estimates by the similar discussion as Sec. 8.3, resulting in the possible another assignments of 2^+ or 3^+.

Significant change of β-decay intensity was also obtained in the present work for the 2.466-MeV level as the negligibly small value of $I_\beta = 0.02(57)$. The latest β branch reported so far is $I_\beta = 3.8(5)$ [NND11]. This difference was deduced by finding 6 new γ rays which populate the 2.466-MeV level (2216, 2227, 2254, 2946, 3431, and 3598 keV γ rays) in the present measurement. As a result, large logft value of >7.0 compared with the reported values of 5.9 [GUI84] and 6.1 [BAU89] was deduced for this level in the present experiment in spite of the allowed β decay of $^{30}\mathrm{Na}_{\mathrm{g.s.}}$ $(2^+) \rightarrow {}^{30}\mathrm{Mg}$ [2.466 MeV: (2^+ [MAC05])].

It is to be emphasized that the spin-parity assignment of 2^+ for the 2.466-MeV level is one possible candidate because it was tentatively assigned by the fact that the $M1$ dominant decay of 984-keV γ ray as a $2^+ \rightarrow 2^+$ decay seems reasonable by the $B(E2)$ value deduced from the life time of the 2.466-MeV level [MAC05]. The possible another spin-parity assignments for this level were speculated to be 0^+ or 3^+ from the comparison of γ-transition intensities with Weisskopf estimates by the similar discussion as Sec. 8.3.

8.4.2 Spin-parity assignment from γ-ray angular distribution by residual polarization

The spins and parities of the 1.788- and 2.466-MeV levels were speculated from the angular distribution of γ rays emitted from ^{30}Mg excited state with the large residual polarization (see Sec. 3.3.2). The ratios of intensities of the 2499-, 3179-, and 3484-keV γ rays detected by the Ge detector placed at 180° to the one detected by the detector placed at 90° [R(180°/90°)] are listed in Table 8.12. It is found that the intensity of the 3484-keV γ ray [4.967 MeV (1^+)

Table 8.12: Gamma-ray angular distribution of the 3484-, 3179-, and 2499-keV γ rays in ^{30}Mg. $R(180°/90°)$ represent the anisotropy of the γ ray detected at 90° and 180°.

γ transition (keV)	$E_i \rightarrow E_f$ (MeV) $\rightarrow$ (MeV)	$I_i^\pi \rightarrow I_f^\pi$	$R(180°/90°)$
3484	4.967 $\rightarrow$ 1.482	$1^+ \rightarrow 2^+$	0.991(7)
3179	4.967 $\rightarrow$ 1.788	$1^+ \rightarrow (0^+)$	1.191(8)
2499	4.967 $\rightarrow$ 2.466	$1^+ \rightarrow (2^+)$	1.072(13)

$\rightarrow$ 1.482 MeV (2^+)] detected at 180° is almost similar to the one detected at 90°, showing the consistent result with the calculated value of $1^+ \rightarrow 2^+$ transition in Fig. 3.5(a).

The contrast values of $R(180°/90°) = 1.191(8)$ and 1.072(13) were obtained for the 3179-keV [4.967 MeV $(1^+) \rightarrow$ 1.788 MeV] and 2499-keV [4.967 MeV $(1^+) \rightarrow$ 2.466 MeV] γ rays, respectively. As the possible I^π assignment is 0^+, 2^+, or 3^+ for the 1.788-MeV level as discussed in Sec. 8.4.1, the 3179-keV transition can be $1^+ \rightarrow 0^+$, $1^+ \rightarrow 2^+$, or $1^+ \rightarrow 3^+$. The 180°/90° anisotropies of $1^+ \rightarrow 0^+$, $1^+ \rightarrow 2^+$, and $1^+ \rightarrow 3^+$ due to the residual polarization are listed in Table 8.13. Of these three transitions, $1^+ \rightarrow 0^+$ decay only shows large anisotropy. Therefore, the 3179-keV transition is most likely to be $1^+ \rightarrow 0^+$, resulting in the assignment of 0^+ for the 1.788-MeV level. In this case, residual polarization of $1^+ \rightarrow 0^+$ can be calculated by the 3179-keV γ ray; $P = (1-1.191)/(1-1.907) \sim 0.21(1)$. Then, the reduced anisotropies of γ rays under this polarization are calculated as listed in rightmost column in Table 8.13. It is found that the anisotropies of the 2499-keV γ traisntion shows good accordance with the calculated $R(180°/90°)$ values for $1^+ \rightarrow 2^+$ or $1^+ \rightarrow 3^+$ transitions. Therefore, 0^+ assignment can be excluded for the 2.466-MeV level. As discussed in this section, the plausible spins and parities of the 1.788- and 2.466-MeV levels were speculated to be 0^+, and 2^+ or 3^+, respectively, by the γ-ray anisotropy due to the residual polarization and comparison of γ-ray intensities with Weisskopf estimates.

The spins and parities assigned in the present work are summarized in Table 8.14.

Table 8.13: Estimations of γ-ray angular distribution for the 3 transitions of $1^+ \to 0^+$, $1^+ \to 2^+$, and $1^+ \to 3^+$ due to the residual polarization. These values are calculated by taking into account the solid angle of the detectors placed at 180° and 90°. $R(180°/90°)$ values for $P = 1.0$ and $P = 0.21$ are listed.

$I_i^\pi \to I_f^\pi$	$R(180°/90°)_{calc}$ ($P = 1.0$)	$R(180°/90°)_{calc}$ ($P = 0.21$)
$1^+ \to 0^+$	1.907	1.191
$1^+ \to 2^+$	1.071	1.015
$1^+ \to 3^+$	0.904	0.980

Table 8.14: Spins and parities of levels in ^{30}Mg.

E_x [MeV]	$I^{\pi a}$	$I^{\pi b}$	$I^{\pi c}$	$I^{\pi d}$	$I^{\pi e}$
g.s.	0^+	0^+	0^+	0^+	0^+
1.482	2^+	2^+	2^+	2^+	2^+
1.788	(0^+)	(0^+)	–	–	(0^+)
2.466	(2^+)	(2^+)	–	(2^+)	(2^+)
2.543	–	–	–	$(2^-, 3^-)$	$(2^-, 3^-)$
3.302	$(2, 3)^+$	–	4^+	–	–
3.380	(4^+)	–	–	(4^+)	(4^+)
3.460	$(2)^+$	(1, 2, 3)	–	(4^+)	(4^+)
3.542	$(1)^+$	–	–	–	$(1, 2)^+$
4.184	–	–	–	(5)	(5)
4.260	–	–	–	–	–
4.359	–	–	–	–	–
4.683	$(2, 3)^+$	–	–	–	–
4.694	$(2, 3)^+$	–	–	–	–
4.967	1^+	$(1, 2)^+$	–	–	$(1, 2)^+$
5.022	1^+	–	–	–	$(1, 2)^+$
5.095	2^+	–	–	–	$(1, 2)^+$
5.313	–	–	–	–	–
5.414	2^+	–	–	–	$(1, 2)^+$
5.897	$(2)^+$	–	–	–	–
6.064	2^+	–	–	–	–

[a]Present work.
[b]Taken from Ref. [SCW09].
[c]Taken from Ref. [TAK09].
[d]Taken from Ref. [DEA10].
[e]Taken from Ref. [NND11].

CHAPTER IX

Discussion: Structures of ^{28}Mg, ^{29}Mg, and ^{30}Mg

In order to clarify the nuclear structures of neutron-rich ^{28}Mg, ^{29}Mg, and ^{30}Mg, the experimental levels observed in the present work are compared with theoretical predictions based on shell model. The calculations were performed with the USD Hamiltonian [WIL84; BRO88] and its revised versions of the USDA and USDB Hamiltonians [BRO06] where nucleon excitations are restricted only in the *sd* shell. The NuShell code [BRO07] was used. The experimental levels of ^{29}Mg and ^{30}Mg are also compared with the shell-model calculations by the SDPF-M interaction, which nucleon excitations are not only in the *sd* shell but also in $1f_{7/2}$ and $2p_{3/2}$ orbits. Low-lying level structure in ^{30}Mg are also compared with the theoretical prediction by the calculation based on the constrained Hartree-Fock-Bogoliubov plus local quasiparticle random-phase approximation (CHFB+LQRPA) method [HIN11], resulting in the existence of possible collective motion. As will be described below, the comparison with these predictions revealed the change of shell structures from ^{28}Mg to ^{30}Mg as neutron number increases.

9.1 Dominant normal configurations in the levels of ^{28}Mg

Prior to estimating the β-decay probability of ^{28}Na$_{\text{g.s.}}$ the wave function of ^{28}Na$_{\text{g.s.}}$ was calculated, and it was confirmed that the experimental value of the ^{28}Na$_{\text{g.s.}}$ magnetic moment $\mu = +2.420(2)\mu_N$ [KEI00] was reproduced well ($\mu_{\text{calc}} = 2.316\mu_N$). The log$ft$ values were evaluated by assuming a quenching factor of 0.6 for the Gamow-Teller matrix element B(GT) [BRO06].

9.1.1 Levels below 5 MeV, and 5.269- and 7.461-MeV levels

Figure 9.1(a) compares the experimental levels of ^{28}Mg to the shell-model calculations with the USDB Hamiltonian. Since the detailed information of energies, spins and parities

(I^π), γ-decay branching ratios, β-decay branching ratios (I_β), and logft values were obtained in the experimental results, the comparison on a level-by-level basis has been carried out. It is to be noted that the calculated positive-parity levels show reasonable correspondence with the levels assigned in the present work as shown by the dashed lines in Fig. 9.1(a), in particular for levels below 5 MeV (1.474-, 3.862-, 4.021-, 4.555-, and 4.878-MeV levels). It is found that there are four 2^+ levels above 7.5 MeV in the calculation. Among them the 7.671-MeV level with the smallest logft value (4.4) corresponds most likely to the newly found 2^+ level at 7.461 MeV [logft = 4.6(1)]. By taking into account the spins and logft values, the predicted level at 5.519 MeV ($I^\pi = 1^+$, logft = 5.06) seem to correspond to the experimental level at 5.269 MeV [1^+, 5.2(2)]. The γ-decay branching ratios by the USDB calculation reproduce the experimental intensities well for the levels discussed in this subsection.

9.1.2 5.193-, 5.469-, 5.917-, 6.546-, and 7.200-MeV levels

Another correspondence between the experimental levels and predicted ones by taking into account the logft values and/or decay patterns, as shown by the dotted lines in Fig. 9.1(a); the experimental and predicted levels of 5.469-MeV (2, >6.0) and 5.567-MeV (2^+, 6.18), 5.917-MeV [$(0, 1, 2)^+$, 5.8(1)] and 6.070-MeV (2^+, 5.12), 6.546 MeV [$(2)^+$, 5.8(2)] and 6.948 MeV (2^+, 5.66), and 7.200 MeV [$(0, 1, 2)^+$, 5.2(2)] and 7.599-MeV (2^+, 5.80). Therefore, 2^+ spin-parity assignments are proposed for the both 5.469-, 5.917-, 6.545-, and 7.200-MeV levels. No predicted levels were calculated for the 5.171- ($I^\pi = 3^-$) and 5.193-MeV ($I = 1$) levels. The latter level has been assigned to be 1^- in Ref. [MID64] for the first time, but reassigned to be 1 by the later work in Ref. [FIS73; NND11]. Our results of the comparison between the experimental and theoretical levels seem to support the 1^- assignment.

Even though some predicted levels in higher energy show inconsistent results, the experimental levels are in good agreement with the shell-model calculation where the model space is restricted in the *sd* shell. These fact indicates negligible contribution of the intruder configurations for the positive-parity levels in ^{28}Mg. It is concluded that ^{28}Mg is located outside the region of the island of inversion.

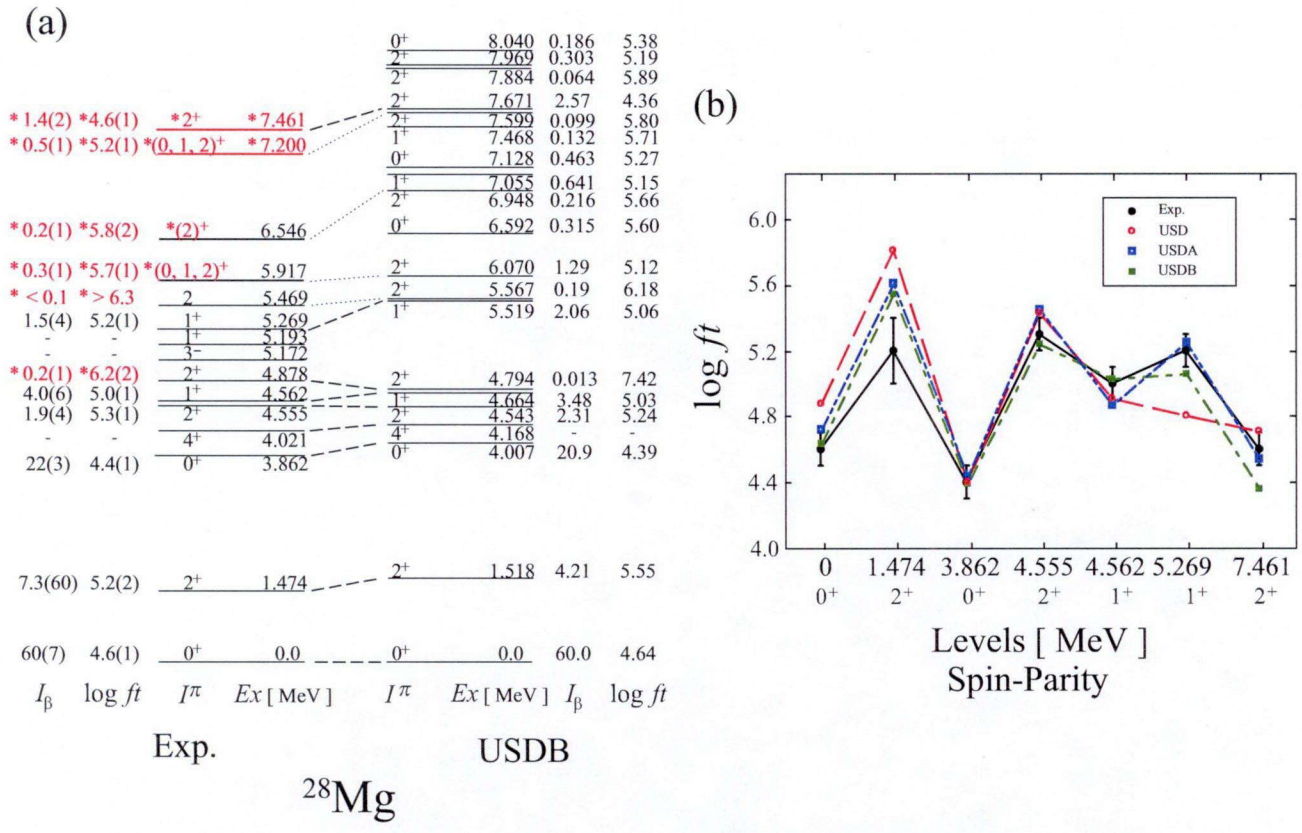

Figure 9.1: (Color online) (a) Comparison of experimental energy levels, I_β, and logft values in ^{28}Mg with the results of shell-model calculation with the USDB Hamiltonian. The newly observed β transitions, energy levels, logft values, and newly assigned spin-parity values in the present work are labeled by asterisks in red color. The corresponding levels are interconnected by dashed and dotted lines (see text in detail). (b) Comparison of logft values in ^{28}Mg. The theoretical values by the USD, USDA, and USDB Hamiltonians are denoted by the open circles (red), open (blue) and closed squires (green), respectively. The lines are to guide the eye.

9.2 Intruder levels in ^{29}Mg

Figure 9.2(a) compares the experimental levels of ^{29}Mg to the shell-model calculations with the USDB and SDPF-M Hamiltonians. The correspondences between the experimental and predicted levels are discussed by taking into account the spins and parities, level energies, logft values, and γ-decay branching ratios in the following subsections.

The comparison of logft values of the experimental and calculations with the three USD Hamiltonians is shown in Fig. 9.2(b). The logft values of the ground state and 1st excited level at 0.055 MeV are not in present since each β branching ratio could not be obtained experimentally. It is to be noted that all the spin-parity assigned levels are reasonably reproduced by the USDB Hamiltonian except for the 1.094- and 1.430-MeV levels. The precise discussions are described below.

9.2.1 Levels with normal configurations

The relative intensity of the two γ rays of 1583 keV (1.638 $\rightarrow$ 0.055 MeV) and 1638 keV (1.638 MeV $\rightarrow$ g.s.) are compared with the USDB calculations. The experimental levels at 0.055 and 1.638 MeV are assumed to be the theoretical levels at 0.045 MeV ($1/2_1^+$) and 1.594 MeV ($5/2_1^+$), respectively, by taking into account the logft values and excitation energies. Table. 9.1 shows the relative intensities of the γ rays deexciting these levels. The intensity of 2 γ rays deexciting the 1.638-MeV level is well reproduced by the calculation. Therefore, the spin-parity assignments of $1/2^+$ and $5/2^+$ for the 0.055- and 1.638-MeV levels, respectively, were confirmed to be plausible.

Similarly, the spin-parity assignments of another spin-assigned levels at 2.614, 3.223, 3.227, 3.673, and 3.985 MeV are discussed by comparing the level energies, logft values, and γ-transition branching ratios between the experimental and theoretical (USDB) results. By the consistence accordance of these physical quantities, the correspondences between the experimental and theoretical levels, as shown by the interconnected lines in Fig. 9.2(a);

Table 9.1: Relative intensities of the two γ transitions from the experimental 1.638-MeV level and the theoretical 1.594-MeV level in the USDB calculation. The intensities to the 1st excited states in both results are normalized to be 1.

γ transition (MeV)	$I_\gamma^{\rm exp}$ (normalized)	$I_\gamma^{\rm calc}$
1.638 $\rightarrow$ 0.055	1.0	1.0
1.638 $\rightarrow$ g.s.	22	26

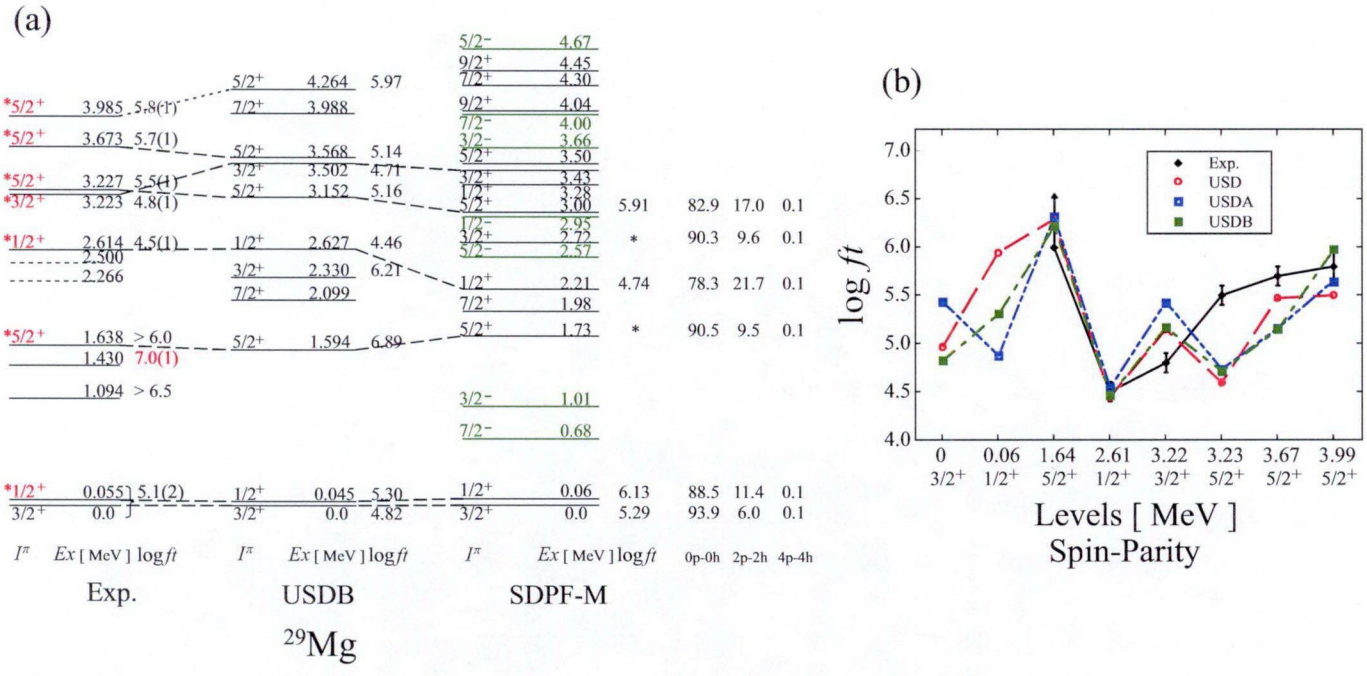

Figure 9.2: (a) Comparison of experimental levels in ^{29}Mg with shell-model calculations by the USDB and SDPF-M Hamiltonians. The newly assigned spin-parity values in the present work are labeled by asterisks in red color. The negative-parity levels reproduced by SDPF-M Hamiltonian are shown in green color. The particle occupations of normal (0p-0h) and intruder (2p-2h, 4p-4h) configurations are listed in the right 3 columns right next to the SDPF-M levels. Corresponding levels are interconnected with dashed and dotted lines (see text in detail). (b) Comparison of logft value of experimental levels in ^{29}Mg with shell-model calculation by the USDB Hamiltonian. The theoretical values by the USD, USDA, and USDB Hamiltonians are denoted by the open circles (red), open (blue) and closed squires (green), respectively. The lines are to guide the eye.

reasonable correspondences of level energies, logft values, and γ-transition branching ratios between the experimental and theoretical levels as, (experimental and theoretical levels) = {2.614 MeV [I^π = 1/2$^+$, logft = 4.5(1)] and 1.594 MeV (1/2$^+$, 6.89)}, {3.223 MeV [3/2$^+$, 4.8(1)] and 3.502 MeV (3/2$^+$, 4.71)}, {3.227 MeV [(5/2)$^+$, 5.5(1)] and 3.152 MeV (5/2$^+$, 5.16)}, and {3.673 MeV [5/2$^+$, 5.7(1)] and 3.568 MeV (5/2$^+$, 5.14)} as shown by the dashed line in Fig. 9.2(a). Another correspondence between the experimental 3.985-MeV level [(5/2)$^+$, 5.8(1)] and theoretical 4.303-MeV level (5/2$^+$, 5.97) by the level energy and logft value as shown by the dotted line in Fig. 9.2(a).

The 2.500-MeV level, which was reported in ^{29}Mg by the ^{29}Na β-decay experiment [BAU87], was not observed in the present measurement. The very small γ-decay intensities of 0.4(1) and 0.2(1) for the 2499- and 2500-keV γ rays, respectively [BAU87], are out of sensitivity in the present measurement by the estimation from background noise in the energy spectrum. By taking into account the logft value of 6.7(1) for this level in Ref. [BAU87], this level seems to correspond with the theoretical level at 2.300-MeV ($3/2_2^+$, logft = 6.21).

The correspondences between the experimental levels at 0.055, 1.638, 2.614, 3.223, and 3.227 MeV and theoretical levels at 0.06, 1.73, 2.21, 3.43, and 3.00 MeV by the SDPF-M Hamiltonian by taking into account the level energies and logft values. It is to be seen that normal configurations are dominant for these 5 levels.

9.2.2 Intruder levels at 1.094 and 1.430 MeV

It is to be noted that all the spin-parity assigned levels in ^{29}Mg in the present work shows reasonable correspondence with the USDB calculations, except for the levels at 1.094 and 1.430 MeV (see Fig. 9.2(a)). It is to be seen that the unassigned $3/2_2^+$ and $7/2_1^+$ positive-parity levels are predicted at 2.330 and 2.099 MeV, respectively, by the USDB Hamiltonian in Fig. 9.2. It is difficult to account for the 1.094- and 1.430-MeV levels by these 2 positive-parity levels because the energy discrepancies are almost 1 MeV. In fact, the 2.500-MeV level observed in the previous ^{29}Na β-decay experiment [BAU87] shows reasonable correspondence with the predicted 2.330-MeV level ($3/2_2^+$) shown later in the next subsection.

In the SDPF-M calculation, negative-parity levels are predicted at 0.68 MeV (7/2$^-$) and 1.01 MeV (3/2$^-$). The possibility of these negative-parity assignments are discussed as follows. Assuming the 3/2$^-$ and 7/2$^-$ assignments for these two levels, the possible assignments are ($I^\pi_{1.094}$, $I^\pi_{1.430}$) = (7/2$^-$, 3/2$^-$) or ($I^\pi_{1.094}$, $I^\pi_{1.430}$) = (3/2$^-$, 7/2$^-$). In the former case, possible γ transition of the 1040 keV (1.094 $\rightarrow$ 0.055 MeV) and 1385 keV (1.430 $\rightarrow$ 0.055 MeV) are $E3$ and $E1$, respectively, and vice versa in the latter case. The strongly

observed γ transition of the 1040 keV (1.094 $\rightarrow$ 0.055 MeV) favors the latter case. Therefore, we proposed the spin-parity assignments of $(I^{\pi}_{1.094}, I^{\pi}_{1.430}) = (3/2^-, 7/2^-)$. The large log$ft$ values of >6.5 and 7.0(1) for the 1.094- and 1.430-MeV levels supports these negative-parity assignments. These assignments are consistent with the previous discussion [BAU89].

9.2.3 Systematics of odd neutron-rich isotopes

As discussed above, the experimental positive-parity levels in ^{29}Mg observed in the present work are well reproduced by the shell-model calculation with the USDB Hamiltonian as shown in Fig. 9.2(a). However, 2 levels at 1.094 and 1.430 MeV could not be assigned by the USDB calculation. The $7/2^-$ and $3/2^-$ levels reproduced at 0.68- and 1.01-MeV by the SDPF-M Hamiltonian suggests that the 2 levels at 1.094 and 1.430 MeV have negative-parity with single neutron occupation in the $1f_{7/2}$ and $2f_{3/2}$ single particle orbits.

To investigate the structures of odd neutron-rich nuclei as a change of proton-neutron ratio, the lowest negative-parity levels of $3/2^-$ and $7/2^-$ are compared in the systematics of (a) $Z = 12$ isotopes and (b) $N = 17$ isotones in Fig. 9.3. The lowest 2 negative-parity levels in ^{25}Mg, ^{27}Mg, ^{31}Si, and ^{33}S are taken from Ref. [END98], and ^{33}Mg from [YOR10][7], respectively. The observed levels at 0.221 and 0.461 MeV in ^{31}Mg are tentatively assigned to be $3/2^-$ and $7/2^-$, respectively, by the AMD calculation [KIM07]. It is to be found that the sharp decreases of the energies of $3/2^-$ and $7/2^-$ levels can be seen as a neutron number increases in the neutron-rich Mg ($Z = 12$) isotopes, and as a proton number decreases in $N = 17$ isotones.

Another negative-parity level has been reported at the 2.266-MeV level ($1/2^-$ or $3/2^-$) in ^{29}Mg [BAU89]. By taking into account the $1/2^-_1$ and $3/2^-_2$ levels at over 4 MeV in ^{31}Si and ^{33}S as shown in Fig. 9.3(b), same lowering can be seen in ^{29}Mg in $N = 17$ isotopes.

To investigate the systematic change of collective behavior in these $Z = 12$ and $N = 17$ shown in Fig. 9.3, the $M1$ and $E2$ transitions related to the $(1/2^+_1, 3/2^+_1)$ and $(7/2^-_1, 3/2^-_1)$ levels, respectively, are discussed by comparing the experimental γ-transition probabilities with the ones of Weisskopf estimations as follows. Table 9.2 and 9.3 show the comparison of γ-transition probabilities deduced from life time (τ) and transition probability of Weisskopf estimate $T_W(\sigma\lambda)$ in unit of s^{-1} for $M1$ and $E2$ decay, respectively. The partial life time of the 0.975- and 3.221-MeV levels in ^{25}Mg and ^{33}S were used to calculate the $M1$ and $E2$ decay intensities, respectively. The $E2$ values between $7/2^-_1$ and $3/2^-_1$ levels were not

[7]This negative-parity assignment has been performed by laser spectroscopy experiment [YOR10], but the result is still under discussion because the low value of logft = 5.2(1) was reported [TRI08] for the β transition of ^{33}Mg(g.s.) $\rightarrow$ ^{33}Al(g.s.), which shows the possibility of positive-parity nature.

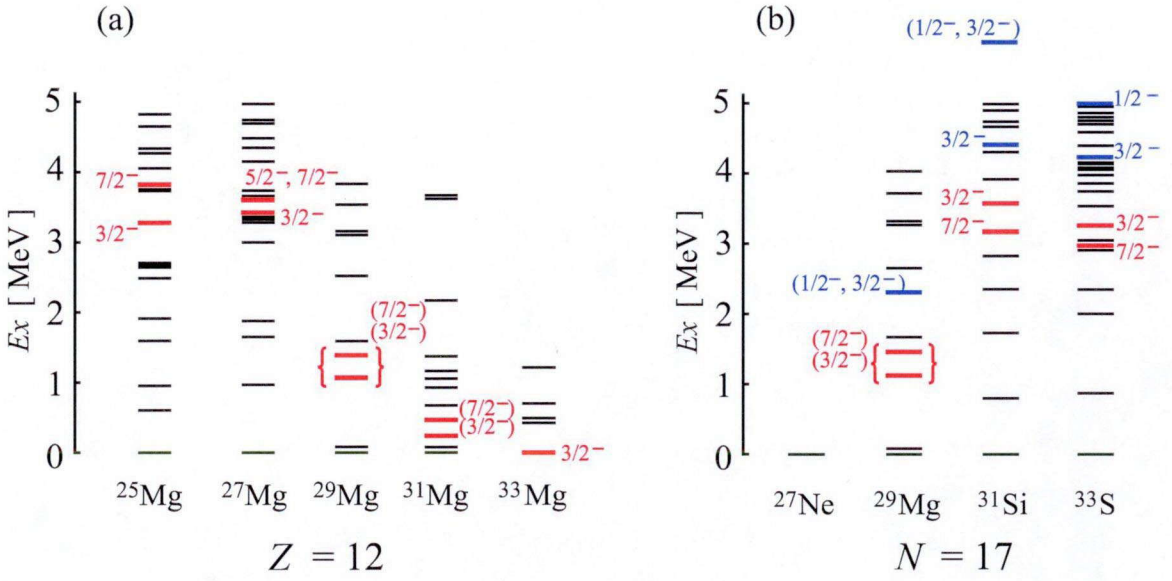

Figure 9.3: Low-lying negative parity levels of $3/2_1^-$ and $7/2_1^-$ in odd isotopes for (a) $Z = 12$ and (b) $N = 17$ (indicated by red color). The $3/2_2^-$ or $1/2_1^-$ levels are also represented with blue color in (b). These spin-parity assignments are taken from Ref. [END98], except for ^{31}Mg [MAC05; NEY05] and ^{33}Mg [YOR10].

Table 9.2: Comparison of γ-transition probabilities of $M1$ decay between the $1/2_1^+$ and $3/2_1^+$ levels in the nuclei shown in Fig. 9.3 deduced from life time and transition probability by Weisskopf estimates $T_W(\sigma\lambda)$ in unit of s^{-1}.

Nucleus	$E_i(I^\pi)$	$E_f(I^\pi)$	τ	$T_W(\sigma\lambda)$	$(1/\tau)/T_W(\sigma\lambda)$
^{25}Mg	0.975 MeV$(3/2_1^+)$	0.585 MeV$(1/2_1^+)$	10.1 psec	1.83×10^{12}	1.7×10^{-2}
^{27}Mg	0.985 MeV$(3/2_1^+)$	g.s.$(1/2_1^+)$	0.97 psec	2.96×10^{13}	2.4×10^{-2}
^{29}Mg	0.055 MeV$(1/2_1^+)$	g.s.$(3/2_1^+)$	1.27 nsec	5.16×10^{9}	0.11
^{31}Mg	0.050 MeV$(3/2_1^+)$	g.s.$(1/2_1^+)$	16 nsec	3.88×10^{9}	1.1×10^{-2}
^{31}Si	0.752 MeV$(1/2_1^+)$	g.s.$(3/2_1^+)$	530 fsec	1.32×10^{13}	0.10
^{33}S	0.841 MeV$(1/2_1^+)$	g.s.$(3/2_1^+)$	1.15 psec	1.84×10^{13}	0.10

Table 9.3: Comparison of γ-transition probabilities of $E2$ decay between the negative-parity levels in the nuclei shown in Fig. 9.3 deduced from life time and transition probability by Weisskopf estimates $T_W(\sigma\lambda)$ in unit of s^{-1}.

Nucleus	$E_i(I^\pi)$	$E_f(I^\pi)$	τ	$T_W(\sigma\lambda)$	$(1/\tau)/T_W(\sigma\lambda)$
^{25}Mg	3.971 MeV($7/2_1^-$)	3.413 MeV($3/2_1^-$)	22 fsec	2.93×10^8	-
^{27}Mg	3.761 MeV($7/2_1^-$)	3.562 MeV($3/2_1^-$)	0.42 psec	1.87×10^6	-
^{29}Mg	1.430 MeV($7/2_1^-$)	1.095 MeV($3/2_1^-$)	1.4 nsec	2.78×10^7	18
^{31}Mg	0.461 MeV($7/2_1^-$)	0.221 MeV($3/2_1^-$)	10.5 nsec	5.74×10^6	12
^{31}Si	3.533 MeV($3/2_1^-$)	3.134 MeV($7/2_1^-$)	<10 fsec	7.29×10^7	-
^{33}S	3.221 MeV($3/2_1^-$)	2.935 MeV($7/2_1^-$)	27 fsec	1.50×10^7	1.1

deduced in ^{25}Mg, ^{27}Mg and ^{31}Si because no γ transitions were reported for these nuclei. Of the two reported assignments of $5/2^-$ and $7/2^-$ at the 3.761-MeV level in ^{27}Mg, $7/2^-$ assignment is assumed. By considering the hindrance factor of 10^{-2} in the case of l-forbidden $M1$ transition in this nuclear region [MOR76], consistent values are obtained in ^{25}Mg, ^{27}Mg and ^{31}Mg, whereas the anomalous large values of 0.11, 0.10, and 0.10 were obtained for ^{29}Mg, ^{31}Si, and ^{33}S, respectively, indicating the collective nature of the related energy levels. However, it is understood that systematic change of $M1$ transition probability cannot be seen as proton number decreases or neutron number increases. In the case of $7/2^- \rightarrow 3/2^-$ $E2$ decay, the anomalous large values are obtained in ^{29}Mg and ^{31}Mg, indicating the collectivity for the related levels. However, it is difficult to discuss the systematic change of $E2$ transition probabilities because of no data in ^{25}Mg and ^{27}Mg.

9.3 Shape coexistence in ^{30}Mg

9.3.1 Different structures in ^{30}Mg

Figure 9.4 shows the comparison of the experimental levels in ^{30}Mg with the shell-model calculations using the USDB and SDPF-M Hamiltonians. The fractions of particle-hole configurations for the levels predicted by the SDPF-M calculation are presented in the right 3 columns.

It is to be noted that the 0_2^+ level is predicted quite high energy (5.818 MeV) by the USDB Hamiltonian compared to the experimental level at 1.788 MeV. This result indicates the insufficient model space with only *sd*-shell to reproduce the levels in ^{30}Mg. On the contrary, the levels of 0_2^+, 2_2^+, and 4_1^+ were reasonably reproduced by the SDPF-M Hamiltonian (2.120, 3.000, and 3.850 MeV, respectively). This fact suggests the dominant intruder configurations

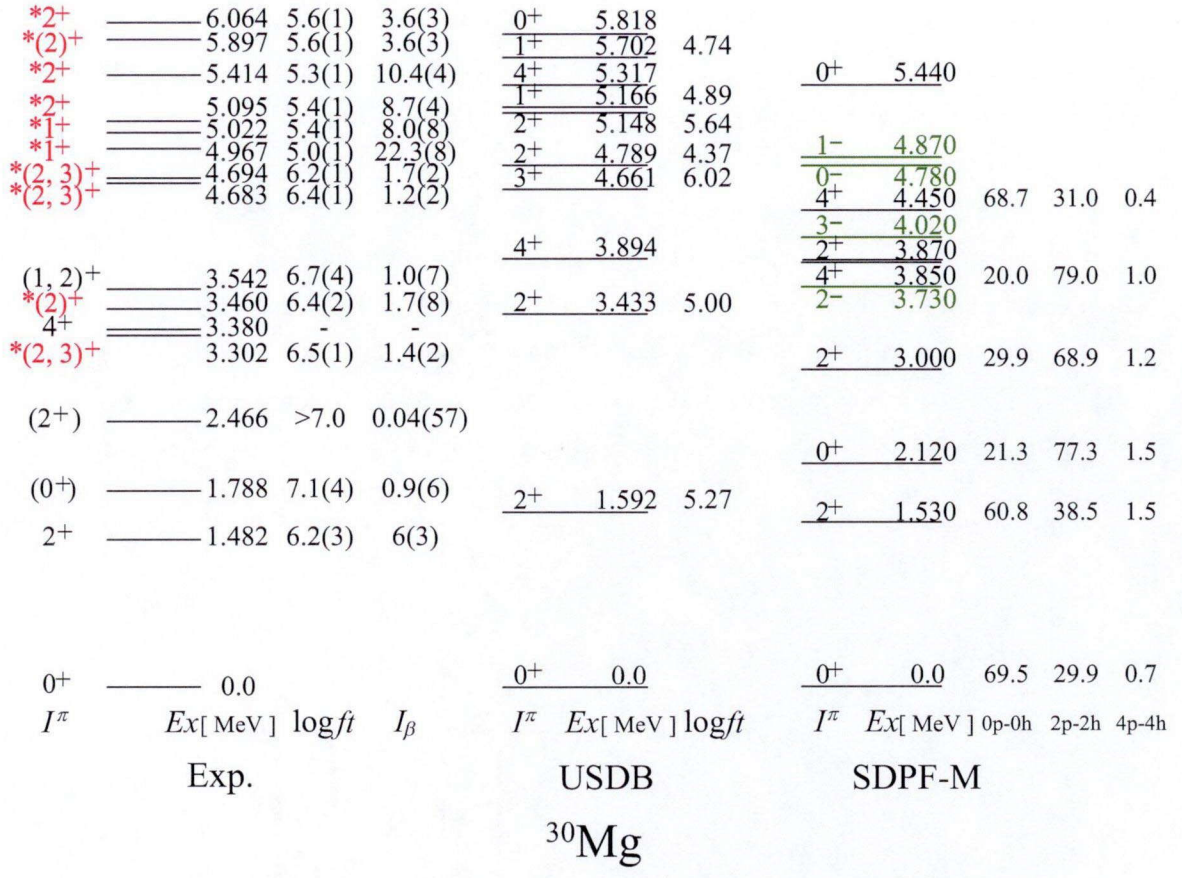

Figure 9.4: Comparison of experimental levels in ^{30}Mg with shell model calculations by the USDB and SDPF-M Hamiltonians. The newly assigned spin-parity values in the present work are indicated by asterisks in red color. The values of the three columns right next to the levels by the SDPF-M Hamiltonian represent the probabilities to occupy normal (0p-0h) and intruder (2p-2h, 4p-4h) configurations.

in these levels, resulting in the large deformation. It is also to be mentioned that higher levels above 3 MeV are not successfully reproduced by the both Hamiltonians. Further modifications are necessary for the both theoretical calculations to reproduce higher excited states.

9.3.2 Exotic natures in 1.788-, 2.466-, 3.460-, 4.967-, and 5.414-MeV levels

It is to be noted that the β branch of the 1.788-MeV level was deduced to be 0.9(6)%, resulting in the extraordinary small logft value of 7.1(4) in spite of the second forbidden β transition by taking into account the 0^+ assignment for the 1.788-MeV level as discussed in

Sec. 8.4.1. This fact suggests that the 1.788-MeV level have very close nuclear structure to the ^{30}Na ground state which have been reported to have large deformed shape [TRI07]. This result is consistent with the large deformation for this level [SCW09].

It is also worth noting that the 0_2^+ level is populated by γ-transitions from higher two levels 5 times more than the β-transition, and that the two higher levels are associated with large β-transition probabilities. This situation is illustrated in Fig. 9.5 as a partial decay scheme of ^{30}Na. It is found that the largest β-transition (22.3%) goes to the 4.967-MeV level (1^+), then leads to the 0_2^+ level with 5.6% intensity, and the next largest one (10.4%) goes to the 5.414-MeV level (2^+) and finally to the 0_2^+ level (1.3%). The fact that $^{30}\mathrm{Na}_{\mathrm{g.s.}}$ is well deformed suggests that these two levels have also intruder configurations to a large extent.

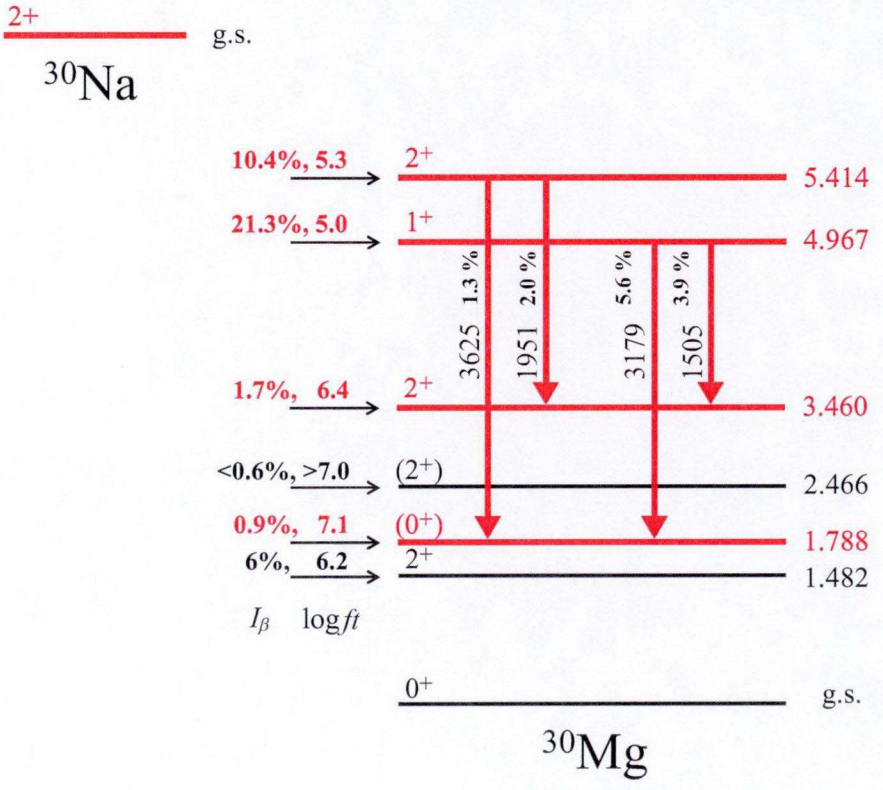

Figure 9.5: Partial decay scheme of ^{30}Na.

It is also to be noted that the 3.460-MeV level are largely populated by the γ transitions from the 4.967- and 5.414-MeV levels as shown in Fig. 9.5. To discuss more quantitatively, the observed γ-transition probabilities from the 4.967-MeV and 5.414-MeV levels are compared with the Weisskopf estimates as summarized in Table 9.4 and 9.5, respectively. It is found that the transitions 4.967 (1^+)$\rightarrow$ 3.460 (2^+) and 5.414 (2^+) $\rightarrow$ 3.460 (2^+) show very large

values compared to the Weisskopf estimates. This fact suggests that the 3.460-MeV level has also deformed shape with intruder configuration.

Table 9.4: Experimental transition intensities and transition probabilities by Weisskopf estimates [$T_W(\sigma\lambda)$] for the γ transitions deexciting the 4.967-MeV level (1^+). Both the experimental and Weisskopf estimates are normalized to those of the ground state transition.

	$E_x^f(I_f^\pi)$	0.0 (0_1^+)	1.482 (2_1^+)	1.788 (0_2^+)	3.460 (2^+)
	$\sigma\lambda$	$M1$	$M1$	$M1$	$M1$
I_γ	experiment	1.0	0.66(7)	0.78(8)	0.55(5)
	Weisskopf est.	1.0	0.35	0.26	0.03

Table 9.5: Experimental transition intensities and transition probabilities by Weisskopf estimates [$T_W(\sigma\lambda)$] for the γ transitions deexciting the 5.414-MeV level (2^+). Both the experimental and Weisskopf estimates are normalized to those of the ground state transition.

	$E_x^f(I_f^\pi)$	0.0 (0_1^+)	1.788 (0_2^+)	1.482 (2_1^+)	3.460 (2^+)
	$\sigma\lambda$	$E2$	$E2$	$M1$	$M1$
I_γ	experiment	1.0	0.43(6)	1.0	0.79(9)
	Weisskopf est.	1.0	0.13	1.0	0.12

Note that the β-decay intensity to the level at 2.466 MeV (2^+) was found to be negligibly small in the present work, whereas the previous work reported 3.8(5)% [NND11]. By taking into account the large β-decay intensity of 5(1)% for the allowed transition of $^{30}\mathrm{Na}_{\mathrm{g.s.}}$ (2^+) $\rightarrow$ 1.482 MeV (2^+) in spite of the transition between different nuclear structures ($^{30}\mathrm{Na}_{\mathrm{g.s.}}$: deformed [TRI07], 1.482 MeV: spherical [TER08]), the negligibly small β-decay intensity of $^{30}\mathrm{Na}_{\mathrm{g.s.}}$ (2^+) $\rightarrow$ 2.466 MeV (2^+) suggests that this level have different nuclear structure from both spherical and deformed shapes.

9.3.3 Collective nature in ^{30}Mg levels

The low-lying ^{30}Mg levels are compared with the predicted level structures by the CHFB + LQRPA method as shown in Fig. 9.6. The $B(E2)$ values are listed in the right side (calculation), and the experimental transition intensities are listed in the left side (experiment). It is to be confirmed that the ratios of energies of 2_1^+ and 4_1^+ levels (R_{42}) for both experiment and calculation show almost same values [$R_{42} = 2.3$ (exp.) and $R_{42} = 2.4$ (calc.)]. This fact shows the capability of producing the experimental levels by this calculation.

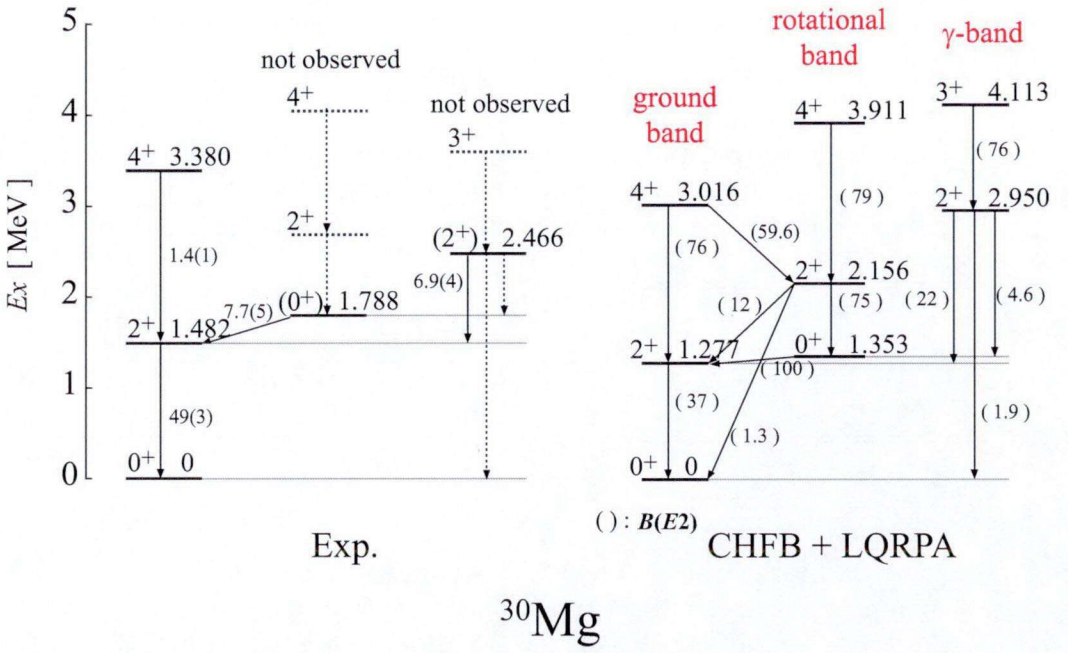

Figure 9.6: Comparison of low-lying levels in ^{30}Mg with the predicted level structures (partial) by the CHFB + LQRPA method.

The second 0^+ level is reproduced at 1.353 MeV as the ground state of rotational band in the calculation, showing good correspondence between the experimental 1.788-MeV level (0_2^+) with large deformation. The upper levels of 2_2^+, 4_2^+, etc., in the rotational band could not be confirmed in the present experimental data. This may be due to the reason that the rotating levels with large deformation could not be populated by the β decay experiment.

The quite small $\log ft$ value of >7.0 has been obtained for the 2.466-MeV level (2^+) in the present measurement in spite of the allowed β transition, indicating the unique structure compared to the other 2^+ level such as 1.482-MeV [I_β = 6(3), $\log ft$ = 6.2(3)]. By taking into account the fact that the $M1$ decay of $2_3^+ \rightarrow 2^+$ transition is hindered when competing with $E2$ transtion for the actual case, good agreement of levels at the 2.466 MeV (exp) and 2.950 MeV (calc) can be seen by the energy and decay pattern of γ rays depopulating these levels. Therefore, the 2.466-MeV level (2^+) is a good candidate of the band head of γ-vibrational band. This collective nature is consistent with the conclusion that this level have different structure from the levels with intruder dominant configurations (see Sec. 9.3.2). Unfortunately, the upper levels of this band structure connecting to the 2.466-MeV level could not be confirmed in the present study. This is because these collective levels is difficult to populate by the β-decay work. Therefore, another experimental approaches are necessary

to populate these collective levels such as rotational or γ-vibrational band.

To summarize the discussion for ^{30}Mg, the coexistence of 3 different shapes of spherical, deformed, and γ-vibrational have been found in ^{30}Mg in the present work. Firm spin-parity assignments for respective levels in a wide excitation energy range made it enable to discuss such anomalous shapes.

CHAPTER X

Summary and perspective

The level structures of ^{28}Mg, ^{29}Mg, and ^{30}Mg have been investigated by the unique experimental method in the present work. The spins and parities of levels in ^{28}Mg, ^{29}Mg, and ^{30}Mg were unambiguously assigned by measuring the anisotropic decay of β ray emitted from spin-polarized ^{28}Na, ^{29}Na, and ^{30}Na, respectively. By the detailed β-γ and γ-γ analyses, the decay schemes of ^{28}Na, ^{29}Na, and ^{30}Na were revised drastically by finding many new γ rays, β transitions, and energy levels, and assigning the spins and parities of many excited levels in ^{28}Mg, ^{29}Mg, and ^{30}Mg. By the consistent spin-parity assignments for the 3 levels in ^{28}Mg have shown the validity of this experimental method. It is to be mentioned that the spins and parities of all the excited levels in ^{29}Mg were assigned for the first time, except for the 2 levels at 1.094 and 1.430 MeV. For ^{30}Mg, it is to be found that most of the β decays from ^{30}Na are concentrated on to the levels above 5 MeV in ^{30}Mg. Another discriminative result was obtained in ^{30}Mg that nuclear structure at 2.466-MeV level have shown by the negligibly small β branch in spite of its allowed β-decay nature.

Firm establishments of level schemes of ^{28}Mg, ^{29}Mg, and ^{30}Mg enabled us to discuss the level structures of these nuclei by comparing with the theoretical predictions on a level-by-level basis. As a result, structure change due to the increasing neutron number have been clarified. For ^{28}Mg, the excited levels were well reproduced by the shell-model calculations with the USD interactions in a wide energy range. The levels in this nucleus are well explained by the nucleon excitations in the *sd* shell. For ^{29}Mg, good correspondences are shown between the experiment and predicted levels by the shell-model calculation with the USD interactions, except for the 1.094- and 1.430-MeV levels. By the large logft values for the 1.094- and 1.430-MeV levels and the predicted $7/2^-$ and $3/2^-$ levels at 0.68 and 1.01 MeV in the SDPF-M calculation, negative-parity assignments for these two levels were highly suggested. These facts suggest the narrowing of $N = 20$ shell gap in ^{29}Mg. For ^{30}Mg, the large deformations were suggested for the 4 excited levels at 1.788, 3.460, 4.967, and

5.414 MeV by the experimental facts and the comparison with the shell-model calculations. Furthermore, the very different nature from spherical or deformed shapes was suggested for the 2.466-MeV level by taking into account the predicted level structures by the CHFB + LQRPA method. Namely, 3 different shapes are found to coexist in ^{30}Mg.

In the present study, this experimental method to investigate the level structures placing emphasis on spin-parity assignment have been proven to be very successful. The structure change have been clarified in ^{28}Mg, ^{29}Mg, and ^{30}Mg as a neutron number increases. This systematic study goes on to heavier Mg isotopes across through the island of inversion.

ACKNOWLEDGEMENTS

I would like to express my gratitude to many people who have offered warm encouragements, valuable discussions and kind advices to make my research work in the master's and Ph.D courses at Osaka University most fruitful.

Most of all, I am deeply grateful to Prof. Tadashi Shimoda who gave me the opportunity to engage in the great research project and nourish me to see things more deeply. My heartfelt appreciation also goes to Assistant Professor Atsuko Odahara who helps me to carry out my study in many precise ways, and gave me comments and suggestions of inestimable value. I would also like to thank Prof. T. Kishimoto, Prof. M. Asakawa, and Prof. N. Aoi to judge me in the doctoral dissertation.

I would like to thank all the Osaka and KEK collaborators of the S1114 project at TRIUMF; to Dr. T. Suzuki for supporting and giving me fruitful advices and discussions. to Dr. Y. Hirayama for supporting and give me fruitful advices and suggestions on the whole of this work, to Dr. N. Imai for your help during the experimental time, to Prof. H. Miyatake for discussion about the experimental results, to R. Leguillon and C. Petrache for supporting me during experiment in 2010, to the students in Shimoda laboratory for staying at TRIUMF and helping this work; T. Hori, T. Masue, A. Takashima, M. Kazato, Y. Ito, Y. Kenmoku, J. Takatsu, K. Nishibata, R. Yokoyama, N. Hamatani, especially to K. Kura and M. Suga for supporting in various parts of the present work.

I wish to express my gratitude to the staff members of TRIUMF for their kind and excellent collaboration. Special thanks goes to Dr. J-M. Poutissou and G. Ball, the head persons of Science Division at the experimental times carried out in 2007 and 2010, respectively, who kindly took every arrangement at TRIUMF to make the present experiments successful. My appreciation also goes to Dr. Matt Pearson for his technical support with great care during our stay in all the experimental time, to Dr. C. D. P. Levy for providing us largely spin-polarized Na beams, to Dr. A. C. Morton and other staffs for sending us unstable beams of Na isotopes as much as possible, to Dr. K. Olchanski for helping me to establish DAQ system, and to other staffs at TRIUMF who provided us every support and useful information.

I would also like to express my gratitude to the researchers for their supports and discussions about establishing data acquisition system, providing us the useful equipments, and theoretical calculations, etc.; to Prof. K. Matsuyanagi, and Dr. N. Hinohara for theoretical discussions of collective nuclear motions, to Prof. H. Sagawa for fruitful discussion about shell-model calculations, to Dr. Y. Utsuno, for sending us the large-scale shell-model calculation data, to Prof. B. A. Brown for providing NuShell code, to Dr. M. Asai for providing us another experimental result about ^{29}Mg, to Prof. T. Ishii for providing us Ge detectors with high efficiency and great energy resolution, to Dr. T. Koike for providing us many Ge detectors and equipments, to Dr. H. Baba for many advises of NBBQ, to Dr. S. Takeuchi for analysis code Anapaw.

Finally, I wish to express my heartfelt gratitude to my family to support and encourage me throughout my academic life for several years.

APPENDICES

APPENDIX A

Data pre-sorting for analysis

A.1 Gain shift correction for Ge detectors

The gain shift of all ADC channels for energy signal of Ge detectors were checked. Some signal showed gain shift during the experiment of ^{29}Na, and ^{30}Na. Table A.1 and A.2 show the energy signal check of Ge detectors for every block data (RUN) during the experiments of ^{29}Na, and ^{30}Na, respectively. The symbols of ◯, †, and × represent the signal with no gain shift, shift-corrected, and not used, respectively.

Table A.1: The gain shift check of each RUN in ^{29}Mg: ○, †, and ×, represent no gain shift, shift-corrected, not used, respectively.

signal \ RUN	1	2	3	4	5	6	7	8	9	10	11	12	13	14	15	16	17	18	19	20	21	22
1	○	○	○	○	○	○	○	○	○	○	○	○	○	○	○	○	○	○	○	○	○	○
2	○	○	○	○	○	○	○	○	○	○	○	○	○	○	○	○	○	○	○	○	○	○
3	○	○	○	○	○	○	○	○	○	○	○	○	○	○	○	○	○	○	○	○	○	○
4	○	○	○	○	○	○	○	○	○	○	○	○	○	○	○	○	○	○	○	○	○	○
5	†	†	†	†	†	†	†	†	†	†	†	†	†	†	†	†	†	†	†	†	†	†
6	○	○	○	○	○	○	○	○	○	○	○	○	○	○	○	○	○	○	○	○	○	○
6 high	○	○	○	○	○	○	○	○	○	○	○	○	○	○	○	○	○	○	○	○	○	○
7	○	○	○	○	○	○	○	○	○	○	○	○	○	○	○	○	○	○	○	○	○	○
R	○	○	○	○	○	○	○	○	○	○	○	○	○	○	○	○	○	○	○	○	○	○
R low	○	○	○	○	○	○	○	○	○	○	○	○	○	○	○	○	○	○	○	○	○	○
L	†	†	†	†	†	†	†	†	†	†	†	†	†	†	†	†	†	†	†	†	†	†
L low	○	○	○	○	○	○	○	○	○	○	○	○	○	○	○	○	○	○	○	○	○	○

	23	24	25	26	27	28	29	30	31	32	33	34	35	36	37	38	39	40	41	42	43
1	○	○	○	○	○	○	○	○	○	○	○	○	○	○	○	○	○	○	○	○	○
2	○	○	○	○	○	○	○	○	○	○	○	○	○	○	○	○	○	○	○	○	○
3	○	○	○	○	○	○	○	○	○	○	○	○	○	○	○	○	○	○	○	○	○
4	○	○	○	○	○	○	○	○	○	○	○	○	○	○	○	○	○	○	○	○	○
5	†	†	†	†	†	†	†	†	†	†	†	†	†	†	†	†	†	†	†	†	†
6	○	○	○	○	○	○	○	○	○	○	○	○	○	○	○	○	○	○	○	○	○
6 high	○	○	○	○	○	○	○	○	○	○	○	○	○	○	○	○	○	○	○	○	○
7	○	○	○	○	○	○	○	○	○	○	○	○	○	○	○	○	○	○	○	○	○
R	○	○	○	○	○	○	○	○	○	○	○	○	○	○	○	○	○	○	○	○	○
R low	○	○	○	○	○	○	○	○	○	○	○	○	○	○	○	○	○	○	○	○	○
L	†	†	†	†	†	†	†	†	†	†	†	†	†	†	†	†	†	†	†	†	†
L low	○	○	○	○	○	○	○	○	○	○	○	○	○	○	○	○	○	○	○	○	○

Table A.2: The gain shift check of each RUN in ^{30}Mg I: ○, †, and ×, represent no gain shift, shift-corrected, not used, respectively.

signal \ RUN	1	2	3	4	5	6	7	8	9	10	11	12	13	14	15	16	17	18	19	20	21	22	23	24	25	26
1	†	†	†	†	†	†	†	†	†	†	†	†	†	†	†	†	†	†	†	†	†	†	†	†	†	†
2	×	×	×	×	×	×	×	×	×	×	×	×	×	×	×	×	×	×	×	×	×	×	×	×	×	×
3	○	○	○	○	○	○	○	○	○	○	○	○	○	○	○	○	○	○	○	○	○	○	○	○	○	○
4	○	○	○	○	○	○	○	○	○	○	○	○	○	○	○	○	○	○	○	○	○	○	○	○	○	○
5	×	×	×	×	×	×	×	×	×	×	×	×	×	×	×	×	×	×	×	×	×	×	×	×	×	×
6	†	†	†	†	†	†	†	†	†	†	†	†	†	†	†	†	†	†	†	†	†	†	†	†	†	†
7	○	○	○	○	○	○	○	○	○	○	○	○	○	○	○	○	○	○	○	○	○	○	○	○	○	○
R	×	×	×	×	×	×	×	×	×	×	×	×	×	×	×	×	×	×	×	×	×	×	×	×	×	×
R low	○	○	○	○	○	○	○	○	○	○	○	○	○	○	○	○	○	○	○	○	○	○	○	○	○	○
L	○	○	○	○	○	○	○	○	○	○	○	○	○	○	○	○	○	○	○	○	○	○	○	○	○	○
L low	×	×	×	×	×	×	×	×	×	×	×	×	×	×	×	×	×	×	×	×	×	×	×	×	×	×

	27	28	29	30	31	32	33	34	35	36	37	38	39	40	41	42	43	44	45	46	47	48	49	50	51	52
1	†	†	†	†	†	†	†	†	†	†	†	†	†	†	†	†	†	†	†	†	†	†	†	†	†	†
2	×	×	×	×	×	×	×	×	×	×	×	×	×	×	×	×	×	×	×	×	×	×	×	×	×	×
3	○	○	○	○	○	○	○	○	○	○	○	○	○	○	○	○	○	○	○	○	○	○	○	○	○	○
4	○	○	○	○	○	○	○	○	○	○	○	○	○	○	○	○	○	○	○	○	○	○	○	○	○	○
5	×	×	×	×	×	×	×	×	×	×	×	×	○	○	○	○	○	○	○	○	○	○	○	○	○	○
6	†	†	†	†	†	†	†	†	†	†	†	†	†	†	†	†	†	†	†	†	†	†	†	†	†	†
7	○	○	○	○	○	○	○	○	○	○	○	○	○	○	○	○	○	○	○	○	○	○	○	○	○	○
R	×	×	×	×	×	×	×	×	×	×	×	×	×	×	×	×	×	×	×	×	×	×	×	×	×	×
R low	○	○	○	○	○	○	○	○	○	○	○	○	○	○	○	○	○	○	○	○	○	○	○	○	○	○
L	○	○	○	○	○	○	○	○	○	○	○	○	○	○	○	○	○	○	○	○	○	○	○	○	○	○
L low	×	×	×	×	×	×	×	×	×	×	×	×	×	×	×	×	×	×	×	×	×	×	×	×	×	×

Table A.3: The gain shift check of each RUN in ^{30}Mg II: ○, †, and ×, represent no gain shift, shift-corrected, not used, respectively.

signal \ RUN	53	54	55	56	57	58	59	60	61	62	63	64	65	66	67	68	69	70	71	72	73	74	75	76	77	78
1	†	†	†	†	†	†	†	†	†	†	†	†	†	†	†	†	†	†	†	†	†	†	†	†	†	†
2	×	×	×	×	×	×	×	×	×	×	×	×	×	×	×	×	×	×	×	×	×	×	×	×	×	×
3	○	○	○	○	○	○	○	○	○	○	○	○	○	○	○	○	○	○	○	○	○	○	○	○	○	○
4	○	○	○	○	○	○	○	○	○	○	○	○	○	○	○	○	○	○	○	○	○	○	○	○	○	○
5	○	○	○	○	○	○	○	○	○	○	○	○	○	○	○	○	○	○	○	○	○	○	○	○	○	○
6	†	†	†	†	†	†	†	†	†	†	†	†	†	†	†	†	†	†	†	†	†	†	†	†	†	†
7	○	○	○	○	○	○	○	○	○	○	○	○	○	○	○	○	○	○	○	○	○	○	○	○	○	○
R	×	×	×	×	×	×	×	×	×	×	×	×	×	×	×	×	×	×	×	×	×	×	×	×	×	×
R low	○	○	○	○	○	○	○	○	○	○	○	○	○	○	○	○	○	○	○	○	○	○	○	○	○	○
L	○	○	○	○	○	○	○	○	○	○	○	○	○	†	†	†	†	†	†	†	†	†	†	†	†	†
L low	×	×	×	×	×	×	×	×	×	×	×	×	×	×	×	×	×	×	×	×	×	×	×	×	×	×

signal \ RUN	79	80	81	82	83	84	85	86	87	88	89	90	91	92	93	94	95	96	97	98	99	100	101	102
1	†	†	†	†	†	†	†	†	†	†	†	†	†	†	†	†	†	†	†	†	†	†	†	†
2	×	×	×	×	×	×	×	×	×	×	×	×	×	×	×	×	×	×	×	×	×	×	×	×
3	○	○	○	○	○	○	○	○	○	○	○	○	○	○	○	○	○	○	○	○	○	○	○	○
4	○	○	○	○	○	○	○	○	○	○	○	○	○	○	○	○	○	○	○	○	○	○	○	○
5	○	○	○	○	○	○	○	○	○	○	○	○	○	○	○	○	○	○	○	○	○	○	○	○
6	†	†	†	†	†	†	†	†	†	†	†	†	†	†	†	†	†	†	†	†	†	†	†	†
7	○	○	○	○	○	○	○	○	○	○	○	○	○	○	○	○	○	○	○	○	○	○	○	○
R	×	×	×	×	×	×	×	×	×	×	×	×	×	×	×	×	×	×	×	×	×	×	×	×
R low	○	○	○	○	○	○	○	○	○	○	○	○	○	○	○	○	○	○	○	○	○	○	○	○
L	†	†	†	†	†	†	†	†	†	†	†	†	†	†	†	†	†	†	†	†	†	†	†	†
L low	×	×	×	×	×	×	×	×	×	×	×	×	×	×	×	×	×	×	×	×	×	×	×	×

A.2 Gated spectra for new γ rays and levels

A.2.1 ^{28}Mg

The γ-ray energy spectra in coincidence with the γ rays in ^{28}Mg observed in the present work are shown in Fig. A.1 to A.12. It is to be noted that the 2008-keV γ ray, which was found as the transition of 7.200 $\rightarrow$ 5.193 MeV, is confirmed to be in coincidence with the 1474-keV γ ray as shown in Fig. A.4 although the cascade transition(s) between the 5.193- and 1.473-MeV levels were not confirmed in the present work. This might caused by the small sensitivity for the intertransition in the present measurement expected from the small intensity of 2008-keV γ ray. Another possibilities are (i) cascade of 2008-5193-1474 keV transition and (ii) the existence of another 2008 keV γ ray which is in coincidence relation with the 1474 keV. The solution (i) is impossible because the lower neutron threshold level at S_n = 8.5 MeV compared with the 2.008 + 5.193 + 1.474 = 8.676 MeV. The solution (ii) is also preferable. However, we could not confirm the 2008 keV γ ray in the γ-ray energy spectrum gated on the 1474 keV shown in Fig.A.4. Hence, the coincidence relation of 2008 and 1474 keV was confirmed incompletely. At least, we established the assignments of 2008-keV γ transition (7.200 $\rightarrow$ 5.193 MeV) as indicated in Fig. 6.2.

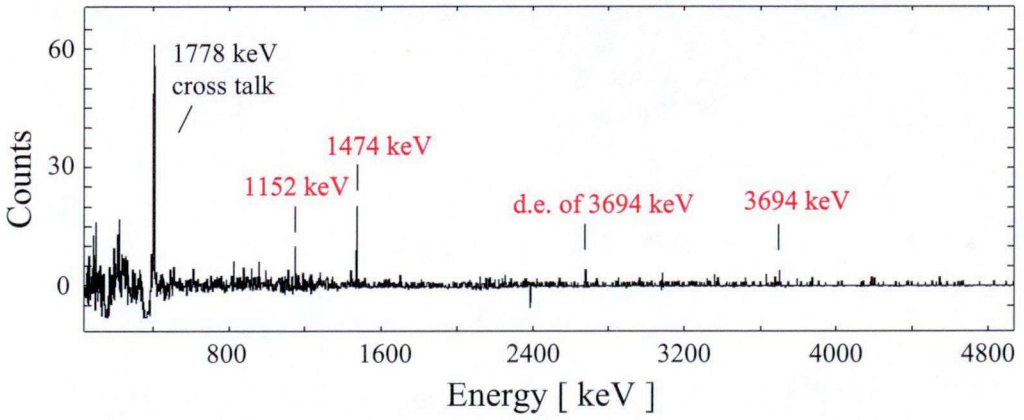

Figure A.1: Gamma-ray energy spectrum in coincidence with the 1373-keV γ ray.

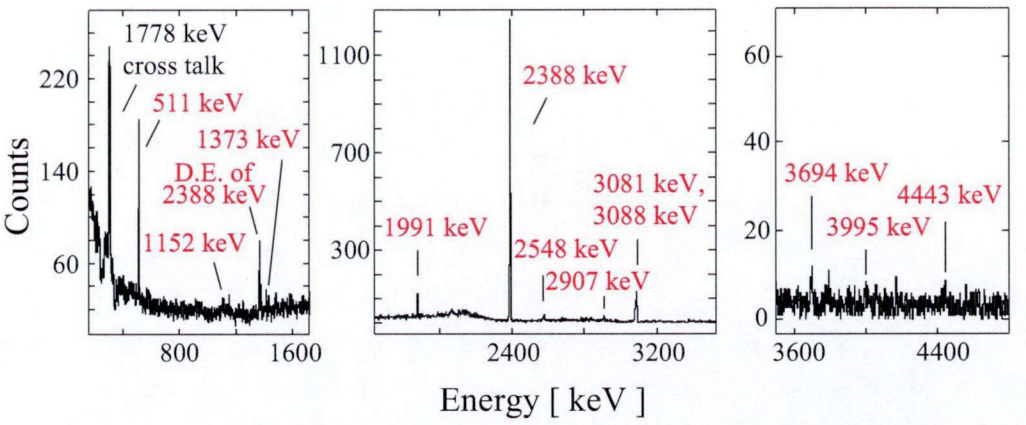

Figure A.2: Gamma-ray energy spectrum in coincidence with the 1474-keV γ ray.

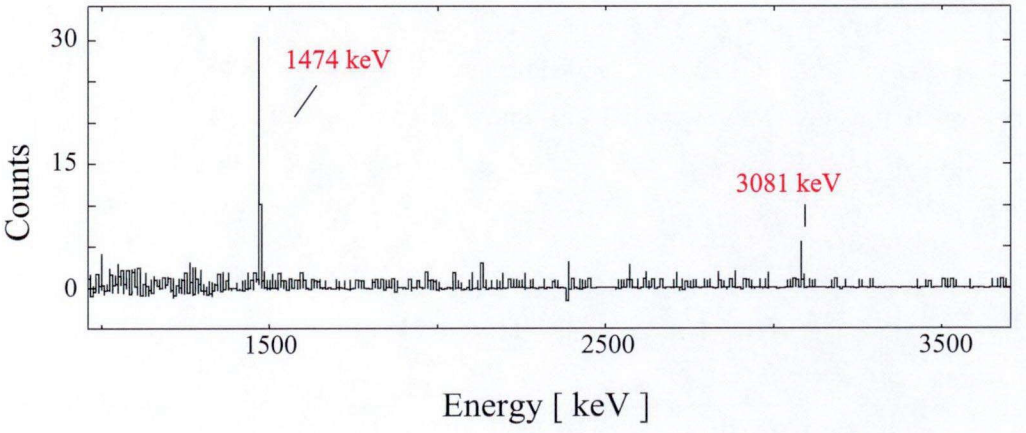

Figure A.3: Gamma-ray energy spectrum in coincidence with the 1991-keV γ ray.

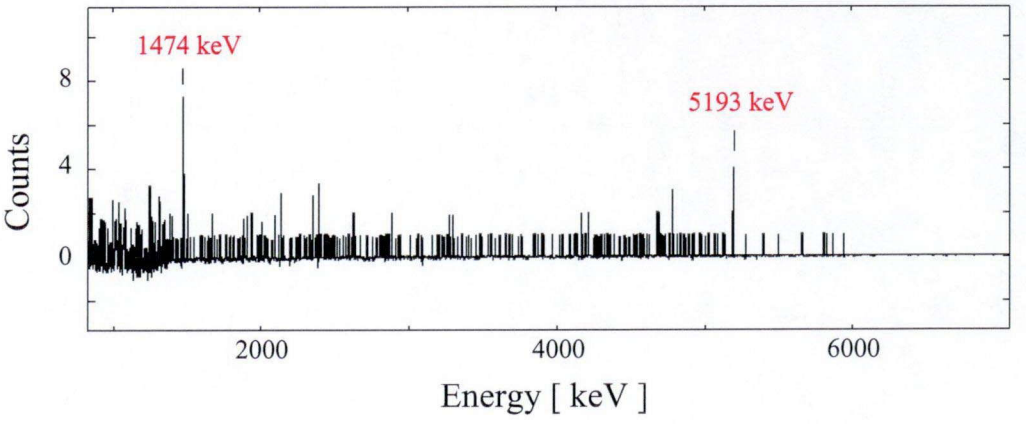

Figure A.4: Gamma-ray energy spectrum in coincidence with the 2008-keV γ ray.

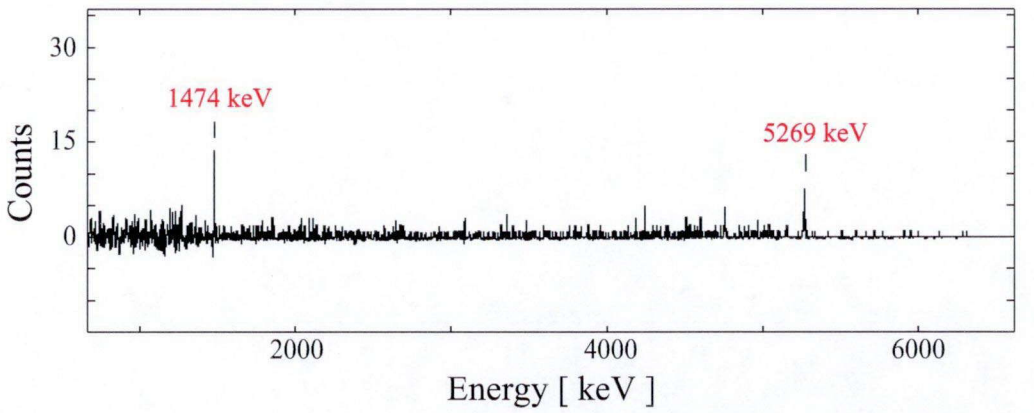

Figure A.5: Gamma-ray energy spectrum in coincidence with the 2192-keV γ ray.

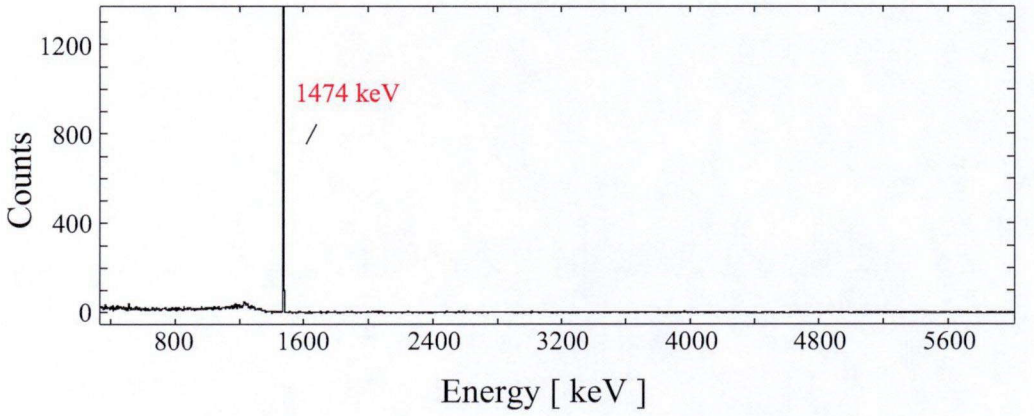

Figure A.6: Gamma-ray energy spectrum in coincidence with the 2388-keV γ ray.

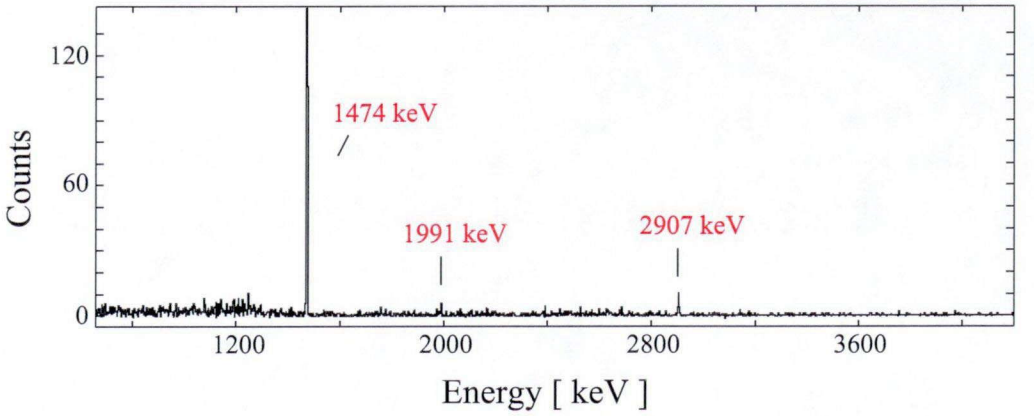

Figure A.7: Gamma-ray energy spectrum in coincidence with the 3081-keV γ ray.

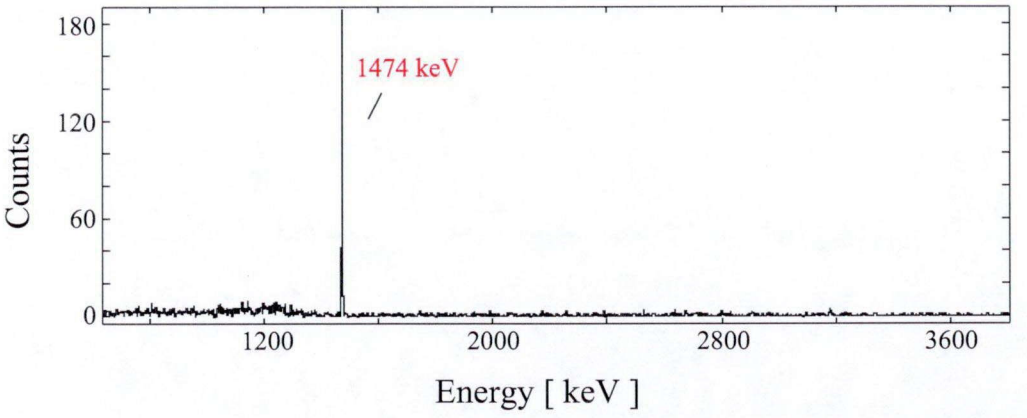

Figure A.8: Gamma-ray energy spectrum in coincidence with the 3088-keV γ ray.

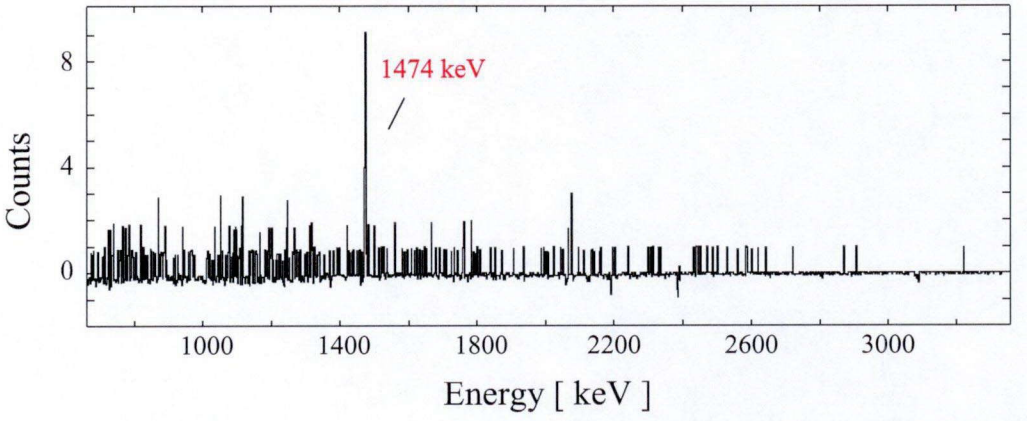

Figure A.9: Gamma-ray energy spectrum in coincidence with the 3405-keV γ ray.

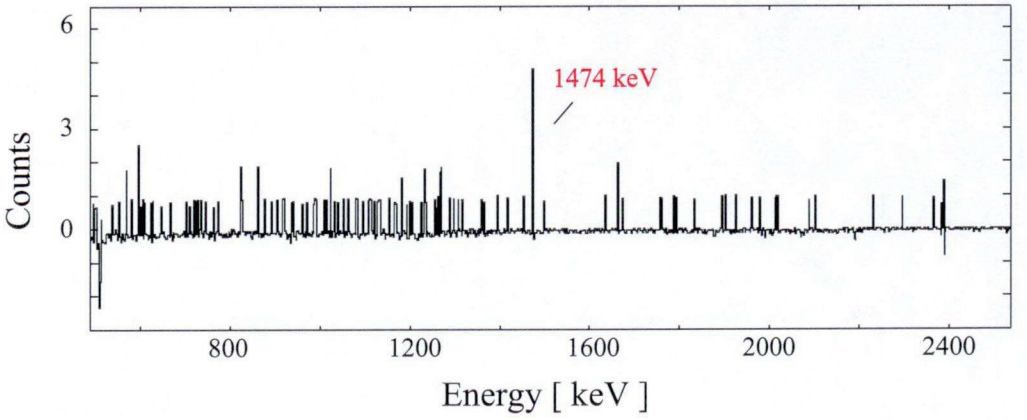

Figure A.10: Gamma-ray energy spectrum in coincidence with the 3995-keV γ ray.

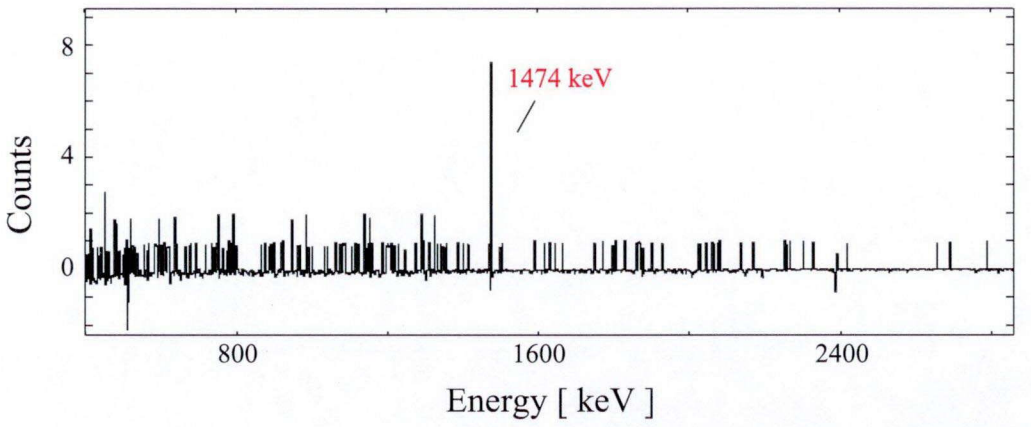

Figure A.11: Gamma-ray energy spectrum in coincidence with the 4443-keV γ ray.

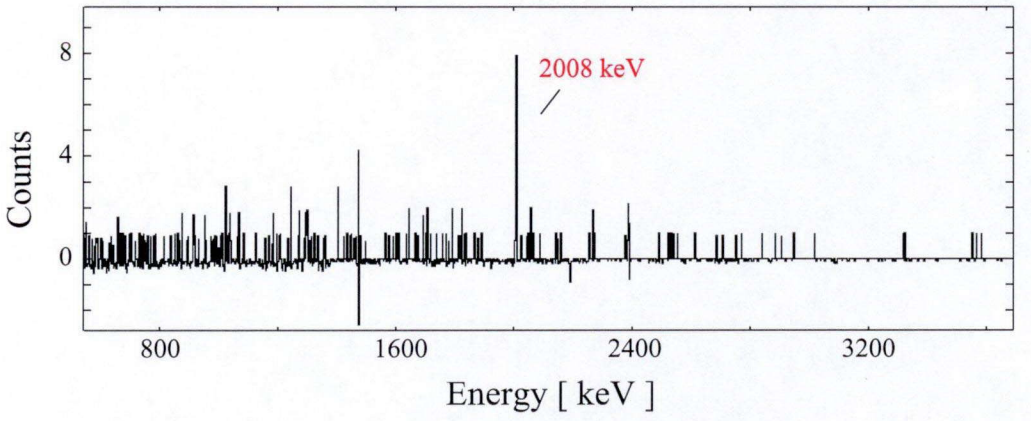

Figure A.12: Gamma-ray energy spectrum in coincidence with the 5193-keV γ ray.

A.2.2 ^{29}Mg

The γ-ray energy energy spectra in coincidence with the γ rays in ^{29}Mg observed in the present work are shown in Fig. A.13 to A.17.

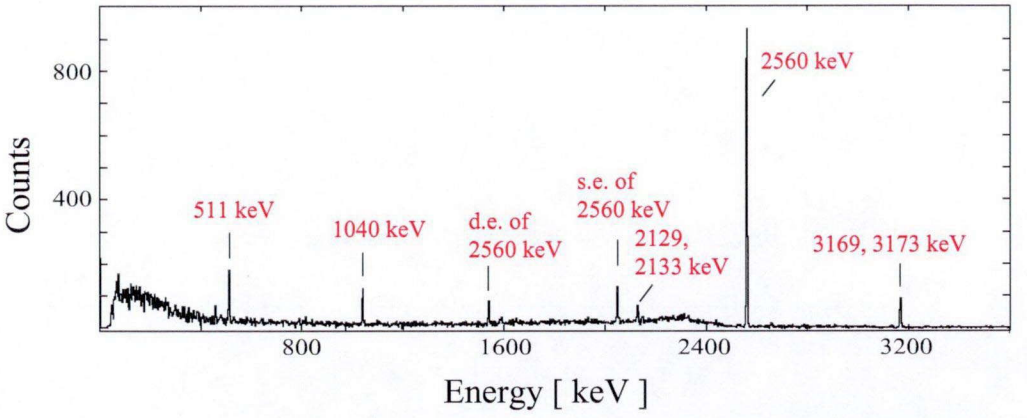

Figure A.13: Gamma-ray energy spectrum in coincidence with the 55-keV γ ray.

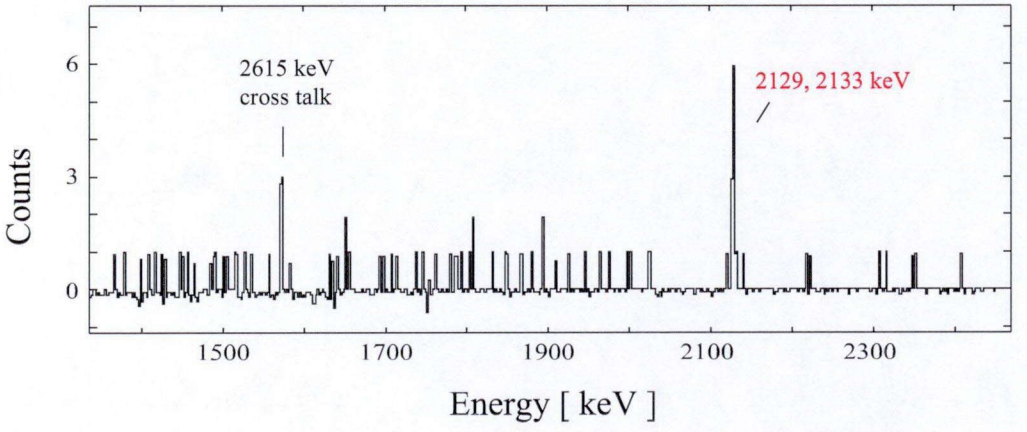

Figure A.14: Gamma-ray energy spectrum in coincidence with the 1040-keV γ ray.

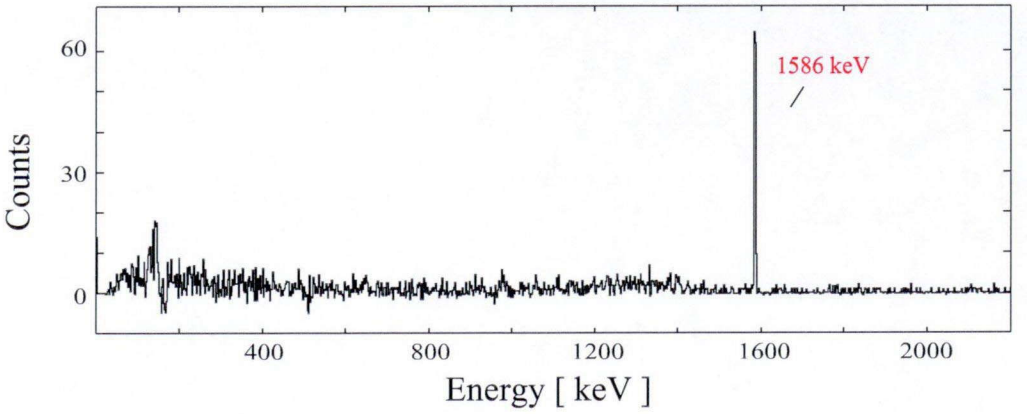

Figure A.15: Gamma-ray spectrum in coincidence with the 1638-keV γ ray.

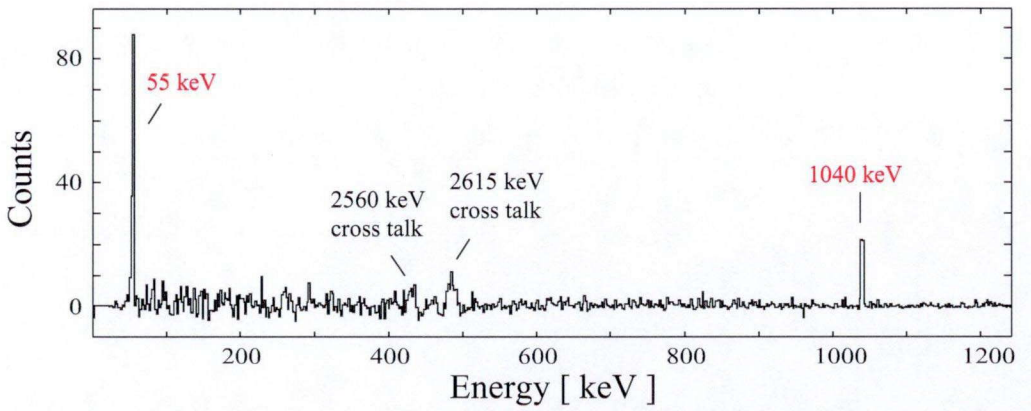

Figure A.16: Gamma-ray energy spectrum in coincidence with the 2129- and 2133-keV γ rays.

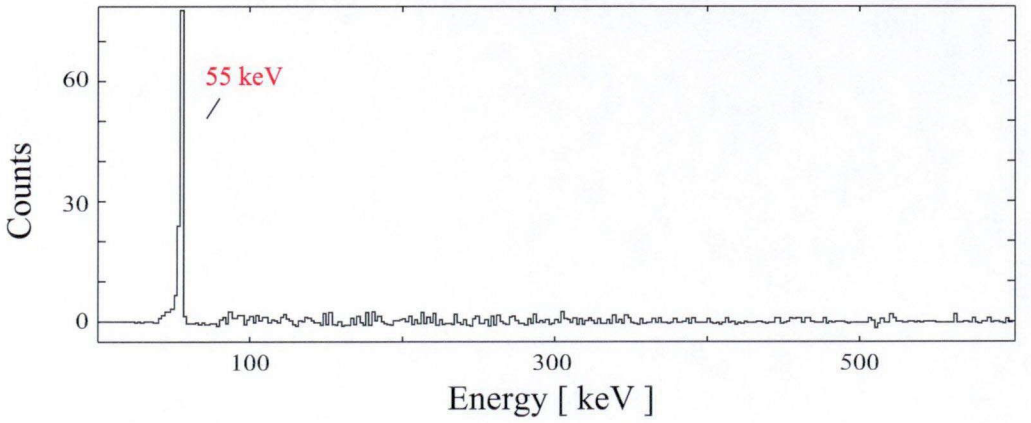

Figure A.17: Gamma-ray energy spectrum in coincidence with the 3169- and 3173-keV γ rays.

A.2.3 ^{30}Mg

The γ-ray energy spectra in coincidence with the γ rays in ^{30}Mg observed in the present work are shown in Fig. A.18 to A.40. It is to be mentioned that the spurious peaks caused by Compton cross talk are rarely observed in γ-γ analysis in the ^{30}Mg data compared with ^{28}Mg and ^{29}Mg. Although many peak-like structures can be seen in the γ-ray gated energy spectra, these peaks were not confirmed in the coincidence relation with the γ rays in ^{30}Mg in γ-γ analysis.

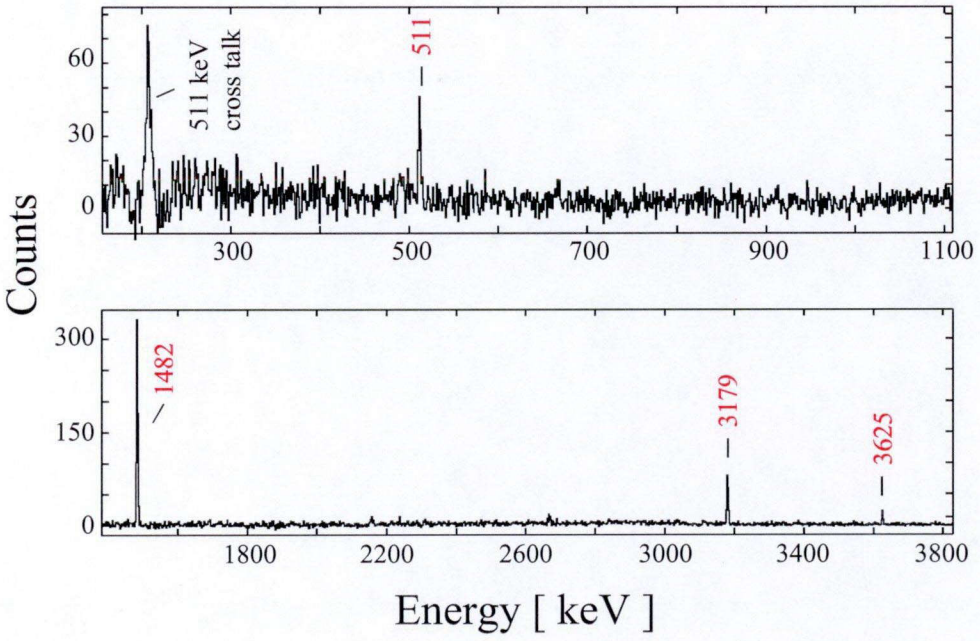

Figure A.18: Gamma-ray energy spectrum in coincidence with the 305-keV γ ray.

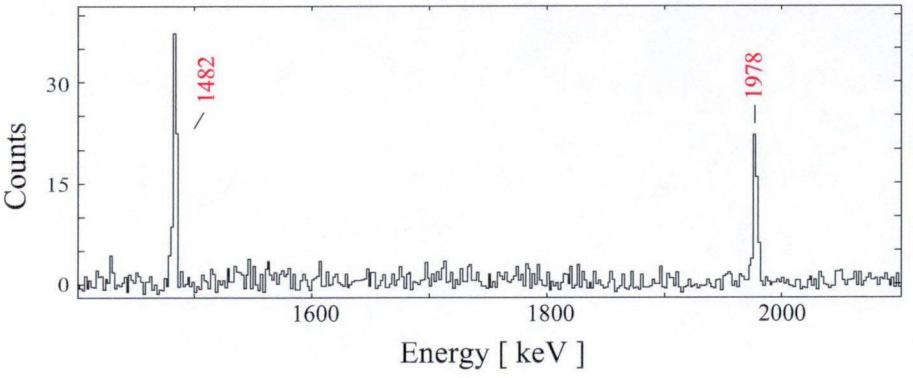

Figure A.19: Gamma-ray energy spectrum in coincidence with the 1505-keV γ ray.

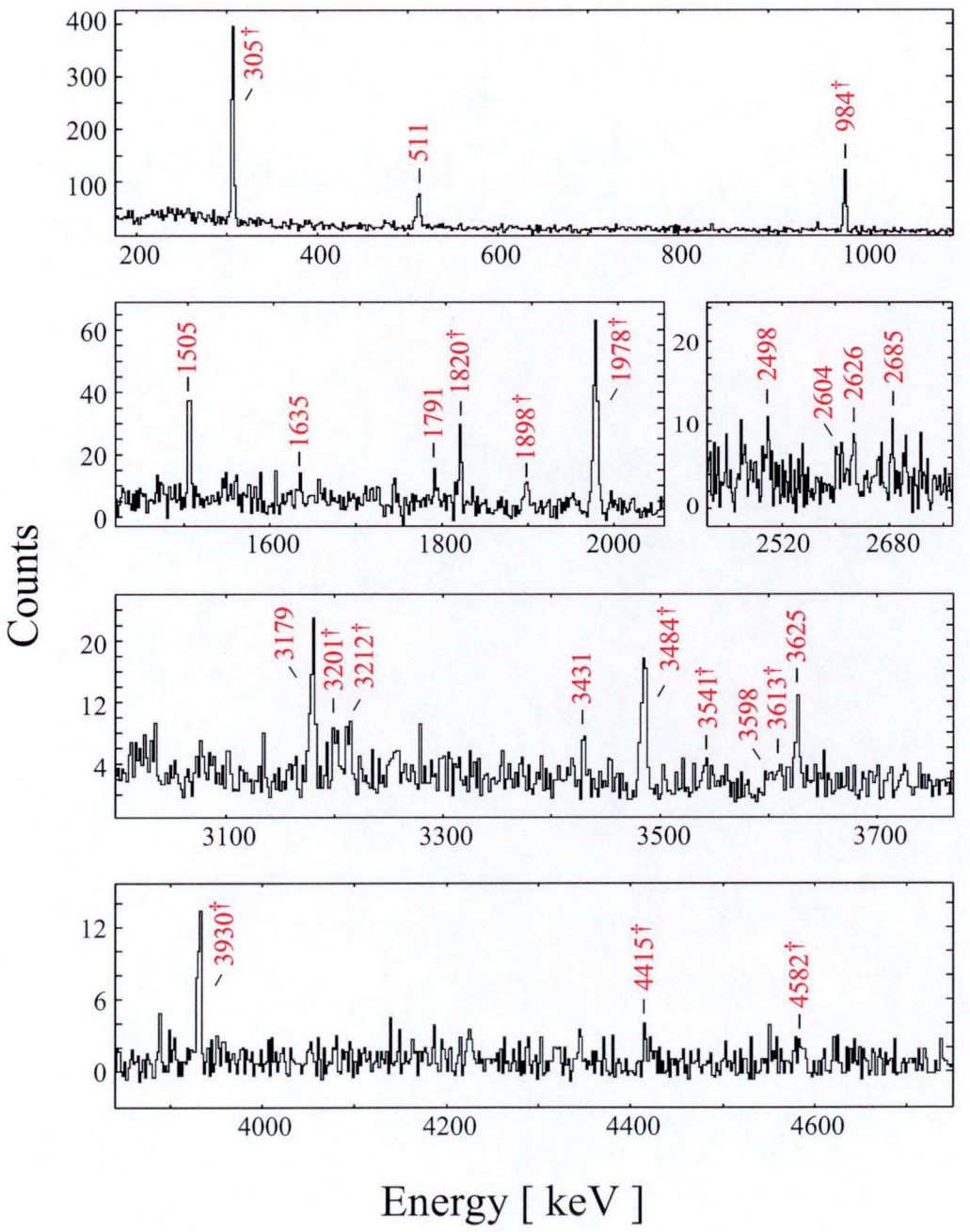

Figure A.20: Gamma-ray energy spectrum in coincidence with the 1482-keV γ ray. The γ-rays which directly populate the 1.482-MeV level are labeled by asterisks.

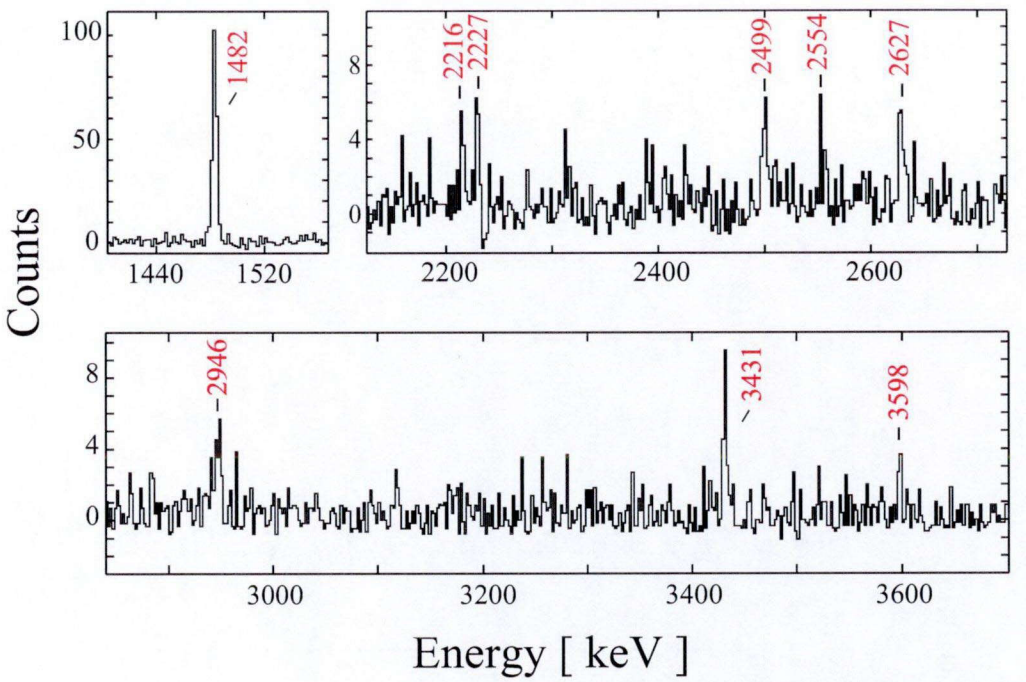

Figure A.21: Gamma-ray energy spectrum in coincidence with the 984-keV γ ray.

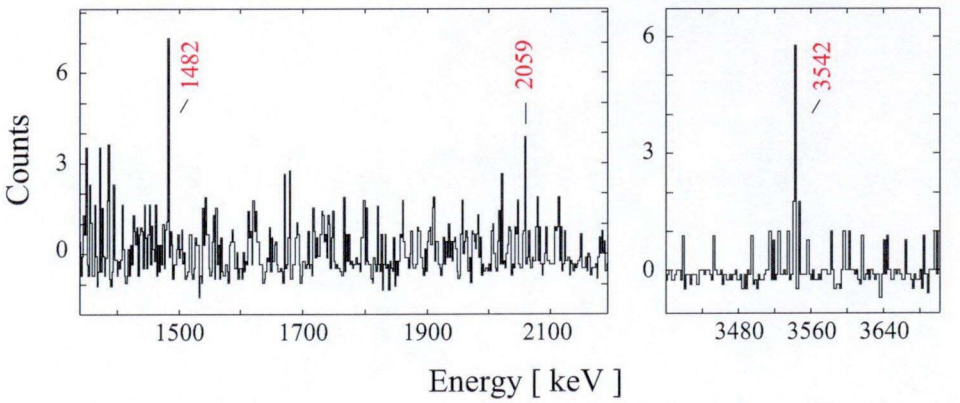

Figure A.22: Gamma-ray energy spectrum in coincidence with the 1552-keV γ ray.

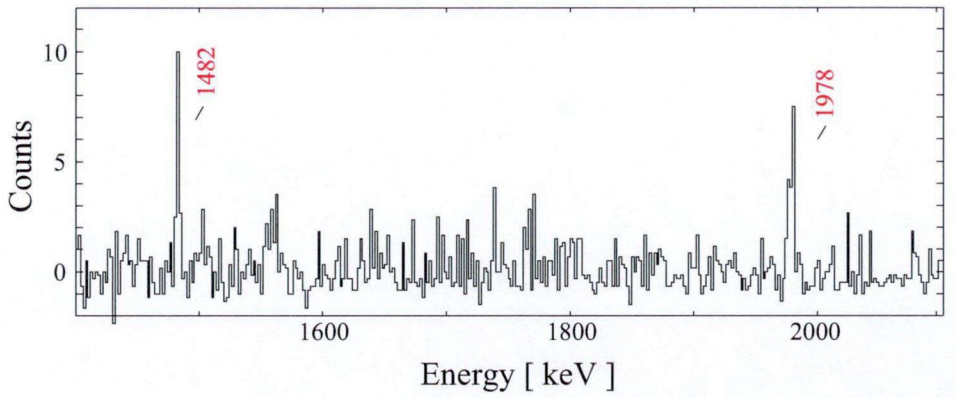

Figure A.23: Gamma-ray energy spectrum in coincidence with the 1559-keV γ ray.

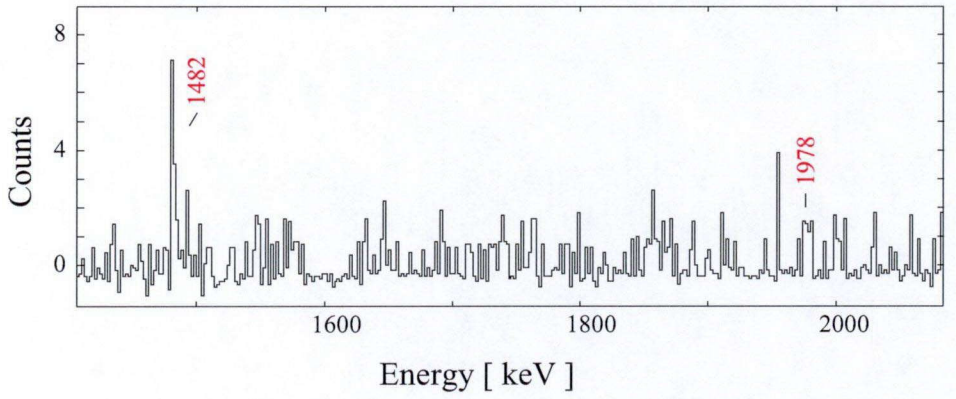

Figure A.24: Gamma-ray energy spectrum in coincidence with the 1635-keV γ ray.

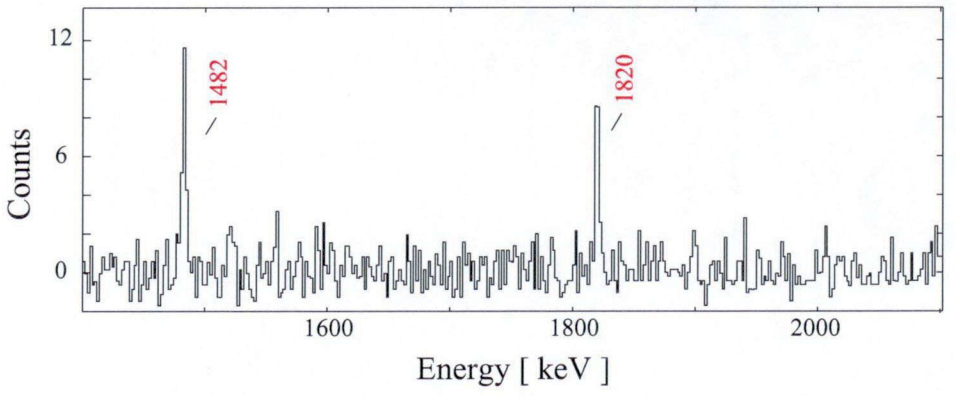

Figure A.25: Gamma-ray energy spectrum in coincidence with the 1791-keV γ ray.

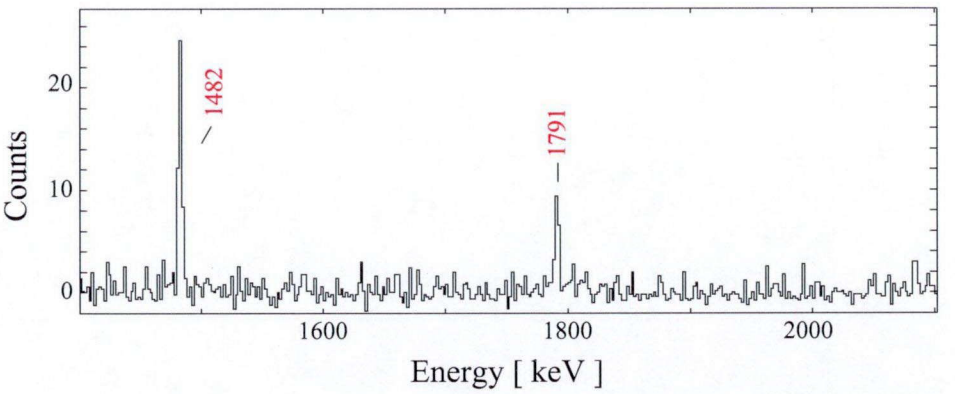

Figure A.26: Gamma-ray energy spectrum in coincidence with the 1820-keV γ ray.

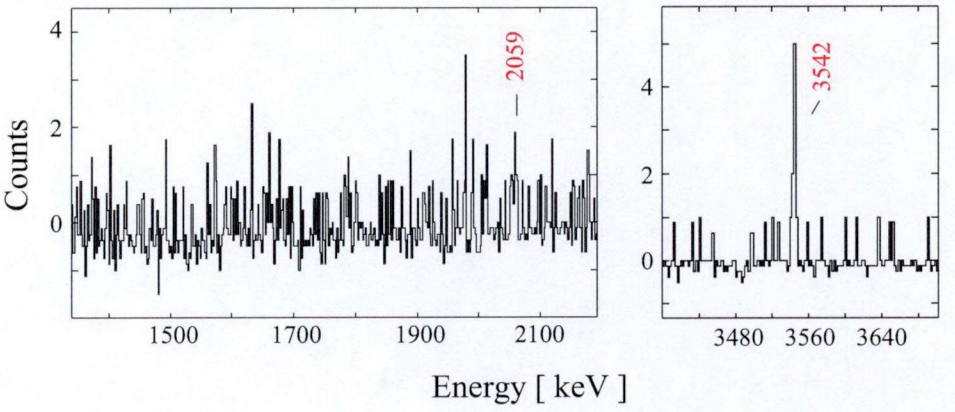

Figure A.27: Gamma-ray energy spectrum in coincidence with the 1871-keV γ ray.

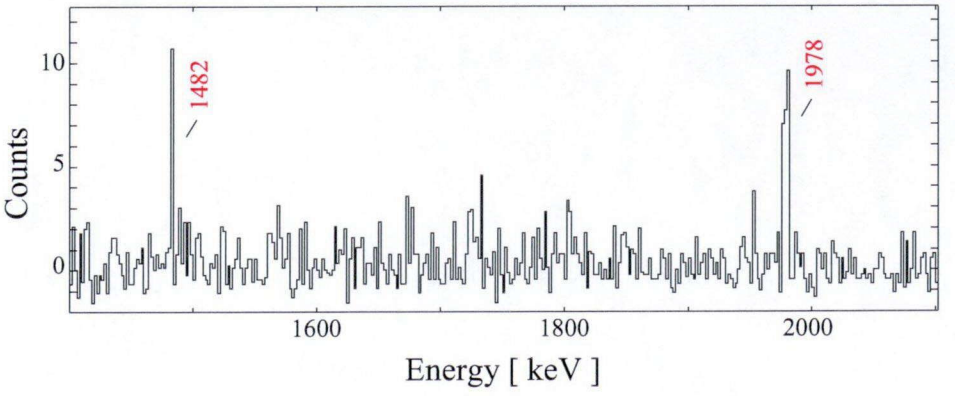

Figure A.28: Gamma-ray energy spectrum in coincidence with the 1951-keV γ ray.

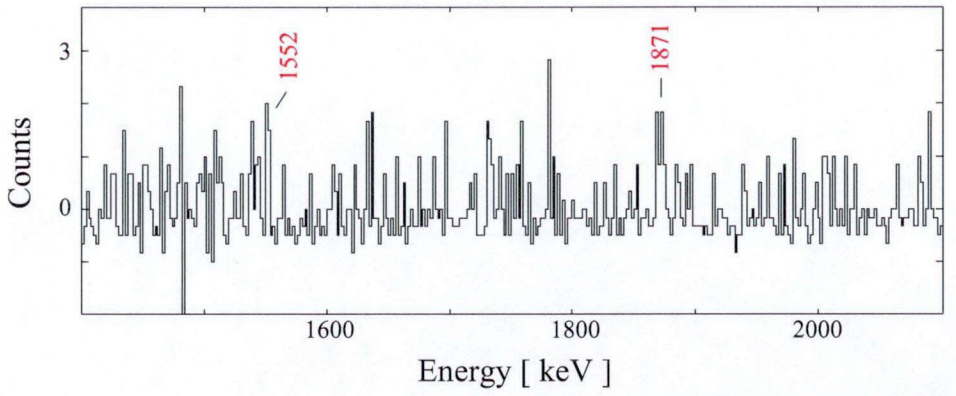

Figure A.29: Gamma-ray energy spectrum in coincidence with the 2059-keV γ ray.

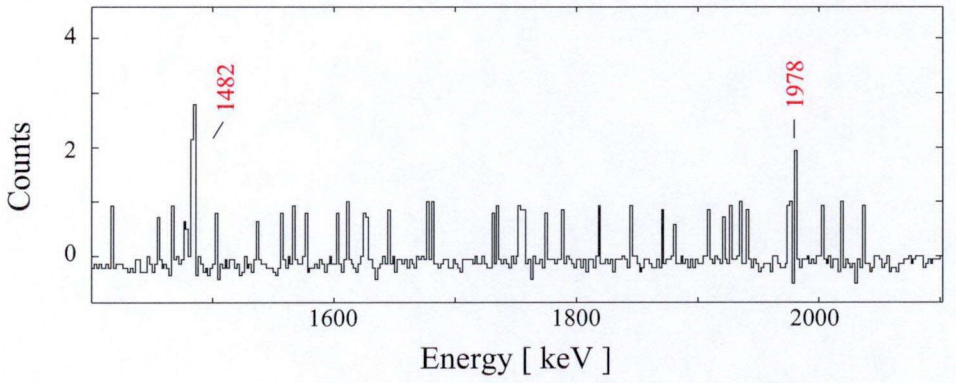

Figure A.30: Gamma-ray energy spectrum in coincidence with the 2437-keV γ ray.

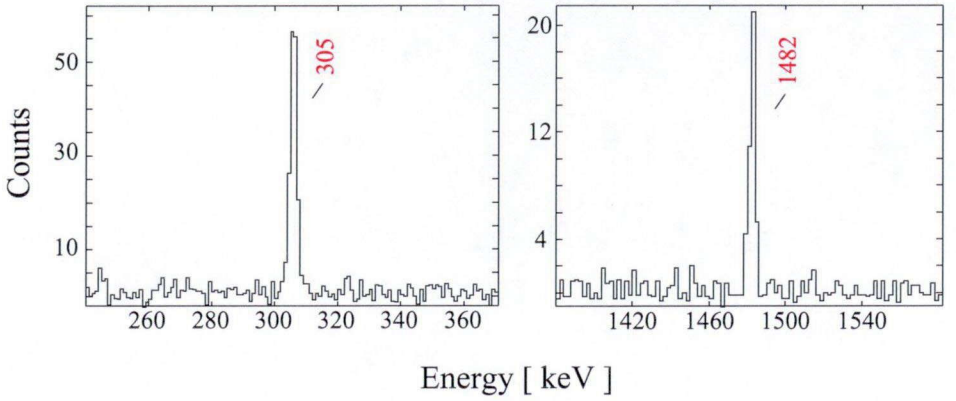

Figure A.31: Gamma-ray energy spectrum in coincidence with the 3179-keV γ ray.

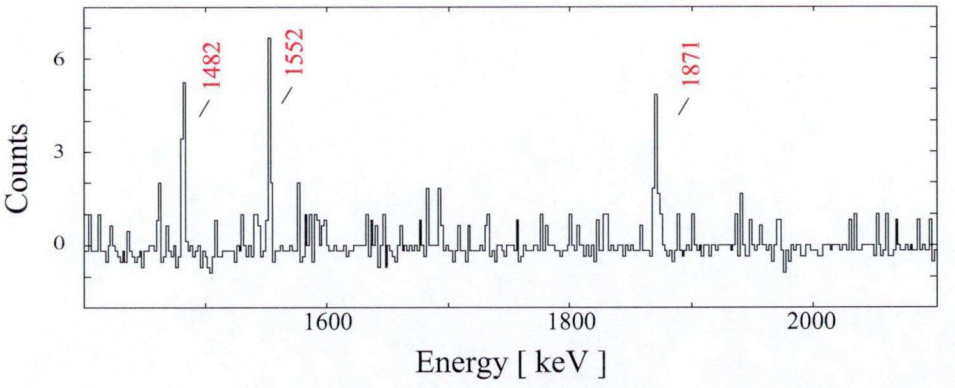

Figure A.32: Gamma-ray energy spectrum in coincidence with the 3541- and 3542-keV γ rays.

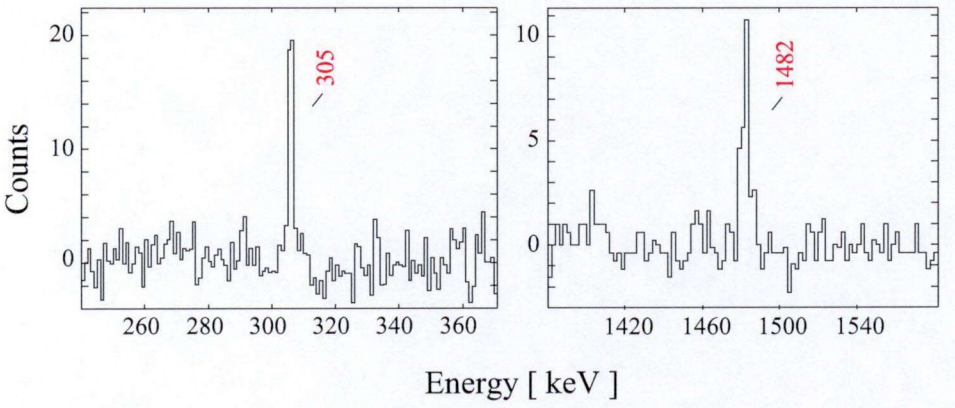

Figure A.33: Gamma-ray energy spectrum in coincidence with the 3625-keV γ ray.

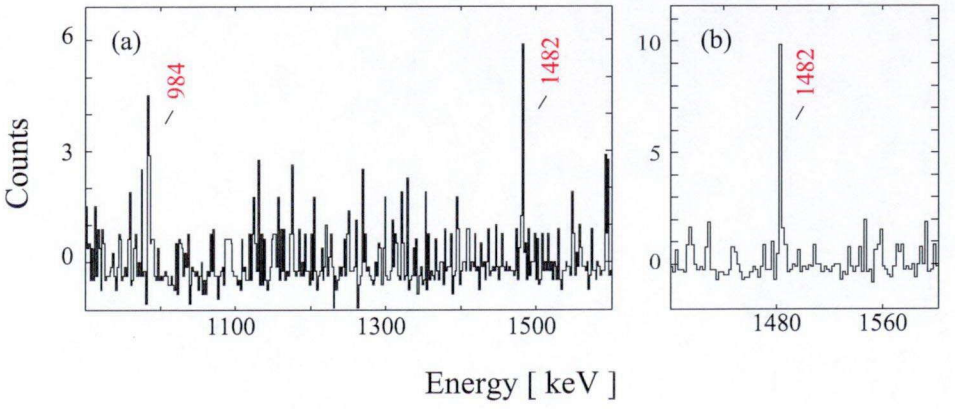

Figure A.34: Gamma-ray energy spectrum in coincidence with the (a) 2216-keV and (b) 3201-keV γ rays.

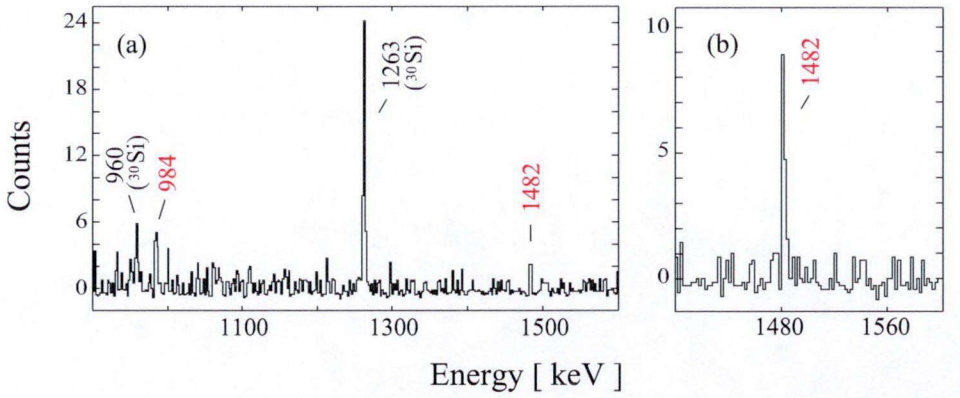

Figure A.35: Gamma-ray energy spectrum in coincidence with the (a) 2227-keV and (b) 3211-keV γ rays.

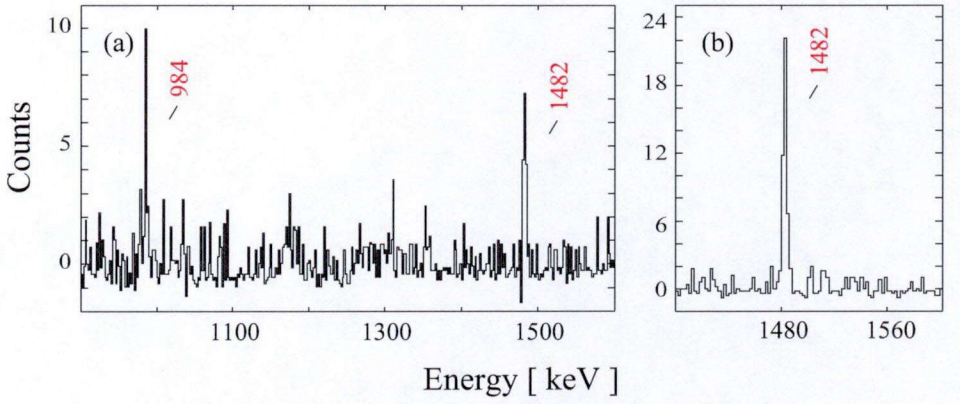

Figure A.36: Gamma-ray energy spectrum in coincidence with the (a) 2499-keV and (b) 3484-keV γ rays.

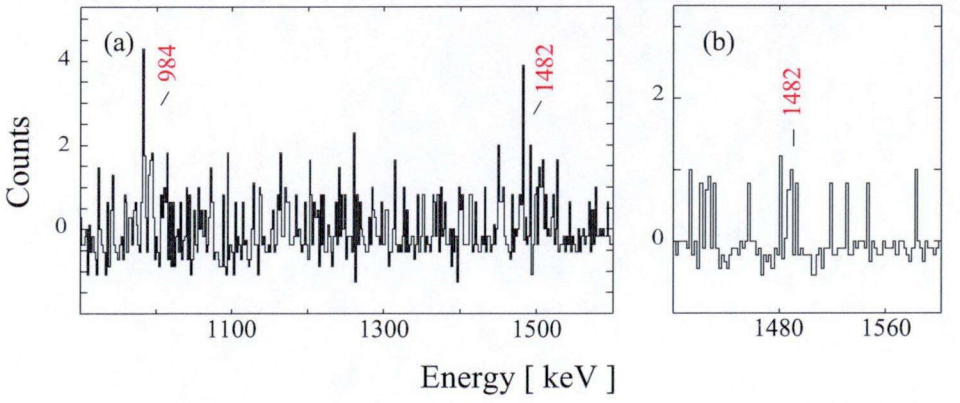

Figure A.37: Gamma-ray energy spectrum in coincidence with the (a) 2554-keV and (b) 3613-keV γ rays.

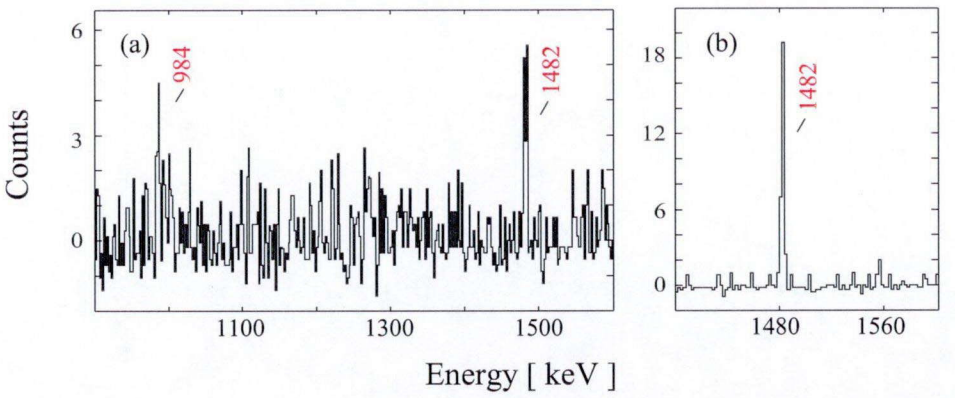

Figure A.38: Gamma-ray energy spectrum in coincidence with the (a) 2627-keV and (b) 3930-keV γ rays.

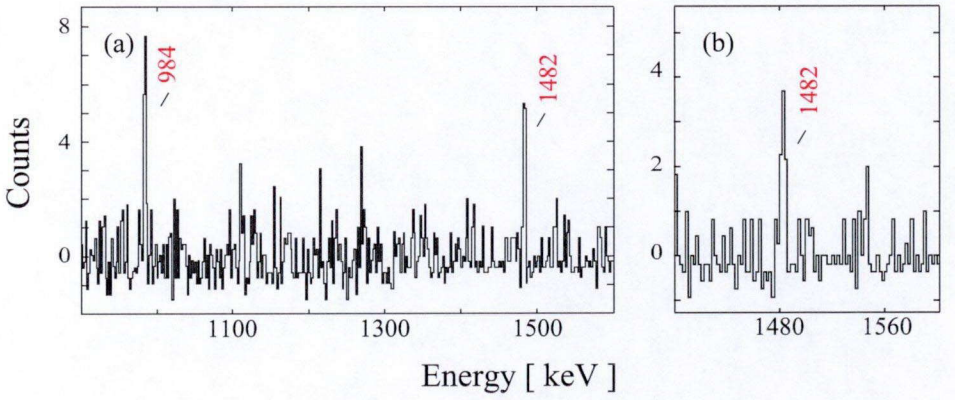

Figure A.39: Gamma-ray energy spectrum in coincidence with the (a) 2946-keV and (b) 4582-keV γ rays.

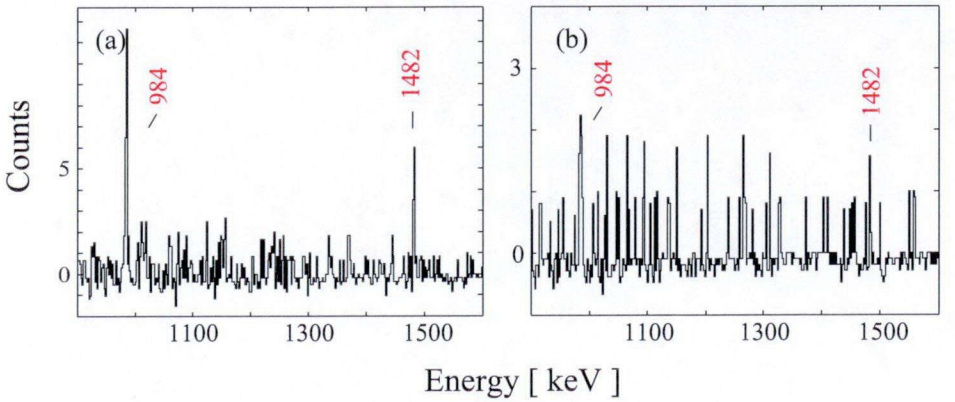

Figure A.40: Gamma-ray energy spectrum in coincidence with the (a) 3431-keV and (b) 3598-keV γ rays.

APPENDIX B

GEANT4 simulation code

The energy deterioration of β ray by the setup materials was estimated by Monte Carlo simulation code GEANT4. GEANT4(GEometry ANd Tracking 4) is a software package composed of tools which can be used to accurately simulate the passage of particles through matter. The concept of GEANT4 is briefly explained as follows.

Let us define the probabilities of $P(x)$: probability for particle to travel a distance of x with no interaction, and wdx: probability for particle to interact with other material between x and $x+dx$. Here, w is expressed by using number density N and interaction cross section δ as w=$N\delta$. Then, the probability $P(x+dx)$ can be described as,

$$P(x+dx) = exp(-wdx). \tag{B.1}$$

When initial value of $P(0)$=1 is given, the probability of interaction between x and $x+dx$, $P_{int}(x)$ is expressed as

$$P(x+dx) = P(x)wdx. \tag{B.2}$$

This value is called probability density function. By integrating this value, the probability for particle to interact in a distance of x is obtained as

$$P_C = \int_0^x P_{int}(x)dx = 1 - exp(-wx). \tag{B.3}$$

This is called cumulative distribution funcition. To replace P_C with uniform random number η[0,1], and mean free path λ=1/w, Eq. (B.3) can be modified as

$$x/\lambda = -ln(1-\eta). \tag{B.4}$$

Here, we obtain the information of physical process of particle and material described only by uniform random number. The value x/λ is called "number of mean free path (NMFP)".

The motions of particle can be chased by making steps with NMFP. When a particle travels in a material, particle is transferred as following steps. Here we explain by using photon for example.

1. In a first step, NMFP of the physical process (e.g. photoelectric absorption, Compton scattering, pair creation) of particle (photon) is expressed by random number.
2. By multiplying NMFP by cross section of material at the particle position (σ), Physical Length (PL) is obtained.
3. Shortest value obtained in process "2" is selected as a step length.
4. Transfer the particle by the distance obtained in process "3".
5. When particle energy is still alive, random number is selected again to NMFP, interaction begins again from process "1".
6. If the particle disappear after interaction, transferring is over.

APPENDIX C

Shell model calculation

C.1 Nuclear shell model and calculation code

Nucleus is quantum many-body system composed of proton and neutron. In the nuclear shell model, these nuclei move in the energy orbit calculated by

$$V(r) = V_{central}(r) + V_{ls}(r) \times \frac{l \cdot s}{\hbar^2}, \tag{C.1}$$

where $V_{central}(r)$ is central force represented by the potential of harmonic oscillator, finite well, or Woods-Saxon type, and the latter term $V_{ls}(r) \times \vec{l} \cdot \vec{s}/\hbar^2$ is the potential of $\vec{l} \cdot \vec{s}$ interaction. Figure C.1 shows the energy levels (so-called single particle energy) calculated by harmonic oscillator and $\vec{l} \cdot \vec{s}$ interaction. With only harmonic oscillator, the levels are explained by main quantum number n and angular momentum l, whereas the levels calculated by harmonic oscillator and $\vec{l} \cdot \vec{s}$ interaction can be explained by not only l and n, but also j=l+s as a good quantum number. Since nucleon is fermion, proton and neutron occupy these levels from the bottom. As a matter of convenience, the level sets of ($1p_{3/2}$, $1p_{1/2}$), ($1d_{5/2}$, $2s_{1/2}$, $1d_{3/2}$), and ($1f_{7/2}$, $2p_{3/2}$, $1f_{5/2}$, $2p_{1/2}$) are categorized to be p-, sd, and pf-shell, respectively, as shown in Fig. C.1.

The calculations were performed by the code NuShell [BRO07], which is the set of programs for carrying out shell-model calculation of general versatility with dimension up to about 100,000 in the J-T scheme and about 2,000,000 in the M-scheme. The nucleui with the valence nucleons in p-shell and sd-shell can be calculated with full model space, whereas those with pf-shell can be calculated with limited model space because it is necessary to use high-end machine. The J-T scheme is the method with diagonalizing the Hamiltonian taking advantage of the symmetric property of angular momentum J and isospin T. The M-scheme is the method with diagonalizing the Hamiltonian by classifying wave functions

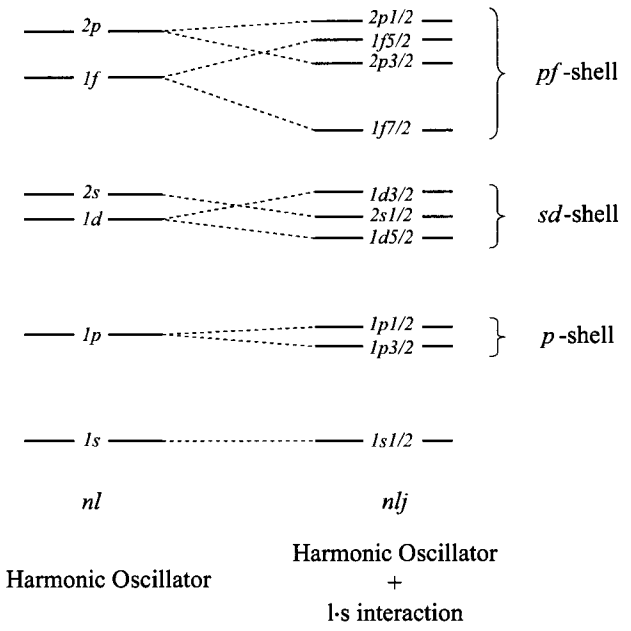

Figure C.1: Single particle levels calculated by harmonic oscillator and $\vec{l} \cdot \vec{s}$ interaction.

by magnetic quantum number M or z-component of isospin T_z. The calculation by NuShell is done using projecting the base of M-scheme to J direction. With the inputs of model space, number of valence particle, interaction, spin, isospin, and parity, we can calculate the energy eigen value, wave function, one body transition density, etc. Then, the energy, γ-transition probabilities, $\log ft$ values of the levels in these Mg isotopes can be obtained. In the case of ^{28}Mg, for expample, the calculation was done with the 12 valence nucleons in *sd*-shell assuming the core ^{16}O.

C.2 USD Hamiltonian

The Hamiltonians of USD [BRO06] and its modified versions of USDA and USDB [BRO06] were used as an interaction. The model spaces of these interactions are limited in *sd*-shell. The Hamiltonian of shell-model is expressed by the sum of one-body (single particle energy) and two-body matrix element as,

$$H = \sum_a \varepsilon_a \hat{n}_n + \sum_{a \le b, c \le d} \sum_{JT} V_{JT}(ab;cd) \hat{T}_{JT}(ab;cd) \tag{C.2}$$

where $\hat{n}_n$ is number operator of orbit a in the quantum numbers (n_a, l_a, j_a) in the spherical symmetric potential, and

$$\hat{T}_{JT}(ab;cd) = \sum_{MT_Z} A^{\dagger}_{JMTT_Z}(ab) A_{JMTT_Z}(cd) \tag{C.3}$$

is the scalar two-body density operator of nucleon pair in the orbit a, b and c, d which in connected with spin quantum number J, M, and isospin quantum number T, T_z. Here, this Hamiltonian is written by brief expression as

$$H = \sum_{i=1}^{p} x_i O_i \tag{C.4}$$

where x_i and O_i correspond to the single particle energy ε_i or two-body matrix element $V_{JT}(ab;cd)$, and $\hat{n}$ or $\hat{T}$, respectively. Assuming this Hamiltonian have eigen function ϕ_k with eigen value λ_k, the eigen value is obtained as

$$\lambda_k = \langle \phi_k \mid H \mid \phi_k \rangle = \sum_{i=1}^{p} x_i \langle \phi_k \mid O_i \mid \phi_k \rangle = \sum_{i=1}^{p} x_i \beta_i^k \tag{C.5}$$

$$\beta_i^k = \langle \phi_k \mid O_i \mid \phi_k \rangle, \tag{C.6}$$

where the Hamiltonian is defined to be $\vec{x} = (x_1, x_2, \cdots, x_p)$. By using experimental data β_i^k as a parameter, λ_k can be obtained to make χ^2 be minimized, as

$$\chi^2 = \sum_{k=1}^{N} \left(\frac{E_{exp}^k - \lambda_k}{\sigma_{exp}^k} \right)^2, \tag{C.7}$$

where E_{exp}^k and σ_{exp}^k are the experimental energy and its error, respectively. For x_i, partial differential equation is calculated as,

$$\frac{\partial \chi^2}{\partial x_j} = \sum_{k=1}^{N} 2 \frac{(E_{exp}^k - \lambda_k)}{(\sigma_{exp}^k)^2} \frac{\partial}{\partial x_j} \left(- \sum_{i=1}^{p} x_i \beta_i^k \right) = 0, \tag{C.8}$$

and we can obtain the system of equations of p-th degree, as

$$\sum_{k=1}^{N} 2 \left(E_{exp}^k - \sum_{i=1}^{p} x_i \beta_i^k \right) \frac{\beta_j^k}{(\sigma_{exp}^k)^2} = e_j - \sum_{i=1}^{p} \gamma_{ij} x_i = 0, \tag{C.9}$$

Table C.1: USD Hamiltonians and number of linear combination.

Interaction	N_E^{exp}	Number of linear Comb. (p)
USD	380	30
USDA	608	30
USDB	608	56

where $j = 1, 2, \cdots, p$. Using the matrix of $p \times p$ and p-th dimensional vector

$$G = (\gamma_{ij}) = \sum_{k=1}^{N} \frac{\beta_i^k \beta_j^k}{(\sigma_{exp}^k)^2} \tag{C.10}$$

$$\vec{e} = (e_i) = \sum_{k=1}^{N} \frac{E_{exp}^k \beta_i^k}{(\sigma_{exp}^k)^2}. \tag{C.11}$$

Then, we can obtain the new hamiltonian as

$$\vec{x} = G^{-1}\vec{e}. \tag{C.12}$$

By applying this calculation to be *sd*-shell, we can obtain USD Hamiltonian. The Hamiltonians of USDA and USDB are the revised version of USD by applying more experimental data recently. Table C.1 shows the number of energy point and p-th degree equation for USD, USDA, and USDB interactions.

C.3 Levels calculated by shell model

The levels in ^{28}Mg, ^{29}Mg, and ^{30}Mg calculated by the shell-model code NuShell with the USD, USDA, and USDB Hamiltonians are listed in Table C.2, C.3, and C.4, respectively.

Table C.2: The levels in ^{28}Mg calculated by the USD, USDA, and USDB Hamiltonians.

levels	E_x [MeV] (I_π) (USD)	E_x [MeV] (I_π) (USDA)	E_x [MeV] (I_π) (USDB)
1	0.0 (0_1^+)	0.0 (0_1^+)	0.0 (0_1^+)
2	1.543 (2_1^+)	1.526 (2_1^+)	1.518 (2_1^+)
3	3.802 (0_2^+)	3.981 (0_2^+)	4.007 (0_2^+)
4	4.126 (4_1^+)	4.200 (4_1^+)	4.168 (4_1^+)
5	4.264 (2_2^+)	4.719 (1_1^+)	4.543 (2_2^+)
6	4.396 (1_1^+)	4.753 (2_2^+)	4.664 (1_1^+)
7	4.773 (2_3^+)	4.892 (2_3^+)	4.794 (2_3^+)
8	5.186 (4_2^+)	5.301 (4_2^+)	5.211 (4_2^+)
9	5.403 (2_4^+)	5.550 (1_2^+)	5.519 (1_2^+)
10	5.412 (1_2^+)	5.620 (2_4^+)	5.543 (3_1^+)
11	5.582 (3_1^+)	5.635 (3_1^+)	5.567 (2_4^+)
12	6.013 (2_5^+)	6.031 (2_5^+)	6.070 (2_5^+)
13	6.187 (0_3^+)	6.685 (3_2^+)	6.582 (3_2^+)
14	6.402 (3_2^+)	6.795 (1_3^+)	6.592 (0_3^+)
15	6.741 (3_3^+)	6.814 (3_3^+)	6.883 (3_3^+)
16	6.757 (2_6^+)	6.844 (0_3^+)	6.934 (4_3^+)
17	6.790 (4_3^+)	6.986 (4_3^+)	6.948 (2_6^+)
18	6.855 (0_4^+)	6.990 (0_4^+)	7.054 (3_4^+)
19	6.864 (1_3^+)	7.023 (2_6^+)	7.055 (1_3^+)
20	6.963 (4_4^+)	7.088 (3_4^+)	7.128 (0_4^+)
21	7.059 (3_4^+)	7.185 (4_4^+)	7.141 (4_4^+)
22	7.198 (3_5^+)	7.231 (3_5^+)	7.226 (3_5^+)
23	7.317 (4_5^+)	7.386 (4_5^+)	7.443 (4_5^+)
24	7.330 (2_7^+)	7.445 (2_7^+)	7.468 (1_4^+)
25	7.381 (1_4^+)	7.545 (1_4^+)	7.599 (2_7^+)
26	7.420 (2_8^+)	7.703 (2_8^+)	7.671 (2_8^+)
27	7.542 (4_6^+)	7.755 (4_6^+)	7.765 (4_6^+)
28	7.619 (2_9^+)	7.818 (0_5^+)	7.884 (2_9^+)
29	7.691 (3_6^+)	7.830 (3_6^+)	7.955 (3_6^+)
30	7.819 (2_{10}^+)	7.845 (2_9^+)	7.969 (2_{10}^+)

Table C.3: The levels in ^{29}Mg calculated by the USD, USDA, and USDB Hamiltonians.

levels	E_x [MeV] (I_π) (USD)	E_x [MeV] (I_π) (USDA)	E_x [MeV] (I_π) (USDB)
1	0.0 $(1/2_1^+)$	0.0 $(1/2_1^+)$	0.0 $(3/2_1^+)$
2	0.040 $(3/2_1^+)$	0.090 $(3/2_1^+)$	0.045 $(1/2_1^+)$
3	1.543 $(5/2_1^+)$	1.610 $(5/2_1^+)$	1.594 $(5/2_1^+)$
4	2.106 $(7/2_1^+)$	2.249 $(7/2_1^+)$	2.099 $(7/2_1^+)$
5	2.193 $(3/2_2^+)$	2.269 $(3/2_2^+)$	2.330 $(3/2_2^+)$
6	2.438 $(1/2_2^+)$	2.905 $(1/2_2^+)$	2.627 $(1/2_2^+)$
7	3.039 $(5/2_2^+)$	3.147 $(5/2_2^+)$	3.152 $(5/2_2^+)$
8	3.227 $(3/2_3^+)$	3.619 $(3/2_3^+)$	3.502 $(3/2_3^+)$
9	3.532 $(5/2_3^+)$	3.628 $(5/2_3^+)$	3.568 $(5/2_3^+)$
10	3.974 $(5/2_4^+)$	3.992 $(7/2_2^+)$	3.982 $(9/2_1^+)$
11	4.071 $(9/2_1^+)$	4.077 $(9/2_1^+)$	3.988 $(7/2_2^+)$
12	4.147 $(7/2_2^+)$	4.253 $(5/2_4^+)$	4.264 $(5/2_4^+)$
13	4.184 $(9/2_2^+)$	4.365 $(9/2_2^+)$	4.302 $(9/2_2^+)$
14	4.624 $(7/2_3^+)$	4.668 $(3/2_4^+)$	4.795 $(7/2_3^+)$
15	4.836 $(3/2_4^+)$	4.718 $(7/2_3^+)$	4.891 $(3/2_4^+)$
16	4.870 $(7/2_4^+)$	5.047 $(7/2_4^+)$	5.095 $(7/2_4^+)$
17	4.935 $(5/2_5^+)$	5.160 $(5/2_5^+)$	5.143 $(5/2_5^+)$
18	4.984 $(5/2_6^+)$	5.175 $(1/2_3^+)$	5.214 $(5/2_6^+)$
19	5.083 $(3/2_5^+)$	5.399 $(5/2_6^+)$	5.433 $(1/2_3^+)$
20	5.261 $(1/2_3^+)$	5.602 $(5/2_7^+)$	5.515 $(3/2_5^+)$
21	5.280 $(5/2_7^+)$	5.619 $(3/2_5^+)$	5.586 $(9/2_3^+)$
22	5.477 $(7/2_5^+)$	5.680 $(9/2_3^+)$	5.730 $(7/2_5^+)$
23	5.532 $(9/2_3^+)$	5.807 $(7/2_5^+)$	5.770 $(5/2_7^+)$
24	5.794 $(7/2_6^+)$	5.913 $(5/2_8^+)$	5.876 $(9/2_4^+)$
25	5.842 $(5/2_8^+)$	5.921 $(9/2_4^+)$	6.014 $(3/2_6^+)$
26	5.844 $(1/2_4^+)$	5.945 $(3/2_6^+)$	6.052 $(7/2_6^+)$
27	5.850 $(9/2_4^+)$	6.070 $(3/2_7^+)$	6.093 $(1/2_4^+)$
28	5.861 $(3/2_6^+)$	6.074 $(7/2_6^+)$	6.205 $(5/2_8^+)$
29	5.928 $(3/2_7^+)$	6.214 $(1/2_4^+)$	6.232 $(7/2_7^+)$
30	6.127 $(7/2_7^+)$	6.226 $(5/2_9^+)$	6.314 $(3/2_7^+)$

Table C.4: The levels in ^{30}Mg calculated by the USD, USDA, and USDB Hamiltonians.

levels	E_x [MeV] (I_π) (USD)	E_x [MeV] (I_π) (USDA)	E_x [MeV] (I_π) (USDB)
1	0.0 (0_1^+)	0.0 (0_1^+)	0.0 (0_1^+)
2	1.671 (2_1^+)	1.592 (2_1^+)	1.592 (2_1^+)
3	3.466 (2_2^+)	3.413 (2_2^+)	3.433 (2_2^+)
4	3.961 (4_1^+)	3.847 (4_1^+)	3.894 (4_1^+)
5	4.692 (3_1^+)	4.573 (2_3^+)	4.661 (3_1^+)
6	4.802 (2_3^+)	4.654 (3_1^+)	4.789 (2_3^+)
7	5.193 (2_4^+)	4.912 (1_1^+)	5.148 (2_4^+)
8	5.242 (1_1^+)	5.100 (2_4^+)	5.166 (1_1^+)
9	5.465 (4_2^+)	5.350 (4_2^+)	5.317 (4_2^+)
10	5.710 (0_2^+)	5.424 (1_2^+)	5.702 (1_2^+)
11	5.959 (1_2^+)	5.498 (0_2^+)	5.818 (0_2^+)
12	6.325 (4_3^+)	6.112 (4_3^+)	6.343 (4_3^+)
13	6.495 (2_5^+)	6.258 (3_2^+)	6.583 (3_2^+)
14	6.499 (3_2^+)	6.549 (0_3^+)	6.767 (2_5^+)
15	6.597 (0_3^+)	6.592 (2_5^+)	6.854 (2_6^+)
16	6.747 (2_6^+)	6.779 (3_3^+)	6.989 (0_3^+)
17	7.124 (4_4^+)	6.887 (2_6^+)	7.035 (3_3^+)
18	7.268 (3_3^+)	7.005 (2_7^+)	7.062 (4_4^+)
19	7.302 (4_5^+)	7.088 (4_4^+)	7.280 (2_7^+)
20	7.304 (1_3^+)	7.313 (4_5^+)	7.331 (4_5^+)
21	7.315 (2_7^+)	7.392 (1_3^+)	7.420 (3_4^+)
22	7.450 (3_4^+)	7.397 (3_4^+)	7.522 (1_3^+)
23	7.792 (2_8^+)	7.435 (2_8^+)	7.820 (2_8^+)
24	7.988 (2_9^+)	7.922 (2_9^+)	8.150 (2_9^+)
25	8.068 (4_6^+)	7.935 (4_6^+)	8.187 (4_6^+)
26	8.247 (3_5^+)	8.094 (3_5^+)	8.292 (3_5^+)
27	8.303 (4_7^+)	8.345 (4_7^+)	8.459 (4_7^+)
28	8.449 (1_4^+)	8.371 (1_4^+)	8.569 (2_{10}^+)
29	8.559 (0_4^+)	8.405 (3_6^+)	8.618 (3_6^+)
30	8.606 (2_{10}^+)	8.414 (2_{10}^+)	8.719 (1_4^+)

BIBLIOGRAPHY

BIBLIOGRAPHY

[AGO03] S. Agostinelli, J. Allison, K. Amako, J. Apostolakis, H. Araujo, P. Arce, M. Asai, D. Axen, S. Banerjee, G. Barrand, *et al.* Geant4-a simulation toolkit. *Nuclear Instruments and Methods in Physics Research A*, 506, 250, 2003.

[ALI06] J. Allison, K. Amako, J. Apostolakis, H. Araujo, P. A. Dubois, M. Asai, G. Barrand, R. Capra, S. Chauvie, R. Chytracek, *et al.* Geant4 Developments and Applications. *Nuclear Science, IEEE Transactions on Nuclear Science*, 53, 270, 2006.

[ARG07] EPICS (Experimental Physics and Industrial Control System) is a set of Open Source software tools, libraries and applications developed collaboratively and used worldwide to create distributed soft real-time control systems for scientific instruments such as a particle accelerators, telescopes and other large scientific experiments. http://www.aps.anl.gov/epics/index.php.

[AUD95] G. Audi and A. H. Wapstra. The 1995 update to the atomic mass evaluation. *Nuclear Physics A*, 595, 409, 1995.

[AUD03] G. Audi, A. H. Wapstra, and C. Thibault. The AME2003 atomic mass evaluation (II). Tables, graphs and references. *Nuclear Physics A*, 729, 337, 2003.

[BRE77] W. Brendler, P. Betz, E. Bitterwolf, and H. Röpke. The Structure of ^{27}Mg from the ^{26}Mg$(d, p\gamma)$ Reaction. *Zeitschrift für Physik A Hadrons and Nuclei*, 281, 75, 1977.

[BAU87] P. Baumann, P. Dessagne, A. Huck, G. Klotz, A. Knipper, G. Marguier, C. Miehé, M. Ramdane, C. Richard-Serre, G. Walter, *et al.* Gamow-Teller beta decay of ^{29}Na and comparison with shell-model predictions. *Physical Review C*, 36, 765, 1987.

[BAU89] P. Baumann, P. Dessagne, A. Huck, G. Klotz, A. Knipper, C. Miché, M. Ramdane, G. Walter, G. Marguier, H. Gabelmann, *et al.* Beta decay of ^{30}Na: Experiment and theory. *Physical Review C*, 39, 626, 1989.

[BRO10] B. A. Brown. Islands of insight in the nuclear chart. *Physics*, 3, 104, 2010.

[BRO06] B. A. Brown and W. A. Richter. New "USD" Hamiltonians for the *sd* shell. *Physical Review. C*, 74, 034315, 2006.

[BRO07] B. A. Brown and W. D. M. Rae. Nushell@MSU. *MSU-NSCL report*, 2007.

[BRO88] B. A. Brown and B. H. Wildenthal. Status of the Nuclear Shell Model. *Annual Review of Nuclear and Particle Science*, 38, 29, 1988.

[CHU05] J. A. Church, C. M. Campbell, D. C. Dinca, J. Enders, A. Gade, T. Glasmacher, Z. Hu, R. V. F. Janssens, W. F. Mueller, H. Olliver, *et al.* Measurement of $E2$ transition strengths in ^{32,34}Mg. *Physical Review C*, 72, 054320, 2005.

[CAM75] X. Campi, H. Flocard, A. K. Kerman, and S. Koonin. Shape Transition in the Neutron Rich Sodium Isotopes. *Nuclear Physics A*, 251, 193, 1975.

[CHI01] V. Chisté, A. Gillibert, A. Lepine-Szily, N. Alamanos, F. Auger, J. Barrette, F. Braga, M. D. Cortina-Gil, Z. Dlouhy, V. Lapoux, *et al.* Electric and nuclear transition strength in ^{30,32}Mg. *Physics Letters B*, 514, 233-239, 2001.

[DOM06] Zs. Dombradi, Z. Elekes, A. Saito, N. Aoi, H. Baba, K. Demichi, Z. Fülöp, J. Gibelin, T. Gomi, H. Hasegawa, *et al.* Vanishing $N = 20$ Shell Gap: Study of Excited States in ^{27,28}Ne. *Physical Review Letters*, 96, 182501, 2006.

[DET79] C. Détraz, D. Guillemaud, G. Huber, R. Klapisch, M. Langevin, F. Naulin, C. Thibault, L. C. Carraz, and F. Touchard. Beta decay of $^{27-32}$Na and their descendants. *Physical Review C*, 19, 164, 1979.

[DET83] C. Détraz, M. Langevin, D. Guillemaud, M. Epherre, G. Audi, C. Thibault, and F. Touchard. Mapping of the Onset of a New Region of Deformation: The Masses of ^{31}Mg and ^{32}Mg. *Nuclear Physics A*, 394, 378, 1983.

[DOO09] P. Doornenbal, H. Scheit, N. Aoi, S. Takeuchi, K. Li, E. Takeshita, H. Wang, H. Baba, S. Deguchi, N. Fukuda, *et al.* Spectroscopy of ^{32}Ne and the " Island of Inversion ". *Physical Review Letters*, 103, 32501, 2009.

[DEA10] A. N. Deacon, J. F. Smith, S. J. Freeman, R. V. F. Janssens, M. P. Carpenter, B. Hadinia, C. R. Hoffman, B. P. Kay, T. Lauritsen, C. J. Lister, *et al.* Cross-shell excitations near the " island of inversion ": Structure of ^{30}Mg. *Physical Review C*, 82, 034305, 2010.

[END90] P. M. Endt. Energy Levels of $A = 21 - 44$ Nuclei (VII). *Nuclear Physics A*, 310, 1, 1978.

[END98] P. M. Endt. Supplement to Energy Levels of $A = 21 - 44$ Nuclei (VII). *Nuclear Physics A*, 633, 1, 1998.

[ETT08] S. Ettenauer, H. Zwahlen, P. Adrich, D. Bazin, C. M. Campbell, J. M. Cook, A. D. Davies, D. C. Dinca, A. Gade, T. Glasmacher, *et al.* Intermediate-energy Coulomb excitation of ^{30}Na. *Physical Review C*, 78, 017302, 2008.

[FIS73] T. R. Fisher, T. T. Bardin, J A. Becker, L. F. Chase Jr., D. Kohler, R. E. McDonald, A. R. Poletti, and J. G. Pronko. Gamma-Ray Spectroscopy of Low-Lying Levels in ^{28}Mg. *Physical Review C*, 7, 1878, 1973.

[FIF85] L. K. Fifield, P. V. Drumm, M. A. C. Hotchkis, T. R. Ophel, and C. L. Woods. The ^{26}Mg(^{18}O,^{17}F)^{27}Na and ^{26}Mg(^{18}O,^{15}O)^{29}Mg Reactions and the Level Schemes of ^{27}Na and ^{29}Mg. *Nuclear Physics A*, 437, 141, 1985.

[FOR11] H. T. Fortune. The puzzle of ^{32}Mg. *Physical Review C*, 84, 24327, 2011.

[FAL06] P. Fallon, E. Rodriguez-Vieitez, D. Bazin, C. M. Campbell, J. M. Cook, R. M. Clark, D. C. Dinca, A. Gade, T. Glasmacher, I. Y. Lee, *et al.* Transition to the Island of Inversion: Study of Excited States in $^{28-30}$Ne. *Journal of Physics: Conference Series*, 49, 165, 2006.

[GAD07] A. Gade, P. Adrich, D. Bazin, M. D. Bowen, B. A. Brown, C. M. Campbell, J. M. Cook, S. Ettenauer, T. Glasmacher, K. W. Kemper, *et al.* Spectroscopy of ^{36}Mg: Interplay of Normal and Intruder Configurations at the Neutron-Rich Boundary of the "Island of Inversion". *Physical Review Letters*, 99, 72502, 2007.

[GAD11] A. Gade, D. Bazin, B. A. Brown, C. M. Campbell, J. M. Cook, S. Ettenauer, T. Glasmacher, K. W. Kemper, S. McDaniel, A. Obertelli, *et al.* In-beam γ-ray spectroscopy of ^{35}Mg and ^{33}Na. *Physical Review C*, 83, 044305, 2011.

[GUI84] D. Guillemaud-Mueller, C. Détraz, M. Langevin, M. Naulin, *et al.* β-Decay Schemes of Very Neutron-Rich Sodium Isotopes and Their Descendants. *Nuclear Physics A*, 426, 37, 1984.

[HIM08] P. Himpe, G. Neyens, DL Balabanski, G. Bélier, J. M. Daugas, F. de Oliveira Santos, M. De Rydt, K. T. Flanagan, I. Matea, P. Morel, *et al.* g factor of the exotic $N = 21$ isotope ^{34}Al: probing the $N = 20$ and $N = 28$ shell gaps at the border of the "island of inversion". *Physics Letters B*, 658, 203, 2008.

[HIN61] S. Hinds, H. Marchant, and R. Middleton. The Energy Levels of the Magnesium Isotopes of Mass 25 to 28. *Proceedings of the Physical Society*, 78, 473, 1961.

[HIN08] T. A. Hinners, Vandana Tripathi, S. L. Tabor, A. Volya, P. C. Bender, C. R. Hoffman, Sangjin Lee, M. Perry, P. F. Mantica, A. D. Davies, *et al.* Complementary studies of $T = 2$ ^{30}Al and the systematics of intruder states. *PHYSICAL REVIEW C* 77, 034305, 2008.

[HIN11] N. Hinohara, K. Sato, K. Yoshida, T. Nakatsukasa, M. Matsuo, and K. Matsuyanagi. Shape fluctuations in the ground and excited 0^+ states of ^{30,32,34}Mg. *Physical Review C*, 84, 061302, 2011.

[HIN] N. Hinohara Private communication

[HIR05] Y. Hirayama, T. Shimoda, H. Izumi, A. Hatakeyama, K. P. Jackson, C. D. P. Levy, H. Miyatake, M. Yagi, and H. Yano. Study of ^{11}Be structure through β-delayed decays from polarized ^{11}Li. *Physics Letter B*, 611, 239, 2005.

[HUB78] G. Huber, F. Touchard, S. Büttgenbach, C. Thibault, R. Klapisch, H. T. Duong, S. Liberman, J. Pinard, J. L. Vialle, P. Juncar, *et al.* Spins, magnetic moments, and isotope shifts of $^{21-31}$Na by high resolution laser spectroscopy of the atomic D_1 line. *Physical Review C*, 18, 2342, 1978.

[IWA01] H. Iwasaki, T. Motobayashi, H. Sakurai, K. Yoneda, T. Gomi, N. Aoi, N. Fukuda, Zs. Fülöp, U. Futakami, Z. Gacsi, *et al.* Large collectivity of ^{34}Mg. *Physics Letters B*, 522, 227, 2001.

[KLO93] G. Klotz, P. Baumann, M. Bounajma, A. Huck, A. Knipper, G. Walter, G. Marguier, C. Richard-Serre, A. Poves, and J. Retamosa. Beta decay of ^{31,32}Na and ^{31}Mg: Study of the $N = 20$ shell closure. *Physical Review C*, 47, 2502, 1993.

[KAN95] Y. Kanada-En ' yo, H. Horiuchi, and A. Ono. Structure of Li and Be isotopes studied with antisymmetrized molecular dynamics. *Physical Review C*, 52, 628, 1995.

[KEI00] M. Keim, U. Georg, A. Klein, R. Neugart, M. Neuroth, S. Wilbert, P. Lievens, L. Vermeeren, and B. A. Brown. Measurement of the electric quadrupole moments of $^{26-29}$Na. *The European Physical Journal A - Hadrons and Nuclei*, 8, 31, 2000.

[KIM07] M. Kimura. The intruder feature of ^{31}Mg and the coexistence of many particle and many hole states. *Physical Review C*, 75, 041302(R), 2007.

[KIM11] M. Kimura. Systematic Study of the Many-Particle and Many-Hole States in and around the Island of Inversion. *International Journal of Modern Physics E*, 20, 893, 2011.

[KAN10] R. Kanungo, C. Nociforo, A. Prochazka, Y. Utsuno, T. Aumann, D. Boutin, D. Cortina-Gil, B. Davids, M. Diakaki, F. Farinon, *et al.* Structure of ^{33}Mg sheds new light on the $N = 20$ island of inversion. *Physics Letters B*, 685, 253, 2010.

[KOW08] M. Kowalska, D. T. Yordanov, K. Blaum, P. Himpe, P. Lievens, S. Mallion, R. Neugart, G. Neyens, and N. Vermeulen. Nuclear ground-state spins and magnetic moments of^{27}Mg, ^{29}Mg, and ^{31}Mg. *Physical Review C*, 77, 034307, 2008.

[LEV04] C. D. P. Levy, R. Baartman, J. A. Behr, R. F. Kiefl, M. Pearson, R. Poutissou, A. Hatakeyama, and Y. Hirayama. The Collinear Laser Beam Line at ISAC. *Nuclear Physics A*, 746, 206, 2004.

[LEV04] C. D. P. Levy, A. Hatakeyama, Y. Hirayama, R. F. Kiefl, R. Baartman, J. A. Behr, H. Izumi, D. Melconian , G. D. Morris, R. Nussbaumer, *et al.* Polarized radioactive beam at ISAC. *Nuclear Instruments and Methods in Physics Research B*, 204, 689, 2003.

[LAN84] M. Langevin, C. Détraz, D. Guillemaud-Mueller, A. C. Mueller, C. Thibault, F. Touchard, and M. Epherre. β-Delayed Neutrons from Very Neutron-Rich Sodium and Magnesium Isotopes. *Nuclear Physics A*, 414, 151, 1984.

[MAR05] F. Maréchal, DL Balabanski, D. Borremans, J.M. Daugas, F. De Oliveira Santos, P. Dessagne, G. Georgiev, J. Giovinazzo, S. Grévy, P. Himpe, *et al.* β decay of ^{31}Mg: Extending the " island of inversion ". *Physical Review C*, 72, 044314, 2005.

[MAC05] H. Mach, L. M. Fraile, O. Tengblad, R. Boutami, C. Jollet, W. A. Płóciennik, D. T. Yordanov, M. Stanoiu, M. J. G. Borge, P. A. Butler, *et al.* New structure information on ^{30}Mg, ^{31}Mg and ^{32}Mg. *The European Physical Journal A - Hadrons and Nuclei*, 25, 105, 2005.

[MAC09] H. Mach *et al.*

[MOT95] T. Motobayashi, Y. Ikeda, K. Ieki, M. Inoue, N. Iwasa, T. Kikuchi, M. Kurokawa, S. Moriya, S. Ogawa, H. Murakami, *et al.* Large deformation of the very neutron-rich nucleus ^{32}Mg from intermediate-energy coulomb excitation. *Physics Letters B*, 346, 9, 1995.

[MIN04] K. Minamisono, K. Matsuta, T. Minamisono, C. D. P. Levy, T. Nagatomo, M. Ogura, T. Sumikama, J. A. Behr, K. P. Jackson, H. Fujiwara, *et al.* Quadrupole Moments of ^{20,21}Na. *Nuclear Physics A*, 746, 501, 2004.

[MIN05] K. Minamisono, K. Matsuta, T. Minamisono, C. D. P. Levy, T. Nagatomo, M. Ogura, T. Sumikama, J. A. Behr, K. P. Jackson, H. Fujiwara, *et al.* Production of Nuclear Polarization of Na Isotopes at ISAC/TRIUMF and its Hyperfine Interaction. *Hyperfine Interactions*, 159, 261, 2004.

[MID64] R. Middleton and D. J. Pullen. A Study of Some (t,p) Reactions (III). Results for Mg^{26}, Si^{28}, Si^{29}, Ca^{40} and Cd^{110}. *Nuclear Physics*, 51, 77, 1964.

[MEU74] F. Meurders and A. Van Der Steld. Investigation of the ^{26}Mg$(d,p)^{27}$Mg Reaction. *Nuclear Physics A*, 230, 317, 1974.

[MOR76] H. Morinaga and T. Yamazaki. *IN-BEAM GAMMA-RAY SPECTROSCOPY.* North-Holland Publishing Company, 1976.

[NEY05] G. Neyens, M. Kowalska, D. Yordanov, K. Blaum, P. Himpe, P. Lievens, S. Mallion, R. Neugart, N. Vermeulen, Y. Utsuno, *et al.* Measurement of the spin and magnetic moment of ^{31}Mg: Evidence for a Strongly Deformed Intruder Ground State. *Physical Review Letters*, 94, 22501, 2005.

[NND11] National Nuclear Data Center, Brookhaven National Laboratory. http://www.nndc.bnl.gov/.

[OTS10] T. Otsuka, T. Suzuki, M. Honma, Y. Utsuno, N. Tsunoda, K. Tsukiyama, and M. Hjorth-Jensen. Novel Features of Nuclear Forces and Shell Evolution in Exotic Nuclei. *Physical Review Letters*, 104, 12501, 2010.

[PRI00] B. V. Pritychenko, T. Glasmacher, B. A. Brown, P. D. Cottle, R. W. Ibbotson, K. W. Kemper, L. A. Riley, and H. Scheit. First observation of an excited state in the neutron-rich nucleus ^{31}Na. *Physical Review C*, 63, 011305, 2000.

[PRI99] B. V. Pritychenko, T. Glasmacher, P. D. Cottle, M. Fauerbach, R. W. Ibbotson, K. W. Kemper, V. Maddalena, A. Navin, R. Ronningen, A. Sakharuk, *et al.* Role of intruder configurations in ^{26,28}Ne and ^{30,32}Mg. *Physics Letters B*, 461, 322, 1999.

[PRI02] B. V. Pritychenko, T. Glasmacher, P. D. Cottle, R. W. Ibbotson, K. W. Kemper, L. A. Riley, A. Sakharuk, H. Scheit, M. Steiner, and V. Zelevinsky. Structure of the "island of inversion" nucleus ^{33}Mg. *Physical Review C*, 65, 061304, 2002.

[PAN81] A. D. Panagiotou, P. K. Kakanis, E. N. Gazis, M. Bernas, C. Détraz, M. Langevin, D. Guillemaud, and E. Plagnol. A new mass measurement of ^{29}Mg. observation of excited states via the ^{13}C(^{18},2p)^{29}Mg reaction. *Zeitschrift für Physik A Hadrons and Nuclei*, 302, 117, 1981.

[RAD11] RadWare is a software package for interactive graphical analysis of gamma-ray coincidence data developed by David Radford of the Physics Division at Oak Ridge National Laboratory. http://radware.phy.ornl.gov/main.html.

[ROE74] E. Roeckl, P. F. Dittner, C. Détraz, R. Klapisch, C. Thibault, and C. Rigaud. Decay properties of the neutron-rich isotopes, ^{11}Li and $^{27-31}$Na. *Physical Review C*, 10, 1181, 1974.

[RAS74] B. Rastegar, G. Guillaume, P. Fintz, and A. Gallmann. Étude du Noyau ^{28}Mg par la Réaction ^{26}Mg($t, p\gamma$)^{28}Mg. *Nuclear Physics A*, 225, 80, 1974.

[SCO74] D. K. Scott, B. G. Harvey, D. L. Hendrie, L. Kraus, C. F. Maguire, J. Mahoney, Y. Terrien, and K. Yagi. Spectroscopy of Exotic Nuclei using Heavy-Ion Transfer Reactions. *Physical Review Letters*, 33, 1343, 1974.

[SOR08] O. Sorlin and M. G. Porquet. Nuclear magic numbers: New features far from stability. *Progress in Particle and Nuclear Physics*, 61, 602, 2008.

[SCW09] W. Schwerdtfeger, P. G. Thirolf, K. Wimmer, D. Habs, H. Mach, T. R. Rodriguez, V. Bildstein, J. L. Egido, L. M. Fraile, R. Gernhäuser, *et al.* Shape Coexistence Near Neutron Number $N = 20$: First Identification of the $E0$ Decay from the Deformed First Excited $J^\pi = 0^+$ State in ^{30}Mg. *Physical Review Letters*, 103, 12501, 2009.

[TAK09] S. Takeuchi, N. Aoi, T. Motobayashi, S. Ota, E. Takeshita, H. Suzuki, H. Baba, T. Fukui, Y. Hashimoto, K. Ieki, *et al.* Low-lying states in ^{32}Mg studied by proton inelastic scattering. *Physical Review C*, 79, 054319, 2009.

[TER08] J. R. Terry, B. A. Brown, C. M. Campbell, J. M. Cook, A. D. Davies, D. C. Dinca, A. Gade, T. Glasmacher, P. G. Hansen, B. M. Sherrill, *et al.* Single-neutron knockout from intermediate energy beams of ^{30,32}Mg: Mapping the transition into the " island of inversion ". *Physical Review C*, 77, 014316, 2008.

[THI75] C. Thibault, R. Klapisch, C. Rigaud, A. M. Poskanzer, R. Prieels, L. Lessard, and W. Reisdorf. Direct measurement of the masses of ^{11}Li and $^{26-32}$Na with an on-line mass spectrometer. *Physical Review C*, 12, 644, 1975.

[TOS11] OPERA-3D (an operating environment for electromagnetic research and analysis) is the preprocessing and postprocessing system for electromagnetic analysis programs such as TOSCA (for nonlinear magnetostatic or electrostatic field and current flow problems) developed by Vector Fields Limited, England. http://www.cobham.com/about-cobham/aerospace-and-security/about-us/antenna-systems/kidlington.aspx, 2011.

[TRI11] MIDAS (Maximum Integrated Data Acquisition System) is a versatile Data Acquisition System (DAQ) for medium scale physics experiments. http://ladd00.triumf.ca/ daqweb/doc/midas/html/, https://daq-plone.triumf.ca/SR/MIDAS/.

[TRI07] V. Tripathi, S.L . Tabor, P. F. Mantica, Y. Utsuno, P. Bender, J. Cook, C. R. Hoffman, S. Lee, T. Otsuka, J. Pereira, *et al.* Competition between normal and intruder states inside the " island of inversion ". *Physical Review C*, 76, 021301, 2007.

[TRI08] V. Tripathi, S. L. Tabor, P. F. Mantica, Y. Utsuno, P. Bender, J. Cook, C. R. Hoffman, S. Lee, T. Otsuka, J. Pereira, *et al.* Intruder Configurations in the $A = 33$ Isobars: ^{33}Mg and ^{33}Al. *Physical Review Letters*, 101, 142504, 2008.

[UTS04] Y. Utsuno, T. Otsuka, T. Glasmacher, T. Mizusaki, and M. Honma. Onset of intruder ground state in exotic Na isotopes and evolution of the $N = 20$ shell gap. *Physical Review C*, 70, 044307, 2004.

[UTS08] Y. Utsuno. private communication.

[WAR90] E. K. Warburton, J. A. Becker, and B. A. Brown. Mass systematics for $A = 29 - 44$ nuclei: The deformed $A \sim 32$ region. *Physical Review C*, 41,1147, 1990.

[WOO88] C. L. Woods, W. N. Catford, L. K. Fifield, N. A. Orr, and R. J. Sadleir. Studies of the $T_z = 5/2$ Nuclei ^{31}Al and ^{29}Mg. *Nuclear Physics A*, 476, 392, 1988.

[WIL84] B. H. Wildenthal. Empirical strengths of spin operators in nuclei. *Progress in Particle and Nuclear Physics*, 11, 5, 1984.

[WIM10] K. Wimmer, T. Kröll, R. Krücken, V. Bildstein, R. Gernhäuser, B. Bastin, N. Bree, J. Diriken, P. Van Duppen, M. Huyse, *et al.* Discovery of the Shape Coexisting 0^+ State in ^{32}Mg by a Two Neutron Transfer Reaction. *Physical Review Letters*, 105, 252501, 2010.

[YOR10] D. T. Yordanov for the COLLAPS Collaboration. Laser spectroscopy in the island of inversion. *Hyperfine Interactions*, 196, 53, 2010.

[YAN03] Y. Yanagisawa, M. Notani, H. Sakurai, M. Kunibu, H. Akiyoshi, N. Aoi, H. Baba, K. Demichi, N. Fukuda, H. Hasegawa, *et al.* The first excited state of ^{30}Ne studied by proton inelastic scattering in reversed kinematics. *Physics Letters B*, 566, 84, 2003.